THE INERTISATION OF THE ZEOLITES ZSM-5, MORDENITE AND BETA BY CHEMICAL VAPOUR DEPOSITION USING TETRAETHOXYSILANE

Reinier Willem Weber
BSc. Eng. (Chem.), MSc. Eng. (Chem.)

Submitted to the University of Cape Town

In fulfillment of the requirements for the degree of

DOCTOR OF PHILOSOPHY

Department of Chemical Engineering
University of Cape Town
Rondebosch
Cape Town
South Africa

May 1998

ACKNOWLEDGEMENTS

Thanks are due to my supervisors, Prof. Cyril O'Connor and Dr. Klaus Möller, for sharing their wisdom and advice when help was most needed, and for the motivation which they have given me throughout this study. Also many thanks to Dr. Eric van Steen and Prof. Mark Dry for their input, and to Dr. Koos Jansen for several fruitful discussions. I wish to express my appreciation to the Catalysis Research Unit and the FRD for their financial contributions.

It has been a great pleasure to work with a cosmopolitan group of guys and girls willing to share their academic and social acumen : to all those Ghanaians, Mauritians, the Dutch and the Flemish, the Swedes, the "Eastern" Europeans, to the occasional local and of course the German hordes - it's been loads of fun ! Many thanks must go to Ashli, Frank, Andrew, Sarah and Julian, for the many lively debates and deliberations, not infrequently on our travels around the fairest Cape looking for that ageless bottle of Cabernet. To all the "Thermodynamix" players who through the years kept doing their best not to let their goalkeeper fall asleep - Thanks for the extra practice, lads !

Thanks to Leslie, Pam and Lorna, without whom all the things we take for granted would never get done. My gratitude for the technical support received from Peter Dobias, Joachim Macke, Bill Randall and Granville de la Cruz, as well as the numerous other people who "make things happen".

Last but certainly not least, a special word of gratitude to my parents, Ton and Ank, for their unassuming belief in all their children, and a big thank you to my siblings Marc and Marjolijn.

SYNOPSIS

The structural characteristic of greatest interest for catalysis in zeolites is the channel system, because these catalysts may display shape selective properties if the reactions take place within the channel system. However, the external surface of zeolites is accessible to all molecules and behaves in a non-shape selective manner. Coke formation on the external surface of zeolites may prevent access to the channel system of the zeolite due to pore blocking. It would thus be of great benefit to study the effects of inertising the external acidity of zeolites, thereby enhancing the shape selective properties of these catalysts, and possibly also to reduce coke formation at the entrances to the pores. Given the industrial importance of ZSM-5, this is a particularly good zeolite to study in this regard.

Chemical vapour deposition (CVD) and chemical liquid deposition (CLD) methods have shown great promise in inertising the external surface acidity of zeolites and thus increasing their selectivity for various reactions. The external surface acidity can be inertised by a thin layer of silica coating the external surfaces of the zeolites. The silica layer can also narrow the pore openings uniformly, thus increasing the shape selective properties of the zeolites even more. By implication, coating ZSM-5 in a shell of iso-structural Silicalite-I may provide an inert layer around the ZSM-5 crystals, without necessarily altering the pore opening size.

In this study, the following methods have been used to inertise the external surface acidity of ZSM-5, Mordenite and Beta:

(i) *Chemical vapour deposition* - Tetraethoxysilane (TEOS) was contacted with the catalyst using a vapour phase flow system and static vacuum system. The effects of deposition temperature and time were varied in order to vary the amount of TEOS deposited on the samples. The effect of the decomposition species formed during TEOS deposition on the complete inertisation of the external surface acidity was investigated.

(ii) *Chemical liquid deposition* - Pure tetraethoxysilane (TEOS) or tetraethoxysilane diluted in water, ethanol or *n*-hexane was contacted with the catalyst at ambient temperatures. The effect on the inertisation

of the external surface acidity in the presence of diluents, similar in nature to typical decomposition products formed at certain different temperatures, was studied.

(iii) *Coating with Silicalite shells* - Parent ZSM-5 seed crystals were immersed into a Silicalite-I synthesis mixture in order to obtain an iso-structural coating. The seed crystals used for modification were (a) the as-synthesized material, (b) detemplated but not ion-exchanged parent crystals (Na-form), and (c) detemplated and ion-exchanged parent crystals (NH_4-form).

The primary objective of these studies was to determine how complete inertisation of the external surface acidity could be achieved. By modifying samples under different conditions as outlined above, information was obtained on the uniformity of the coating of samples modified in each of the different systems. ZSM-5, Mordenite and Beta samples modified using similar CVD and CLD modification conditions were compared. Post-modification treatment was employed to determine whether the silica layer deposited during CVD treatment was irreversibly attached to the external surface of the samples.

A temperature programmed desorption (TPD) technique was developed in which 4-methyl quinoline (critical diameter = 7.3 Å) was used to probe the external surface acidity, because this molecule was not expected to enter the channels of the zeolites. Although for reasons explained in the thesis, quantitative measurements of the number of acid sites on the external surface could not be made, it was possible to obtain relative external surface acidity values which could be compared to the parent sample. The external surface activity of selected samples was determined by the conversion of 1,3,5-triisopropyl benzene (TiPB) (kinetic diameter = 8.5 Å). Temperature programmed desorption studies of pyridine (critical diameter = 5.1 Å) were used to probe the total acidity of the zeolites. Changes in Si/Al ratio brought about by the various modifications were measured by atomic absorption spectroscopy (AA). Adsorption studies using a range of different sized adsorbates (*n*-hexane (4.3 Å), *p*-xylene (5.85 Å), *o*-xylene (6.6 Å) and 1,2,4-trimethyl benzene (6.6 Å)) were used to determine whether the modification of the external surface had resulted in changes in pore structure such as pore mouth narrowing or pore blocking.

The extent of TEOS deposition was found to be strongly dependent on temperature in both vapour phase flow and static vacuum systems. The amount of TEOS deposited at relatively low temperatures was shown to be small because acid sites were required to decompose TEOS to ethanol, leaving residual partially decomposed alkoxy silane species on the external surface. Water, which catalyses the deposition reaction at higher temperatures, was not formed via ethanol dehydration at low temperatures. TEOS did not appear to decompose but was shown to physisorb onto the silanol groups on the external surface.

At relatively high temperatures, both the acid sites and the SiOH groups were able to decompose TEOS, although it appeared that the rate of decomposition was much greater on acid sites than on SiOH groups. Ethylene and water were formed at temperatures above about 200°C, probably via ethanol dehydration. Water catalyses the decomposition of surface alkoxy silane species to SiOH and ethanol. This creates new active sites for further TEOS deposition, while ethanol can again be dehydrated to ethylene and water, thereby allowing the deposition to proceed.

The competitive adsorption of decomposition products onto external surface acid sites resulted in incomplete inertisation by rendering these sites inaccessible to inertisation. Due to its static nature, samples modified in a vacuum system were affected more by competitive adsorption of decomposition products than samples modified in a vapour phase flow system. Thus, where necessary, decomposition products had to be removed from the sample with the use of repeated deposition-evacuation cycles, re-exposing acid sites to fresh TEOS. This procedure resulted in the relative external surface acidities of samples modified in a static vacuum system being reduced by 97% or more as measured by TPD of 4-methyl quinoline, using 4 cycles or less regardless of zeolite type.

ZSM-5, Mordenite and Beta samples modified in a vapour phase flow system showed significant pore mouth narrowing and increases in Si/Al ratio even though inertisation of the external surface acidity was not complete (viz. 20% or more relative to the respective parent sample). Consequently the silane was not deposited uniformly, and not all the external surface acid sites are necessarily inertised before pore mouth narrowing is observable. It is proposed here that the static environment of the vacuum system would be more

conducive to smaller TEOS concentration gradients compared to the relatively turbulent environment of the vapour phase flow system, thereby possibly favouring a kinetically controlled process in a vacuum system. Therefore it was possible to obtain complete inertisation of the external surface acidity in a static vacuum system without significant pore mouth narrowing. On the other hand, TEOS concentration gradients through the catalyst bed, and possible concentration gradients near the catalyst surface, may have favoured a diffusion controlling process contributing to non-uniform TEOS deposition in a vapour phase flow system. Ensuring low TEOS conversion levels in a vapour phase flow system is likely to improve the uniformity of the silica layer, but in a large or industrial scale operation unreacted TEOS will need to be recycled. The use of fluidised bed reactors for CVD may also be considered to obtain improved uniformity of the silane deposition.

The potential inhibiting effect of the decomposition products on the complete inertisation of the external surface acidity was further highlighted by the liquid phase deposition studies. The polar water and ethanol molecules inhibited TEOS deposition due to competitive adsorption on the acid sites. The relative external surface acidities of ZSM-5 samples modified using water and ethanol as diluents were reduced by 47 and 59% respectively compared to their parent sample. The non-polar *n*-hexane molecules were less strongly adsorbed by the acid sites, enabling a greater extent of inertisation of the external surface acidity to occur than for the polar diluents, viz. a reduction of at least 69% in external surface acidity compared to the parent sample for each of the zeolite types used. The samples modified using *n*-hexane as diluent showed slight pore mouth narrowing. The presence of diluents may provide an environment in which a more gradual and therefore more uniform deposition occurs than when pure TEOS is used, and diluents may disperse agglomerate particles, thus improving both the uniformity and completeness of the deposition during CLD treatment. However, a liquid phase system may be prone to incomplete inertisation of the external surface acidity because decomposition products, such as ethanol, are likely to be adsorbed onto the acid sites as soon as they are formed. Repeated deposition-calcination cycles may overcome this problem, but large scale manufacturing using such a procedure would be expensive.

Particle size distributions have shown that grinding caused agglomerates to break up, exposing new acid sites on the external surfaces that would not have been inertised previously during the CVD treatment. For example, the relative

external surface acidity of a Mordenite sample increased from 0% after CVD treatment to 57% after being subjected to grinding. Transport and handling of these catalysts when the powder form is modified may thus be detrimental to the effectiveness of the coating. For industrial applications it may therefore be necessary to consider *in-situ* chemical vapour deposition techniques, or modification of pellet or extrudate forms of the catalysts.

The amount of TEOS deposited during chemical vapour and liquid deposition at low temperatures is small and therefore excessive pore mouth narrowing is prevented. Repeated deposition-calcination cycles may be needed to completely inertise the external surface acidity, and to increase the amount of silane deposited on the external surface gradually with each cycle. Operating at relatively high temperatures will increase the amount of TEOS that can be deposited per cycle, but probably at the expense of controlled pore mouth narrowing. Co-feeding diluents or diluent mixtures and using fluidised bed reactors could be ways in which fewer deposition-calcination cycles are needed at high deposition temperatures while maintaining good control over pore mouth narrowing.

Inertisation of the external surface acidity using the Silicalite shell coating method on ZSM-5 seed particles was successful when the NH_4-form of the parent seed particles was used. The relative external surface acidity of this sample was reduced by 93%. No conclusive explanation is apparent as to why the NH_4-form of the seed particles would have been more successfully inertised than the Na-form. A Silicalite-I (or possibly a highly siliceous ZSM-5) phase was formed in samples modified using the Silicalite shell method, but separate Silicalite-I particles may also have been formed. The channel structure and internal acid sites remained accessible to probe molecules. It is possible that small amounts of amorphous material were formed in the mesopores of the parent seed particles, causing significant changes in the mesopore size distributions. The use of undetemplated seed particles may be preferred, in that the deposition of amorphous species in the mesopores or even the channels can be prevented during the modification process. Obvious shortcomings of the Silicalite shell method of modification are that this method applies to ZSM-5 only, and that the presence of large amounts of Silicalite-I will add substantially to the reactor size.

TABLE OF CONTENTS

APPENDICES

LIST OF FIGURES

LIST OF TABLES

NOMENCLATURE

AA	Atomic Absorption Spectroscopy
BET	Brunauer, Emmett and Teller
CLD	Chemical Liquid Deposition
CVD	Chemical Vapour Deposition
DEA	Diethylamine
EDTA	Ethylenedinitrilo Tetraacetic Acid
EELS	Electron Energy Loss Spectroscopy
EFAI	Extra Framework Aluminium
EXAFS	Extended X-ray Absorption Fine Structure
FID	Flame Ionization Detector
FT-IR	Fourier Transform Infra-Red
GC	Gas Chromatograph
HERI	errionite
HOFF	offretite
HY (USHY)	zeolite Y (ultrastable)
I.R.	Infra-red
MS	Mass Spectrometer
4MQ	4-Methyl Quinoline
n.m.r.	nuclear magnetic resonance
Py	Pyridine
SBU	Secondary Building Unit
SEM	Scanning Electron Microscopy
SIM	Selected Ion Mode
TBA	Tributylamine
TCD	Thermal Conductivity Detector
TEM	Transmission Electron Microscopy
TEOS	Tetraethoxysilane
TIC	Total Ion Chromatogram
TiPB	Triisopropyl benzene
TMB	Trimethyl benzene
TMOS	Tetramethoxysilane
TPA (-Br)	Tetrapropylammonium (Bromide)
TPD	Temperature Programmed Desorption
MQ-TPD	Temperature Programmed Desorption of 4-methyl quinoline
NH_3-TPD	Temperature Programmed Desorption of ammonia
Py-TPD	Temperature Programmed Desorption of pyridine
WHSV	Weight Hourly Space Velocity
XPS	X-ray Photoelectron Spectroscopy
XRD	X-ray Diffraction

PUBLICATIONS TO DATE FROM THIS THESIS

Journal Publications:

R.W. Weber, J.C.Q. Fletcher, K.P. Möller, C.T. O'Connor, "The characterization and elimination of the external acidity of ZSM-5", *Microporous Materials*, **7** (1996) 15-25

R.W. Weber, K.P. Möller, M. Unger, C.T. O'Connor, "The chemical vapour and liquid deposition of tetraethoxysilane on the external surface of ZSM-5", Accepted by *Microporous and Mesoporous Materials* (1998)

Conference Presentations (Oral):

R.W. Weber, H.P. Röger, K.P. Möller, C.T. O'Connor, "The chemical vapour deposition of TEOS on the external surface of zeolites", Presented by C.T. O'Connor at the 1st Conference of the Indo-Pacific Catalysis Association, Cape Town, South Africa, 26-28 January 1998

Conference Presentations (Poster):

R.W. Weber, C.T. O'Connor, "Synthesis and characterization of ZSM-5 by elimination of the external acidity", The National Conference on Catalysis, Pretoria, South Africa, 28-30 October 1994

R.W. Weber, C.T. O'Connor, "The elimination of the external acidity of ZSM-5", The Catalysis Conference, Rustenberg, South Africa, 25-27 June 1995

R.W. Weber, H.P. Röger, M. Unger, K.P. Möller, C.T. O'Connor, "Chemical vapour deposition of TEOS on HZSM-5", 11th International Zeolite Conference, Seoul, South Korea, 12-17 August 1996

R.W. Weber, H.P. Röger, K.P. Möller, C.T. O'Connor, "Effect of different silanisation procedures on the external surface activity and shape selectivity of HZSM-5", Accepted for the 12th International Zeolite Conference, Baltimore, United States of America, 5-10 June 1998

CHAPTER 1

INTRODUCTION

"We do not know one millionth percent about nothing" - **Edison**

1.1 INTRODUCTION

This thesis presents an investigation into the inertisation of the external surface acidity the zeolites ZSM-5, Mordenite and Beta by chemical vapour deposition (CVD) and chemical liquid deposition (CLD) using tetraethoxysilane (TEOS) and of ZSM-5 by coating with Silicalite shells.

The uniform pore dimensions, ion-exchange properties, ability to possess acidity and high thermal stability make zeolites suitable catalysts for a wide range of industrial applications. The structural characteristic of greatest interest for catalysis in zeolites is the channel system, because these catalysts may display shape selective properties if the reactions take place within the channel system. It has been shown recently that the external surface of, for example, ZSM-5 is not smooth and that many protrusions occur on the external surface [Koegler *et al.*, 1997]. The external surface area may consequently form a significant part of the total surface area. Because the external surface of zeolites is fully accessible to all molecules it behaves in a non-shape selective manner. Coke formation on the external surface of zeolites may prevent access to the channel system of the zeolite due to pore blocking. It would thus be of great benefit to study the effects of inertising the external surface acidity of zeolites, thereby enhancing the shape selective properties of these catalysts, and possibly also to reduce coke formation at the entrance to the pores.

Several methods of altering the acidity of zeolites, including leaching methods and hydrothermal or chemical treatments, have been reported and are reviewed in Chapter 2. Chemical vapour deposition (CVD) and chemical liquid deposition (CLD) methods have shown great promise in selectively inertising the external surface acidity of zeolites and thus increasing their selectivity for various reactions. Chemical deposition of alkoxy silanes has been reported using static vacuum systems, vapour phase flow systems and liquid phase systems, as will be shown in Chapter 2. The external surface acidity could be inertised using CVD or CLD techniques by a thin layer of silica which coated the external surfaces of the zeolites. The silica layer can also narrow the pore openings uniformly, thus increasing the shape selective properties of the zeolites even more.

In the investigation covered by this thesis, the modification of ZSM-5, Mordenite and Beta was carried out by chemical vapour deposition (CVD) in both a static vacuum system and a vapour phase flow system and by chemical liquid deposition (CLD). Tetraethoxysilane (TEOS) was used to inertise the external surface acidity of the samples. The primary objective of these studies was to determine how complete inertisation of the external surface acidity could be achieved. By modifying samples under different conditions as outlined above, information was obtained on the uniformity of the silica layer covering the samples modified in each of the three systems.

The temperature and time of deposition were varied in order to vary the amount of TEOS deposited on the samples. TEOS deposition studies on ZSM-5, Silicalite-I and silica at different temperatures were used to provide information on the influence of the catalyst acidity on the deposition process. The effect of the decomposition species formed during TEOS deposition on complete inertisation of the external surface acidity was compared for each method of deposition. Liquid phase deposition using pure TEOS or using TEOS diluted in water, ethanol or *n*-hexane was used to investigate the effect of different types of diluents. Post-modification treatment was employed to determine whether the silica layer was irreversibly attached to the external surface of the samples. Given the industrial importance of ZSM-5, most of the modifications by CVD and CLD and the characterization studies were carried out using this zeolite. The results obtained with ZSM-5 were compared with results obtained for Mordenite and Beta using similar conditions.

Coating ZSM-5 in a shell of iso-structural Silicalite-I may be used as an alternative method of inertising the external surface acidity, without necessarily altering the pore opening size. The influence of the seed crystal on epitaxial growth was investigated. The seed crystals used for modification were (i) the as-synthesized material, (ii) detemplated but not ion-exchanged parent crystals (Na-form), and (iii) detemplated and ion-exchanged parent crystals (NH_4-form).

Chapter 2 reviews the relevant literature on the structure, acidity and synthesis of zeolites, the concept of shape selectivity as well as coke formation and deactivation of zeolites. Several methods of altering the acidity of zeolites are discussed, the emphasis being placed on chemical vapour and liquid deposition, and on coating ZSM-5 with Silicalite shells, because these methods were most likely to inertise selectively the external surface acidity with a minimum of

change to the internal acidity. Characterization techniques relevant to this study are discussed. The literature review deals more specifically with zeolites ZSM-5, Mordenite and Beta, because these zeolites were used in this investigation. Finally, the specific objectives of research are listed.

Chapter 3 describes the experimental procedures followed to synthesize and modify the zeolites, the characterization techniques and the equipment used. The primary analytical tool used to quantify the extent of inertisation of the external surface acidity was temperature programmed desorption (TPD). Pyridine (critical diameter = 5.1 Å) was used to probe the total acidity of the zeolites, and a TPD technique in which 4-methyl quinoline (critical diameter = 7.3 Å) was used to probe the external surface acidity was developed. The detector chosen for the TPD studies was a mass spectrometer, by virtue of its flexibility in monitoring all desorbing species simultaneously for the duration of the experiment. The external surface activity of selected samples was determined by the conversion of 1,3,5-triisopropyl benzene (TiPB) (kinetic diameter = 8.5 Å) and compared with 4-methyl quinoline TPD results.

Changes in Si/Al ratio brought about by the various modifications were measured by atomic absorption spectroscopy (AA), and the aluminium content measured by AA was compared with the number of acid sites measured by Py-TPD studies. Adsorption studies using a range of different sized adsorbates (*n*-hexane (4.3 Å), *p*-xylene (5.85 Å), *o*-xylene (6.6 Å) and 1,2,4-trimethyl benzene (6.6 Å)) were used to determine whether the modification of the external surface had resulted in changes in pore structure such as pore mouth narrowing or pore blocking.

Chapter 4 details the results of the physico-chemical catalyst characterization, the temperature programmed desorption studies, the adsorption studies and probe reaction work. The results are discussed in Chapter 5, and concluding remarks are made in Chapter 6.

CHAPTER 2

LITERATURE REVIEW

"If you go into a labyrinth, take a clue with you"

2.1 ZEOLITES

Zeolites are 3-dimensional crystalline aluminosilicates consisting of cornerlinked tetrahedra in which small atoms (collectively denoted T atoms) lie at the centers of the tetrahedra, with oxygen atoms at the corners. The T sites of all natural zeolites are dominated by Al and Si atoms, such that the ratio $O/(Al+Si) = 2$ [Barrer, 1982], but chemically related atoms such as Ga, Ge and P can be incorporated in synthetic zeolites. The substitution of aluminium atoms into the silicon based structure results in a net negative charge on the zeolite framework. This is compensated for by the presence of charge balancing cations, typically Na, K, Mg, Ca or Ba. The unit cell formula is given by

$$M_pD_q(Al_{p+2q}Si_rO_{2p+4q+2r}).{}_sH_2O \qquad \text{[Smith, 1979]}$$

where M and D represent monovalent and divalent cations respectively. The arrangement of the tetrahedral units in the macroscopic crystal results in the formation of open channels and cavities in the zeolite structure. Different arrangements yield the various zeolite types. It is this intracrystalline porosity which confers on zeolites their remarkable properties.

In addition to the cations needed to neutralize the framework charge, there is room for salts and water molecules in the channels and cavities of the zeolite. The open frameworks of zeolites also provide an environment in which cations and water have a high degree of mobility, resulting in good ion-exchange properties and the capacity for reversible hydration. The uniform pore dimensions, ion-exchange properties, ability to possess acidity and high thermal stability make zeolites suitable for a wide range of industrial applications. The four main areas in which zeolites are used are the following:

Adsorbents and separation processes:

Including applications such as drying agents, gas purification and separation processes which utilize their shape selective properties.

Catalysts:

Mainly in petroleum refining, synfuels production and petrochemicals production.

Detergents:

As a substitute for phosphates (limited nearly exclusively to zeolite A).

Miscellaneous:

For waste water treatment, nuclear effluent treatment, animal feed supplements and soil improvement.

Figure 2.1 shows the dominance of zeolite A in this market as it has been estimated that 67% of all synthetic zeolites produced was A-type zeolite for detergent builders. The estimate for zeolite usage in North-America, Western Europe and Japan in 1988 was a total of approximately 550 000 metric tons, of which the breakdown is given in Figure 2.2.

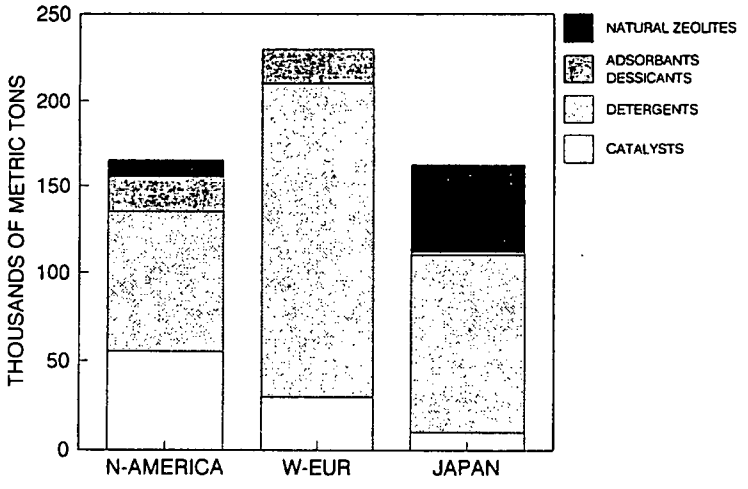

FIGURE 2.1: Estimated relative consumption of zeolites in 1988 for various applications in North-America, Western Europe and Japan [From Moscou, 1991]

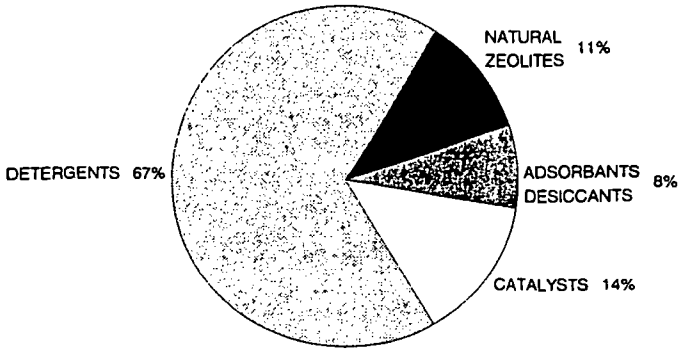

FIGURE 2.2: Estimated zeolite consumption in 1988 [From Moscou, 1991]

2.1.1 THE STRUCTURE OF ZEOLITES

2.1.1.1 The primary building unit

The primary building units of zeolites are the tetrahedra, as shown in Figure 2.3.

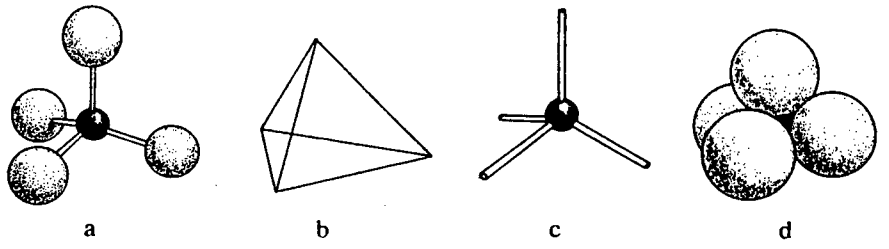

FIGURE 2.3: Representations of TO_4 tetrahedra

2.1.1.2 The secondary building units

In order to facilitate the description and systematization of the vast diversity of zeolite topologies, Meier [1968] suggested the use of 8 secondary structural units based on simple groupings of linked tetrahedra. The number of these so-called secondary building units (SBU's) was later increased to 16 as shown in Figure 2.4 [Meier and Olson, 1992]. Zeolites can be reduced to combinations of secondary building units.

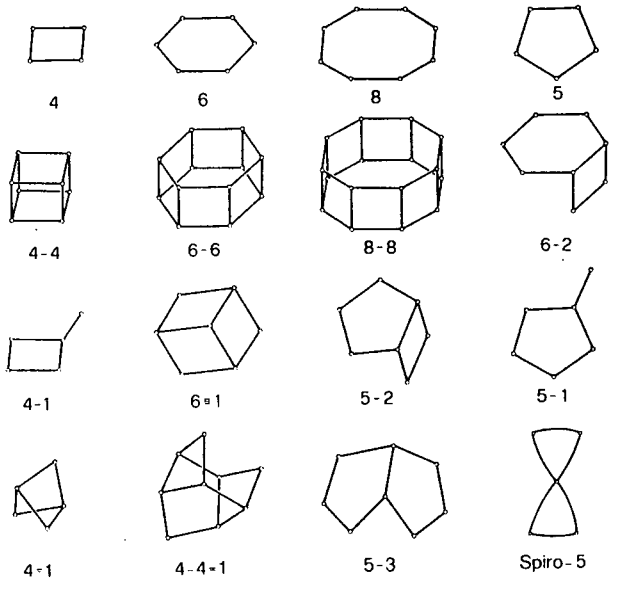

FIGURE 2.4: Secondary building units [Meier and Olson, 1992]

The T atoms in Figure 2.4 are represented by the corners or apices. The O atoms are not shown, but would lie approximately at the midpoints of the lines joining the T atoms.

2.1.1.3 Building blocks

The SBU's may be combined to form building blocks. An example of such a building block is the sodalite unit, depicted in Figure 2.5a, which is found in faujasite zeolites, X and Y. The sodalite unit is a truncated cubo-octahedron composed of 24 silicon and aluminium ions in tetrahedral coordination with oxygen atoms. These sodalite units are linked together via their hexagonal faces by so-called hexagonal prisms yielding the faujasite structure shown in Figure 2.5b.

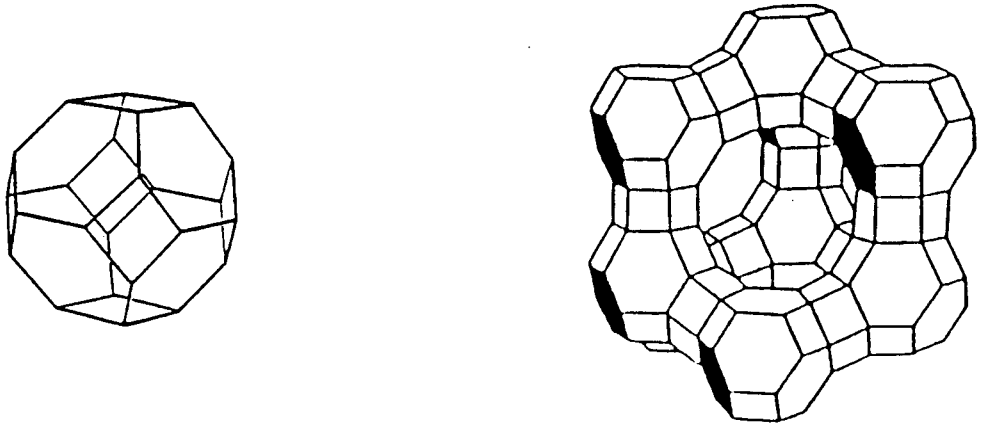

a b

FIGURE 2.5: Structure of faujasite (b) showing the sodalite unit (a)

This arrangement of sodalite units and hexagonal prisms results in the formation of large, almost spherical cavities interconnected by distorted 12 sided windows. This cavity is referred to as the supercage. In this manner a network of channels and cages is formed. Similarly, in other zeolites, such networks

exist, although not all zeolites will have cages. Also, the channel network may consist of straight parallel channels as in Mordenite, or of an intersecting network as in ZSM-5. Figure 2.6 shows the topology of several well-known zeolites.

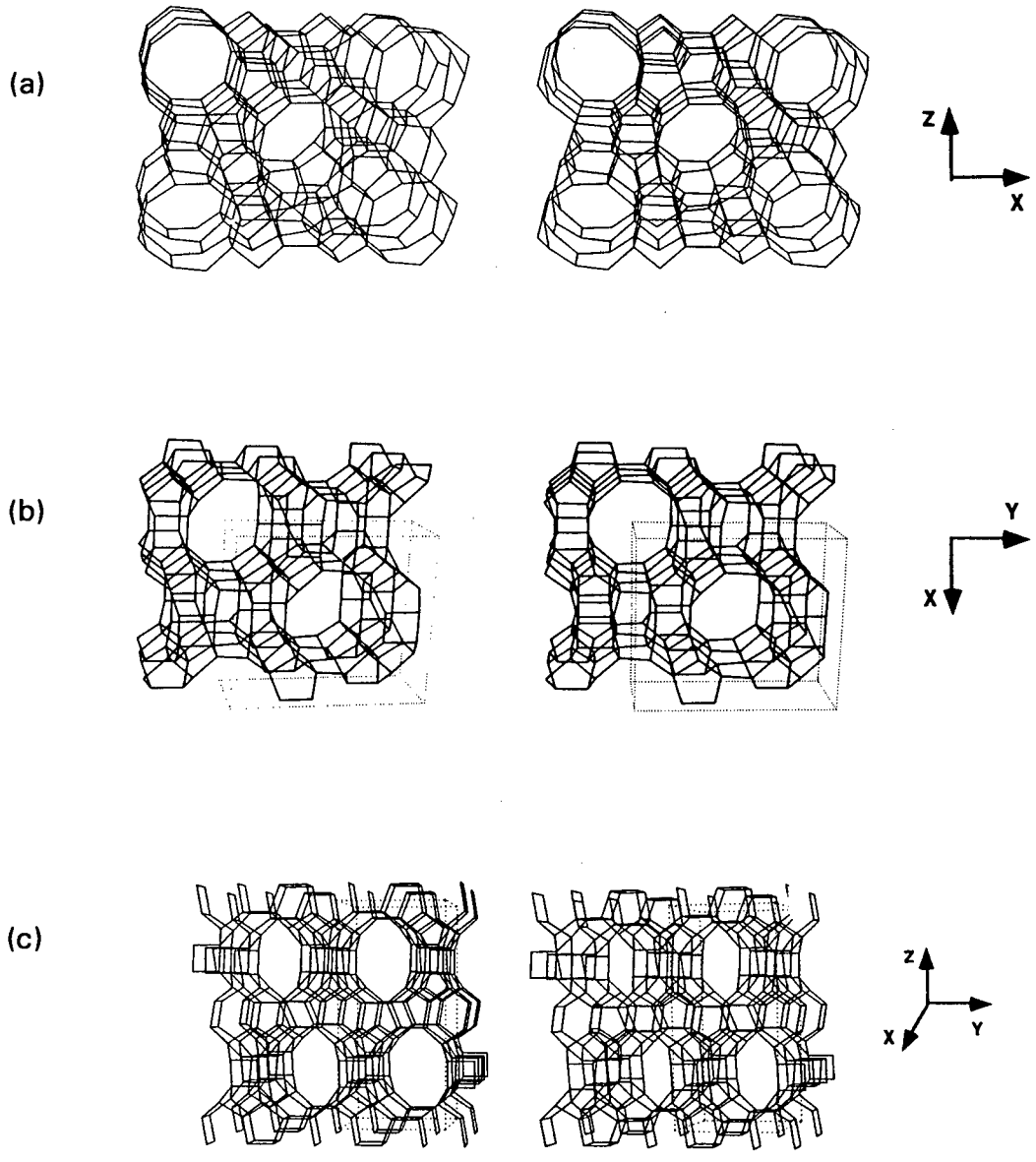

FIGURE 2.6: Stereoscopic representations of zeolite topologies (a) ZSM-5, (b) Mordenite and (c) Beta [Meier *et al.*, 1996]

2.1.1.4 Zeolite groups

The structural characteristic of greatest interest for catalysis is the channel system, which is described for some zeolites in Table 2.1. Depending on the largest channel, zeolites are characterized as small, medium or large pore zeolites if they contain apertures made by rings of 8, 10 or 12 linked tetrahedra respectively [Haag and Chen, 1987]. Small pore zeolites, which include chabazite and erionite, adsorb only straight-chain molecules such as *n*-paraffins and *n*-olefins. Medium pore zeolites, such as ZSM-5, ZSM-11, ZSM-22 and ZSM-23, are of most interest to the design of shape-selective catalysts. Synthetic faujasites, zeolite X and Y, and Mordenite are large pore zeolites.

The channel system may be one-dimensional (ZSM-22 and ZSM-48), two-dimensional (ferrierite) or three-dimensional (ZSM-5). Multidimensional channels often intersect one another, but this is not always the case. The interconnecting channels may be straight (ZSM-11) or tortuous (ZSM-5). The connectivity of the channel system has major consequences for diffusion and ageing characteristics.

TABLE 2.1: Channel systems of some representative zeolites [after Haag and Chen, 1987]

TYPE	NAME	RING SIZE OF CHANNELS	LARGEST CHANNEL SIZE (Å)
SMALL PORE	Linde type A	8-8-8	4.1
	Chabazite	8-8-8	3.6 x 3.7
	Erionite	8-8	3.6 x 5.2
MEDIUM PORE	ZSM-22	10	4.5 x 5.5
	ZSM-23	10	4.5 x 5.6
	ZSM-48	10	5.3 x 5.6
	Ferrierite	10-8	4.3 x 5.5
	ZSM-5	10-10	5.4 x 5.6
	ZSM-11	10-10	5.1 x 5.5
LARGE PORE	ZSM-12	12	5.7 x 6.1
	Linde type L	12	7.1
	Mazzite	12	7.4
	Mordenite	12-8	6.7 x 7.0
	Beta	12-12	6.4 x 7.6
	Offretite	12-8-8	6.4
	Faujasite	12-12-12	7.4

2.1.1.5 The zeolite ZSM-5

ZSM-5 synthesis was first reported by researchers at Mobil [Argauer and Landolt, 1972]. It is a medium pore zeolite belonging to the pentasil group. The unit cell formula of the sodium form of ZSM-5 is shown below, with n typically having a value of 3 or less (but not greater than 27) [Kokotailo *et al.*, 1978].

$$Na_nAl_nSi_{96-n}O_{192} \cdot 16H_2O \qquad n < 27$$

It has been shown from X-ray diffraction studies that as-synthesized ZSM-5 crystallizes with orthorhombic symmetry and has lattice constants a = 20.1, b = 19.9 and c = 13.4 Å [Meier *et al.*, 1996]. However, monoclinic symmetry has also been observed [De Vos Burchart *et al.*, 1993].

The framework of ZSM-5 consists of linked tetrahedra which may be considered to join to form eight 5-membered rings (SBU = 5-1). The units are connected through edges to form chains as shown in Figure 2.7. These chains are connected to form sheets and the linking of sheets leads to a three dimensional framework structure. The sheets parallel to the (010) and (100) planes are shown in Figure 2.8.

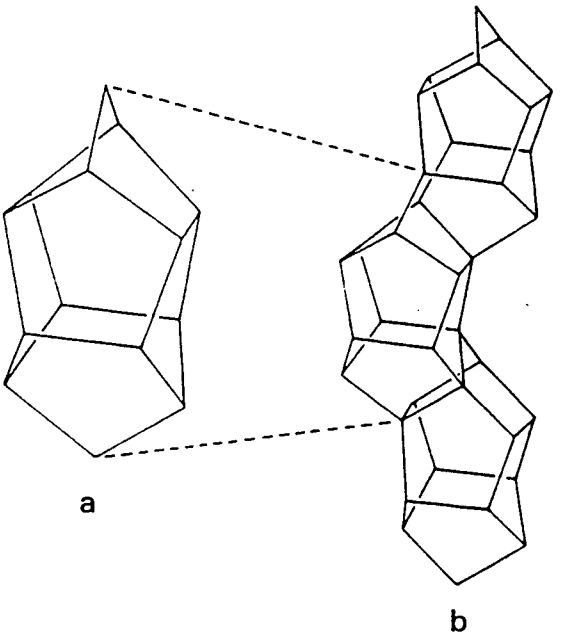

FIGURE 2.7: The building blocks of ZSM-5

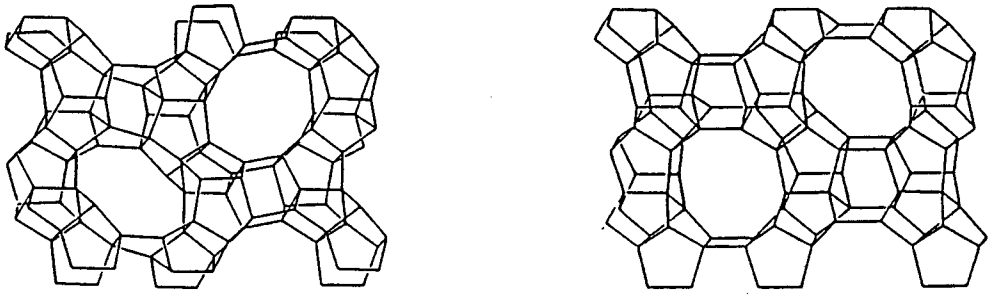

a b

FIGURE 2.8: The skeletal diagrams of (a) the (010) plane of the ZSM-5 unit cell, showing the channel opening of the straight channel, and of (b) the (100) plane of the ZSM-5 unit cell, showing the channel opening of the sinusoidal channel

The ZSM-5 framework contains two intersecting channel systems, one sinusoidal running parallel to the (010) plane and the other straight and parallel to the (100) plane, as indicated by Figure 2.9. The elliptical 10-membered ring openings (10 Al or Si atoms) controlling the channels can be seen clearly in Figure 2.8. The sinusoidal channels have a diameter of 5.1 x 5.5 Å, whereas the straight channels have a diameter of 5.3 x 5.6 Å [Meier *et al.*, 1996].

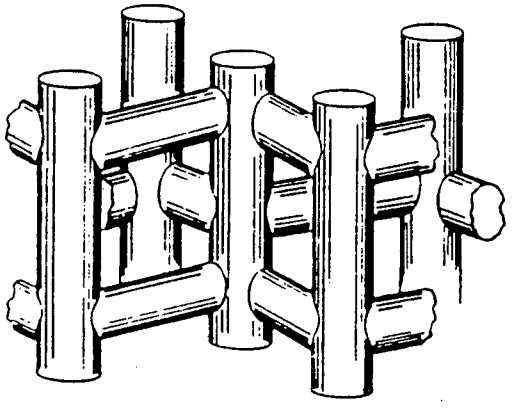

FIGURE 2.9: The channel structure of ZSM-5

2.1.1.6 The zeolite Mordenite

Mordenite synthesis was reported by Barrer in 1948. Mordenite is a large pore zeolite, and crystallizes with orthorhombic symmetry. The lattice constants are a = 18.1 Å, b = 20.5 Å and c = 7.5 Å [Meier *et al.*, 1996]. The unit cell formula is shown below.

$$Na_nAl_nSi_{48-n}O_{96} \cdot 24H_2O \qquad n \approx 8$$

The building units of Mordenite consist of four- and five-membered rings, crosslinked by the sharing of neighbouring oxygens to form chains [Szostak, 1992]. Mordenite contains a two-dimensional channel system, but for practical applications it is considered to be a uni-dimensional large pore molecular sieve with side pockets because of the constraint on the 8-member ring openings for diffusion. The large channels have a diameter of 6.5 x 7.0 Å, whereas the small channels have a diameter of 2.6 x 5.7 Å [Meier *et al.*, 1996]. Figure 2.10 shows the framework topology of Mordenite.

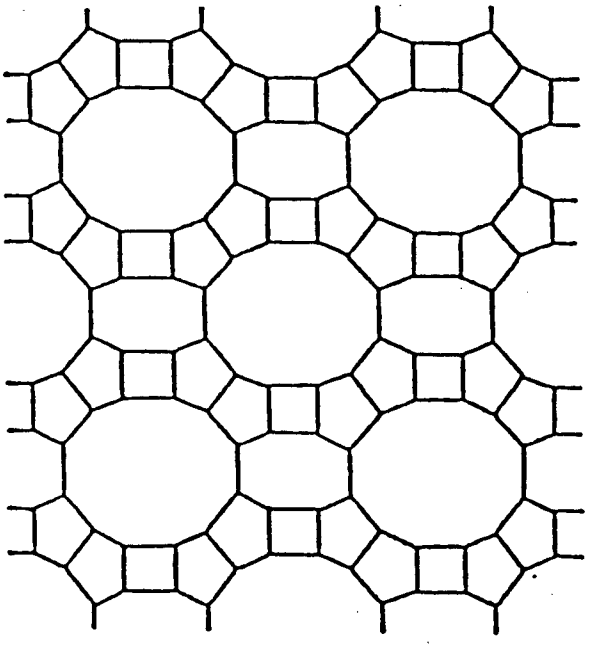

FIGURE 2.10: Framework topology of Mordenite

2.1.1.7 The zeolite Beta

Zeolite Beta was first synthesized by Wadlinger *et al.* [1967]. Zeolite Beta is a large pore zeolite, and crystallizes with both tetragonal and monoclinic symmetry. The unit cell formula is shown below [Meier *et al.*, 1996].

$$Na_nAl_nSi_{64-n}O_{128} \qquad n < 7$$

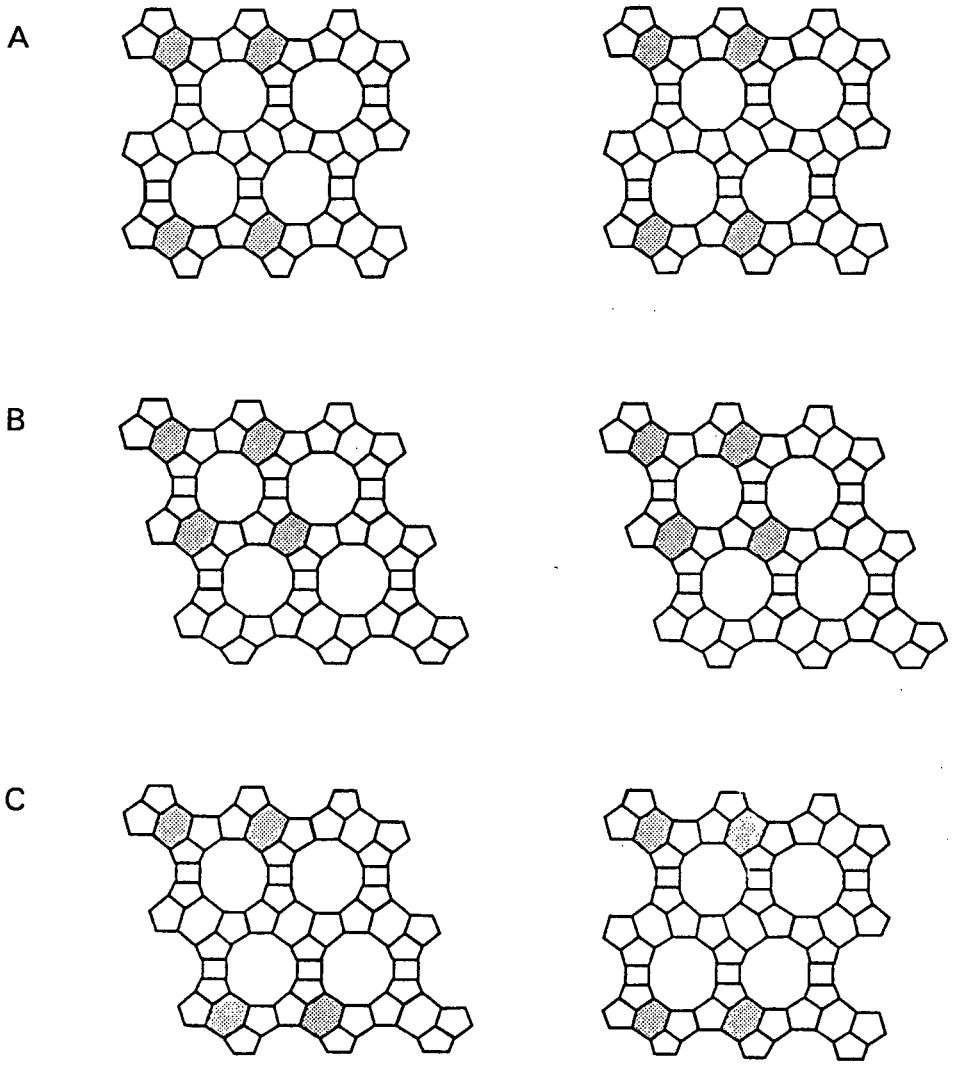

FIGURE 2.11: Polymorphs A, B and C of zeolite Beta

The framework structure of zeolite Beta is disordered along the (001) plane. Zeolite Beta consists of a highly intergrown hybrid of three distinct, but closely related structures (polymorphs) that have fully three-dimensional channel systems with 12-rings as minimum constricting apertures. These polymorphs (A, B or C) are arranged in layers, interconnecting in either a left- or right-handed fashion [Ratnasamy *et al.*, 1989]. Figure 2.11 shows the three polymorphs of zeolite Beta.

Zeolite Beta's pore system consists of three intersecting 12-membered ring channels. Two of these channels are identical and linear. They are mutually orthogonal and perpendicular to the c-axis. The third channel is nonlinear and parallel to the c-axis [Higgins *et al.*, 1988]. The tortuosity of the third channel is determined by the stacking faults found in zeolite Beta. The pore dimensions of the two linear channels are 7.6 x 6.4 Å, and 5.5 x 5.5 Å for the nonlinear channel [Meier *et al.*, 1996].

The lattice constants are a = 12.469 Å, b = 12.469 Å and c = 26.330 Å for polymorph A, a = 17.634 Å, b = 17.635 Å and c = 14.416 Å for polymorph B, and a = 12.470 Å, b = 12.470 Å and c = 27.609 Å for polymorph C [Szostak, 1992].

2.1.2 THE ACIDITY OF ZEOLITES

In Section 2.1.1 it was mentioned that zeolites are composed of tetrahedrally bound silicon and aluminium ions, joined by bridging oxygen ions. The tetrahedral coordination of the aluminium ion induces a negative framework charge for each aluminium ion. This charge is neutralized by the presence of exchangeable cations. It is this charge balancing phenomenon that is responsible for the acidity and activity of zeolites.

Zeolites are commonly synthesized in the sodium form, and the sodium cations are replaced by ammonium cations. On heating ammonium-exchanged zeolites ammonia is released, thereby yielding the active protonic form, as shown in Figure 2.12 [Uytterhoeven *et al.*, 1965; Niewenhuys *et al.*, 1993].

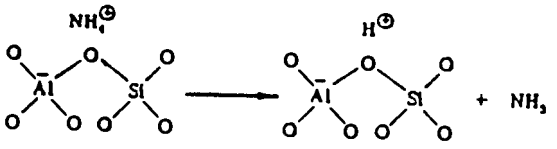

FIGURE 2.12: The formation of the proton form of zeolites

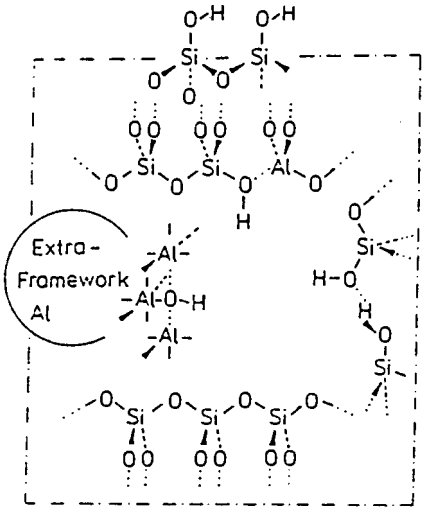

FIGURE 2.13: Schematic of hydroxyl groups in zeolites [Sauer, 1989]

Several different hydroxyl groups are found in zeolite structures. Figure 2.13 shows a schematic view of a microcrystallite of a zeolite catalyst showing (non-acidic) terminal hydroxyls on the outer surface and (acidic) bridged hydroxyls on the walls of the micropores. Further hydroxyl groups may be found on extra-framework aluminium species or may be connected with open Si-O-Si links (lattice defects) [Sauer, 1989].

Ward [1967] investigated the nature of the active sites on proton exchanged zeolite Y, and observed three hydroxyl group stretching bands in the infrared spectrum of zeolite Y at 3742, 3643 and 3540 cm^{-1}. These observations were in agreement with Uytterhoeven *et al.* [1965]. The 3742 cm^{-1} band probably represented Si-OH terminal groups (similar to those on silica) or they may be associated with amorphous impurities in the structure [Ward, 1967]. The bands at 3643 and 3540 cm^{-1} represented hydroxyl groups at different crystallographic locations.

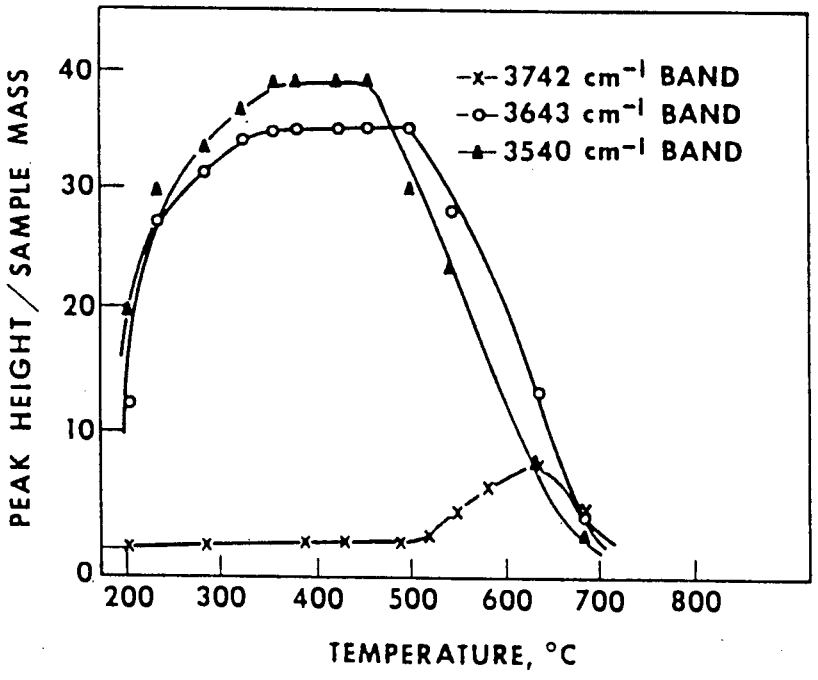

FIGURE 2.14: Intensity of the hydroxyl group stretching frequencies of zeolite Y for different calcination temperatures [Ward, 1967]

Ward [1967] noted that the maximum intensity of the hydroxyl group bands of zeolite Y was reached at calcination temperatures of 350°C. From this

temperature to 500°C the intensities remained constant, after which they decreased (Figure 2.14). The 3742 cm^{-1} band intensity increased to a maximum at a calcination temperature of 640°C before decreasing. Ward [1967] concluded that the hydroxyl groups, functioning as Brönsted acid sites, were largely responsible for catalytic activity.

The OH bond is covalent [Kazansky, 1994; Van Santen, 1994]. The acid strength for the different types of hydroxyl groups in zeolites differ [Sauer, 1989]. It has been widely accepted that the number of Brönsted sites is determined by the number of aluminium atoms in the framework [Stach *et al.*, 1992]. An important factor which controls the acid strength of the Brönsted sites is the lattice composition. As the aluminium content changes, the deprotonation energy, and thus the strength of the Brönsted sites, varies.

Kazansky [1991] found that the covalent hydroxyl interaction energy varied little with acidity and concluded that the factor contributing most to strong acidity was the stabilization of the negative charge left on the framework after deprotonation. The existence of other negative centres (i.e. other aluminium atoms in the lattice) in close proximity would hinder this stabilization. Aluminium atoms in the second coordination sphere (i.e. the 12 T-atoms which are linked to the acid site by an -O-Si-O- group) lead to a decrease in acid strength [Niewenhuys *et al.*, 1993].

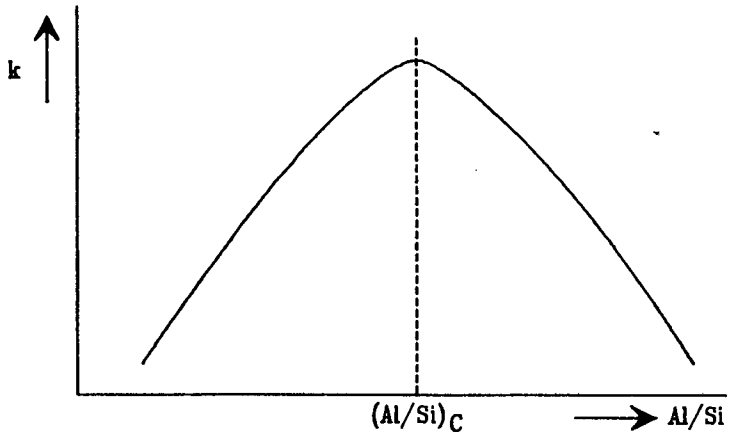

FIGURE 2.15: Dependence of acid-catalyzed reaction on zeolite Al/Si ratio [Niewenhuys *et al.*, 1993]

Brönsted acid-catalyzed reactions will be proportional to the proton content of a zeolite as long as the intrinsic acidity of a proton remains unchanged, since the proton concentration is proportional to the Al/Si ratio. As shown in Figure 2.15, once the Al/Si ratio exceeds a critical value $(Al/Si)_c$, the intrinsic acidity of a zeolitic proton starts to decrease, resulting in an overall decrease in the rate of reaction [Niewenhuys *et al.*, 1993].

While Brönsted acidity decreases rapidly above calcination temperatures of 500°C, the concentration of Lewis acid sites is small below 475°C, but increases rapidly at higher temperatures (Figure 2.16).

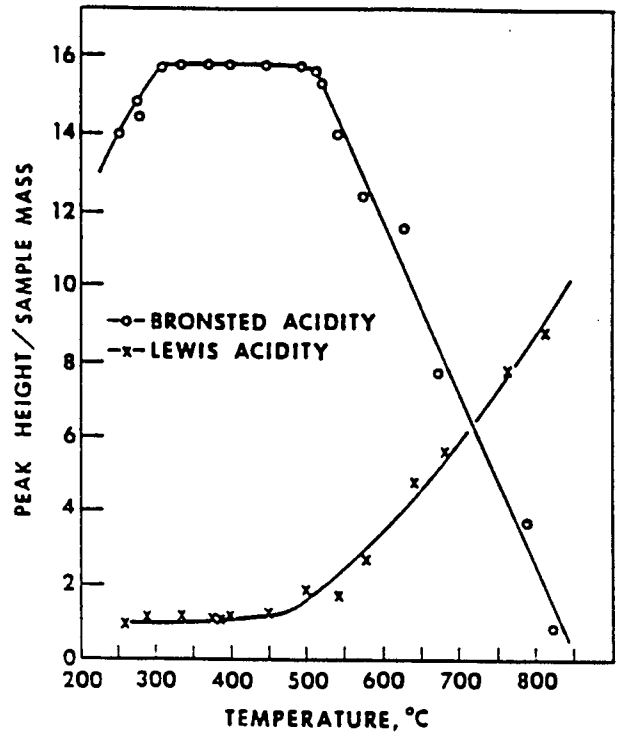

FIGURE 2.16: Acid site populations on zeolite Y as a function of calcination temperature [Ward, 1967]

Ward [1967] and Uytterhoeven *et al.* [1965] suggested that if the Brönsted acid sites are hydroxyl groups, then a conversion to Lewis acid sites should occur with increasing temperature, according to Figure 2.17, such that dehydroxylation of the zeolite occurs leaving tri-coordinated silicon and aluminium species.

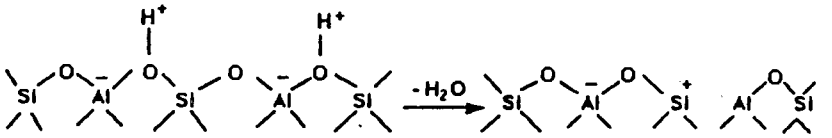

FIGURE 2.17: The formation of Lewis acid sites by dehydroxylation

However, Kühl [1973 and 1977] proposed that tri-coordinated aluminium would be removed from the crystal structure by the formation of oxyaluminium species. These AlO^+ or $Al_xO_y^{n+}$ clusters were termed the "true" Lewis sites, and are frequently formed when zeolites are dealuminated by acid or steam treatment [Scherzer, 1984; Karge and Dondur, 1990; Karge *et al.*, 1991; O'Donovan *et al.*, 1995].

2.1.3 ZEOLITE SYNTHESIS

Zeolites, with the possible exception of silicalites, are synthesized in an oxide system containing H_2O-SiO_2-Al_2O_3-(alkali, alkaline earth, organic cation) at temperatures below 200°C and at autothermal pressures [Sand, 1980]. The chemical sources which are needed in principle for zeolite synthesis are given in Table 2.2.

The silicon sources, such as colloidal silica, waterglass or fumed silica, might be different in terms of the degree of polymerization of the Si species. Zeolites are typically synthesized at a pH ranging from 8 - 12 [Jansen, 1991]. In these alkaline solutions, the most abundant forms of Si are monomeric and oligomeric Si species [Jansen, 1991], while the most abundant form of Al is monomeric $Al(OH)_4^-$ [Barrer, 1981 and 1989]. The mono- and oligomeric Si and monomeric Al species react to produce aluminosilicate structures [Feijen *et al.*,

1994]. Ageing of the gel or raising the temperature of the gel increases the depolymerization or dissolution of the Si species. This dissolution will increase the concentration of dissolved silica [Feijen *et al.*, 1994].

TABLE 2.2: Chemical sources and their function in zeolite synthesis [from Jansen, 1991]

Source	Function(s)
SiO_2	Primary building unit of framework
AlO_2^-	origin of framework charge
OH^-	Mineralizer, guest molecule
Alkali cation, template	Counterion of framework charge, guest molecule
H_2O	Solvent, guest molecule

The increase in concentration of solute will transform a stable solution into a metastable solution, and finally into a labile one, as shown by Figure 2.18 [Jacobs, 1992]. In the labile region nucleation as well as crystal growth are possible, in the metastable region only crystal growth is possible, whereas no nucleation or crystal growth can occur in the stable region. Hence the achievement of supersaturation by depolymerization of Si species is a requirement for nucleation in the labile region.

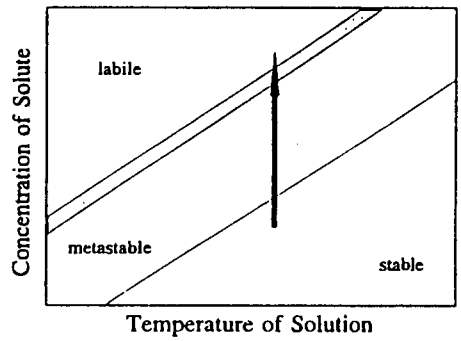

FIGURE 2.18: The solubility-supersolubility diagram [after Jacobs, 1992]

Primary nucleation from a supersaturated solution can be divided into homogeneous nucleation (spontaneous nucleation from clear solutions) and heterogeneous nucleation (induced by impurities, gel phase). Secondary nucleation is induced by the presence of seed crystals [Jacobs, 1992; Feijen *et al.*, 1994]. Heterogeneous nucleation occurs at the liquid-gel interface, and crystallization proceeds *into* the gel, whereas the driving force for crystallization is equal in all directions in homogeneous nucleation [Jansen *et al.*, 1989].

Nuclei will grow by addition or condensation of precursor species towards full-grown crystals. There is general agreement that zeolite crystal growth occurs in solution, specifically at the crystal plane-solution interface, probably by condensation of dissolved species onto the growing crystal surface [Feijen *et al.*, 1994]. Hence, as reacting species are being depleted, the system changes from a labile to a metastable and finally to a stable region. There are at least three types of crystal building units involved in crystal growth that have been proposed, viz. the primary building unit (the tetrahedral monomeric species), the secondary building units (resembling the SBU's of Meier and Olson described in section 2.1.1.2), and the cation templating theory [Jansen, 1991].

The chemical composition of a synthesis hydrogel influences the nucleation and crystal growth, nature of the crystalline material, the lattice aluminium content and distribution, the crystal size and morphology. These variables and their influence on catalyst characteristics are briefly discussed in Sections 2.1.3.1 - 2.1.3.3, as well as some effects that synthesis variables have on the synthesis of zeolites ZSM-5, Mordenite and Beta (Sections 2.1.3.4 - 2.1.3.6).

2.1.3.1 Temperature and Time

An increase in temperature will increase both nucleation and the crystal growth rate [Feijen *et al.*, 1994]. However, H_2O is required to fill the pores and thereby stabilize the porous structure. As a liquid phase is required for this, an upper temperature limit for zeolite formation is to be expected [Barrer, 1982]. Crystallinity normally increases with time, although according to Ostwald's rule of successive phase transformations the thermodynamically most stable phase will in time be formed [Barrer, 1982; Katovic *et al.*, 1989].

2.1.3.2 Alkalinity

The pH of alkaline synthesis solutions is usually between 8 and 12. The role of the OH^- anions is that of a mineralizing or mobilizing agent. The mineralizing agent brings the Si and Al species into solution at an adequate rate to create a supersaturated solution, such that nucleation and crystal growth can occur. In general, increasing the pH shortens the time required for formation of nuclei, and accelerates crystal growth [Barrer, 1981]. The Si/Al ratio tends to decrease with increasing pH, as Al incorporation is greater at higher pH [Barrer, 1981].

2.1.3.3 Templates (structure directing species)

In aqueous solutions, cations are known to influence the ordering of H_2O molecules. *Structure-making* cations such as Na^+ or Li^+ interact strongly with the H_2O molecules because of their high charge density, and the H_2O molecules are (re-)organised around the cations [Gilson, 1992]. Cations such as NH_4^+, K^+ and Rb^+ are *structure-breaking* cations because their interaction with the H_2O molecules is not strong enough to form organised H_2O clusters, thereby "breaking" the H_2O structure [Gilson, 1992]. The hydrophobic character of the alkyl chains of organic cations such as tetraalkylammonium ions may be responsible for the H_2O organizing effect near the alkyl chains, thereby stabilizing the H_2O network near the alkyl-chain containing cation. These organised H_2O molecules can be replaced by silicate and aluminate tetrahedra and in this way lead to the formation of zeolite crystal structures [Feijen *et al.*, 1994].

The H_2O molecule is an important templating species. Apart from its templating effect by interaction with cations, as discussed above, and its solvating and hydrolyzing ability, it enhances the formation of a zeolite structure during crystal growth by filling the pore system and thereby stabilizes the porous lattices [Barrer, 1982].

2.1.3.4 ZSM-5 synthesis

ZSM-5 can be synthesized with a wide Si/Al ratio, the siliceous analogue of ZSM-5 being Silicalite-I [Flanigen *et al.*, 1978; Fyfe *et al.*, 1983]. The synthesis of ZSM-5 usually takes place using the tetrapropylammonium (TPA^+) cation as organic template, although the synthesis of ZSM-5 in the presence of other amines, alcohols or in fact without organic template has been reported [Jacobs and Martens, 1987; Gilson, 1992]. It has been reported by Nagy *et al.* [1983] that the number of TPA^+ cations in ZSM-5 corresponded with number of channel intersections, suggesting that the TPA^+ cations act as structure directing templates located at the channel intersections.

Nucleation of ZSM-5 was found to be more rapid for structure-making alkali cations (Li^+, Na^+) than for structure-breaking alkali cations (K^+, Rb^+, Cs^+) [Gabelica *et al.*, 1983] and at higher pH values [Derouane and Gabelica, 1986; Szostak, 1989]. A high nucleation rate resulted in many smaller crystals, whereas fewer but larger crystals were formed at low nucleation rates.

It has been observed that the crystallization rate and crystallite size decreased for increased Al content in ZSM-5 synthesis [Van der Gaag *et al.*, 1985]. The incorporation of Al into the structure is disruptive, and thus the more Al present in the synthesis gel the more difficult it becomes to be incorporated into the structure. This then leads to the growth of smaller crystals. In ZSM-5, aluminium zoning may occur in the crystals [Suib *et al.*, 1980; Derouane *et al.*, 1981; Von Ballmoos and Meier, 1981; Hughes *et al.*, 1983; Chao and Chern, 1988]

2.1.3.5 Mordenite synthesis

The effect of varying the synthesis gel composition on the final crystalline product is illustrated for Mordenite in Figure 2.19. Early synthetic Mordenites had Si/Al ratios ranging between 4.5 and 5.5. The synthesis of more siliceous Mordenites was first reported by Whittemore [1972], with Si/Al ratios ranging between 6 and 10. No organic template is required for the synthesis of Mordenite [Itabashi *et al.*, 1986].

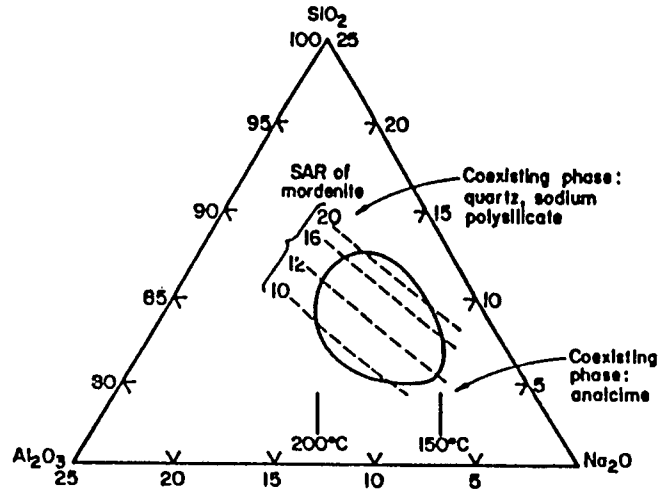

FIGURE 2.19: Composition diagram of synthesis gel composition and temperature required for the synthesis of siliceous Mordenite [from Itabashi *et al.*, 1986]

2.1.3.6 Beta synthesis

According to the patent by Wadlinger *et al.* [1967] the Si/Al ratio for zeolite Beta can be between 5 and 100. Recently, this lower limit was reached [Borade and Clearfield, 1996]. The composition of the synthesis gel for the formation of zeolite Beta is important. Tetraethoxysilane [Pérez-Pariente *et al.*, 1987, Eapen *et al.*, 1994], silica gel and sol [Eapen *et al.*, 1994] and fumed silica [Borade and Clearfield, 1996] have been used as silicon source. Sodium aluminate as aluminium source gave faster crystallization rates and increased yields when compared to aluminium sulphate and aluminium isopropoxide [Eapen *et al.*, 1994]. Camblor and Pérez-Pariente [1991] reported that no zeolite Beta could be obtained in the absence of alkali cations (Na^+, K^+). The tetraethyl ammonium cation (TEA^+) is the only organic cation with which zeolite Beta has been obtained [Eapen *et al.*, 1994].

2.1.4 SHAPE SELECTIVITY IN ZEOLITES

If the majority of the catalytic sites are confined in the channel structure and if the channels are small, the fate of the reactant molecules and the probability of forming product molecules are determined mostly by molecular dimension and configuration. Only molecules whose dimensions are less than a critical size can enter the channels, have access to internal catalytic sites, and react there. Furthermore, only molecules which can leave appear in the final product. Catalysts displaying such properties are said to be shape selective.

Csicsery [1979] distinguished between three types of shape selectivity. In *reactant shape selectivity* some of the molecules in a reactant mixture are too large to diffuse through the catalyst channels to reach active sites. In *product shape selectivity* only product molecules with sufficiently small dimensions can diffuse out of the channels and appear as products. In *restricted transition state shape selectivity* certain reactions are prevented because the corresponding transition state requires more space than is available in the cavities or channels of the catalyst. Reactant and product selectivities are mass transfer limited and are therefore affected by crystallite size, whereas transition state selectivity is not.

Choudhary and Akolekar [1989] suggested a shuttlecock-shuttlebox model for the sorbate-zeolite channel system to explain how the dimensions and configurations of molecules can influence the selectivity. Penetration of bulkier molecules into the zeolite channel is expected to take place only when the molecule enters the channel opening in an orientation in which its compression to the size of the channel is accomplished with relative ease. Otherwise its sorption is either totally rejected or expected to occur with a low probability, because of a much greater steric hindrance experienced by the molecule. Similarly, diffusion of the molecules in the channels is favoured in the direction in which the resistance to movement of the compressed group of the diffusing molecule is at a minimum, as shown in Figure 2.20.

Experimental observations corresponding both to Csiscery's classification of shape selective effects in zeolites and Choudhary and Akolekar's model have been reported by Haag *et al.* [1982], who compared the cracking of various

hydrocarbon compounds over small crystal and large crystal ZSM-5 by calculating the rate constant and effectiveness factor in each case.

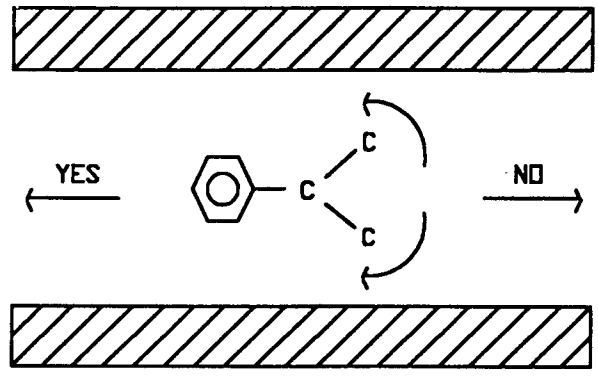

FIGURE 2.20: Diffusion limitations due to steric hindrance

An additional concept of secondary shape selectivity was introduced by Santilli and Zones [1990]. When, as in the above cases, shape selectivity is a result of direct interactions between molecules and a channel system, the term *primary* shape selectivity is applied. In zeolite catalysis, *secondary* shape selectivity occurs when one molecule interferes with the reactivity of another because of steric constraints imposed by the channels. Secondary shape selectivity is a phenomenon which does not happen in an unhindered environment. Santilli and Zones [1990] stated that it is likely that several types of secondary shape selectivity exist, such as reactant, product and transition state secondary shape selectivity, and that these could be caused by both reactants and products.

An extension of this type of shape selectivity is *inverse* shape selectivity [Santilli *et al.*, 1993]. Shape selectivity occurs when the repulsive forces between the zeolite and the reactants, transition states or products tend to favour the reaction, production or diffusion of sterically smaller molecules. Inverse shape selectivity occurs when attractive forces alter the catalytic and adsorptive selectivities of molecules. Hence sterically larger molecules may be adsorbed or converted preferentially because of greater attractive forces between the channel walls and the larger molecules [Santilli *et al.*, 1993].

Derouane [1986] suggested that molecular shape selective effects are not necessarily restricted to the intracrystalline volume of the zeolites, although that would clearly favour their occurrence. He suggested that molecular shape selectivity should occur whenever a catalyst selects or prefers specific reactants or products on the basis of their size and shape in order to match its own active site steric requirements. The external surface of zeolites offers channel openings and cut channels (*half cavities*) due to their framework structure. Derouane [1986] proposed that such hilly environments will facilitate the preferential selection and reaction of certain molecules, depending on their stereochemistry and their ability to optimize their Van der Waals interaction with the framework, or their capacity to "*nest*". Such external surface molecular shape selective effects are more likely to be observed for bulky molecules, small crystals and crystals with restricted access to their interior (coked or modified crystals).

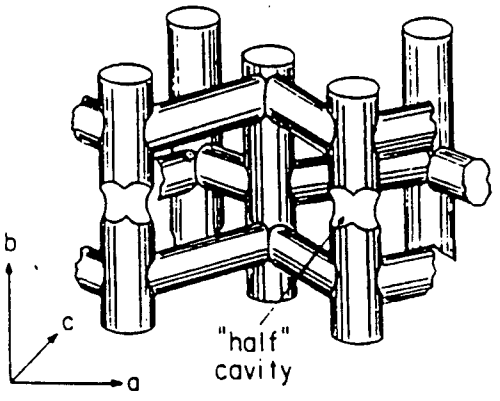

FIGURE 2.21: "Half" channel intersection cavities [Fraenkel *et al.*, 1984]

Experimental observations of the nesting effect on the external surface described by Derouane [1986] have been claimed by Fraenkel *et al.* [1984]. Fraenkel *et al.* [1984 and 1986] and Fraenkel and Levy [1989a and 1989b] further speculated that the external Brönsted acid sites were located in *"half"* channel intersection cavities. These "half" cavities were characterized by larger-than-10-ring openings (Figure 2.21). Fraenkel *et al.* [1984] proposed that

there were two types of catalytic sites on ZSM-5. The first type was located inside the crystal, corresponding to 100% *p*-selectivity in xylene production or isomerization. The other resided on the external surface of the zeolite, and was not shape-selective (i.e. it gave the thermodynamic equilibrium mixture). Any xylene product composition obtained over ZSM-5 would thus be analyzed as the sum of the two contributions: that of the selective and that of the unselective sites.

These findings have been disputed by Neuber and Weitkamp [1989] and Weitkamp *et al.* [1989], who suggested that the observed effects could be rationalized in terms of diffusional restrictions inside the channels rather than in terms of shape selective sieving effects on the external surface.

The effects of cation exchange and poisoning have been investigated by Choudhary and Akolekar [1991]. H.Na-ZSM-8 and H.Na-ZSM-5 showed an increase in shape selectivity for xylene isomerization and toluene disproportionation with increasing Na content due to an increase in the diffusional resistance with increasing Na exchange. Similarly, poisoning of these catalysts with pyridine resulted in an increase in shape selectivity for the above mentioned reactions, also due to increased diffusional resistances.

The internal surface of ZSM-5 certainly plays a major role in shape selective catalysis. The effect of the external surface is less certain. Larger molecules, either in the reaction or product mixtures, will have greater diffusional resistances inside the channels than smaller molecules. Therefore the acid sites on the external surface will play a greater role in the reaction of large molecules than molecules that readily diffuse through the channels. Therefore, even though the number of acid sites on the external surface is small compared to the total number of acid sites, these easily accessible and non-shape selective acid sites may provide a high turnover rate for non-shape selective reactions. This will be most noticeable for small crystallite sizes, as these crystals will have the largest ratio of external/internal surface area.

2.1.5 COKE FORMATION AND DEACTIVATION OF ZEOLITES

Deactivation of catalysts is of considerable importance in catalysis because many catalysts show a loss of activity with time. The loss in activity of zeolites may be caused by [Bhatia *et al.*, 1989-90]:

(i) The formation of coke, which will accumulate on the surface and/or block the channels,
(ii) The selective adsorption of undesirable agents, especially basic compounds, which poison the active sites,

All reactions of organic compounds on solid acid catalysts are accompanied by the formation of heavy by-products which form a hydrogen-deficient deposit, viz. coke, on the surface and result in deactivation. The deactivation rate depends on the relative rate of formation of these by-products, which can be very different from one catalytic system (catalyst + reaction + reaction conditions) to another [Magnoux *et al.*, 1987; Guisnet and Magnoux, 1989; Bhatia *et al.*, 1989-90]. The deactivation rate depends also on the mode of deactivation.

Rollmann [1977] suggested that coke formation was a shape selective reaction and that deactivation rates were intrinsic properties of the channel structure. Cyclo-paraffin pre-cursors, and hence coke, cannot readily form in the restrictive pore system of shape selective catalysts. Large pore catalysts offer little restriction to coke formation and deactivation becomes significant. Not all coke is formed in the intracrystalline pore system, but intracrystalline coke formation is a shape selective reaction directly controlled by the zeolite channel structure. Therefore not all zeolites have the same propensity to coke. Rollmann and Walsh [1979] further suggested that while catalyst composition and crystal size can influence coke formation, these are secondary effects.

The nature and the location of the coke and the modes of coke formation and deactivation have been studied widely [Rollmann, 1977; Magnoux *et al.*, 1987; Guisnet and Magnoux, 1989; Anderson *et al.*, 1989b; Karge, 1991]. This is briefly summarized in Sections 2.1.5.1 to 2.1.5.4.

2.1.5.1 The nature of the coke

Coke can be divided into two types [Guisnet and Magnoux, 1989; Karge, 1991], namely *soft* (or *soluble, non-graphitic*) coke and *hard* (or *insoluble, graphitic*) coke. Soft coke consists mainly of paraffinic, olefinic and polyolefinic species (H/C ratio > 1), whereas hard coke consists predominantly of alkylaromatics and polyaromatics (H/C ratio < 1). According to Guisnet and Magnoux [1989] soluble coke molecules are intermediates in the formation of insoluble coke. They concluded that insoluble coke was not formed at low coke content, and that the aromaticity of the soluble coke increased with the coke content.

Schulz *et al.* [1987] and Magnoux *et al.* [1987] reported that the coke found in the channels of HZSM-5 consisted mainly of alkylated 2-ring aromatics, although the exact nature of the coke may depend on the feed [Bhatia *et al.*, 1989-90]. In the case of HY bulky aromatic rings (more than 3 rings) were found in the supercages [Magnoux *et al.*, 1987; Bhatia *et al.*, 1989-90].

The coke on HZSM-5, H-OFF and USHY was studied by Gallezot *et al.* [1988] using TEM and EELS. The external coke formed on HZSM-5 and H-OFF gave EELS spectra not much different from that of coronene, indicating that the coke was made up of graphite-like polyaromatic molecules. The external coke formed on USHY consisted of linear polyaromatic filaments protruding from the channels.

2.1.5.2 The mode of coke formation

The coke formation on zeolites probably occurs through cracking of paraffins and olefins, oligomerization of the olefins, transformations through hydrogen transfer into monoaromatics, alkylation of these monoaromatics and cyclization and hydrogen transfer to polyaromatics [Guisnet and Magnoux, 1989].

Bülow *et al.* [1987] investigated the cracking of *n*-hexane and mesitylene on HZSM-5. Coke deposits formed from *n*-hexane cracking were distributed homogeneously throughout the crystal, while coke deposits formed from

mesitylene cracking were deposited on or near the external surface. Hence bulky molecules such as mesitylene promote coke formation on the external surface, while smaller molecules, at least initially, promote coke formation in the channels.

2.1.5.3 The location of coke

An important problem related to the coking of zeolites is the location of the coke deposits, namely in the channels, in the cavities or on the external surface. Most researchers believe that coke is initially formed in the channels of HZSM-5 and later on the external surface [Bibby *et al.*, 1986; Bülow *et al.*, 1987; Anderson *et al.*, 1989b for example]. Magnoux *et al.* [1987] also proposed that initial coke formation occurs in the channels and cavities of HM and HY before coke is formed on the external surface.

The amount of coke deposited on HZSM-5 before external coke was detected varied. Bibby *et al.* [1986] reported values of 14 - 18 wt% before the onset of external coke formation, whereas Behrsing *et al.* [1989] reported a value of 6 wt%. However, Anderson *et al.* [1989b] reported that migration of coke from the channels to the external surface occurred as the temperature was raised. Hence the amount of coke on the external surface may depend on the reaction and/or reaction conditions. This is in agreement with Bhatia *et al.* [1989-90].

Bibby *et al.* [1986] also stated that on HZSM-5 coke continued to form during thermal cracking reactions on the hot catalyst bed, even after complete deactivation. Furthermore, the amount of coke formed was found to be in excess of the pore volume, with ratios of external coke to internal coke ranging from 5 - 14 for different particle sizes. Anderson *et al.* [1989b] reported that deacidification of the external surface of HZSM-5 with $SiCl_4$ reduced the amount of aromatic residue held externally, especially at higher temperatures.

2.1.5.4 The mode of deactivation

Magnoux *et al.* [1987] investigated the deactivation modes of HM, HY and HZSM-5 during *n*-heptane cracking. Coke formation, initially very rapid on HM and HY, was very slow on HZSM-5. As mentioned in Section 2.1.5.3, coke is formed initially in the channels and cavities, and then on the external surface. The modes of deactivation are described below [Magnoux *et al.*, 1987].

(i) In the uni-dimensional pore structure of HM, deactivation is mainly due to pore blockage.

(ii) On HY small polyaromatics are initially formed on the strongest sites, until diffusion becomes slow and the bulky molecules block the entry to the cavities. Then the coke content increases at a slower rate as new coke molecules are formed, but also due to the growth of existing coke deposits, both in the channels and on the external surface.

(iii) For HZSM-5 deactivation is initially due to coverage of acid sites located at channel intersections by small (1 or 2 ring) aromatics. Later on, bulkier polyaromatics form extremely slowly on external acid sites or from acid sites located near the external surface, thereby blocking the channels.

2.2 THE INERTISATION OF THE EXTERNAL ACIDITY OF ZEOLITES

From Sections 2.1.4 and 2.1.5 it has become clear that the external surface of zeolites, especially in ZSM-5, can play a major role in non-shape selective reactions and in the coke induced deactivation of these zeolites. Bhatia *et al.* [1989-90] state that, "for shape selectivity to occur, essentially all the catalytic active sites must be in the interior of the pores". Koegler *et al.* [1997] have shown that the external surface of ZSM-5 crystals is not smooth, but that many protrusions occur on the external surface. The external surface area may thus form a significant part of the total surface area. Especially when diffusion limitations are significant, it may be necessary to poison or inactivate exterior sites so they do not contribute excessively to the reaction. Anderson *et al.* [1989b] state that "retained products may function as possible precursors to coke formation and deactivation of the catalyst. Deacidification of the external surface would reduce the amount of aromatic residue held externally."

There are several methods of altering the acidity of zeolites. This section discusses some of these methods, the main emphasis being placed on the methods which are most likely to eliminate selectively the external acidity with a minimum of change to the bulk of the zeolite and on methods which improve the shape selectivity.

2.2.1 CHEMICAL VAPOUR AND LIQUID DEPOSITION

The use of chemical vapour deposition (CVD) or chemical liquid deposition (CLD) to cover the external surface of zeolites with silicon alkoxides and other silicon based compounds has been investigated by several research groups. These silicon based compounds were chosen for their size and were not expected to enter the channels of the zeolite. Hence these compounds are deposited only on the external surface, where they can be decomposed to form a silica layer inertising the external surface of the zeolite.

The silicon based compounds that have been used include $Si(OCH_3)_4$ [for example Niwa *et al.*, 1984b], $Si(OC_2H_5)_4$ [for example Wang *et al.*, 1988; Das *et al.*, 1993], $Si(OC_4H_9)_4$ [Wang *et al.*, 1988], $Si(OCH_3)(CH_3)_3$, $Si(OCH_3)_2(CH_3)_2$,

$Si(OCH_3)_3(CH_3)$ and $Si(OCH_3)(C_3H_7)_3$ [Kim *et al.*, 1996], $Si(CH_3)_4$ [Niwa *et al.*, 1988a] or $((CH_3)_2SiO)_4$ (octamethylcyclotetrasiloxane) [Chamoumi *et al.*, 1994]. The most commonly used compounds in chemical vapour or liquid deposition are silicon alkoxides such as tetramethoxysilane ($Si(OCH_3)_4$ or TMOS) and tetraethoxysilane ($Si(OC_2H_5)_4$ or TEOS). The molecular diameters of TMOS and TEOS are 8.9 ± 0.2 Å [Niwa *et al.*, 1984b] and 9.6 Å [Yue *et al.*, 1997] respectively.

Chemical deposition methods have been used to deposit silicon compounds on the external surfaces of zeolites such as Mordenite [for example Niwa *et al.*, 1984a and 1984b; Gründling *et al.*, 1996], HZSM-5 [for example Wang *et al.*, 1988; Hibino *et al.*, 1991; Bhat *et al.*, 1996], Beta [Tsai and Wang, 1991], zeolite A [Niwa *et al.*, 1991 and 1994], zeolite Y [Yue *et al.*, 1997], Offretite [Chamoumi *et al.*, 1994], zeolite ZK-5 [Bergna *et al.*, 1989; Fetting and Dingerdissen, 1992] and zeolite Rho [Bergna *et al.*, 1989]. Furthermore, chemical vapour deposition has also been used to create Brönsted acidity by depositing silica on, for example, alumina [Sato *et al.*, 1991; Sheng and Gay, 1994] or titania and zirconia [Niwa *et al.*, 1992].

A similar modification has been reported by Richter *et al.* [1991], who used 12-tungstosilicic acid. They claimed that the Keggin unit $(SiW_{12}O_{40})^{4-}$ could not penetrate the ZSM-5 channel system but became deposited on the external surface. However, thermal decomposition of the acid yielded WO_3 at high loading accompanied by a loss of acid sites in the channel system. This was not exclusively caused by further dealumination but was partially attributed to site blocking by WO_3. Obviously, the decomposition of the acid involved mobile species of smaller sizes which were able to migrate into the interior of the zeolite.

2.2.1.1 Methods of deposition

Three methods of depositing silicon compounds have been employed, viz. (i) a static vacuum system [Niwa *et al.*, 1984a and 1986a], (ii) a vapour phase flow system [Wang *et al.*, 1988; Bhat *et al.*, 1994], and (iii) liquid phase deposition [Bergna *et al.*, 1989; Gründling *et al.*, 1996; Yue *et al.*, 1996]. The conditions used for the deposition have varied considerably.

In chemical liquid deposition the silicon alkoxide was typically deposited at ambient temperature in the presence of a diluent such as toluene or *n*-hexane. In a vapour phase flow system the silicon alkoxide was typically passed over the catalyst at elevated temperatures in the presence of combinations of toluene, methanol or water. Usually the silicon alkoxide was pure when using a static vacuum system, although sometimes the sample was exposed to water as well. Deposition temperatures ranged from ambient to 420°C. The following sections deal with the deposition mechanism and characterization more closely.

2.2.1.2 Deposition mechanism of silicon alkoxides

Niwa and co-workers have analyzed the deposition of silicon alkoxides on Mordenite [Niwa *et al.*, 1984a and 1988a] and HZSM-5 [Niwa *et al.*, 1986a]. A static vacuum system was used, and deposition temperatures ranged from ambient to 420°C [Niwa *et al.*, 1984a]. The amount of deposition was controlled by varying the catalyst mass, partial pressure of the silicon alkoxide and by repeating the deposition procedure. The weight gain was measured using a microbalance.

Niwa *et al.* [1988a] reported that during deposition of TMOS ($Si(OCH_3)_4$) at ambient temperatures, decomposition products (methanol, dimethyl ether) were adsorbed by Mordenite. These could subsequently be desorbed by raising the temperature. Indeed, when TMOS was deposited at 220°C methanol and dimethyl ether were detected by gas chromatography. At higher deposition temperatures, viz. 320°C, lower hydrocarbons such as ethylene and propane were observed, possibly due to methanol conversion on Mordenite. However, hydrocarbons with more than 4 carbon atoms were not observed.

The layer deposited on Mordenite was studied by I.R. spectroscopy [Niwa *et al.*, 1984a]. Deposition of TMOS at 200°C revealed the C-H stretching absorption at 2900 cm^{-1} as well as at 1600, 1480 and 1370 cm^{-1}. The band corresponding to the hydroxide of Mordenite at *ca.* 3600 cm^{-1} became broad upon deposition. The sample was then evacuated successively at 265, 315, 370 and 400°C. Evacuation at 265°C did not change the I.R. spectrum. At 315°C the C-H stretching vibration at 2900 cm^{-1} was removed, the 1480 cm^{-1} band diminished and the hydroxide band at 3600 cm^{-1} was restored. The

sample was finally exposed to oxygen at 400°C, which restored the I.R. spectrum to that of the original Mordenite sample, as calcination removed the absorptions at 1600 and 1370 cm^{-1}. Hence adsorbed residue formed during the deposition of TMOS was desorbed above ± 300°C, and irreversibly deposited carbonaceous material was removed only by calcination. Furthermore, Brönsted acid sites were not altered by the deposition of TMOS, although they were affected by the adsorbed organic molecules at relatively low temperatures.

When TMOS was deposited on SiO_2, the intensity of the isolated Si-OH group decreased, whereas a band at 1460 cm^{-1} strongly indicated the presence of a methoxy group on the sample. A broad band at 3400 cm^{-1} indicated the presence of adsorbed methanol [Niwa *et al.*, 1988a]. The methoxide bands were not removed completely by evacuation alone, and the intensity of the Si-OH was not recovered. However, all the methoxide bands disappeared upon reaction with water at 320°C.

Niwa *et al.* [1988a] employed various silanes, viz. $Si(OCH_3)_4$, $Si(OCH_3)(CH_3)_3$ and $Si(CH_3)_4$. $Si(OCH_3)_4$ was found to be the most reactive. Because $Si(CH_3)_4$ was physically adsorbed but not deposited on Mordenite, it was concluded that the methoxy group had to be present for successful deposition of the silane. Furthermore, it was found that $Si(OCH_3)_4$ was more reactive than $Si(OC_2H_5)_4$ [Niwa *et al.*, 1989]. Kim *et al.* [1996] investigated the use of $Si(OCH_3)(CH_3)_3$, $Si(OCH_3)_2(CH_3)_2$, $Si(OCH_3)_3(CH_3)$, $Si(OCH_3)_4$ and $Si(OCH_3)(C_3H_7)_3$. They concluded that $Si(OCH_3)(CH_3)_3$, $Si(OCH_3)_2(CH_3)_2$ and $Si(OCH_3)_3(CH_3)$ could enter the channels of HZSM-5 and inertise the internal acid sites, whereas $Si(OCH_3)_4$ and $Si(OCH_3)(C_3H_7)_3$ could not. As $Si(OCH_3)(C_3H_7)_3$ only has one methoxide group, Kim *et al.* [1996] proposed that it be stabilized as an isolated species. $Si(OCH_3)_4$ has four functional methoxide groups, and can be polymerized into a siloxane network structure (...-Si-O-Si-...), which can ultimately lead to effective control of the pore-opening size (Section 2.2.1.3).

Based on the above considerations, a reaction mechanism for the deposition of TMOS on zeolites, shown in Figure 2.22, was proposed by Niwa *et al.* [1988a]. First, the alkoxide reacts with the hydroxyl on the external surface to yield the anchored trimethoxide and methanol. Secondly, the trimethoxide is hydrolyzed, either by exposing the sample to water after the deposition or from water remaining in the zeolite system, thereby forming new hydroxyl groups. The newly formed hydroxyl groups react further with the gaseous alkoxide or the

vicinal trimethoxide. A polymeric silica layer consisting of siloxane bonds (...-Si-O-Si-...) is obtained. The final carbonaceous residue can be removed by calcination.

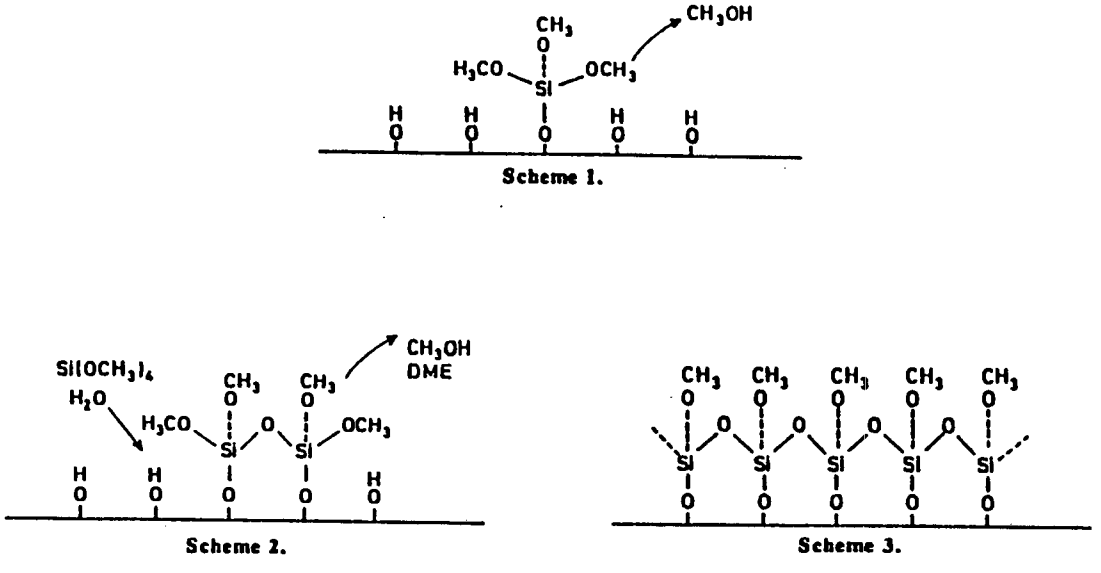

FIGURE 2.22: Reaction scheme for the Chemical Vapour Deposition of TMOS [Niwa *et al.*, 1988a]

2.2.1.3 Conservation of the internal zeolite structure and acidity

NH_3-TPD studies of HM [Niwa *et al.*, 1984a] and HZSM-5 [Niwa *et al.*, 1986a] indicated that neither the peak maximum temperature nor the amount of NH_3 desorbed changed for the samples modified by TMOS deposition in a static vacuum system. Bhat *et al.* [1995] reported no change in the NH_3-TPD spectrum or the amount of NH_3 desorbed from HZSM-5 when TEOS was deposited on the catalyst in a vapour phase flow system. Similar findings have been reported for NH_3-TPD studies of HZSM-5 where TEOS was used in liquid phase to modify the catalyst [Cejka *et al.*, 1996; Yue *et al.*, 1996].

Both the H_2O (2.65 Å) and N_2 (3.64 Å) adsorption capacities and adsorption rates of TMOS modified Mordenite and HZSM-5 samples remained unchanged from the respective parent samples [Niwa *et al.*, 1984a and 1986a; Hibino *et*

al., 1991]. However, for larger molecules such as *p*-xylene (5.85 Å) and *o*-xylene (6.8 Å) the adsorption rates decreased significantly for TMOS modified samples with increasing amounts of deposition, although the equilibrium adsorption capacities were not altered. Niwa *et al.* [1984b] also reported that the rates of hexane, 2-methyl pentane and 2,2-dimethyl butane sorption on modified Mordenite were suppressed by increasing amounts of TMOS deposition, especially for the branched molecules. Adsorption experiments carried out by Yue *et al.* [1996 and 1997] on ZSM-5 samples modified by TEOS in liquid phase showed that the adsorption capacities of larger molecules decreased while the adsorption capacities of smaller molecules were not affected by the deposition, suggesting that some pore blocking had occurred.

The NH_3-TPD and adsorption capacity studies showed that the internal zeolite structure and acidity were conserved (i.e. TMOS and TEOS deposition did not affect the internal volume and acid sites of the zeolites), but the decrease in adsorption rates implied that the channel openings were narrowed by the deposition of the silicon alkoxide. Presumably, pore mouth narrowing ultimately leads to pore blocking. However, it has been shown by Niwa *et al.* [1994] that lower olefins (C_2H_4, C_3H_6, and 1-C_4H_8) can be separated by controlling the pore-opening size of TMOS modified zeolite A, and that oxygen and nitrogen can be separated by controlling the pore-opening size of TMOS modified zeolite A [Niwa *et al.*, 1991].

XPS showed an increase in the silicon content of the surface layer of Mordenite samples modified with TMOS in a static vacuum system [Niwa *et al.*, 1984a], and of HZSM-5 samples modified with TEOS in liquid phase [Yue *et al.*, 1996]. This confirmed that the silicon alkoxides were not deposited uniformly in the zeolite bulk, but that the external surface was enriched in silicon.

2.2.1.4 Control of the pore-opening size

Niwa *et al.* [1984b and 1986a] have calculated the number of layers of silica that were formed on the external surface from the weight gain, assuming that the deposited silica formed a layer structure. The number of layers required to obtain shape-selectively improved HZSM-5 was about four to six layers [Niwa *et al.*, 1986a], but only one to three layers were required for Mordenite [Niwa *et al.*, 1984b and 1986a]. Furthermore, Hibino *et al.* [1993] have shown that

the acidity became weaker with each layer, and that approximately four silica layers were required to eliminate the conversion of 1,3,5-triisopropyl benzene over both Mordenite and HZSM-5.

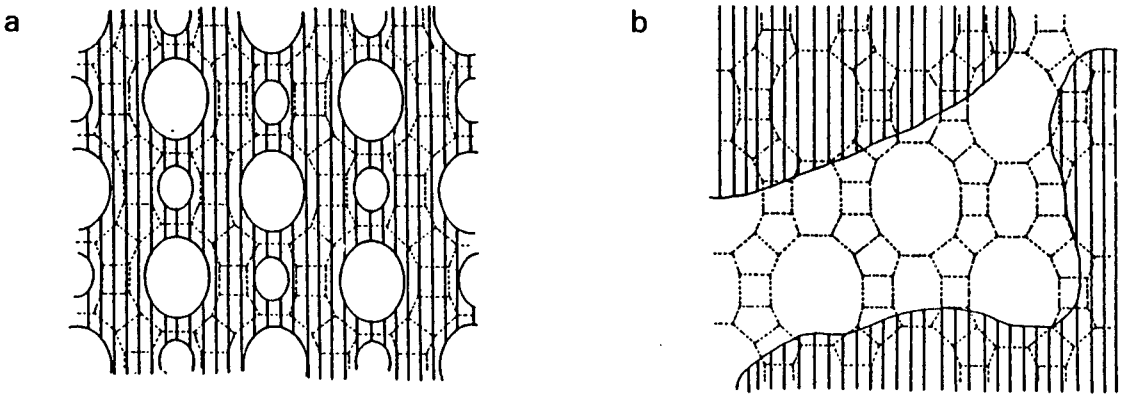

FIGURE 2.23: Schematic for the control of pore-opening size by GeO_2 : (a) before, and (b) after deterioration of the GeO_2 layer [Hibino *et al.*, 1989]

In order to obtain a better understanding of the deposited layer and its control of pore-opening size, germanium alkoxides have been used to form a GeO_2 layer on the external surface of Mordenite, as it is possible to distinguish between the deposited GeO_2 layer and the zeolite [Niwa *et al.*, 1986b; Hibino *et al.*, 1989]. Spectroscopic techniques such as EXAFS, XPS and TEM could thus be used to analyze the structure of the deposited GeO_2 layer. $Ge(OCH_3)_4$ was said to be more reactive than $Si(OCH_3)_4$, because Niwa *et al.* [1986b] reported that the deposition temperature had to be lowered from 320°C for $Si(OCH_3)_4$ to 60 - 150°C for $Ge(OCH_3)_4$ to obtain a uniformly controlled pore-opening size. The uniformity of the pore-opening size was based on sorption profiles of molecules such as water, *n*-hexane and *p*-xylene. However, when the GeO_2 layer was exposed to water and subsequently heated to 500°C, a deterioration in the shape-selective properties of Mordenite was observed. EXAFS and TEM

measurements revealed that the deposited GeO_2 crystallized and grew into particles on the external surfaces of Mordenite, as shown in Figure 2.23 [Hibino *et al.*, 1989]. This did not occur for samples stored under dry conditions.

Hence the GeO_2 had to deposit as an ultra-thin layer to improve the shape selectivity effectively by pore mouth narrowing. Since the pore mouth narrowing observed by the deposition of silicon alkoxides was analogous to that of germanium alkoxide, the structure of the deposited silica may also be an ultrathin layer [Hibino *et al.*, 1989]. However, as the tetrahedral germanium unit is soluble in water, the deposited GeO_2 layer may be unstable when exposed to water. This may have caused a deterioration in the shape-selective properties. Whether a similar deterioration can occur for a SiO_2 layer is unclear.

2.2.1.5 Factors influencing the deposition

To obtain different amounts of silica on the external surfaces, various parameters have been altered for the different methods of deposition. Using a static vacuum system, Niwa *et al.* [1984a and 1986a] varied the deposition amount, measured by an *in situ* microbalance, by changing the sample size or the partial pressure of the silicon alkoxide. To obtain highly deposited samples, the deposition was repeated up to 7 times after the evacuation of the gas phase [Niwa *et al.*, 1986a]. The deposition temperature or the time period for which the silicon alkoxide mixture was exposed to the catalyst in a vapour phase flow system was typically varied to change the amount of deposition on the sample [Tsai and Wang, 1991; Bhat *et al.*, 1995]. In liquid phase deposition, the concentration of the silicon alkoxide mixture was typically varied [Bergna *et al.*, 1989; Yue *et al.*, 1996].

By varying the temperature to obtain 50% TEOS conversion over HZSM-5, SiO_2-Al_2O_3, γ-Al_2O_3 and kieselguhr in a vapour phase flow system, Wang *et al.* [1988] concluded that the rate of TEOS decomposition strongly depended on the strength of the acid sites. Hibino *et al.* [1993] reported that Mordenite samples with Si/Al ratios of 9.9, 19.9 and 36.8 required similar amounts of TMOS deposition to reduce the conversion of 1,3,5-triisopropyl benzene, used as a measure of the external surface acidity, by the same degree. I.R. work showed that the alkoxide reacted with the terminal silanol (Si-OH) groups

(Section 2.2.1.2.). As the external surface acidic hydroxide (Al-OH) groups were inertised for the conversion of 1,3,5-triisopropyl benzene, Hibino *et al.* [1993] concluded that the alkoxide also reacted with the external surface acidic hydroxyl groups. Because the Si/Al ratio had no effect on the degree of inertisation of the Mordenite samples, Hibino *et al.* [1993] proposed that the alkoxide reacted equivalently with both terminal silanol and acidic hydroxyl groups, contrary to the conclusions of Wang *et al.* [1988].

However, the pore-opening size was dependent on the Si/Al ratio [Hibino *et al.*, 1993]. The pore-opening size of highly siliceous Mordenite was not readily narrowed. The silica layer consists of Si-O-Si bonds, whereas the zeolite contains both Si-O-Si and Si-O-Al bonds, resulting in different bond lengths or bond angles between the silica layer and the zeolite, which become larger as the aluminium content of the zeolite increases. Hibino *et al.* [1993] proposed that the Si-O-Si bond of the silica layer protruded into the pore, narrowing the pore-opening size to a greater extent for zeolites with a low Si/Al ratio than for siliceous zeolites (Figure 2.24). This may explain why the shape-selectivity of a relatively aluminium-rich Mordenite was improved with the deposition of one to three layers of silica, whereas four to six layers were required for a relatively siliceous HZSM-5 [Niwa *et al.*, 1986a].

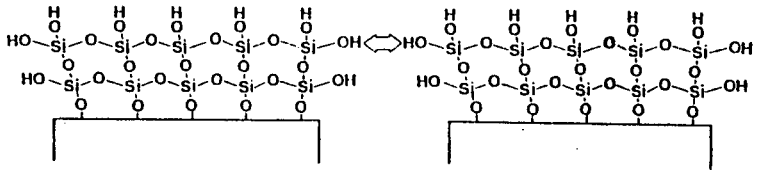

Scheme 1

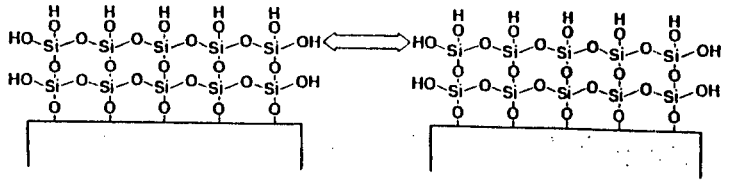

Scheme 2

FIGURE 2.24: Schematic illustration of the narrowing of pore-opening sizes by silica layers on low Si/Al ratio zeolites (Scheme 1) and high Si/Al ratio zeolites (Scheme 2) [Hibino *et al.*, 1993]

Comparing HZSM-5 samples with varying morphologies and crystal sizes, Wang *et al.* [1988] and Bhat *et al.* [1996] showed that crystallites with greater specific external surfaces (e.g. small or rough crystals) required greater amounts of silica deposition than crystallites with relatively smaller specific external surfaces (e.g. large or regular crystals). In addition, it has been reported that when extra-framework aluminium species existed on the external surface of HZSM-5, the amount of silica deposition required to inertise the external surface increased [Hibino *et al.*, 1991 and 1993; Bhat *et al.*, 1996].

Hibino *et al.* [1993] reported that the degree of inertisation of the external surface of Mordenite did not depend on the included cation, viz. Na^+ or H^+. However, because the concentration of acidic surface hydroxyls was lower on NaZSM-5 than on HZSM-5, Yue *et al.* [1996] reported that in their liquid phase work a more concentrated solution was required to obtain the same pore controlling effect for NaZSM-5 than for HZSM-5.

2.2.1.6 Reaction studies

It has been shown in the previous sections that the characterization studies indicated that the external surfaces of the catalysts were inertised effectively by the silica deposition, and that controlling the extent of pore-mouth narrowing is possible. Both these phenomena may lead to better selectivities, either by preventing non-shape selective reactions on the external surface or by controlling the reactant or product shape selectivity of the catalyst.

(i) Inertisation of the external surface

To determine the activity of the external surface of HZSM-5 and Mordenite, cracking of 1,3,5-triisopropyl benzene (TiPB) was carried out at 300°C by Hibino *et al.* [1991 and 1993]. TiPB (8.5 Å) is much larger than the pore size of HZSM-5 (5.4 - 5.6 Å) and the cracking of this molecule takes place only on the external surface [Namba *et al.*, 1986]. Similarly, Hibino *et al.* [1993] showed that TiPB was not able to enter the channels of Mordenite (6.7 - 7.0 Å). Hibino *et al.* [1991 and 1993] observed that the conversion of TiPB could be decreased from 14% for HZSM-5 and from 18% for Mordenite to near zero on the respective silica modified catalysts, depending on the amount of silica

deposition. Cejka *et al.* [1996] reported a decrease in TiPB conversion from 84% for the parent HZSM-5 to 2% for TEOS modified ZSM-5. Kim *et al.* [1996] showed that the amount of silica deposition required to completely inertise the external surface of HZSM-5 for the conversion of TiPB was dependent on the type of silicon alkoxide, the better being TEOS.

Therefore the TiPB probe reaction confirmed that the external surface was inertised by chemical deposition methods. In addition, the cracking of C_8-paraffins on Mordenite showed that the cracking of octane remained unaffected, whereas 2,2,4-trimethyl pentane was unreactive on modified samples [Niwa *et al.*, 1984b]. Hence the inertisation of the external surface acid sites by the silica deposition did not affect the internal acid sites.

(ii) Activity and selectivity of the modified samples

Chemical vapour and liquid deposition methods have frequently been used to improve *p*-selectivities for several reactions. These studies have included the isomerization of *o*-xylene [Hibino *et al.*, 1991], the disproportionation of toluene [Hibino *et al.*, 1991], the alkylation of toluene and ethylbenzene with methanol or ethylene on ZSM-5 [Wang *et al.*, 1988 and 1989; Hibino *et al.*, 1991; Das *et al.*, 1993; Bhat *et al.*, 1994 and 1995; Mirth *et al.*, 1994; Cejka *et al.*, 1996], as well as toluene isopropylation [Parikh *et al.*, 1992] and cumene disproportionation [Tsai and Wang, 1991] over zeolite Beta.

Hibino *et al.* [1991] reported that the fraction of the *p*-isomer in the xylene fractions for toluene disproportionation, alkylation of toluene with methanol and *o*-xylene isomerization all reached 98% using ZSM-5 samples with 13.3 wt% silica deposition. Wang *et al.* [1988 and 1989] and Das *et al.* [1993] also reported that *p*-selectivities greater than 98% were attainable for the ethylation of toluene and ethylbenzene on silica modified ZSM-5. However, the modification may result in decreased conversions when modified samples are compared to the parent sample [Wang *et al.*, 1988; Hibino *et al.*, 1991; Das *et al.*, 1993]. Hibino *et al.* [1991] and Kim *et al.* [1996] reported that the increase in *p*-selectivity was caused mainly by the narrowing of the pore-opening rather than by the inertisation of the acid sites on the external surface.

Similarly, the selective synthesis of dimethylamine (DMA) has been looked at over silica modified zeolites ZK-5 [Bergna *et al.*, 1989; Fetting and Dingerdissen, 1992], Rho [Bergna *et al.*, 1989] and Mordenite [Gründling *et al.*, 1996]. The activities of Rho [Bergna *et al.*, 1989] and Mordenite [Gründling *et al.*, 1996] were not significantly altered, whereas the activity of ZK-5 was greatly reduced [Bergna *et al.*, 1989]. Gründling *et al.* [1996] concluded that the increase in selectivity towards the smaller mono- and dimethylamine on silica modified Mordenite was as a result of pore mouth narrowing, which reduced the diffusion rate of the larger trimethylamine. Hence only MMA and DMA could diffuse out of the Mordenite pores with reasonable rates.

Methanol conversion on silica modified HZSM-5 [Niwa *et al.*, 1986a] and silica modified Mordenite [Sawa *et al.*, 1990a] showed a decrease in large (aromatic) molecules and a corresponding increase in that of small olefins. Details of the aromatic product distribution revealed a remarkable change towards the smaller isomers with increasing deposition, indicating greatly enhanced shape selectivity due mainly to pore narrowing but also due to inertisation of the external surface. The lifetime of silica modified ZSM-5 was not significantly altered by the deposition [Niwa *et al.*, 1986a], although the silica deposition caused a rapid loss of activity in dealuminated Mordenite [Sawa *et al.*, 1990a].

(iii) The adsorbed species during reaction

The adsorbed species during reaction work on silica modified catalysts have been analyzed using I.R. techniques. Mirth *et al.* [1994] reported that the narrowing of the pore-opening resulted in decreased diffusion rates of larger molecules. Hence in the alkylation of toluene with methanol or ethylene, it was found that the concentration of the adsorbed reaction products, such as *o*- and *m*-isomers or trimethyl benzenes, increased for modified samples because these bulky molecules became trapped in the channels [Mirth *et al.*, 1994; Cejka *et al.*, 1996]. Furthermore, isomerization of the trapped *o*- and *m*-isomers to the *p*-isomer resulted in a high *p*-selectivity. However, it was noted that the molecules trapped in the channels due to their low diffusion rates blocked the acid sites, resulting in a decrease in activity. Similar results have been obtained by Gründling *et al.* [1996] for the selective synthesis of dimethylamine over Mordenite.

2.2.2 SILICALITE SHELLS

A US patent by Rollmann [1980] reported on the Silicalite-i coating of ZSM-5 by reintroduction of the ZSM-5 crystals into an aluminium-free synthesis mixture. This was said to yield ZSM-5 crystals with an Al-rich core and an Al-free shell with an isostructural configuration. Handreck and Smith [1990] investigated this method of coating the external surface and concluded that this method did not restrict access to the channels of the zeolite. However, the possible presence, in the final product, of acidic amorphous silica that has the potential to catalyze reactions in a non-shape selective manner may place a limit on the overall effectiveness of this method.

Barrer [1982] noted that when seed crystals are used not all crystal surfaces grow at the same rate, and that flawed surfaces grow more rapidly than corresponding surfaces without flaws. Warzywoda *et al.* [1991], however, investigated seeding Al-free ZSM-5 crystallizations with Al-free crystals to study the role of the seed crystal in promoting the synthesis of a subsequent batch. They noted that very little growth was observed, but that new populations were observed to form both around the seeds and on the seed surface. Jacobs and Martens [1987] note that for successful seeding the template-to-silica ratio should be kept low when large amounts of seeds are used.

Lee *et al.* [1993] reported that the inactivation of the acid sites on the external surface by coating the crystals with a Silicalite shell increased the *p*-selectivity in toluene alkylation, without narrowing of the channels. In this case Na-ZSM-5 crystals were used as seeds. XRD patterns of coated crystals showed reduced intensities of the peaks near 2θ values of 7.9° and 23.1°. Crystal sizes could not be compared quantitatively by SEM pictures only, as a catalyst with a shell-to-core weight ratio of 1:1 was only expected to be 1.26 times larger than the seed. NH_3-TPD spectra showed decreased peak intensities and the peak maximum temperatures were also lower for the coated samples. Both these observations were probably due to the reduction in the number of acid sites per unit weight of catalyst, because the modified catalysts consisted of both ZSM-5 and Silicalite-I phases.

The conversion of 1,2,4-trimethyl benzene was used to probe the effects of inertisation of the external surface of HZSM-5 with Silicalite shells by Röger *et al.* [1997]. It was shown that the isomerization products reflected changes in

external activity, while the disproportionation products and 1,2,4,5- and 1,2,3,5-tetramethyl benzene indicated changes in overall activity and selectivity. Furthermore, cracking of 1,3,5-triisopropyl benzene, which can only occur on the external surface of HZSM-5, decreased from 90% on HZSM-5 to 10% on HZSM-5 coated with Silicalite-I, suggesting that few acid sites on the external surface remained after modification. However, the conversion for *n*-hexane cracking decreased from 25% on HZSM-5 to 12% on the modified HZSM-5, even though the number of aluminium atoms was kept the same in both samples.

The coating of SAPO-11 with an $AlPO_4$-11 shell has been reported by Matsuda *et al.* [1996]. The modified catalyst was less active for the alkylation of biphenyl with propene, but exhibited a higher 4,4'-diisopropylbiphenyl selectivity (> 80% sel.) than the parent SAPO-11 catalyst (70% sel.), due to the inertisation of the external acid sites.

2.2.3 HYDROTHERMAL TREATMENT

The activity of HZSM-5 can be increased by mild steaming treatments [Nayak and Choudhary, 1984; Zholobenko *et al.*, 1990; Andersen, 1991]. Nayak and Choudhary [1984] and Lago *et al.* [1986] reported a decrease in total acidity for steamed HZSM-5 from TPD-studies, due to the dealumination of the catalyst and the formation of extra-framework aluminium species. O'Donovan *et al.* [1995] reported that for H-Mordenite 45% or more of the framework aluminium was removed by mild or severe steaming, although the aluminium remained in the zeolite bulk in the form of extra-framework aluminium. Parikh *et al.* [1994] have reported an increase in Si/Al ratio from 30 for zeolite Beta to 50 for steamed zeolite Beta. XPS studies showed an increase in the concentration of aluminium on the surface of HZSM-5 [Nayak and Choudhary, 1984] and zeolite Beta [Corma *et al.*, 1996], thought to be due to the formation of extra-framework aluminium located on the zeolite surface. Enrichment of the surface with aluminium has also been found for zeolite Y by Akporiaye *et al.* [1986]. Furthermore, steaming caused the formation of mesopores [Szostak, 1991]. Therefore hydrothermal treatment is not suitable for the selective dealumination of the external surface of zeolites.

2.2.4 LEACHING METHODS

Acid leaching with HCl or HNO_3 is a dealumination method which is often used in conjunction with other methods, such as steaming. Extra-framework aluminium species may be removed from zeolites using this method [Scherzer, 1984]. Niwa *et al.* [1988b] reported that the aluminium concentration in HM decreased generally with temperature and time of HCl leaching, and with HCl concentration. Sawa *et al.* [1989] showed a decrease in bulk aluminium concentration from 1.87 mmol/g for HM to ± 0.40 mmol/g for acid leached HM, but XPS measurements showed a higher aluminium concentration in the external layer than in the bulk. This was later attributed to extra-framework aluminium species formed upon dealumination that were located near the surface [Sawa *et al.*, 1992]. Corma *et al.* [1996] used a combination of HCl leaching and $(NH_4)_2SiF_6$ treatment to dealuminate zeolite Beta. The bulk Si/Al ratio increased from 12.8 to 39.5 on treatment, leaving the catalyst almost free of extra-framework aluminium. Similar observations were made by Maache *et al.* [1993] by HCl leaching of zeolite Beta. Steaming followed by acid leaching tended to leave HZSM-5 and HM with an aluminium deficient surface, but left HY with a near uniform aluminium distribution [Szostak, 1991]. However, according to Anderson *et al.* [1989a] and Handreck and Smith [1990] acid leaching was not suitable for selective external surface dealumination of HZSM-5.

The use of H_4-EDTA to dealuminate zeolite Y was first reported by Kerr [1968a and 1968b]. This method resulted in aluminium deficient surfaces [Dwyer *et al.*, 1981], but also in the formation of mesopores [Akporiaye *et al.*, 1986; Szostak, 1991]. However, bulk dealumination, at least for large pore zeolites such as zeolite Y, did occur. In fact, the rate at which H_4-EDTA solution was added to the zeolite was found to be important for zeolite integrity. Kerr [1968a] and Datka *et al.* [1993] showed that when H_4-EDTA was added to zeolite Y relatively quickly, framework vacancies were created by aluminium expulsion which were not healed by silicon from other parts of the framework. Slow addition of H_4-EDTA did not decrease zeolite Y crystallinities [Kerr, 1968a].

Recently, dicarboxylic acids such as oxalic acid have been used to dealuminate zeolite Beta [Apelian *et al.*, 1996]. Bulk aluminium measurements showed that oxalic acid treatment had reduced the Al content by 90%. It was also found

that oxalic acid chelates with aluminium, thereby removing extra-framework aluminium from zeolite Beta. Apelian *et al.* [1996] stated that a limited degree of dealumination with oxalic acid was observed for zeolites with channel openings less than 6.4 Å, such as ZSM-5. Furthermore, a patent by Apelian *et al.* [1993] describes a process for the selective surface dealumination of organic-containing zeolites using dicarboxylic acids. The organic compound may be a structure directing agent used in the zeolite synthesis or introduced in the pores of the zeolite after thermal treatment. The treatment resulted in a reduction in surface acidity without a significant reduction in overall activity.

2.2.5 CHEMICAL TREATMENT

Beyer and Belenykaja [1980] were the first to report on the bulk dealumination of zeolites using $SiCl_4$. They were able to increase the Si/Al ratio of NaY from 2.5 to 50 without the destruction of the zeolite structure, using temperatures ranging from 457 - 557°C. It is believed that Al atoms were replaced by Si atoms according to the following reaction:

$$M_{1/n}\,[AlO_2.(SiO_2)_x] \;+\; SiCl_4 \;\text{--->}\; 1/n\;MCl_n \;+\; AlCl_3 \;+\; [(SiO_2)_{x+1}]$$

where M is the charge balancing cation (in this case Na).

Martens *et al.* [1990] showed this was in fact a 2-step reaction. Beyer and Belenykaja [1980] noted that $AlCl_3$ and NaCl species blocked the channels, but these could be removed by acid leaching.

Namba *et al.* [1986] investigated the dealumination of Na-ZSM-5 using $SiCl_4$. They noted that the structure was not destroyed and that the external acid sites were removed more selectively than the internal acid sites. Furthermore, the rate of 1,3,5-triisopropyl benzene (too large to enter the channels) cracking was found to be lower on $SiCl_4$ dealuminated HZSM-5 than on the parent HZSM-5. $SiCl_4$ dealumination also improved the shape selective alkylation of 1,2,4-trimethyl benzene with methanol. Cracking of cumene resulted in less coke formation on $SiCl_4$ dealuminated HZSM-5.

It was shown by Anderson *et al.* [1989a] that the lowest temperature, time and $SiCl_4$ partial pressure in their studies (600°C, 1 min, 1.04 kPa respectively) resulted in the best external surface dealumination for HZSM-5. However, they noted that for large extents of external surface dealumination, bulk dealumination will take place. On the other hand, for minimal bulk dealumination, external surface dealumination will be incomplete. These findings have also been confirmed by Handreck and Smith [1990], who reported that dealumination using $SiCl_4$, followed by acid leaching, did not remove aluminium selectively from the external surface.

$(NH_4)_2SiF_6$ has been used to dealuminate zeolite Y [Skeels and Breck, 1984; Akporiaye *et al.*, 1986; Neuber *et al.*, 1988]. At least for zeolite Y, this method did not dealuminate the external zeolite surface preferentially, but in fact produced the most homogeneous aluminium dispersion [Szostak, 1991] when compared to H_4-EDTA and steam dealumination. The use of $(NH_4)_2SiF_6$ did not result in the formation of mesopores [Akporiaye *et al.*, 1986]. Liu and Xu [1989] claimed that the use of NH_4BF_4 gave a more crystalline product compared to $(NH_4)_2SiF_6$, and that this was achieved without boron insertion into the framework of zeolite Y.

Das *et al.* [1996] reported that the Si/Al ratio for zeolite Beta increased from 30 to 97, 109 and 123 for repeated cycles of dealumination using $(NH_4)_2SiF_6$. A combination of steaming and $(NH_4)_2SiF_6$ treatment resulted in an increase in the Si/Al ratio from 30 for zeolite Beta to 98 for the modified zeolite Beta [Parikh *et al.*, 1994]. This would suggest that for zeolite Beta bulk dealumination occurred. Silva *et al.* [1996] reported that dealumination of Mordenite using $(NH_4)_2SiF_6$ removed aluminium from the external surface more extensively than from the bulk, because extra-framework aluminium (EFAl) was deposited in the channels, thus preventing diffusion of EFAl species out of the channels. The maximum percentage of dealumination of the zeolite framework was found to be 12%, whereas the maximum dealumination of the external surface was found to be about 40%. Hence for large pore zeolites, $(NH_4)_2SiF_6$ and $SiCl_4$ treatment cannot be used to dealuminate the external surface only.

2.3 TEMPERATURE PROGRAMMED DESORPTION

The temperature programmed desorption technique involves the desorption of a probe, previously adsorbed under controlled conditions, from a catalyst into an inert carrier gas, by raising the temperature of the catalyst linearly and measuring the amount of probe desorbed using a suitable detector. Numerous catalysts have been investigated using this method, such as alumina [Amenomiya and Cvetanovic, 1963a; Amenomiya and Cvetanovic, 1963b; Amenomiya and Cvetanovic, 1963c; Amenomiya *et al.*, 1964], silica-alumina [Amenomiya and Cvetanovic, 1970; Schwarz *et al.*, 1978], zeolite X [Kiskinova *et al.*, 1981], Mordenite [Kapustin *et al.*, 1988; Karge and Dondur, 1990], zeolite Beta [Hegde *et al.*, 1989] and ZSM-5 [Topsoe *et al.*, 1981; Hidalgo *et al.*, 1984; Kofke *et al.*, 1988]. The probes which have been used include ammonia [Amenomiya *et al.*, 1964; Post and Van Hooff, 1984; Iwamoto *et al.*, 1986], pyridine [Schwarz *et al.*, 1978; Topsoe *et al.*, 1981; Parrillo *et al.*, 1990], alkenes [Amenomiya and Cvetanovic, 1963a; Kofke and Gorte, 1989], alcohols [Kofke *et al.*, 1988; Kofke *et al.*, 1989] and other amines [Post and Van Hooff, 1984; Parrillo *et al.*, 1990; Pope, 1990]. The detectors used have included infrared [Topsoe *et al.*, 1981; Parrillo *et al.*, 1990], flame ionization [Nayak and Choudhary, 1983] and thermal conductivity [Amenomiya and Cvetanovic. 1963a] detectors, and mass spectrometers [Schwarz *et al.*, 1978; Kofke *et al.*, 1988; Karge and Dondur, 1990; Parrillo *et al.*, 1990].

The desorption spectrum is a plot of desorption rate versus temperature, and consists of one or more peaks which identify specific sites on the catalyst surface. Using suitably calibrated thermal conductivity detectors, flame ionization detectors, mass spectrometers or titration methods, the amount of desorbed material can be determined and, in the case of bases desorbed from acid catalysts, this can be related to the number of acid sites on the catalyst surface. In principle, a distribution of acid site strength with respect to temperature can be obtained. Desorption activation energies can also be obtained [Cvetanovic and Amenomiya, 1972], but valid interpretation of the data is essential.

The peak shape and the position of the peak maximum have been investigated thoroughly, and were found to be functions of readsorption of the probe molecule onto the channel walls [Cvetanovic and Amenomiya, 1967; Gorte,

1982; Rieck and Bell, 1984], diffusion [Jones and Griffin, 1983; Gorte, 1982], particle size [Tronconi and Forzatti, 1985], bed depth [Rieck and Bell, 1984], carrier gas flowrate [Rieck and Bell, 1984], surface heterogeneity [Amenomiya and Cvetanovic, 1963c] and surface coverage [Schwarz *et al.*, 1978; Kiskinova *et al.*, 1981]. The activation energy for desorption can be calculated by using different heating rates, assuming first order desorption and that large pore diffusional effects are absent [Cvetanovic and Amenomiya, 1972]. Usually, the rate limiting step in porous catalysts is the diffusion of the probe out of the catalyst (where readsorption may play a role) [Gorte, 1982; Jones and Griffin, 1983; Demmin and Gorte, 1984; Forni *et al.*, 1992 and 1995]. Gorte [1982] and Demmin and Gorte [1984] have proposed a set of design parameters, in the form of dimensionless groups, by which it is possible to carry out TPD experiments under conditions which will ensure sound data interpretation.

2.3.1 TEMPERATURE PROGRAMMED DESORPTION THEORY

A mathematical model of temperature programmed desorption has been described by Cvetanovic and Amenomiya [1967 and 1972]. They assumed a linear heating rate, first order desorption kinetics, an energetically homogeneous surface and no diffusional or readsorption effects. The following expressions were derived:

$$(k_d)_m = A \exp(-E_d/RT_{max}) = \beta E_d/RT_{max}^2 \qquad (2.1)$$

where,

$(k_d)_m$ = desorption rate constant
A = pre-exponential factor
E_d = desorption activation energy
R = gas constant
T_{max} = temperature of peak maximum
β = heating rate

Equation 2.1 can be rewritten as:

$$2 \ln T_{max} - \ln \beta = E_d/RT_{max} + \ln(E_d/AR) \qquad (2.2)$$

From Equation 2.2 it can be seen that the desorption activation energy can be obtained by plotting (2 ln T_{max} - ln β) versus $1/T_{max}$. It should be noted that when the variation of the heating rate, β, is small, the accuracy of this method will be low. The peak shape can, in principle, provide values of E_d, but only for homogeneous surfaces without readsorption, as in such cases the peak shape is uniquely defined by the ratios E_d/T_{max} [Cvetanovic and Amenomiya, 1972]. However, due to dispersion in the lines linking the sample cell to the detector, significant peak broadening may still occur before the desorbed adsorbate reaches the detector.

More recently other mathematical models have been derived. Sawa *et al.* [1990b] derived a model in which readsorption occurs freely. Niwa *et al.* [1995] proposed two kinds of methods to determine the strength of zeolite acidity based on the model derived by Sawa *et al.* [1990b]. Forni and Magni [1988] proposed three models, viz. (i) desorption controlling with no readsorption, (ii) desorption controlling with free readsorption, and (iii) intracrystalline diffusion controlling.

As previously mentioned Gorte [1982] and Demmin and Gorte [1984] have proposed a set of design parameters, in the form of dimensionless groups, by which it is possible to carry out TPD experiments under conditions which will ensure sound data interpretation. The design parameters are listed in Table 2.3.

Complications due to lag times in the sample cell (Group 1 in Table 2.3), resulting in long residence times, should be avoided. Diffusional limitations in the catalyst channels (Group 2) can be minimized by using low heating rates. Concentration gradients in the catalyst particles will be significant when Group 3 is greater than 0.05. Low flowrates will result in smaller concentration gradients in the catalyst particles. When Group 3 is greater than 10 the flowrate may be considered infinite since the mass transfer process is then diffusion limited. Group 4 determines the extent of back-mixing in the packed bed. When Group 5 is greater than unity readsorption will be important even for infinite flowrates. When flowrates are low enough so that no gradients are present in the particles, the importance of readsorption is determined by Group 6. These parameters are often much greater than 1, especially in porous materials, indicating that readsorption can often significantly increase the observed peak temperature.

TABLE 2.3: TPD design parameters [Demmin and Gorte, 1984]

	Parameter	Definition	Observed Effect	Ideal requirement
1.	$\frac{\varepsilon_B V \beta}{Q(T_f - T_o)}$	Residence time of carrier gas	Convective lag	Must be <0.01 for negligible lag
2.	$\frac{\varepsilon_P r^2 \beta}{D_P(T_f - T_o)}$	Time constant for diffusion out of an individual particle	Diffusive lag	Must be <0.01 for negligible lag
3.	$\frac{Qr}{4\pi r^2 N D_P}$	Ratio of carrier gas flowrate to rate of diffusion	Particle concentration gradients	Must be <0.05 for negligible gradient
4.	$\frac{QL^2}{VD_B}$	Ratio of carrier gas flowrate to axial mixing	Bed concentration gradients	Must be <0.1 for valid CSTR model
5.	$\frac{\alpha \rho s F r^2}{\pi^2 D_P}$	Ratio of adsorption rate to diffusion rate	Readsorption at infinite flowrate	Must be <1 for negligible readsorption
6.	$\frac{\alpha \rho s F V(1-\varepsilon_B)}{Q}$	Ratio of adsorption rate to carrier gas flowrate	Readsorption at low flowrate	Must be <1 for negligible readsorption

where,

α	=	particle surface area (cm^2/g)
β	=	heating rate (K/sec)
D_B	=	bed dispersion coefficient (cm^2/sec)
D_P	=	particle dispersion coefficient (cm^2/sec)
ε_B	=	bed porosity
ε_P	=	particle porosity
F	=	$(RT/2\pi M)^{1/2}$ (cm/sec)
L	=	bed length (cm)
M	=	molar mass (g/mol)
N	=	number of particles in the bed
ρ	=	particle density (g/cm^3)
Q	=	carrier gas flowrate (cm^3/sec)
r	=	radius of particles (cm)
R	=	ideal gas constant (g cm^2/mol sec^2 K)
s	=	sticking coefficient
T	=	temperature (K)
T_f	=	final temperature (K)
T_o	=	initial temperature (K)
V	=	bed volume (cm^3)

When conducting experiments under conditions for which the criteria for cell (convective) and channel (diffusive) lag times are satisfied, yet with flowrates high enough to generate concentration profiles within the channels, then valid comparisons of TPD spectra can still be made if constant heating rates, catalyst masses, carrier gas flowrates and initial surface coverages are used in all cases. Also, since the peak temperature may be raised due to readsorption, when the magnitude of the Group 3 parameter exceeds 10 (infinite flowrate, diffusion limited), both the TPD peak shape and temperature will remain unaffected by changes in the flowrate. Under these conditions comparisons of TPD spectra will be more meaningful than if fluctuations in the carrier gas flowrate would affect the desorption peaks. This does not allow for the determination of absolute values of adsorption energies, but relative values may still be obtained from the peak temperatures.

The parameters proposed by Demmin and Gorte [1984] have been derived assuming first-order desorption kinetics and the bed was modelled as a CSTR. Jones and Griffin [1983] considered the case of Langmuir adsorption kinetics, since this was more appropriate than the assumption that desorption (or readsorption) was independent of surface coverage. They assumed the TPD process to be diffusion limited.

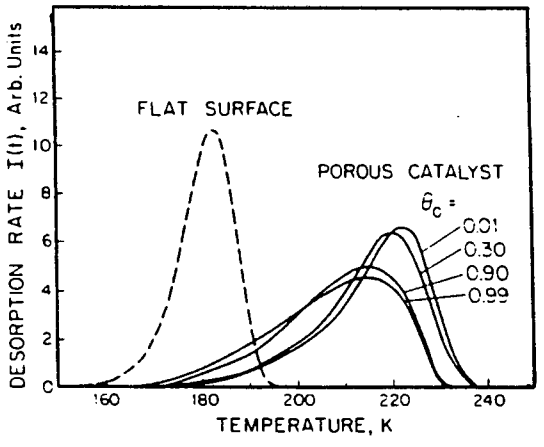

FIGURE 2.25: Simulated TPD spectra [Jones and Griffin, 1983]

For desorption from a flat surface (i.e. no readsorption) the TPD spectrum exhibited essentially a Gaussian distribution [Gorte, 1982; Herz *et al.*, 1982;

Jones and Griffin, 1983; Demmin and Gorte, 1984]. If readsorption occurred the TPD spectrum was skewed towards higher desorption temperatures [Gorte, 1982; Jones and Griffin, 1983; Demmin and Gorte, 1984]. Jones and Griffin [1983] showed that, for higher initial coverages, there was an increase in the desorption rate on the leading edge (low temperature side) of the TPD spectrum. The higher fraction of occupied sites meant that diffusing molecules were less likely to be "restrained" by readsorption, especially at the start of desorption. Also, as a result of readsorption and because of saturation effects associated with Langmuir adsorption kinetics, the peak maximum temperature shifted to lower values as the initial coverage was increased (Figure 2.25).

As mentioned earlier, the peak shape and peak maximum temperature, T_{max}, can be altered by a number of factors. The most important of these are surface heterogeneity, surface coverage, readsorption and diffusion, but heating rate, carrier gas flowrate, bed depth and particle size also affect either the peak shape or the peak maximum temperature.

2.3.1.1 Surface heterogeneity and surface coverage

If the activation energy of desorption and the peak maximum temperature are constant, only the peak size would change depending on the amount of material adsorbed for non-saturated samples. However, by decreasing the amount of material adsorbed on the catalyst, the peak maximum temperature increased [Amenomiya and Cvetanovic, 1963c; Kiskinova *et al.*, 1981]. They noticed that the leading edge (low temperature side) of the peak was gradually removed, whereas the trailing edge (high temperature side) remained unchanged. They concluded that the adsorbate was preferentially adsorbed onto strong sites, and these results indicated surface heterogeneity, or a range of activation energies of desorption (assuming no readsorption). Amenomiya *et al.* [1964] showed similar results for the desorption of ammonia from alumina.

When it is assumed that no readsorption occurs during temperature programmed desorption, the position of T_{max} is independent of initial surface coverage, if all adsorption sites are homogeneous. On heterogeneous surfaces the adsorbate will adsorb preferentially on the strongest acid sites, in which case T_{max} will increase with decreasing surface coverage. Such a shift in T_{max} has therefore been regarded to indicate a potential existence of surface

heterogeneity. However, even with homogeneous adsorption sites there will be a similar shift if readsorption occurs [Cvetanovic and Amenomiya, 1967].

2.3.1.2 Readsorption and diffusion

Readsorption is intrinsic to the adsorption system being studied and can often not be eliminated by changing experimental parameters. The possibility of readsorption in porous catalysts should always be considered since it can raise T_{max} by several hundred degrees. The extent to which readsorption influences the peak position and shape was studied using a model developed by Rieck and Bell [1984] and was found to be comparable to Gorte's findings [Gorte, 1982].

When the desorption of the adsorbate is greater than its diffusion out of the channels of the catalyst, then adsorbate partial pressure builds up inside the catalyst. This can cause a lag in the detection of the desorbing adsorbate [Gorte, 1982]. The desorption is no longer the rate-limiting process, and the measured flux of molecules leaving the sample is determined by the rate of diffusion out of the catalyst channels, as modified by readsorption on the channel walls [Jones and Griffin, 1983; Forni *et al.*, 1992 and 1995]. These effects can be reduced by judicious choice of experimental conditions. However, for microporous solids, especially zeolites and molecular sieves, it may not be possible to eliminate these effects totally.

Readsorption should be considered especially when reaction is occurring along with desorption [Gorte, 1982]. The many desorption and readsorption processes imply that TPD with reaction will not be much different from running a reaction at the instantaneous pressure and temperature of the desorption. Thus only questions about the reaction which cannot be answered by reaction studies should be addressed using TPD.

2.3.1.3 Carrier gas flowrate, heating rate, bed depth and particle size

An increase in carrier gas flowrate resulted in a peak shift to lower temperatures and sharper peaks [Rieck and Bell, 1984]. Such effects also have been reported by Fletcher [1984]. With increasing flowrate, the concentration of the adsorbate in the voids between the particles decreases, thereby increasing the

concentration gradient within the particle and decreasing the concentration at the center of the particle. This accelerates the rate of desorption while suppressing the rate of readsorption, thus shifting the peak temperatures to lower values. Hence equilibrium readsorption prevails when a carrier gas is used to sweep away the desorbing adsorbate. Lowering the heating rate will affect the desorption rate in a similar way to increasing the flowrate, and thus tend to lower T_{max}, as observed by Forni *et al.* [1995] for ZSM-5 and by Moon [1995] for zeolite Beta.

Rieck and Bell [1984] also showed that an increase in particle size increased the peak temperature. However, an increase in carrier gas flowrate would result in a point where the peak position and shape would no longer be sensitive to flowrate, as the desorption process would be dominated by intraparticle mass transfer. These findings correspond to those obtained by Tronconi and Forzatti [1985].

An increase in catalyst mass, or bed depth, may result in axial gradients along the bed [Rieck and Bell, 1984]. This will affect the desorption rate in a similar way to changes in the flowrate. A decrease in catalyst mass will tend to lower T_{max}. Should axial gradients be present, most models used are no longer appropriate as the bed is usually modelled as a CSTR.

2.3.1.4 Summary

The importance of the need for detailed information has been highlighted in the preceding sections when wishing to analyze TPD spectra. The influence of the various experimental parameters is pronounced, and makes comparisons difficult if the experimental parameters are not identical. It is therefore difficult to make claims about the strength of the acid sites of different catalysts, as indicated by T_{max}, based solely on TPD data. Especially when comparing modified catalysts, a change in T_{max} may not be due to a change in acid strength, but rather due to a change in one or more experimental parameters. However, T_{max} and the peak shape may still be instructive indications of changes to the system. The amount of adsorbate desorbed from the catalyst is also an instructive parameter obtained from TPD studies.

2.3.2 TEMPERATURE PROGRAMMED DESORPTION FROM ZEOLITES

2.3.2.1 Physisorption and chemisorption

Topsoe *et al.* [1981] studied the acidic properties of ZSM-5 type zeolites by infrared spectroscopy and temperature programmed desorption. Ammonia was adsorbed at 20°C until saturated, then eluted at 20°C before increasing the temperature linearly. They observed three peaks with maxima in the regions 60-100°C, 150-200°C and 420-500°C, named α, β and γ respectively. They proposed that the γ-peak was associated with the adsorption of NH_3 on strong Brönsted and/or Lewis acid sites, and that these sites would probably be located at the channel intersections. The I.R. band at 3605 cm^{-1} (Si-OH-Al groups) was found to be characteristic of these sites. The β-peak was ascribed to silanol (Si-OH) groups of weaker Brönsted acid strength, corresponding to an I.R. band at 3720-3740 cm^{-1}, or with adsorption of NH_3 on Na counterions. The α-peak was thought to be due to nonzeolitic material and did not seem to have any catalytic function.

These results were confirmed by, amongst others, Hidalgo *et al.* [1984]. NH_3 was adsorbed and evacuated at 100°C. TPD spectra showed two peaks at 147°C (low temperature desorption peak - LTD peak) and 324°C (high temperature desorption peak - HTD peak) respectively, but a third peak was observed at lower temperatures when NH_3 was adsorbed at 20°C. The I.R. band at 3605 cm^{-1} was also ascribed to Si-OH-Al groups, corresponding to the HTD peak. They did, however, suggest that the low temperature desorption peak (147°C) is also in some way related to the I.R. band at 3605 cm^{-1} (Si-OH-Al groups). Indeed, Iwamoto *et al.* [1986] suggested that the LTD peak of NH_3 results from physisorbed or very weakly chemisorbed molecules, but not from NH_3 bonded to weak acid sites. Pope [1990] suggested that, unlike other larger amines, more than one NH_3 molecule can be adsorbed strongly per acid site. For the above reasons Niwa *et al.* [1986c] and Forni *et al.* [1992] stressed the importance of ensuring that the isothermal desorption time, t_{id}, is long enough to obtain the complete removal of excess adsorbate. A peak at higher temperatures (677°C and above) was found to be due to dehydroxylation of the zeolite [Hidalgo *et al.*, 1984; Iwamoto *et al.*, 1986].

Post and Van Hooff [1984] investigated NH_3-TPD and *n*-hexane cracking on HZSM-5 and Silicalite-I (which is isostructural to ZSM-5, but has no acidity). They observed a LTD peak and a HTD peak from HZSM-5, but only a LTD peak from Silicalite-I. The acidity of Silicalite-I arose from Si-OH groups at the crystal surface. Since Silicalite-I showed no activity for *n*-hexane cracking, only the HTD peak from HZSM-5 was of catalytic interest. Hunger *et al.* [1990] increased the NH_3 dosage gradually, and noticed that the HTD peak appeared first, and the LTD peak appeared only when the dosage was increased. This implied that the adsorbate was adsorbed preferentially onto the strong acid sites, as indicated by the HTD peak. This was in agreement with the findings of Cvetanovic and Amenomiya [1967].

2.3.2.2 The influence of zeolite structure and Si/Al ratio

Kofke *et al.* [1989] studied the temperature programmed desorption of 2-propanol and 2-propanamine on HZSM-5, HZSM-12 and HM. On all three zeolites 1:1 adsorption complexes with similar reactivities were formed. The complexes decomposed at the same temperatures and formed the same products on all three zeolites. For this reason Kofke *et al.* [1989] claimed that the acid sites formed by isolated aluminium atoms in the zeolite lattice were chemically equivalent, independent of the structure of the lattice.

However, the influence of acid site strength, number of acid sites and zeolite structure seems to be uncertain. Hidalgo *et al.* [1984] reported the peak maximum temperature of HZSM-5 to be essentially independent of Si/Al ratio. Kapustin *et al.* [1988] reported a decrease in peak maximum temperature with increasing Si/Al ratio. They also compared peak maximum temperatures for HZSM-5 and Mordenite, having similar heats of adsorption, and deduced that the structure influenced peak maximum temperatures, which was contrary to the findings of Kofke *et al.* [1989]. For this reason they concluded that the peak maximum temperature could not be used for comparisons of the acid site strengths of different zeolites.

Iwamoto *et al.* [1986], in agreement with Kapustin *et al.* [1988], found that the aluminium content influenced the peak maximum temperature, but found that the structure had no effect, which was in agreement with Kofke *et al.* [1989]. It has been shown by Forni *et al.* [1992] that for a HZSM-5 sample with a Si/Al

ratio of 16.8, the rate determining step was intracrystalline diffusion, whereas a sample with a Si/Al ratio of 5.2 was controlled by desorption without free readsorption [Forni *et al.*, 1995].

These apparently contradictory findings of various studies may be explained when one considers the potentially overwhelming influence of experimental conditions (catalyst mass, carrier gas flowrate, heating rate, etc.) on the resulting spectra. It seems likely that changes in Si/Al ratios and the use of different zeolites will result in changes to the competitive interaction between the desorption and readsorption phenomena, as shown by Forni *et al.* [1992 and 1995]. This will result in changes to the peak maximum temperature of the desorption spectrum.

Evidence for readsorption in HZSM-5 has been reported by Kapustin *et al.* [1988]. They noticed that an increase in carrier gas flowrate or a decrease in catalyst mass resulted in lower values of T_{max} of the NH_3-TPD spectrum. A decrease in T_{max} was also observed by Hunger *et al.* [1990] for a decrease in catalyst mass. This was in agreement with the models of Demmin and Gorte [1984] and Rieck and Bell [1984].

It was also shown by Hidalgo *et al.* [1984] and Anderson *et al.* [1979] that the peak maximum temperature of the HTD peak decreased with increased cation exchange, whereas that of the LTD peak remained relatively unchanged. This implied that an increase in ion exchange resulted in a corresponding loss of acidity. Forni *et al.* [1992] proposed that ionic Na^+ clusters were likely to restrict the pore size and thus affect the rate of diffusion of desorbing molecules.

2.3.2.3 Probe molecules for the total acidity

Although ammonia is the most commonly used probe molecule, the use of pyridine has also been reported [Topsoe *et al.*, 1981; Karge and Dondur, 1990; Parrillo *et al.*, 1990; Sharma *et al.*, 1993]. Sharma *et al.* [1993] have reported that pyridine has a smaller particle diffusion coefficient than NH_3, due to its greater size. This resulted in higher values of the peak maximum temperature for pyridine. Similar observations in peak maximum temperature values for NH_3 and pyridine have been made by Karge and Dondur [1990] on Mordenite and

Parrillo *et al.* [1990] on ZSM-5. Topsoe *et al.* [1981] reported that pyridine desorption helps the dehydroxylation of the zeolite. The desorption of pyridine from a Brönsted site results in the loss of a H_2O molecule and thus the formation of a Lewis site.

The desorption spectra of NH_3 and pyridine under vacuum conditions have been investigated on dealuminated Mordenite [Karge and Dondur, 1990] and dealuminated Y-type zeolite [Karge *et al.*, 1991], using FT-IR techniques. On deconvolution of the NH_3 desorption spectra, four types of acidic sites were identified from dealuminated Mordenite and zeolite Y samples, viz. weak and strong Brönsted acid sites and weak and strong Lewis acid sites. On deconvolution of the pyridine desorption spectra from dealuminated Mordenite, only the weak and strong Lewis and the weak Brönsted acid sites were identified. For pyridine desorption from dealuminated zeolite Y, only weak and strong Brönsted acid sites were identified. It was proposed that the bulkier pyridine could not reach all the acid sites that could be probed by NH_3.

It has been pointed out that the use of certain amines may give unreliable results for the measurement of acid site concentration due to the reactivity of the molecules upon heating, or the exclusion of two molecules present at adjacent sites [Pope, 1990]. Parrillo *et al.* [1990] examined the desorption of simple amines (methyl-, ethyl-, *n*-propyl-, isopropyl- and *tert*-butylamine) as well as pyridine. For each adsorbate a well defined adsorption state corresponding to a coverage of one molecule per aluminium atom could be identified by using TPD-TGA. Amine molecules adsorbed in excess of one molecule per site desorbed unreacted at much lower temperatures. This excess was thus equivalent to a LTD peak. With the exception of methylamine and pyridine, the 1:1 complexes formed by each amine reacted completely to desorb as ammonia and alkene products (equivalent to a HTD peak). Pyridine desorbed intact above 423°C. Infrared spectroscopy was used to demonstrate that the stoichiometric complexes formed for each amine were protonated and associated with the hydroxyls at the aluminium sites in the zeolite. These results implied that the acid sites in HZSM-5 were simple Brönsted sites. Very similar results were obtained by Kofke *et al.* [1988] using simple alcohols and by Kofke and Gorte [1989] using simple alkenes as adsorbates.

2.3.2.4 Probe molecules for the external surface acidity

Post and Van Hooff [1984] used a probe which was too large to enter the channels to study the external surface of HZSM-5. When triethylamine (TEA) was used instead of NH_3, again both a LTD peak (180°C) and a HTD peak (490°C) were observed on HZSM-5, but only a LTD peak was observed on Silicalite-I. However, since TEA was likely to react upon desorption (as shown for many alkyl amines by Parrillo *et al.* [1990]), the LTD and HTD peak could also be due to the desorption of the different reaction products. Since a TCD was used in these studies as detector, it would not have been possible to differentiate between these two possibilities. It was unlikely that a LTD peak should have existed on HZSM-5 or on Silicalite-I (indicating physisorbed material) if the adsorbate was adsorbed onto the external surface.

Pereira and Gorte [1992] have reported TPD-TGA data using cyclooctylamine and 2-ethylhexylamine from HY and HZSM-5, and concluded that these compounds were adsorbed only on the external surface of HZSM-5. Both cyclooctylamine and 2-ethylhexylamine decomposed to form alkenes and ammonia. Other adsorbates which have been used to probe the external surface of HZSM-5 include ethyldiisopropylamine [Pope, 1990], various nitrogen containing (poly-)aromatic compounds [Rollmann, 1991], and 4-methyl quinoline [Anderson *et al.*, 1979]. However, no desorption spectra have been reported in these studies.

2.4 OBJECTIVES OF RESEARCH

The external surface of zeolites is fully accessible to all molecules and thus behaves in a non-shape selective manner. In this study two methods have been used to inertise the external surface acidity of zeolites, viz. (a) chemical vapour and liquid deposition of zeolites ZSM-5, Mordenite and Beta, and (b) coating the ZSM-5 crystals with a Silicalite shell. The purpose of these modifications is to inertise the external surface acidity and narrow the pore openings in a controlled manner, thereby increasing the shape selective properties of the zeolites, and possibly also to reduce coke formation at the entrance to the pores.

Although chemical deposition of alkoxy silanes has been reported using static vacuum systems, vapour phase flow systems and liquid phase systems, these systems have not been compared in one study. In a number of studies the alkoxy silanes have been co-fed with methanol or water to aid the deposition process, but reasons for the addition of diluents such as toluene and *n*-hexane have not been clarified. The deposition temperatures have ranged from ambient to ± 420°C and the deposition times have also varied widely. Whereas the amount of silica deposited on the external surface appears to be dependent on the deposition temperature and time, the extent to which controlled pore mouth narrowing or undesirable pore blocking takes place has not been addressed fully. The robustness of the silica layer has not been studied to determine whether the silica layer is irreversibly attached to the surface. Lastly, no definitive analytical tool exists to quantitatively measure the number of acid sites on the external surface of zeolites.

Thus the objectives of this study are:

(i) To develop a temperature programmed desorption technique aimed at quantitatively measuring the number of acid sites on the external surface of zeolites.

(ii) To inertise the external surface acidities of ZSM-5, Mordenite and Beta using tetraethoxysilane (TEOS) in a static vacuum system, a vapour phase flow system and a liquid phase system.

(iii) To investigate the effects of deposition temperature, deposition time and of using diluents on the completeness of the inertisation process and on the controlled pore mouth narrowing of the silica layer formed on the external surface by the deposition of TEOS.

(iv) To determine whether the silica layer formed on the surface of the zeolites during TEOS deposition is attached irreversibly.

(v) To inertise the external surface acidity of ZSM-5 by coating the seed crystals with Silicalite shells, changing the post-synthesis treatment of the parent crystals (preparatory treatment) while keeping the modification procedure the same.

(vi) To attempt to develop a consistent explanation for the observations made under the above-mentioned range of experimental conditions.

CHAPTER 3

EXPERIMENTAL METHODS

"A fool is a man who never tried an experiment in his life" - **Darwin**

3.1 CATALYST SYNTHESIS AND MODIFICATIONS

Three zeolites were used during the course of the project.

1. The parent ZSM-5 was synthesized for the project. The synthesis procedures for the parent ZSM-5 are described in Section 3.1.1.
2. A single batch of Na-Mordenite was obtained from a commercial vendor.
3. A single batch of H-Beta was obtained from a commercial vendor.

This section deals with the synthesis and modifications of the catalysts investigated. A list of all reagents and chemicals used can be found in Appendix I.

The complete synthesis and modification procedures for ZSM-5 consisted of several steps. A schematic representation of this is given by Figure 3.1. The ***primary synthesis*** is the synthesis of the unmodified, or parent, ZSM-5 catalyst. Before the catalyst was modified the catalyst was treated in several ways. This was the ***preparatory treatment***, consisting of washing and drying, detemplation, ion exchanging or calcination, after which ***modification*** took place.

ZSM-5 was modified (a) by ***chemical vapour and liquid deposition***, which was achieved by contacting the catalyst with tetraethoxysilane (TEOS) in (i) a static vacuum system, (ii) a vapour phase flow system, or (iii) a liquid phase system, or (b) by coating the parent crystals with a ***Silicalite shell***, which was achieved by reimmersing the parent crystals in an aluminium-free synthesis mixture. Where required the modified samples were prepared for analysis by washing and drying, detemplation, ion exchanging or calcination.

In the case of Mordenite and Beta, preparatory treatment prior to modification was carried out as required. However, these zeolites were only modified using chemical vapour and liquid deposition methods.

To test the durability of the modification, selected samples were subjected to grinding (***post-modification treatment***).

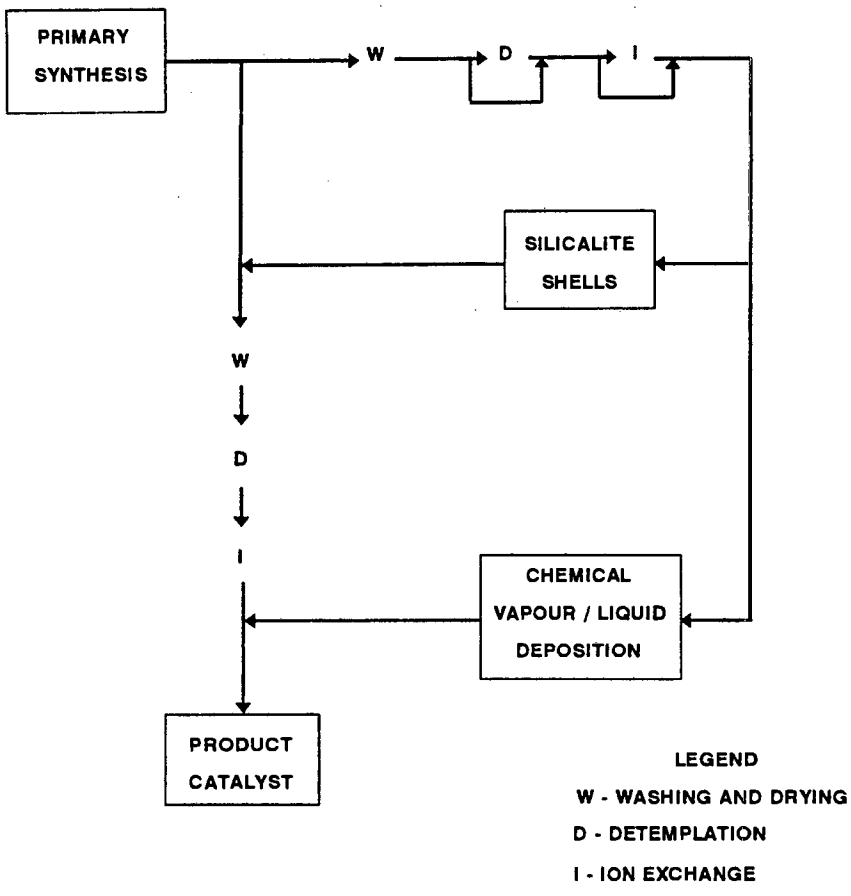

FIGURE 3.1: Schematic representation of ZSM-5 synthesis and modifications

3.1.1 PRIMARY ZSM-5 SYNTHESIS

The synthesis method for ZSM-5 was based on US Patent 3,702,886 by Argauer and Landolt [1972]. The synthesis mixture for the primary, or parent syntheses, consisted of the following weight ratios: H_2O / Ludox HS40 (Du Pont, 40% SiO_2) / TPA-Br (Fluka Chemie AG, 98% pure) / NaOH (Saarchem, 97% pure) / $Al(OH)_3$ (BDH, 99.5% pure) = 100.0 / 31.84 / 25.18 / 1.87 / 0.4751. These synthesis mixtures had a Si/Al ratio of 35. The synthesis mixtures were kept at 160°C for 72 h at autothermal pressure in a Teflon-lined autoclave.

ZSM-5 was prepared by dissolving the full charge of TPA-Br in approximately 1/3 H_2O in a Teflon autoclave beaker (Solution A). The full NaOH charge and the full $Al(OH)_3$ charge was dissolved in a minimum of H_2O (approx. 2-5 ml) in a

50 ml glass beaker by gently heating the mixture to its boiling point (Solution B). Solution B was added to Solution A. The full Ludox charge was added to the above mixture, after which the remaining H_2O was added. The synthesis mixture was placed in an autoclave in which the synthesis mixture was stirred. The autoclave was heated to 160°C at 1°C/min and the temperature was kept at 160°C for 72 h. The autoclave was subsequently cooled to room temperature. To synthesize Silicalite-I no $Al(OH_3)$ was added to the synthesis mixture, but otherwise the procedure remained as described above.

Table 3.1 shows the synthesis variables for eight primary synthesis mixtures (batches Z_1 - Z_8) used for chemical vapour deposition studies on ZSM-5. The eight individual batches were analyzed by AA and XRD and subsequently mixed together to provide a large uniform batch of ZSM-5, denoted batch Z.

TABLE 3.1: Synthesis conditions and synthesis mixture compositions for primary ZSM-5 syntheses (batches Z_1 - Z_8)

CATALYST		Z_1	Z_2	Z_3	Z_4
Temperature	(°C)	159	163	162	163
Time	(h)	72	72	72	72
H_2O	(g)	300.3	299.8	300.1	300.0
TPA-Br	(g)	75.52	75.53	75.55	75.55
Ludox	(g)	95.53	95.50	95.48	95.50
$Al(OH)_3$	(g)	1.4255	1.4255	1.4252	1.4252
NaOH	(g)	5.62	5.61	5.61	5.61

CATALYST		Z_5	Z_6	Z_7	Z_8
Temperature	(°C)	160	161	160	165
Time	(h)	72	72	72	72
H_2O	(g)	300.0	300.0	300.0	300.0
TPA-Br	(g)	75.54	75.54	75.55	75.54
Ludox	(g)	95.52	95.52	95.53	95.52
$Al(OH)_3$	(g)	1.4251	1.4253	1.4254	1.4255
NaOH	(g)	5.61	5.62	5.62	5.61

Table 3.2 shows the synthesis variables for the primary synthesis used to modify ZSM-5 samples by coating with Silicalite shells (batch Z_9). Synthesis variables for Silicalite-I (batch S) are also given in Table 3.2.

TABLE 3.2: Synthesis conditions and synthesis mixture compositions for the primary ZSM-5 synthesis batch used for coating with Silicalite shells (batch Z_9) and for Silicalite-I (batch S)

CATALYST		Z_9	S
Temperature	(°C)	156	161
Time	(h)	72	72
H_2O	(g)	100.1	100.0
TPA-Br	(g)	25.18	25.18
Ludox	(g)	31.82	31.83
$Al(OH)_3$	(g)	0.4751	-
NaOH	(g)	1.87	1.87

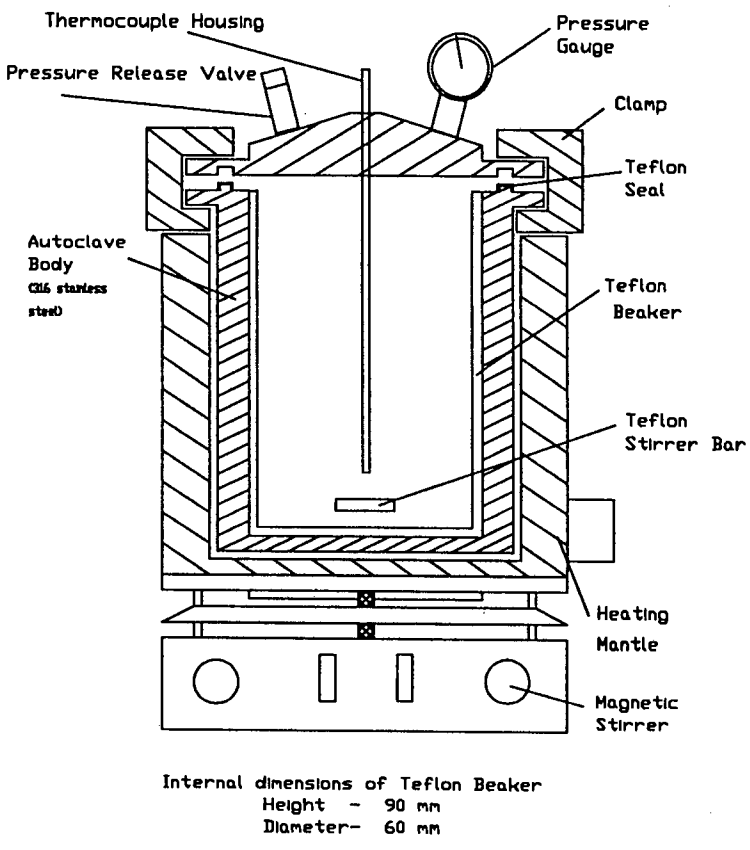

FIGURE 3.2: Magnetically stirred autoclave

Smaller ZSM-5 batches and the Silicalite-I batch (viz. batches Z_9 and S) were synthesized in a magnetically stirred autoclave (Figure 3.2). Larger ZSM-5 batches (viz. batches Z_1 - Z_8) were synthesized in a mechanically stirred autoclave (Figure 3.3).

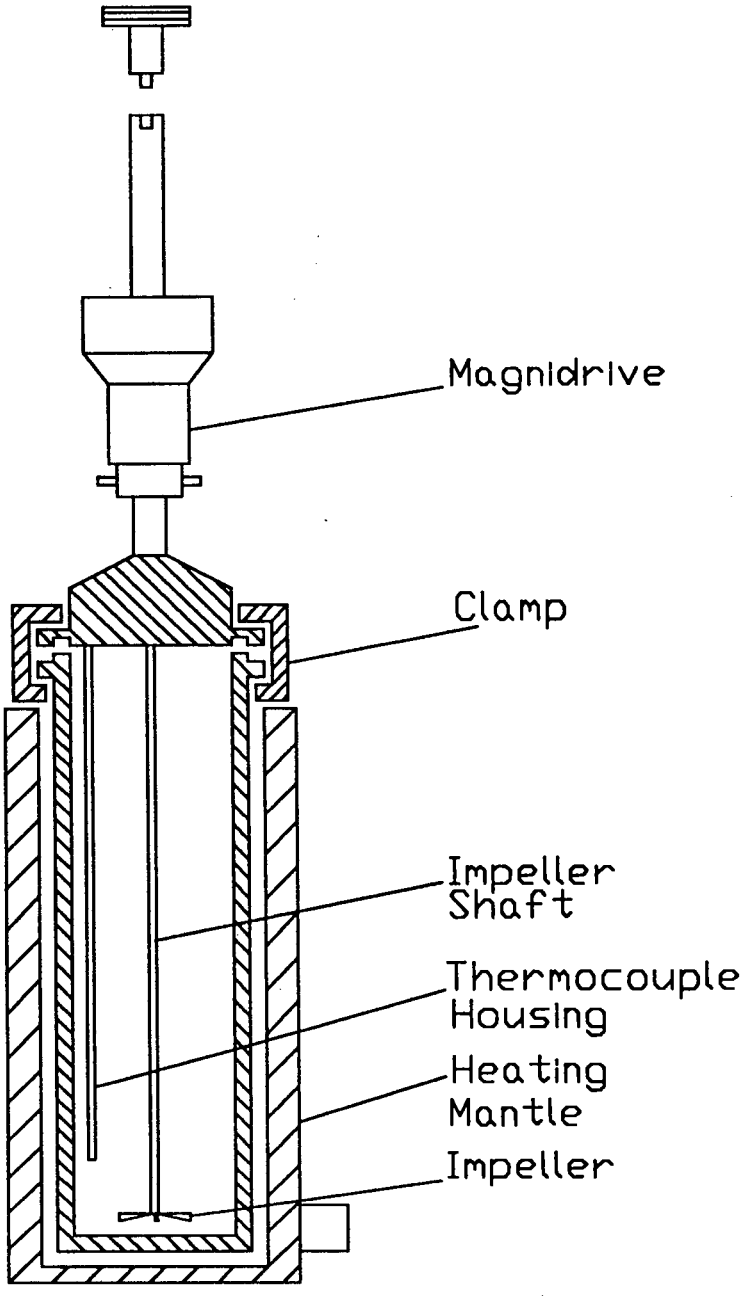

FIGURE 3.3: Mechanically stirred autoclave

3.1.2 PREPARATORY TREATMENT

3.1.2.1 Washing and drying

The supernatant liquor resulting from the synthesis was decanted. The as-synthesized catalyst was mixed thoroughly with 500 ml deionized water. The catalyst was allowed to settle out, and the supernatant liquor was discarded. The catalyst was washed a further three times with deionized water. The catalyst was then dried at 80 - 90°C for 16 h.

3.1.2.2 Detemplation

To remove the template, TPA-Br, the dried catalyst was placed in a 300 mm long, 16 mm I.D. tubular stainless steel reactor. Nitrogen was passed over the catalyst at 500°C (60 ml/min) for 6-8 h, after which air was passed over the catalyst at 500°C (60 ml/min) for a further 16 h.

3.1.2.3 Ion exchanging

After the template had been removed by detemplation, the as-synthesized Na-form of the catalyst was ion exchanged to obtain the NH_4-form of the catalyst. Ion exchange was achieved by gently boiling the Na-form of the catalyst in a 2M NH_4NO_3 solution under reflux conditions for 24 h in a glass culture vessel. Up to 15 g of the Na-form was ion exchanged per liter of 2M NH_4NO_3 solution. After ion exchange, the catalyst was washed and dried as described in Section 3.1.2.1.

3.1.2.4 Calcination

The H-form of the catalyst was obtained by calcination. Usually the sample was calcined *in situ* in the apparatus to be used for a particular experiment. Hence the calcination parameters will be described in detail in the sections dealing with those experiments. Typically air was passed over the catalyst at 500°C (30 - 60 ml/min) for 1 - 16 h.

3.1.3 MODIFICATIONS

3.1.3.1 Chemical vapour and liquid deposition

Modification by means of chemical vapour deposition (CVD) or chemical liquid deposition (CLD) was achieved by exposing the catalyst to tetraethoxysilane (TEOS). Three different methods were used:

(i) a static vacuum system
(ii) a vapour phase flow system
(iii) a liquid phase system

(i) Modification using a static vacuum system

The chemical vapour deposition of TEOS in a static vacuum system was achieved by calcining 2.5 g of the NH_4-form of the catalyst in flowing air (30 ml/min) at 500°C for 8 h. TEOS was deposited *in situ* under vacuum. The vacuum system is described in more detail in Section 3.5. The ultimate vacuum obtained was $< 5x10^{-5}$ mbar, and the TEOS partial pressure was ~ 2.15 mbar. The sample deposition temperature ranged from 100 - 400°C for 4 - 60 h, either using a single deposition cycle (Table 3.3a) or using multiple deposition cycles (Table 3.3b). For multiple deposition cycles, the samples were evacuated at the deposition temperature for 1 h between each deposition cycle. Samples were calcined in flowing air (30 ml/min) at 500°C for 8 - 12 h at the end of the CVD procedure to remove adsorbed carbonaceous residues.

TABLE 3.3a: Modification parameters for samples prepared by a single TEOS deposition cycle using a static vacuum system

CATALYST	Deposition Temperature (°C)	Deposition Time (h)		
		4	21	60
ZSM-5	100	*	*	*
	200	*	*	*
	300	*	*	*
	400	*	*	*
Mordenite	400			*
Beta	400			*

NOTE: * indicates samples were modified using the above conditions in a static vacuum system

TABLE 3.3b: Modification parameters for samples prepared by multiple TEOS deposition cycles using a static vacuum system

CATALYST	Deposition Temperature (°C)	No. of Cycles	Deposition Time per Cycle (h)	Total Deposition Time (h)
ZSM-5	400	4	4	16
	400	6	10	60
Mordenite	400	6	10	60
Beta	400	6	10	60

(ii) Modification using a vapour phase flow system

The chemical vapour deposition of TEOS in a vapour phase flow system was achieved by calcining 0.2 or 1.0 g of the NH_4-form of the catalyst in flowing air (30 ml/min) at 500°C for 8 h. TEOS was fed by saturator (30 or 150 ml/min helium carrier gas to obtain a TEOS WHSV = 0.18 h^{-1}) for a total of 8 - 40 h, using single or multiple deposition cycles. The catalyst deposition temperature ranged from 50 - 400°C. The sample was subsequently calcined in flowing air (30 ml/min) at 500°C for 8 h to remove adsorbed carbonaceous residues. Table 3.4 indicates the samples prepared using a vapour phase flow system.

TABLE 3.4: Modification parameters for samples prepared by TEOS deposition using a vapour phase flow system (single or multiple deposition cycles)

CATALYST	Deposition Temperature (°C)	Deposition Time (h)		
		8	4 x 5h	4 x 10h
ZSM-5	50	*		*
	400	*	*	
Mordenite	400	*		
Beta	400	*		

NOTE: * indicates samples were modified using the above conditions in a vapour phase flow system

The saturator consisted of a 160 mm long, 12 mm I.D. glass tube which was packed with Chromosorb. The Chromosorb bed was saturated with TEOS. The gas feed passed through the saturated Chromosorb bed, ensuring good contact between gas and liquid and reducing pulsation effects commonly found in simple bubble saturators. The saturators were operated in up-flow mode to avoid increasing the pressure drops due to compression of the Chromosorb bed. A water jacket surrounding the Chromosorb bed was used to maintain constant TEOS partial pressures (~ 2.15 mbar).

(iii) Modification using a liquid phase system

The chemical liquid deposition of TEOS was achieved by drying 2.5 g of the H-form of the catalyst at 70°C for 3 h. A diluent was added to the sample before the addition of TEOS. A total of 20 ml of TEOS in H_2O, ethanol, or *n*-hexane, in varying concentrations, or pure TEOS was added in this manner. This mixture was stirred at ambient temperatures for 21 h. The sample was subsequently washed 3 times with H_2O and dried at 70°C. Calcination of these samples was usually carried out *in situ* prior to analysis. Table 3.5 indicates the samples prepared using a liquid phase system.

TABLE 3.5: Modification parameters for samples prepared by TEOS deposition using a liquid phase system

CATALYST	Deposition Temperature (°C)	Diluent			
		water	ethanol	*n*-hexane	none
ZSM-5	20	*	*	*	*
Mordenite	20			*	
Beta	20			*	

NOTE: * indicates samples were modified using the above conditions in a liquid phase system

3.1.3.2 Silicalite shells

To obtain a Silicalite shell around the ZSM-5 crystals, the parent sample was reimmersed into a secondary synthesis mixture. This mixture contained no $Al(OH)_3$, but was otherwise of the same composition as described in Section 3.1.1. Hence the synthesis procedure was similar to that described in Section 3.1.1 for the synthesis of Silicalite-I, with the addition that the parent ZSM-5 crystals were added to the synthesis mixture. The relative amounts of ZSM-5 seeds and secondary synthesis mixture could be varied. Here, the relative amounts of ZSM-5 seeds and secondary synthesis mixture was such that approximately 1.5 g Silicalite-I was expected to form per gram of ZSM-5 added as seed crystal. In some cases samples were not detemplated or ion exchanged prior to reimmersion into the secondary synthesis mixture, but all were washed, detemplated and ion exchanged after the modification (Section 3.1.2). The modification synthesis time was 72 h at 160°C, and the Silicalite shell coating procedure was carried out in a magnetically stirred autoclave (Figure 3.2).

Note that zeolites Mordenite and Beta were not modified using this method.

TABLE 3.6: Synthesis conditions and synthesis mixture compositions for modification using the Silicalite shell method

CATALYST	Z_9-C-templ	Z_9-C-Na	Z_9-C-NH_4
Primary synthesis	Z_9	Z_9	Z_9
Preparatory treatment			
detemplation	no	yes	yes
ion exchange	no	no	yes
Temperature (°C)	164	156	159
Time (h)	72	72	72
H_2O (g)	50.04	31.31	31.25
TPA-Br (g)	12.60	7.87	7.87
Ludox (g)	15.96	9.93	9.95
$Al(OH)_3$ (g)	-	-	-
NaOH (g)	0.936	0.590	0.585
ZSM-5 (g)	4.0	2.5	2.5

3.1.4 POST-MODIFICATION TREATMENT

Post-modification treatment was carried out to determine whether the silica layer deposited during chemical vapour deposition was permanently attached to the external surface. Post-modification treatment consisted of grinding the sample in a mortar and pestle, subjecting the sample to mechanical stresses and breaking up agglomerates. Only a few selected samples were treated in this way.

3.1.5 CATALYST NOMENCLATURE

The catalysts are named according to the following code:

ZEOLITE - MODIFICATION - PARAMETERS

e.g. X_n - Y - T/t/c/d

where

- **X** is the zeolite type.
  - **Z** ZSM-5 (a mixture of several smaller ZSM-5 batches)
  - **M** Mordenite
  - **B** Beta
  - **S** Silicalite-I
  - **n** included when referring to a particular parent ZSM-5 batch

- **Y** is the modification type.
  - **V** modified with TEOS using a static vacuum system
  - **F** modified with TEOS using a vapour phase flow system
  - **L** modified with TEOS using a liquid phase system
  - **C** modified by coating with Silicalite shells (ZSM-5 only)

Nomenclature for samples modified by chemical vapour (CVD) and liquid (CLD) deposition methods

T the deposition temperature (°C) (not CLD samples)

t the deposition time (h) (not CLD samples)

c the volume % TEOS in the liquid phase system (CLD samples only)

d the diluent used in the liquid phase system, (CLD samples only)
where

- **W** Water
- **E** Ethanol
- **H** *n*-Hexane
- **-** pure TEOS was used without diluent

Nomenclature for ZSM-5 samples modified by coating with Silicalite shells

templ sample prepared using the as-synthesized material (i.e. not detemplated and not ion-exchanged parent crystals)

Na sample prepared using detemplated but not ion-exchanged parent crystals (Na-form)

NH_4 sample prepared using detemplated and ion-exchanged parent crystals (NH_4-form)

Nomenclature for post-modification treatment

the term "**(crushed)**" follows the sample name when the modified sample was subjected to grinding

A separate "bookmark" is provided, as well as a fold-out with examples in Appendix II, which can be used as reference guides.

3.2 CATALYST CHARACTERIZATION

3.2.1 CATALYST STRUCTURE AND MORPHOLOGY

3.2.1.1 X-ray diffraction (XRD)

A Philips X-ray Diffractometer was used to obtain X-ray diffraction spectra using Cu-Kα or Co-Kα radiation. The samples were kept at ambient conditions prior to analysis. Relative crystallinities were obtained by integrating the peak areas of the three largest peaks in the range 22-30° 2θ for ZSM-5 [Hardenberg *et al.*, 1992], the five largest peaks in the range 20-35° 2θ for Mordenite and the peak in the range 22-30° 2θ for Beta [Camblor and Pérez-Pariente, 1991]. The peak positions were different depending on whether Cu-Kα (wavelength = 1.542 Å) or Co-Kα (wavelength = 1.769 Å) radiation was used. The peak areas were normalized with respect to the parent sample. The following parameters were used for the X-ray Diffractometer:

- voltage	40	kV
- current	25	mA
- range	2000	
- preset	2000	counts/sec
- time constant	1	sec
- 2θ/step	0.1°	
- 2θ range	6-40°	
- slits	1°	

3.2.1.2 Scanning electron microscopy (SEM)

A Cambridge S200 scanning electron microscope was used to obtain crystallite morphologies and sizes. The following parameters were used:

- accelerating voltage	15	keV
- aperture	30	
- tilt angle	39°	
- resolution	10	
- working distance	10 - 15	mm

The sample was mounted on a stub with a carbon and glue mixture, and coated with AuPd. Care was taken to select representative micrographs of the sample,

and although this characterization method may not have been truly representative of the whole sample, it was considered unlikely that the micrographs varied substantially within the same sample.

3.2.1.3 Particle size distribution

A Malvern Mastersizer S was used to obtain particle size distributions of the parent ZSM-5, Mordenite and Beta samples. The samples were suspended in H_2O using ultra-sound (30% of maximum instrument setting).

3.2.2 ADSORPTION MEASUREMENTS

3.2.2.1 Thermogravimetric analysis (TGA)

The adsorption capacities of the samples were measured using a Stanton Redcroft STA-780 Series Thermal Analyzer. Adsorbates with differing molecular diameters could be adsorbed, thus giving information on pore mouth narrowing or pore blocking. The following adsorbates were used (kinetic diameters given in brackets [Breck, 1974]):

n-hexane	(4.3 Å)
p-xylene	(5.85 Å)
o-xylene	(6.6 Å)
1,2,4-trimethyl benzene	(6.6 Å)

50 mg of sample was loaded in the sample holder and calcined in air (30 ml/min) at 500°C for at least 1 h. The sample was then cooled to the adsorption temperature, viz. 80°C for *n*-hexane, and 150°C for *p*-xylene, *o*-xylene and 1,2,4-trimethyl benzene. The adsorbates were fed by saturators as described in Section 3.1.3.1, which were kept at 0°C using an ice-bath. The partial pressures for *n*-hexane, *p*-xylene, *o*-xylene and 1,2,4-trimethyl benzene were 60.4, 2.36, 1.72 and 0.52 mbar respectively. The carrier gas flowrate through the saturator was 30 ml/min nitrogen. The adsorption times were 60 min for *n*-hexane, and 300 min for *p*-xylene, *o*-xylene and 1,2,4-trimethyl benzene.

All four compounds were adsorbed without changing the sample, the sample being calcined each time to remove the previously adsorbed compound. Usually the following order was used for adsorption: *p*-xylene, *o*-xylene, *n*-hexane and 1,2,4-trimethyl benzene. The moisture content of the sample could be obtained from the weight loss during the first calcination.

3.2.2.2 Nitrogen adsorption (N_2-BET)

The micropore volume of the samples was determined using a Micromeritics ASAP 2000. 0.5 g of sample was dried at 350°C under vacuum. Nitrogen was then adsorbed at liquid nitrogen temperatures at a rate of 3 ml per step until ambient pressure was reached.

3.2.3 CATALYST COMPOSITION

3.2.3.1 Atomic absorption spectroscopy (AA)

Zeolite aluminium, silicon and sodium contents were determined by atomic absorption spectroscopy. A Varian Spectra AA-30 spectrometer, attached to a DS 15 data station was used to obtain the measurements. In most cases the ion exchanged (NH_4- or H-) form of the catalyst was used for these analyses.

The samples were prepared by placing a 100 mg sample in a Teflon Parr bomb. The sample was wetted with a few drops of deionized H_2O. 4 ml of cold 40% HF was added to the sample. The Parr bomb was heated in an oven at 70°C for 16 h to digest the zeolite, after which it was cooled to room temperature. The solution was transferred to a polypropylene volumetric flask, and the solution was made up to 50 ml with deionized H_2O. To obtain silicon readings the solution was diluted further to 1 part solution per 19 parts deionized H_2O.

To obtain aluminium standards the matrix of the standards needed to be matched with the matrix found in the solutions to be analyzed. The standards were prepared by using an equivalent amount of silicon (in the form of 99.9% pure SiO_2) to the amount of silicon that would be expected in the zeolite sample. The amount of silicon expected in the sample could be calculated from

the unit cell formula of the zeolite (e.g. see Section 2.1.1.5. for the unit cell formula of ZSM-5). The required amount of SiO_2 was placed in a Teflon Parr bomb. The SiO_2 was wetted with a few drops of deionized H_2O and 4 ml of cold 40% HF was added to the sample. The Parr bomb was heated in an oven at 70°C for 16 h to digest the SiO_2, after which it was cooled to room temperature. The solution was transferred to a 50 ml polypropylene volumetric flask. For a concentration range of 0, 20, 40, 100 and 200 μg/ml, 0, 1.0, 2.0, 5.0 and 10.0 ml of 1000 PPM Al standard solution were added to the 50 ml volumetric flasks respectively. The solutions were made up to 50 ml with deionized H_2O.

Standards for sodium were prepared similarly to the aluminium standards. However, it was not necessary to match the matrix for the silicon standards, as the aluminium and sodium concentrations were low compared to those of silicon. Hence silicon standards were prepared simply by diluting 1000 PPM Si standard solution to the required concentrations.

The following standards were used:

- Al	0	20	40	100	200	μg/ml
- Si	0	10	40	100	200	μg/ml
- Na	0	0.5	1.0	1.5	3.0	μg/ml

A sample calculation of the theoretical aluminium and silicon content of ZSM-5 is given in Appendix III. A sample calculation of the AA results can be found in Appendix IV.

3.2.3.2 Temperature programmed desorption of pyridine and 4-methyl quinoline (Py-TPD and MQ-TPD)

The apparatus used for these TPD studies was built for this project, and consisted of a heated TPD cell which could be evacuated by means of a vacuum line. It allowed the use of different sized adsorbates, such as NH_3, pyridine (Py) and 4-methyl quinoline (4MQ), to probe different areas on the zeolite surface. The apparatus was also used for the deposition of TEOS under

vacuum conditions. A mass selective detector was used for analysis. Quantitative measurements for all adsorbates could not always be made using a mass selective detector (refer to Section 3.5.3 for discussion). However, quantitative NH_3-TPD measurements were made using the apparatus and procedures described in Section 3.2.3.3 using a thermal conductivity detector, and these values were used to cross-calibrate the two TPD instruments. The operating procedures used to obtain NH_3-TPD spectra using either apparatus is described in Section 3.2.3.3. Only operating procedures to obtain Py-TPD and MQ-TPD spectra will be discussed here. The vacuum line and mass selective detector are described in more detail in Section 3.5.

(i) Sample preparation

When the adsorbate to be used was pyridine, the sample was mixed with approximately 1 g of quartz particles (70 - 212 micron) before it was placed in the TPD cell. This was done for the following reasons (brackets indicate why this did not apply to MQ-TPD studies for practical reasons):

- Because small catalyst samples were used, typically 0.1 g, it ensured that the thermocouple was in the catalyst bed (using 1 g of catalyst for MQ-TPD studies ensured that the thermocouple was in the catalyst bed).
- The quartz particles acted as a heat sink during adsorption and desorption (only a small amount of 4MQ adsorbed onto the catalyst).

To prevent catalyst particles from being swept away in the carrier gas stream, a plug of quartz wool was placed on top of the catalyst bed. These procedures did not affect the TPD spectra in any way.

(ii) Experimental procedures and conditions

The experimental conditions and procedures of a typical TPD experiment are described in the section below for each of the adsorbates. Table 3.7 summarizes typical TPD parameters. Unless otherwise stated in the text, these parameters applied throughout this study. The parameters differed for each

adsorbate, and were chosen to ensure saturation of the sample and complete removal of the physisorbed material while maintaining concentration levels within the detectable range. For example, the catalyst mass and carrier gas flowrate for MQ-TPD experiments differed from Py-TPD experiments in order to obtain detectable signals in the MS. Adsorption temperatures and evacuation times also varied according to the requirements of each system. Conditions for 4MQ are given in brackets where different to Py.

Typically 0.10 g of sample, mixed with 1 g quartz particles, was placed in the TPD cell (1.0 g of sample without quartz particles for 4MQ). The sample was calcined in air at 500°C at a flowrate of 60 ml/min for 8 h, after which the sample was cooled to the required adsorption temperature (200°C for Py, 100°C for 4MQ). The sample was evacuated for 2 h at the adsorption temperature, or until the pressure had been decreased to less than 10^{-4} mbar.

An ice bath was placed around the adsorbate storage reservoir to keep the adsorbate temperature at 0°C, thereby ensuring a constant partial pressure in all experiments (± 5.2 and ± 0.5 mbar for Py and 4MQ respectively). The sample was exposed to Py for 1 h or in the case of 4MQ for 3 h.

After adsorption the sample was evacuated for 1 h at the adsorption temperature (200 and 100°C for Py and 4MQ respectively) to remove physisorbed material. The sample was flushed in helium at a flowrate of 100 ml/min (40 ml/min for 4MQ) for up to 2 h. During this flushing stage the internal standard was used to obtain a response-line. The response-line was obtained by introducing a 1 mol% Ar/He mixture (3 ml/min) into the carrier gas stream, and measuring the intensity of the argon signal for approximately 20 - 30 min at steady state conditions.

The line connecting the vacuum line to the GC/MS was heated to 150°C (280°C for 4MQ) to prevent condensation of desorbing species. In the case of Py, the sample was cooled to 150°C to ensure that the temperature ramp was linear before the start of the desorption. In the case of 4MQ the adsorption temperature was sufficiently low when initiating the temperature ramp. The furnace was ramped at 10°C/min up to a maximum of 1050°C in helium at a flowrate of 100 ml/min (40 ml/min for 4MQ). The signal was detected by mass selective detector.

(iii) Data work-up

Regular calibration experiments were carried out to calibrate the TPD apparatus for Py-TPD and MQ-TPD spectra. The system was calibrated for pyridine using a standard HZSM-5 sample of which the total number of acid sites per gram of sample was known accurately. The signal obtained for the standard sample could be thus converted to give a *Calibration Factor*, which represents the area count equivalent to 1 mmol of pyridine.

The response-line obtained using the internal standard accounted for daily variations in the mass spectrometer response signal. Hence the *ratio of the internal standard response-lines* of the calibration and unknown samples adjusted the signal for the daily variations in the mass spectrometer response signal.

Therefore, the number of acid sites of the unknown sample was obtained by relating its area count to the calibration factor adjusted by the internal standard ratio, as given by the relationship below:

$$[\text{mmol/g}] = \text{Area Count} \times \text{Internal Std. Ratio} / \text{Calibration Factor}$$

It was not possible to obtain accurate values of the number of acid sites on the external surface (see Section 4.2.1.2). Therefore these data are presented as relative values compared to a reference sample. Hence the percentage relative external surface acidity (RESA) is obtained as given below:

$$\%\ \text{RESA} = 100 \times \text{Area Count} \times \text{Internal Std. Ratio} / \text{Area Count of Reference}$$

The apparatus was calibrated prior to analysis of a series of samples, because the calibration factor changed significantly when samples was analyzed with a long time period between analyses. This change could be due to routine maintenance, changes in electron multiplier voltage of the instrument or when the mass spectrometer was used for other studies between the analysis of TPD samples.

Calibration factors, internal standard ratios and area counts of Py-TPD and MQ-TPD spectra are given in Appendix VI and VII respectively.

3.2.3.3 Temperature programmed desorption of ammonia (NH_3-TPD)

To obtain quantitative data of the number of acid sites, as measured by mmol of NH_3 per gram of catalyst, ammonia temperature programmed desorption (NH_3-TPD) studies were carried out using the apparatus and procedures described below. This standard TPD system did not permit the use of adsorbates other than NH_3. The apparatus described here was used mainly to cross-calibrate NH_3-TPD spectra obtained using this standard NH_3-TPD apparatus with spectra obtained using the procedures described in section 3.2.3.2 in which NH_3, pyridine and 4-methyl quinoline could be used as adsorbates.

NH_3-TPD spectra were recorded in the range 100 - 700°C. The sample was placed in a tubular quartz reactor (300 mm long, 14 mm I.D.), which was heated by a suitable furnace. 0.25 g of catalyst was placed in the quartz TPD cell. The sample was calcined in air (45 ml/min) at 500°C for 4 h. The sample was cooled to 150°C for NH_3 adsorption. NH_3/He (1 mol% NH_3) was passed over the sample kept at 150°C for 1 h at a flowrate of 70 ml/min. The sample was flushed for 16 h with helium (70 ml/min) at the adsorption temperature to remove physisorbed NH_3. The furnace was ramped linearly at 10°C/min from the adsorption temperature to 700°C in helium (70 ml/min). The signal was detected by a suitably calibrated thermal conductivity detector (TCD). The furnace was driven by computer which was also used to store data. Back titration was used to confirm the results obtained using the TCD.

TABLE 3.7: Typical variables used in TPD studies

TPD parameters		NH_3 (1)	Py (2)	4MQ (2)
catalyst mass	(g)	0.25	0.10	1.00
adsorption temp.	(°C)	150	200	100
adsorption time	(h)	1	1	3
evacuation temp.	(°C)	–	200	100
evacuation time	(h)	–	1	1
flushing time	(h)	16	2	2
helium flow rate	(ml/min)	70	100	40
internal std. flow rate	(ml/min)	–	3	3

NOTE: Py = pyridine ; 4MQ = 4-methyl quinoline

(1) TPD parameters for NH_3-TPD studies using a thermal conductivity detector or mass selective detector.

(2) TPD parameters for Py-TPD and MQ-TPD studies using a mass selective detector.

3.3 TETRAETHOXYSILANE DEPOSITION STUDIES

3.3.1 TEMPERATURE PROGRAMMED REACTION STUDIES

The deposition of tetraethoxysilane (TEOS) was studied to determine the main decomposition species during a temperature ramp on HZSM-5 and Silicalite-I. 0.2 g of the sample was calcined in flowing air (30 ml/min) at 500°C for 8 h. TEOS was fed by saturator (30 ml/min helium carrier gas) and passed over the sample. The vapour phase flow method of TEOS deposition was used as described in Section 3.1.3.1, with the exception that the temperature of the sample was raised linearly from 50°C to 500°C at 5°C/min while TEOS was being passed over the sample. A non-separating polyimide deactivated fused silica capillary column was used to bleed off part of the product stream, which was analyzed continuously using a mass spectrometer.

3.3.2 ISOTHERMAL REACTION STUDIES

The isothermal deposition of tetraethoxysilane (TEOS) was studied at relatively low (50°C) and relatively high (400°C) temperatures on ZSM-5, Silicalite-I and silica. The vapour phase flow method of TEOS deposition was used as described in Section 3.1.3.1.

0.2 g of the sample was calcined in flowing air (30 ml/min) at 500°C for 8 h. TEOS was fed by saturator (30 ml/min helium carrier gas) and passed over the sample at 50°C or 400°C. When steady state was reached the samples were regenerated (30 ml/min air, 500°C, 2 h) after which the deposition cycle was repeated. Up to 3 deposition-regeneration cycles were used. The sample was subsequently calcined in flowing air (30 ml/min) at 500°C for 8 h to remove adsorbed carbonaceous residues. The product stream was analyzed by mass spectrometer during the course of each deposition cycle, specifically monitoring the main decomposition products as determined by the temperature programmed reaction studies (Section 3.3.1). A non-separating polyimide deactivated fused silica capillary column was used to periodically bleed off part of the product stream, which was analyzed using a mass spectrometer.

3.3.3 THERMOGRAVIMETRIC ANALYSIS

The weight gain during tetraethoxysilane (TEOS) deposition on HZSM-5 was measured using a Stanton Redcroft STA-780 Series Thermal Analyzer at different temperatures. 50 mg of the sample was calcined in air (30 ml/min) at 500°C for 1 h. TEOS was fed by saturator (30 ml/min N_2 carrier gas, part. press. ± 0.5 mbar) for 10 h at the deposition temperature, viz. 100, 270 or 450°C. The sample was subsequently again calcined in air (30 ml/min) at 500°C for 1 h.

3.4 THE CONVERSION OF 1,3,5-TRIISOPROPYL BENZENE

The conversion of 1,3,5-triisopropyl benzene (TiPB) was studied to investigate the external surface activity of selected samples. The kinetic diameter of TiPB is 8.5 Å [Hibino *et al.*, 1991] and it has been shown that cracking of TiPB takes place only on the external surface of ZSM-5 [Namba *et al.*, 1986] and of Mordenite [Hibino *et al.*, 1993] (Section 2.2.1.6).

3.4.1 EXPERIMENTAL APPARATUS

The equipment used for these studies was a multi-purpose probe reaction system, in which it was possible to feed different reactants and an internal standard using dosing systems (Figure 3.4). Each dosing system consisted of a gas feed with an in-line filter, a mass flow controller protected by a one-way valve, and a thermostated saturator. Each saturator could be by-passed. The pressure in the saturators could be controlled using needle valve N1 (Figure 3.4) and pressure sensor. The feed gas proceeded through both an axial and a radial mixer before entering the reactor. The reactor inlet and by-pass pressures were controlled using needle valves N3 and N2 respectively in combination with the upstream pressure sensor (Figure 3.4). The reactor was situated in a kiln, thereby minimizing temperature gradients. The reactor product stream and internal standard stream were mixed using a radial mixer, before passing through an ampoule sampler [Schulz and Nehren, 1986] used for analysis of the products. Finally the product stream passed through a condenser kept at 15°C and a bubble flow meter before being vented (Figure 3.4). The feed, product and internal standard lines were heated to 120°C.

3.4.1.1 The reactor

The reactor consisted of a stainless steel tube of 80 mm length (10 mm I.D., 12.5 mm O.D.). The reactor was operated in down-flow mode. A thermowell (3.1 mm O.D.) was situated centrally in the reactor. The reactor was packed with washed, catalytically inert quartz sand particles in three zones: (i) 4.0 g quartz sand (± 30 mm length) was packed in the upstream part of the reactor,

(ii) 2.9 g quartz sand mixed with 0.1 g sample (± 23 mm length) was packed in the central part of the reactor, and (iii) 3.0 g quartz sand (± 23 mm length) was packed in the downstream part of the reactor. The purpose of the packing procedure was to avoid channelling effects, maintaining isothermal conditions, decreasing the dispersion and enhancing the consequent plug flow behaviour of the catalyst bed. Glass wool plugs were used to keep the packing in place.

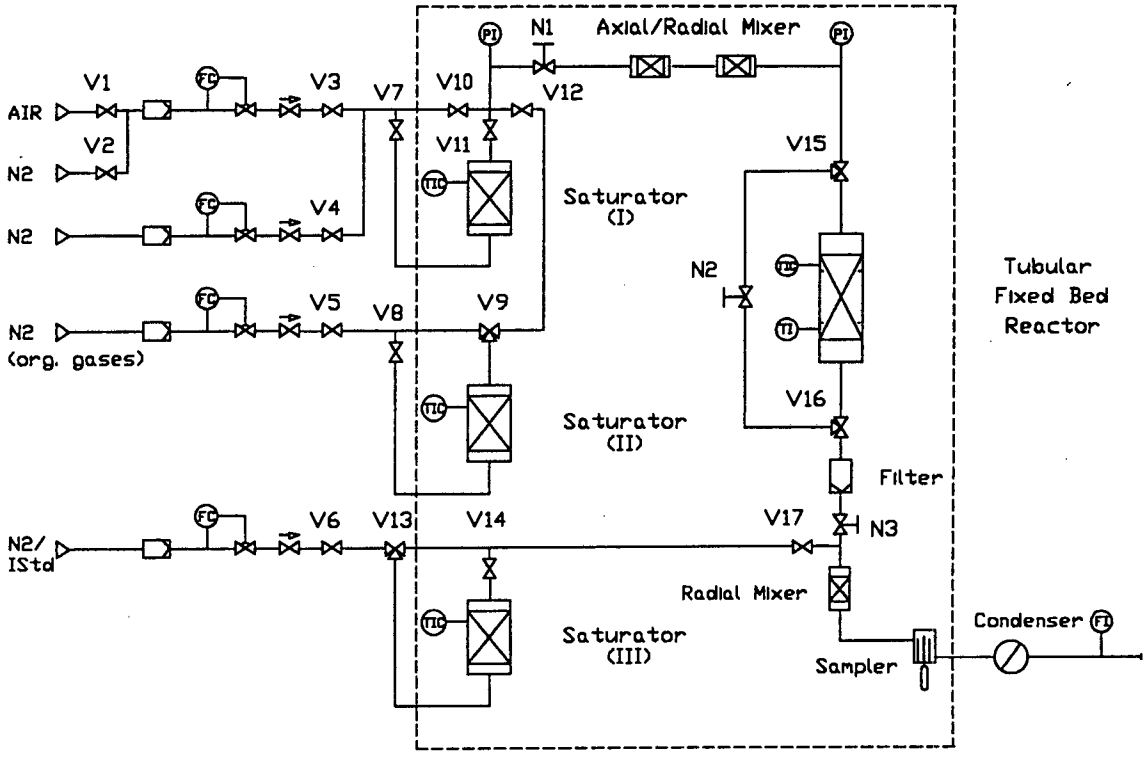

FIGURE 3.4: Flowsheet of the experimental apparatus used for the conversion of 1,3,5-triisopropyl benzene

3.4.1.2 The saturators

The saturators consisted of an upper and a lower compartment (Figure 3.5). The upper compartment was packed with Chromosorb which was saturated

with the substance to be dosed. The gas feed passed through the saturated Chromosorb bed, ensuring good contact between gas and liquid and reducing pulsation effects commonly found in simple bubble saturators. The saturators were operated in up-flow mode to avoid increasing the pressure drops due to compression of the Chromosorb bed. The upper compartment could be heated or cooled using a water jacket surrounding the Chromosorb bed. The lower compartment of the saturator consisted of a reservoir containing the substance to be dosed. The Chromosorb packing was in contact with the liquid in the reservoir. Due to capillary forces the liquid was transported into the Chromosorb bed maintaining a constant loading. The upper and lower compartments were pressure equilibrated.

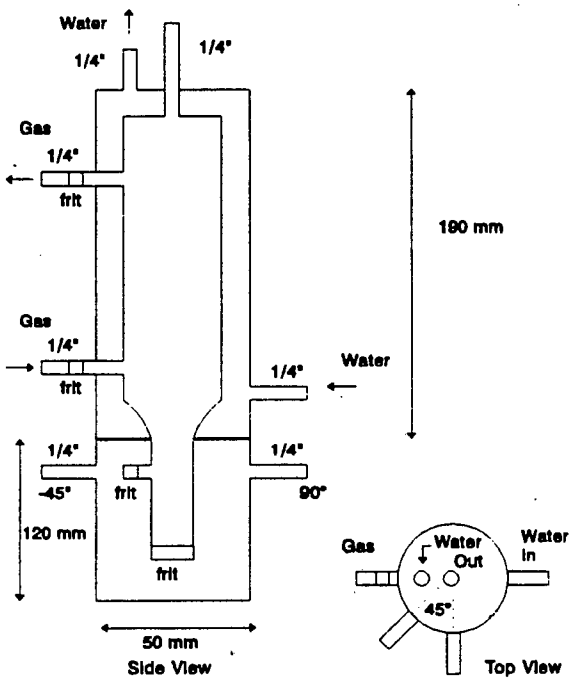

FIGURE 3.5: The saturator

3.4.1.3 The ampoule sampler

This technique of capturing and analyzing gas samples was developed by Schulz and Nehren [1986] and is described in detail in this reference. Glass ampoules were evacuated prior to use, and the capillary of the ampoule was inserted into

the gas stream through the septum of the ampoule sampler. The tip of the capillary was broken, enabling the product gas to fill the evacuated ampoule. The capillary was sealed immediately using a spot flame. This technique decoupled sampling from analysis and samples could be stored over long periods of time, and also allowed frequent capturing of gas samples. The gas samples contained in the glass ampoules were analyzed by breaking the ampoule in a heated ampoule breaker connected to the gas chromatograph via a 6-way valve. The GC carrier gas could either by-pass the ampoule breaker or transport the gas sample to the GC for analysis.

3.4.2 EXPERIMENTAL PROCEDURE

3.4.2.1 Conditions and procedures

The reactor was packed with 0.1 g sample as described in Section 3.4.1.1. The sample was calcined at 500°C for 6 h in air (80 ml/min). Reaction temperatures were chosen to ensure a conversion of 50 - 100 % for the respective parent samples. After calcination the sample was cooled to the reaction temperature (270°C for ZSM-5, 200°C for Mordenite and 160°C for Beta) and air was replaced with nitrogen. The feed and product lines were kept at 120°C. The pressures of the reactor inlet and by-pass lines were adjusted. The TiPB feed (T_{sat} = 60°C, 92 ml/min nitrogen carrier gas, WHSV = 0.6 h^{-1}, partial pressure = 1.7 mbar) and cyclo-hexane internal standard (T_{sat} = 15°C, 8 ml/min nitrogen carrier gas) saturators were switched on-line and the flows were stabilised for ± 4 h while by-passing the reactor. The TiPB saturator head pressure was kept 100 mbar above the reactor inlet pressure. The time at which the flows were switched from by-pass to the reactor was defined as being zero time-on-stream. TiPB was reacted for 60 min at the reaction temperature. Gas samples were taken every 10 min using the ampoule system and were analyzed with a 100 m, 0.32 mm I.D. RH-1 column and a Varian 3300 Gas Chromatograph.

3.4.2.2 Data work-up

From the GC spectra, the conversions were calculated using the ratios of the reactant feed (TiPB) area (A_{tipb}) and the internal standard (cyclo-hexane) area (A_{is}) at time = t and for the by-pass samples:

where $Rc_t = [A_{tipb} / A_{is}]_t$ (t = time)

$Rc_{bp} = [A_{tipb} / A_{is}]_{bp}$ (bp = by-pass)

and

$$\text{Conversion (\%)} = 100 \times [1 - (Rc_t / Rc_{bp})]$$

The mass balances were obtained using the ratios of the total area (A_{tot}) minus the area of cyclo-hexane (A_{is}) divided by the total area at time = t and for the by-pass samples:

where $Rm_t = [(A_{tot} - A_{is}) / A_{tot}]_t$ (t = time)

$Rm_{bp} = [(A_{tot} - A_{is}) / A_{tot}]_{bp}$ (bp = by-pass)

and

$$\text{Mass Balance (\%)} = 100 \times [Rm_t / Rm_{bp}]$$

The accuracy of the mass balance calculation decreases with increasing coke formation. However, coke formation does not influence the calculation of the conversions.

3.5 THE VACUUM SYSTEM

The apparatus used for temperature programmed desorption studies and for the chemical vapour deposition using a static vacuum system was constructed for this project. It allowed the use of different adsorbates, such as NH_3, pyridine (Py) and 4-methyl quinoline (4MQ), to probe the internal or external surface areas of the zeolite during TPD studies and the use of tetraethoxysilane (TEOS) for modification of samples by means of chemical vapour deposition.

3.5.1 EXPERIMENTAL APPARATUS

The apparatus used for temperature programmed desorption studies and for chemical vapour deposition using a static vacuum system consisted of a heated sample cell, which could be evacuated by means of a vacuum line. An on-line mass spectrometer was used as detector. Appendix I lists all items of equipment used to build the apparatus. Figure 3.6 shows a schematic of the apparatus.

3.5.1.1 The vacuum line

The vacuum line consisted of a borosilicate glass vacuum line (25 mm diameter). The vacuum was supplied by a rotary pump and an oil-diffusion pump. The vacuum was monitored using a Pirani and a Penning vacuum gauge. Four pairs of glass reservoirs were attached to the vacuum line. Each pair of reservoirs was used to purify and store a liquid adsorbate (such as pyridine or 4-methyl quinoline) or tetraethoxysilane used for chemical vapour deposition. A liquid nitrogen trap was used to trap condensable contaminants and adsorbates before entering the diffusion pump. A quartz TPD cell, or reactor, could be inserted into the vacuum line and could be attached using Cajon fittings. Stopcocks isolated various sections of the vacuum line. Data of leak testing can be found in Appendix I.

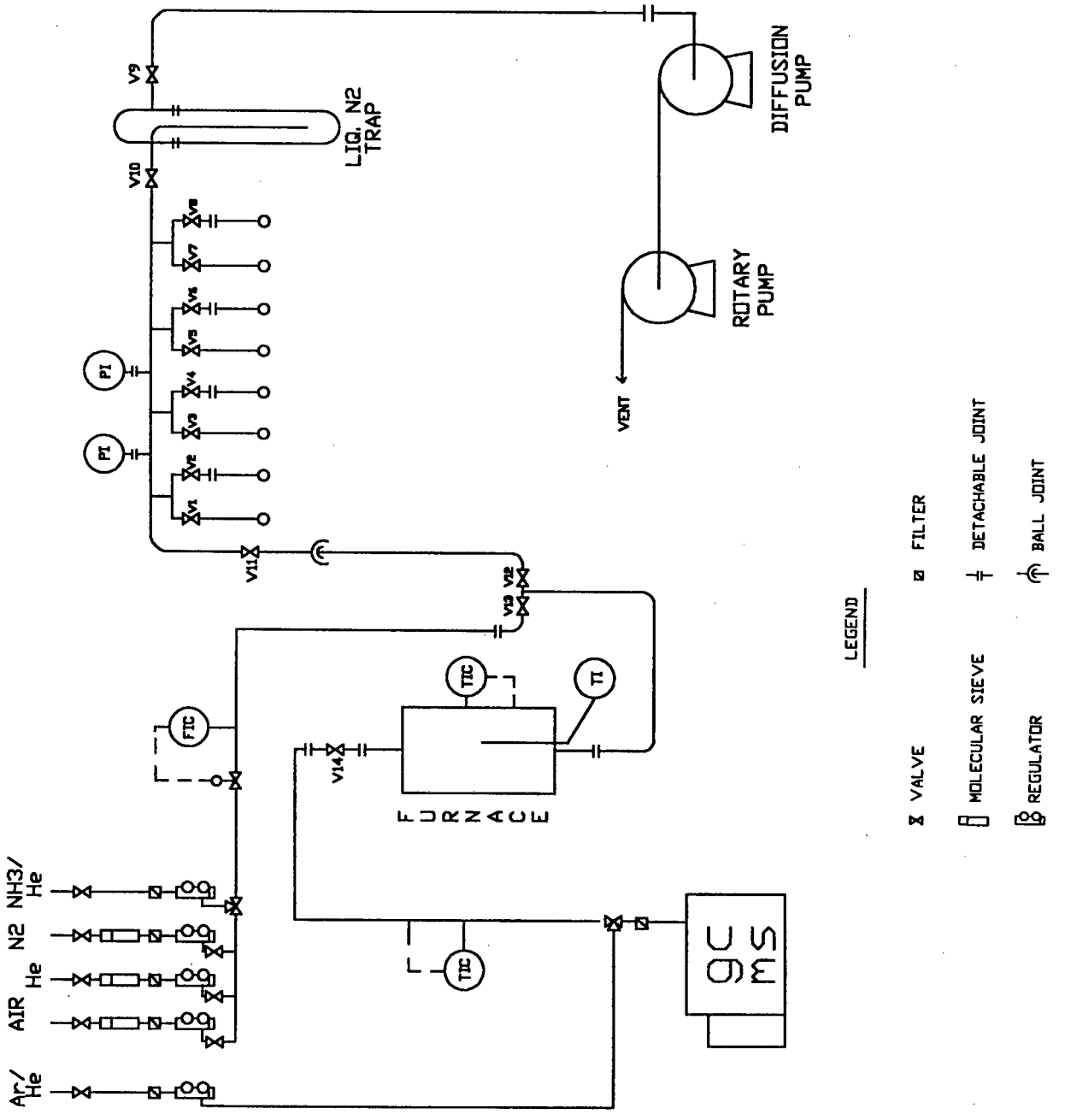

FIGURE 3.6: Schematic of the apparatus used for ammonia, pyridine and 4-methyl quinoline Temperature Programmed Desorption studies and for modification by means of chemical vapour deposition

3.5.1.2 The furnace

The configuration of the furnace can be found in Appendix I. The temperature of the furnace was controlled using a temperature programmer. The thermocouple used to control and monitor the temperature was placed in the thermowell of the reactor cell, thus ensuring that the temperature ramp of the sample was accurate. Appendix I shows a profile of the temperature ramp. As can be seen from this profile, the temperature of the sample could be ramped linearly from ambient temperatures to above 1000°C using a range of temperature ramps. All the thermocouples and temperature controllers were calibrated prior to use.

3.5.1.3 The reactor cell

The reactor cell was a 350 mm long, 10 mm I.D. quartz tube, with a 2 mm I.D. thermowell, as shown in Figure 3.7.

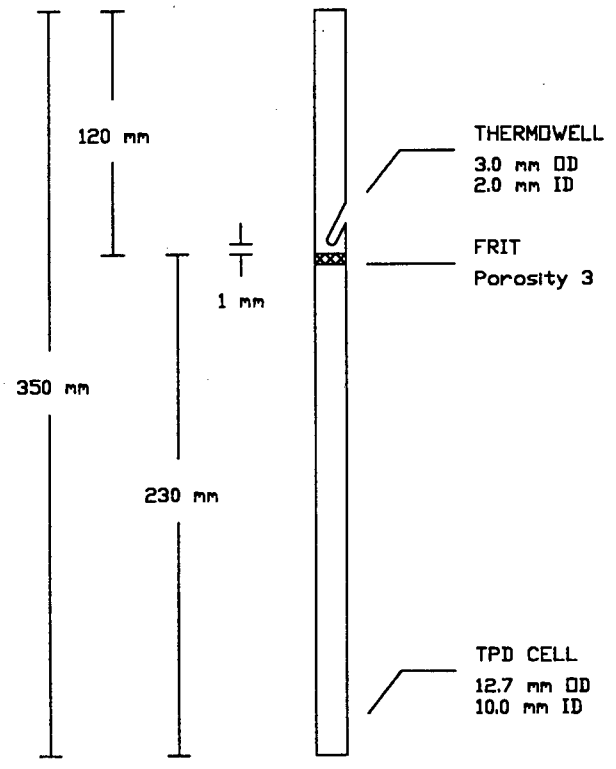

FIGURE 3.7: The reactor cell

3.5.1.4 The carrier gas transfer lines

Several carrier gases were available for use. Air was used for calcination purposes, helium was used during the desorption stage and a NH_3/He mixture (1 mol% NH_3) could be used to adsorb NH_3 onto the catalyst. The gases passed through a 3A molecular sieve and a filter prior to a regulator. The gas flowrate was monitored and controlled using a mass flow controller common to all carrier gases. The mass flow controller was calibrated for helium prior to use. The carrier gases passed through a 1/8 inch stainless steel feed line attached to the vacuum line. An 1/8 inch stainless steel tube connected the vacuum line to the GC/MS. This line was heated to prevent condensation in or adsorption onto the walls of the tube by the adsorbates. An in-line filter prevented contamination of the GC/MS.

3.5.1.5 The internal standard

A 1 mol% argon/helium mixture (3 ml/min) was introduced after the reactor cell, and was used as an internal standard to account for day-to-day changes in sensitivity of the detector for the TPD studies. The gas flowrate was monitored and controlled using a mass flow controller.

3.5.1.6 Signal detection

The total flow entering the GC was split. Only a small fraction, typically 1/100 - 1/250, entered a 15 m long, 0.22 mm I.D. polyimide coated deactivated fused silica capillary column. By adjusting the column head pressure the flow to the MS through the capillary column could be regulated. A Hewlett Packard 5971A Mass Selective Detector was used to monitor the abundance of the ions of the species desorbed from the sample versus time.

Signal recording was initiated after the temperature ramp had been commenced in order to correct for the lag time between the sample and the detector (1 min for NH_3 and Py, 1.5 min for 4MQ). The lag time was due mainly to the time that was required for the signal to travel through the 15 m long GC column. The signal could be adjusted to account for the split ratio (typically 100/1 - 250/1) prior to the GC column or for changes in catalyst mass and carrier gas

flowrate. The time scale was converted to a temperature scale. The gas chromatograph and mass spectrometer settings typically used in these studies are given in Table 3.8.

TABLE 3.8: Gas chromatograph and mass spectrometer settings

GC/MS SETTINGS		NH_3	Py	4MQ
oven temp.	(°C)	150	150	280
detector temp.	(°C)	280	280	280
column head pressure	(psi)	5	5	5
split vent flow	(ml/min)	67	97	37
purge vent flow	(ml/min)	2	2	2
column flow	(ml/min)	1	1	1
dwell time	(sec)	0.985	0.985	5.000
cycle time	(sec^{-1})	0.167	0.167	0.1
total ion maximum		$5x10^7$	$5x10^7$	$5x10^7$
ion maximum		$5x10^6$	$5x10^6$	$5x10^6$
EMVolts		varied	varied	varied
solvent delay	(min)	0	0	0
max. run time	(min)	90	90	95

3.5.2 REAGENT PREPARATION

As mentioned before, the carrier gases were dried using 3A molecular sieves, and passed through a 2 micron filter before use. The liquid adsorbates, such as pyridine and 4-methyl quinoline, were purified by vacuum distillation prior to use. The adsorbate was placed in one of the detachable reservoirs of the vacuum line (Figure 3.6). The adsorbate was heated while being evacuated until approximately 1/3 of the material had been distilled and collected in the liquid N_2 trap of the vacuum line. The adsorbate was then heated further, but the liquid N_2 trap was isolated, and a liquid N_2 dewar was placed around the twin (non-detachable) reservoir, such that approximately a further 1/3 of the adsorbate had been collected in this reservoir. The reservoir contained 3A molecular sieves to adsorb any moisture entering the reservoir during normal operation of the vacuum line. This middle fraction was used as the pure adsorbate for the TPD studies. The fraction trapped in the liquid N_2 trap and the remaining 1/3 were discarded.

3.5.3 THE MASS SPECTROMETER AS DETECTOR

In order to understand the abilities and limitations of the mass spectrometer as a detector for studies of desorption of an adsorbate from a zeolite, a few remarks are included in this section to elucidate on these matters.

A molecule entering the mass spectrometer is ionized. The ratio of the ions formed is specific to that molecule, which can thus be identified. Data can be collected in the following two manners: (i) as a Total Ion Chromatogram (TIC), which monitors all ions in a specified range, or (ii) in the Selected Ion Mode (SIM), which monitors a few selected ions. In this study the TIC was used only to obtain the complete desorption spectrum from the sample. SIM was typically used in all other experiments, as this mode allowed more precise monitoring of ions specific to a particular compound. By choosing ions specific to a particular compound, several species could be monitored, even though they may have desorbed simultaneously. This is not always possible using a TCD or FID as detector.

Table 3.9 shows the ions detected by the mass selective detector for the internal standard, compounds desorbed in TPD studies or compounds observed in the deposition of TEOS (i.e. the experiments described in Sections 3.2.3.2, 3.3.1 and 3.3.2). The ions printed in bold typeface were found to be the two most abundant ions of each species in the desorption or product spectra of the TPD or TEOS deposition studies.

TABLE 3.9: Ions detected by mass selective detector

COMPOUND	
ammonia	**17**, **16**, 15
argon	**40**, **20**
ethylene	**28**, **27**, 26, 25, 29,
ethanol	**31**, **45**, 27, 29, 28, 43
4-methyl quinoline	143, **128**, 79, **78**, 52, 51, 50, 15
pyridine	**79**, **52**, 51, 50, 39, 27
tetraethoxysilane	208, **193**, 163, **149**, 135, 119, 79
water	**18**, **17**, 16

Care must be taken if one ion is a characteristic ion of two different compounds. For example, the three most abundant ions from H_2O are $m/e = 18$, 17 and 16; from NH_3 they are $m/e = 17$, 16 and 15. Hence, if the desorption of NH_3 is monitored from zeolites, it is not advisable to monitor $m/e = 17$ only, as desorption of H_2O from the zeolite is likely to occur, thereby increasing the signal of $m/e = 17$. Thus a judicious choice of the ions to be monitored is required. Even so, it is possible that the ions formed by the ionization of one molecule may themselves ionize other molecules when these molecules reach the detector simultaneously [Middleditch, 1979].

By monitoring the relative intensities of several ions characteristic of one molecule (using SIM), it is possible to determine whether a compound has reacted on the zeolite surface prior to reaching the detector. If the relative intensities change, or if they are not the same as for the pure compound, during the course of the desorption process, then a reaction has taken place on the surface of the zeolite. Care must be taken to check which ions are formed due to the ionization in the MS and which ions arise from reaction products.

The mass spectrometer does not have the same sensitivity to all ions. Therefore, even though the concentration of two compounds are the same, the intensity of the signal, or abundance, may in fact vary by several orders of magnitude for different ions. In this study the sensitivity to H_2O and NH_3 ions was found to be far smaller than to Py ions, probably because H_2O and NH_3 ionize to a much lesser extent than Py. However, the magnitude of the signal can be increased by increasing the concentration of the desorbed species in the carrier gas stream (by increasing the catalyst mass and/or by decreasing the carrier gas flowrate) or by increasing the dwell time (the time period during which the MS "counts" each ion).

Due to the different amounts of adsorbate desorbed for the various probes under investigation, it has been necessary to vary certain experimental parameters in order to acquire the required magnitude of the signal for each of the desorbing species. Therefore it was not always possible to relate the spectra of the different adsorbates directly.

CHAPTER 4

RESULTS

"We are protected against disillusionment by vanity and optimism"

4.1 PHYSICAL AND CHEMICAL CATALYST CHARACTERIZATION

XRD spectra of Silicalite-I, ZSM-5 and modified ZSM-5 samples were obtained using either Cu-Kα radiation (wavelength = 1.542 Å) or Co-Kα radiation (wavelength = 1.769 Å). All Mordenite, Beta and their respective modified samples were obtained using Co-Kα radiation.

4.1.1 STRUCTURE AND MORPHOLOGY OF ZSM-5

4.1.1.1 Relative crystallinity

The XRD patterns of ZSM-5 (sample Z) and Silicalite-I (sample S) are given in Figure 4.1. The XRD patterns of modified ZSM-5 samples are given in Appendix V. The main difference between ZSM-5 and Silicalite-I was the intensity of the reflections at 2θ values of 9.5° and 10.5° (using Co-Kα radiation) (Figure 4.1). These two reflections were more intense for Silicalite-I. From Figure A-V.5 in Appendix V it can be seen that samples Z_9-C-templ, Z_9-C-Na and Z_9-C-NH_4, being ZSM-5 samples coated with a Silicalite shell, showed similar increases in intensity for the reflections at 2θ values of 7.9° and 8.8° compared to sample Z_9 (using Cu-Kα radiation). None of the ZSM-5 samples modified by chemical vapour and liquid deposition methods showed any significant changes in their XRD patterns (Appendix V).

The relative crystallinities of all ZSM-5 and modified ZSM-5 samples are listed in Table 4.1, and were calculated by integrating the area of the three major peaks between 2θ values of 22-25° (using Cu-Kα radiation) or between 2θ values of 27-29° (using Co-Kα radiation), and normalizing these to the peak areas for the parent ZSM-5 sample (sample Z). The relative crystallinities of the ZSM-5 samples coated with a Silicalite shell, viz. samples Z_9-C-templ (94%), Z_9-C-Na (85%) and Z_9-C-NH_4 (89%), were found to be the lowest, although the relative crystallinities of samples Z_9-C-templ and Z_9-C-NH_4 were within the experimental error when compared to the parent batch, viz. sample Z_9 (95%). All values of the relative crystallinities for ZSM-5 samples modified by chemical vapour and liquid deposition were found to be within the experimental error. The estimated error for these data is ± 3%.

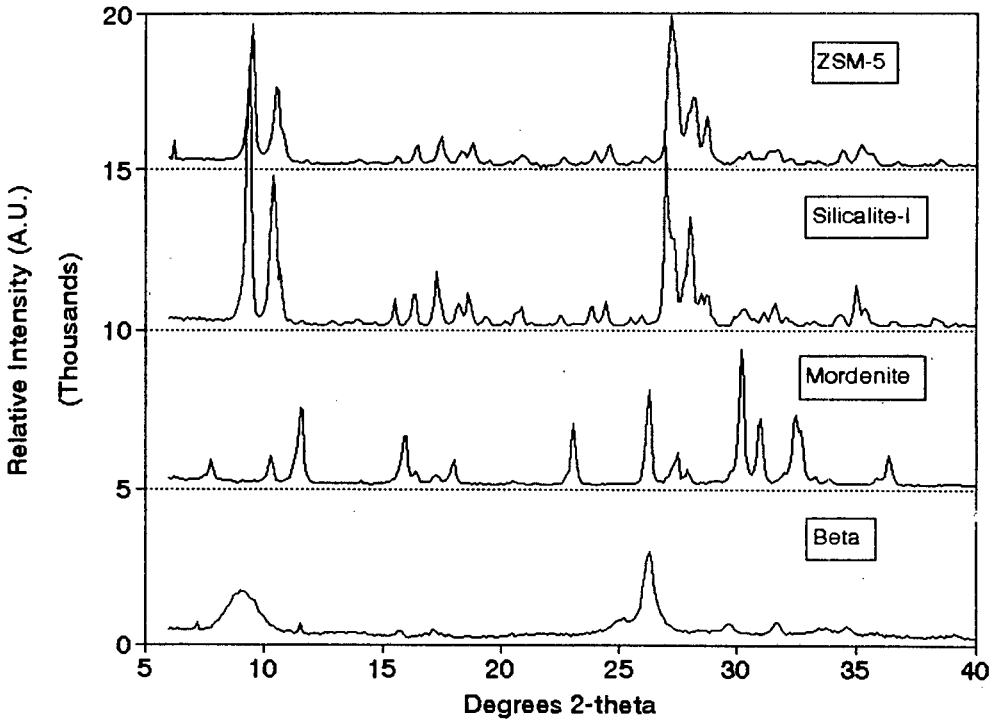

FIGURE 4.1: XRD patterns of ZSM-5 (sample Z), Silicalite-I (sample S), Mordenite (sample M) and Beta (sample B) using Co-Kα radiation

4.1.1.2 Crystallite particle size, particle size distribution and morphology

ZSM-5 crystallite particle sizes were determined from electron micrographs (Figure 4.2). The crystallite particle sizes of sample Z ranged from 1 μm to 5 μm. No significant deposits of amorphous material were seen in the micrographs at these magnifications. Some agglomeration of crystallites could be observed. No differences in crystallite particle sizes or morphologies could be observed for ZSM-5 samples modified using chemical vapour or liquid deposition techniques. The crystallite particle sizes of the samples obtained after coating the parent crystals with Silicalite shells were not noticeably larger than their parent crystals. A particle with a shell-to-core weight ratio of 1.5:1 was only expected to be 1.36 times larger than the seed crystal. Also, separate Silicalite-I crystals may have formed during the Silicalite shell coating procedure.

TABLE 4.1: Catalyst characterization of Silicalite-I, ZSM-5 and modified ZSM-5 samples

Catalyst	Si/Al ratio	Aluminium content (Al/uc)	Aluminium content (mmol/g)	Relative crystallinity (%)
S	500	0.2	0.03	102
Z	34	2.7	0.42	100
Z-V-100/60	41	2.3	0.40	101
Z-V-200/60	37	2.5	0.42	99
Z-V-300/60	39	2.4	0.38	102
Z-V-400/60	36	2.6	0.41	105
Z-V-400/4x4	42	2.2	0.38	102
Z-V-400/6x10	41	2.3	0.38	98
Z-F-50/8	43	2.2	0.39	100
Z-F-400/8	42	2.2	0.40	94
Z-L-100/-	39	2.4	0.38	97
Z-L-100/- (60h)	38	2.5	0.43	104
Z-L-0.5/W	38	2.5	0.40	104
Z-L-5/W	39	2.4	0.40	104
Z-L-5/E	36	2.6	0.44	94
Z-L-5/H	37	2.5	0.42	96
Z_9	39	2.6	0.46	95
Z_9-C-templ	81	1.2	0.19	94
Z_9-C-Na	81	1.2	0.19	85
Z_9-C-NH_4	108	0.9	0.14	89
error	± 7%	± 5%	± 5%	± 3%

NOTE: A statistical error analysis was not possible. The error listed in the table above is a non-statistical estimation, based on accuracy of the equipment and reproducibility of the measurements.

FIGURE 4.2: Electron micrographs of ZSM-5 (sample Z)

The number-based Malvern particle size distribution of the ZSM-5 batch (sample Z) is given in Figure 4.3. The particle size distribution showed two peaks, viz. at ± 2 μm and ± 4 μm. The particle size distribution was found to correspond well with the size range observed by electron microscopy. When subjected to grinding, a more Gaussian distribution was obtained with a mean particle size of ± 1.5 μm.

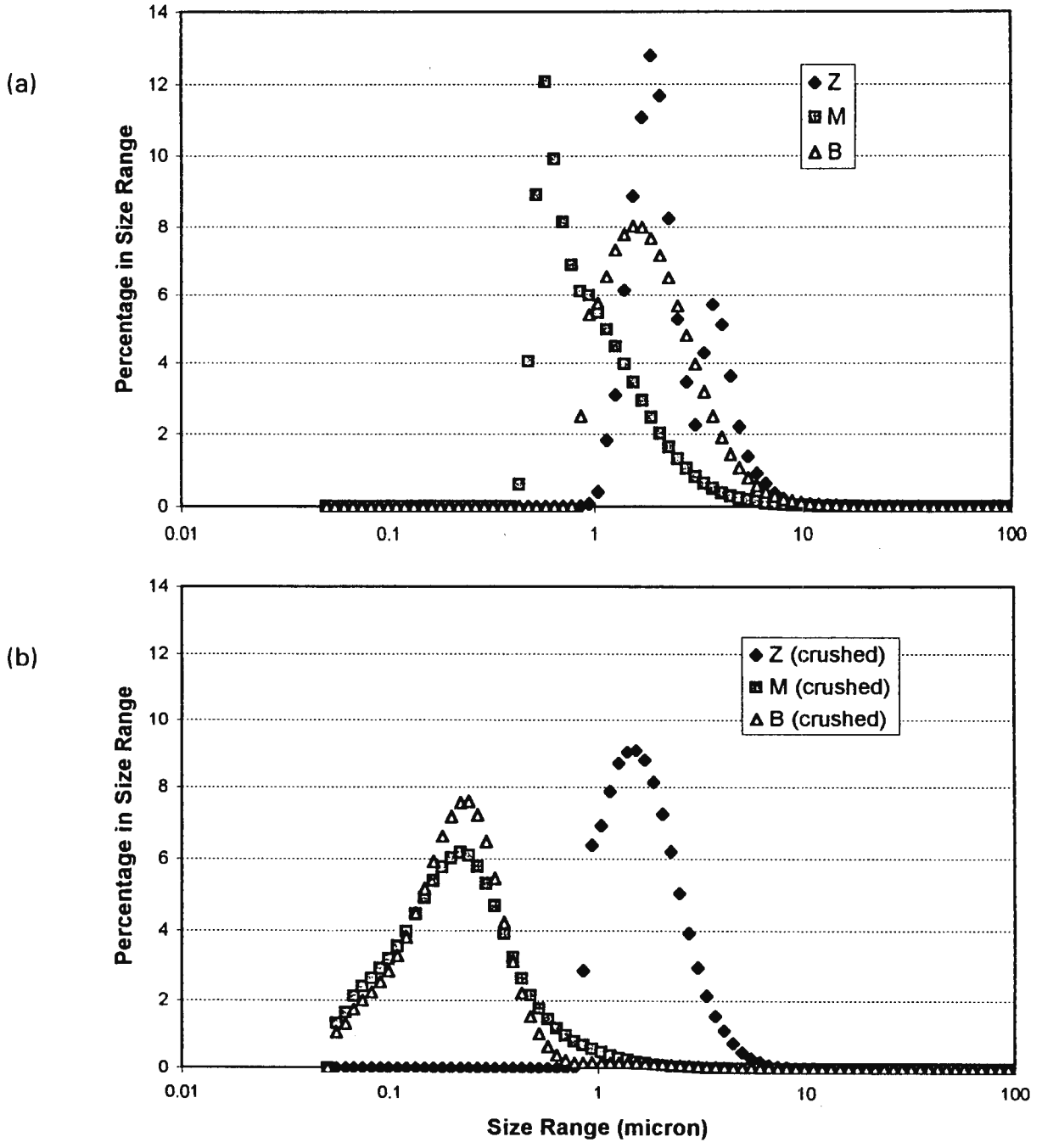

FIGURE 4.3: Particle size distributions of ZSM-5 (sample Z), Mordenite (sample M) and Beta (sample B) before (a) and after (b) being subjected to grinding

4.1.2 STRUCTURE AND MORPHOLOGY OF MORDENITE

4.1.2.1 Relative crystallinity

The XRD pattern of Mordenite (sample M) is shown in Figure 4.1. The XRD patterns of modified Mordenite samples are shown in Figure A-V.6 of Appendix V. The Mordenite samples modified by chemical vapour and liquid deposition methods did not show significant changes in their XRD patterns (Appendix V). The relative crystallinities of the Mordenite and modified Mordenite samples are listed in Table 4.2 and were calculated by integrating the areas of the five major peaks between 2θ values of 20-35° (Co-Kα radiation) and normalizing these to the peak areas for the parent Mordenite sample (sample M). The relative crystallinities of samples M-F-400/8 and M-L-5/H were 90 and 87% respectively, indicating that the relative crystallinities for these samples had decreased significantly. The estimated error for these data is ± 3%.

TABLE 4.2: Catalyst characterization of Mordenite and modified Mordenite samples

Catalyst	Si/Al ratio	Aluminium content (Al/uc)	Aluminium content (mmol/g)	Relative crystallinity (%)
M	10	4.4	1.29	100
M-V-400/60	12	3.7	1.23	95
M-V-400/6x10	11	4.0	1.18	95
M-F-400/8	13	3.4	1.15	90
M-L-5/H	12	3.7	1.17	87
error	± 7%	± 5%	± 5%	± 3%

NOTE: A statistical error analysis was not possible. The error listed in the table above is a non-statistical estimation, based on accuracy of the equipment and reproducibility of the measurements.

4.1.2.2 Crystallite particle size, particle size distribution and morphology

Mordenite crystallite particle sizes were determined from electron micrographs (Figure 4.4). The crystallite sizes ranged from 0.5 μm to 5 μm for Mordenite, but no accurate estimation of the average crystallite size could be made

because of agglomeration of the crystallites into particles. No differences in crystallite sizes or morphologies could be observed for Mordenite samples modified using chemical vapour or liquid deposition techniques.

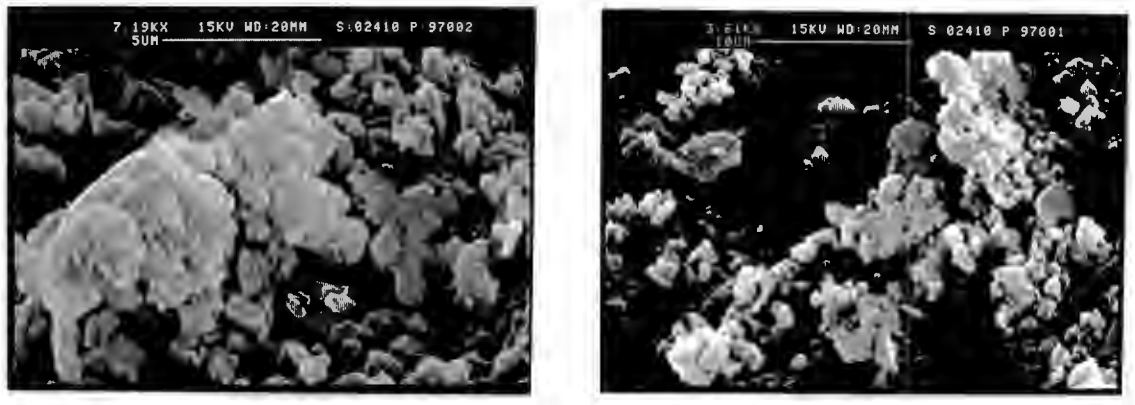

FIGURE 4.4: Electron micrographs of Mordenite (sample M)

The number-based Malvern particle size distribution of the Mordenite batch (sample M) is given in Figure 4.3. The size distribution ranged from ± 0.5 μm to 6 μm, in agreement with the size range observed with electron microscopy, although a large fraction consisted of particles smaller than 1 μm. The mean particle size was ± 0.8 μm but decreased to 0.2 μm after being subjected to grinding, indicating that crystallite agglomerates were broken up during the grinding. A Gaussian distribution was obtained after grinding the sample.

4.1.3 STRUCTURE AND MORPHOLOGY OF BETA

4.1.3.1 Relative crystallinity

The XRD pattern of Beta (sample B) is shown in Figure 4.1. The XRD patterns of modified Beta samples are given in Figure A-V.7 of Appendix V. The Beta samples modified by chemical vapour and liquid deposition methods did not show significant changes in their XRD patterns (Appendix V). The relative crystallinities of the Beta and modified Beta samples are listed in Table 4.3, and

were calculated by integrating the area of the peak at a 2θ value of 26.3° (Co-Kα radiation) and normalizing this to the peak area for the parent Beta sample (sample B). The relative crystallinity of sample B-F-400/8 was 86%, indicating that the relative crystallinity for this sample had decreased significantly compared to sample B. The relative crystallinity of sample B-L-5/H decreased to 93%. The estimated error for these data is ± 3%.

TABLE 4.3: Catalyst characterization of Beta and modified Beta samples

Catalyst	Si/Al ratio	Aluminium content (Al/uc)	Aluminium content (mmol/g)	Relative crystallinity (%)
B	18	3.7	0.84	100
B-V-400/60	19	3.2	0.81	101
B-V-400/6x10	22	2.8	0.77	95
B-F-400/8	20	3.0	0.72	86
B-L-5/H	20	3.0	0.76	93
error	± 7%	± 5%	± 5%	± 3%

NOTE: A statistical error analysis was not possible. The error listed in the table above is a non-statistical estimation, based on accuracy of the equipment and reproducibility of the measurements.

4.1.3.2 Crystallite particle size, particle size distribution and morphology

Beta crystallite particle sizes were determined from electron micrographs (Figure 4.5). The crystallite particle sizes ranged from 0.1 μm to 2 μm for Beta, but no accurate estimation of the average crystallite particle size could be made because of agglomeration of the crystallites. No differences in crystallite particle sizes or morphologies could be observed for Beta samples modified using chemical vapour or liquid deposition techniques.

The number-based Malvern particle size distribution of the Beta batch (sample B) is given in Figure 4.3, and showed a fairly Gaussian size distribution ranging from ± 0.8 μm to 10 μm. The mean particle size was ± 1.7 μm and this was found to be larger than crystallite particle sizes observed by electron microscopy. After grinding the sample, the mean particle size was reduced to

± 0.2 μm. This clearly showed that a large proportion of the crystallites was present as agglomerates.

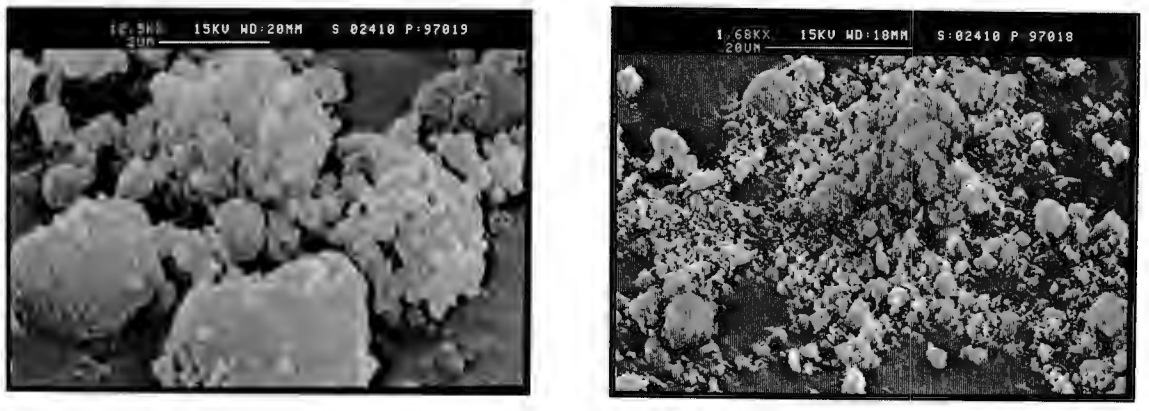

FIGURE 4.5: Electron micrographs of Beta (sample B)

4.1.4 CATALYST COMPOSITION

The silicon and aluminium content of the samples was determined by atomic absorption spectroscopy (Section 3.2.3.1). A sample calculation for the determination of the Si/Al ratio is given in Appendix IV.

4.1.4.1 ZSM-5 silicon and aluminium content

The Si/Al ratios of the Silicalite-I, ZSM-5 and modified ZSM-5 batches are shown in Table 4.1. The number of aluminium atoms per unit cell, and the number of mmol aluminium per gram of dry sample as determined by AA has also been included in Table 4.1. No sodium was detected in any of the samples after ion-exchanging with NH_4NO_3. The Si/Al ratios for the parent ZSM-5 batches were 34 and 39 for samples Z and Z_9 respectively. Trace aluminium was detected in the Silicalite-I sample (Si/Al ~ 500).

The aluminium content for CVD and CLD modified samples generally decreased slightly compared to the parent batch, although these changes were often within the experimental error, and Si/Al ratios increased correspondingly (Table 4.1). Coating sample Z_9 with Silicalite shells produced a large increase in the

Si/Al ratio from 39 to 81-108, sample Z_9-C-NH_4 having the greatest increase (Table 4.1). The aluminium reading contributed the most to the overall error (due to the low levels) and the corresponding error increased with increasing Si/Al ratio. Hence the Si/Al ratios of the samples modified by coating with Silicalite shells have a greater error associated with them than the other samples. However, the aluminium content determined by AA corresponded well with the aluminium in the synthesis mixture, as the expected value should be approximately $1/(1+1.5)$ times that of the parent sample if 1 g of ZSM-5 is reimmersed in a synthesis mixture expected to yield 1.5 g of Silicalite-I (Table 4.1).

4.1.4.2 Mordenite silicon and aluminium content

The Si/Al ratios of the Mordenite and modified Mordenite batches are shown in Table 4.2. The number of aluminium atoms per unit cell, and the number of mmol aluminium per gram of dry sample as determined by AA has also been included in Table 4.2. No sodium was detected in any of the samples after ion exchanging with NH_4NO_3. The parent Mordenite batch (sample M) had a Si/Al ratio of 10. The Si/Al ratio for CVD and CLD modified samples increased slightly compared to the parent batch. Sample M-F-400/8 (Si/Al = 13) was found to have the highest Si/Al ratio. Although the aluminium content was 1.29 mmol/g for sample M and ranged from 1.15 - 1.23 mmol/g for the modified Mordenite samples (Table 4.2), the differences were within the experimental error except for sample M-F-400/8.

4.1.4.3 Beta silicon and aluminium content

The Si/Al ratios of the Beta and modified Beta batches are shown in Table 4.3. The number of aluminium atoms per unit cell, and the number of mmol aluminium per gram of dry sample as determined by AA has also been included in Table 4.3. The parent Beta batch (sample B) had a Si/Al ratio of 18. The Si/Al ratio for CVD and CLD modified samples increased slightly compared to the parent batch, ranging from 19-22. Although the aluminium content was 0.84 mmol/g for sample B and ranged from 0.72 - 0.81 mmol/g for the modified Beta samples (Table 4.3), the differences were within the experimental error with the exception of sample B-F-400/8.

4.2 TEMPERATURE PROGRAMMED DESORPTION STUDIES

4.2.1 PRELIMINARY TEMPERATURE PROGRAMMED DESORPTION STUDIES

4.2.1.1 Choice of appropriate adsorbates

To determine the most appropriate adsorbates for temperature programmed desorption studies of the total acidity and the external surface acidity, several adsorbates were considered. Both ammonia (critical diameter = 2.4 Å) and pyridine (critical diameter = 5.1 Å) have been widely used in TPD studies (see Section 2.3) and were also used in these studies to measure the total number of acid sites of the samples. The total number of acid sites could be obtained by using adsorbates that are small enough to enter the channels of the zeolites, whereas the external surface acidity could be probed by using adsorbates which are too large to enter the channels.

(i) Diethylamine (DEA)

Figure 4.6 shows the TPD spectrum of diethylamine (DEA) from ZSM-5 (1.0 g, 40 ml/min helium, 10°C/min). Similar to findings by Parrillo *et al.* [1990], unreacted DEA was desorbed at low temperatures (T_{max} = 180°C), but at high temperatures ammonia, hydrocarbons and aromatics were observed (400 - 520°C) indicating that DEA decomposed and that the ethyl groups reacted to form hydrocarbon and aromatic species. Hence DEA was not considered further for TPD studies because quantification would not be accurate.

(ii) Tributylamine (TBA)

Figure 4.7 shows the TPD spectrum of tributylamine (TBA) from ZSM-5 (1.0 g, 40 ml/min helium, 10°C/min). No unreacted TBA was desorbed. Butene, hydrocarbons, aromatics and ammonia were observed (180 - 520°C) indicating that TBA decomposed and that the butyl groups reacted to form hydrocarbon and aromatic species. The intensity of the ammonia signal (*m/e* = 17) was low and could not be quantified accurately. Tributylamine was not considered further for TPD studies of the external surface because quantification would not

be accurate. However, the intensity of the total ion chromatogram signal for TBA was 2 orders of magnitude lower than that of DEA, suggesting that TBA was adsorbed on the external surface only.

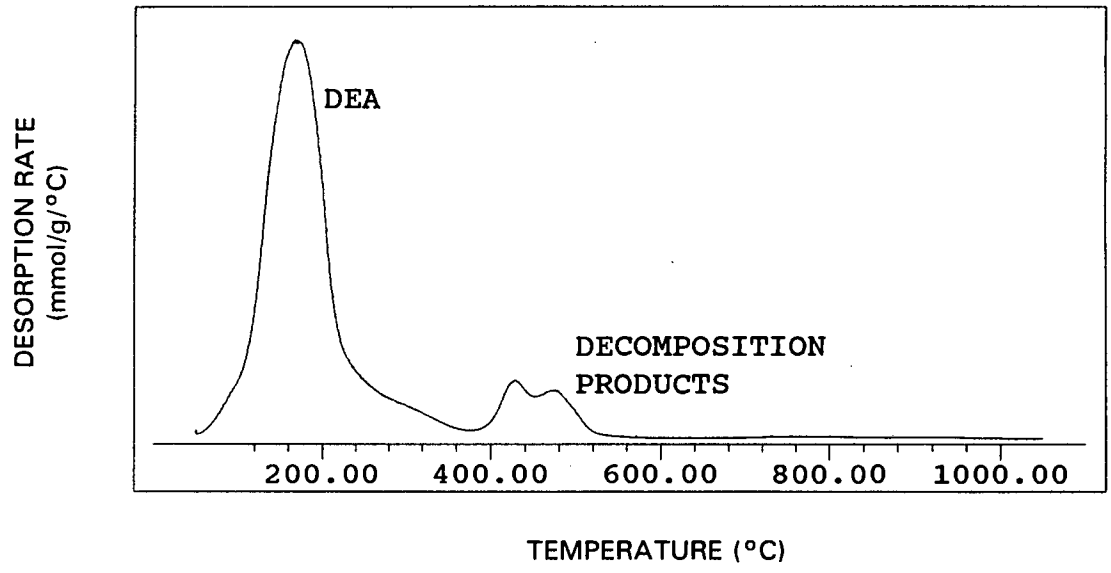

FIGURE 4.6: TPD spectrum of diethylamine from HZSM-5 (sample Z, 1.0 g, 40 ml/min helium, 10°C/min)

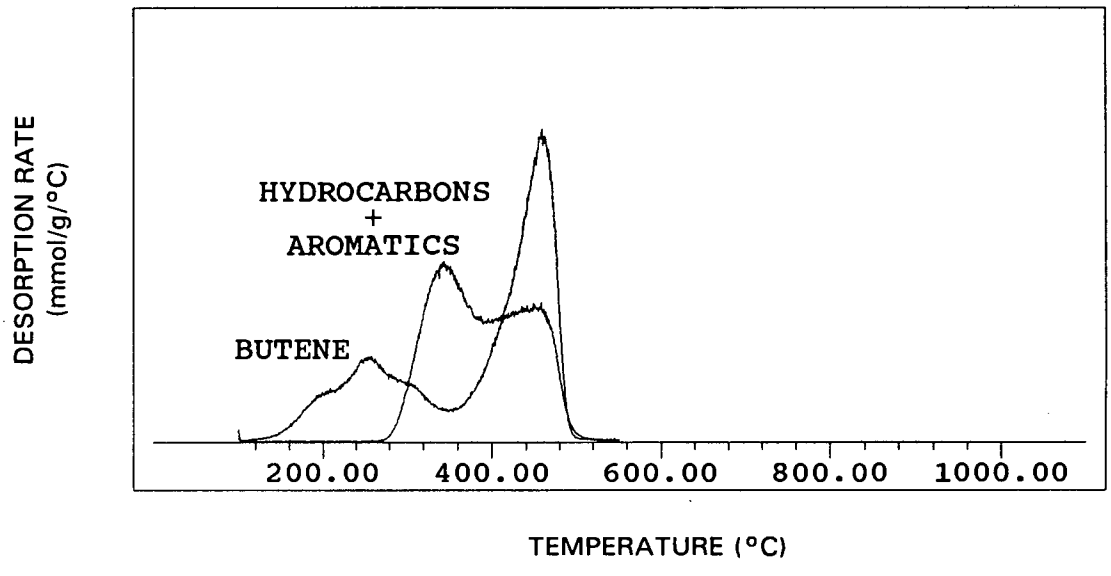

FIGURE 4.7: TPD spectrum of tributylamine from HZSM-5 (sample Z, 1.0 g, 40 ml/min helium, 10°C/min)

(iii) Quinoline

Quinoline was found to decompose primarily into benzene on desorption from HZSM-5. The benzene fraction could be used to monitor the desorption process. However, it was found that quinoline was adsorbed into the channels of HZSM-5, because the amount of quinoline adsorbed over a 24 h period was found to be 11 times greater than the amount of quinoline adsorbed over a 1 h period. Indeed, Weitkamp *et al.* [1989] have reported that naphthalene, which is similar in size and structure to quinoline, is adsorbed into the channels of ZSM-5. Therefore quinoline could not be used to determine the external surface acidity.

(iv) 4-Methyl quinoline (4MQ)

4-Methyl quinoline was also found to decompose primarily into benzene on desorption from HZSM-5. 4-Methyl quinoline was only adsorbed on the external surface of HZSM-5, because the amount of 4-methyl quinoline adsorbed was independent of the adsorption period. Whereas the decomposition products of tributylamine were not easily identifiable and the ammonia signal ($m/e = 17$) was low, when using 4-methyl quinoline the benzene fraction could be used to determine the external surface acidity. The stability of the adsorbates will be discussed in more detail in section 4.2.1.2.

4.2.1.2. The stability of the adsorbates

(i) Ammonia and Pyridine

Ammonia and pyridine did not decompose on desorption from HZSM-5 because the mass fractions detected by the mass spectrometer during TPD were identical to the mass fractions observed for pure ammonia and pyridine, thereby allowing quantification of the ammonia and pyridine TPD results. The mass fractions detected by the mass spectrometer for pyridine are shown in Figure 4.8.

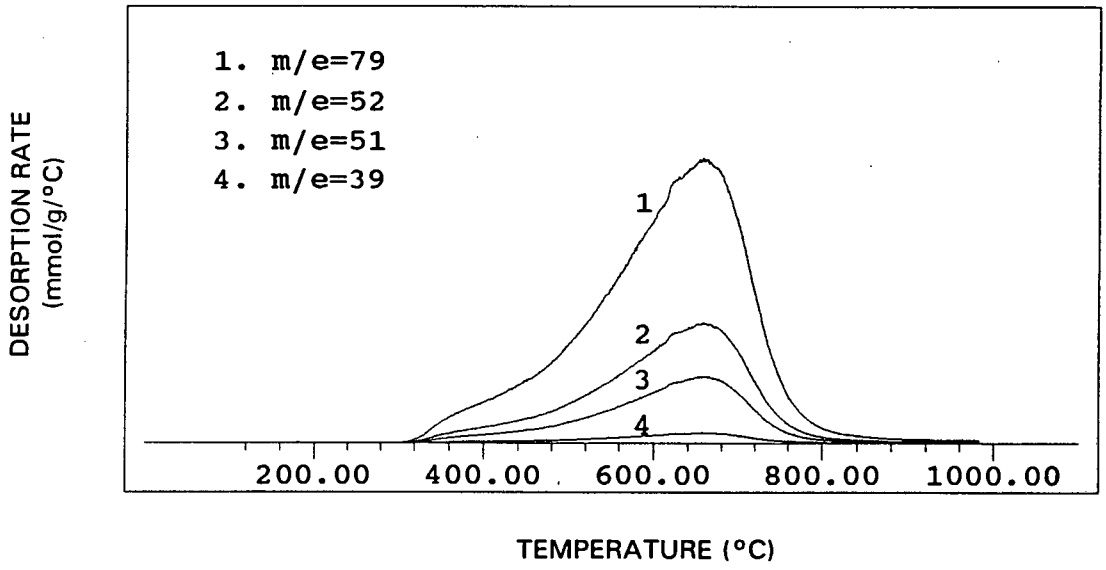

FIGURE 4.8: TPD spectrum of pyridine mass fractions from HZSM-5 (sample Z, 0.10 g, 100 ml/min helium, 10°C/min)

(ii) 4-Methyl quinoline

The mass fractions of the spectrum of 4-methyl quinoline (4MQ) injected directly into the injector port of the detector were compared with the mass fractions obtained in a typical spectrum of a MQ-TPD experiment. The two most abundant mass fractions obtained by injection were found to be $m/e = 143$ and 115, as given in the literature. As can be seen from Figure 4.9, the two most abundant mass fractions obtained by MQ-TPD (viz. $m/e = 78$ and 128) were not the same as those obtained by injection. This indicated that 4-methyl quinoline decomposed at high temperatures in the presence of HZSM-5.

Using a high temperature ramp (20°C/min) and low flowrates (30 ml/min) to increase the concentration of decomposition products in the product stream, an ethylene peak (indicated by $m/e = 27$) was observed at 300°C (Figure 4.10), suggesting that methyl groups dissociated from two 4-methyl quinoline molecules to form ethylene.

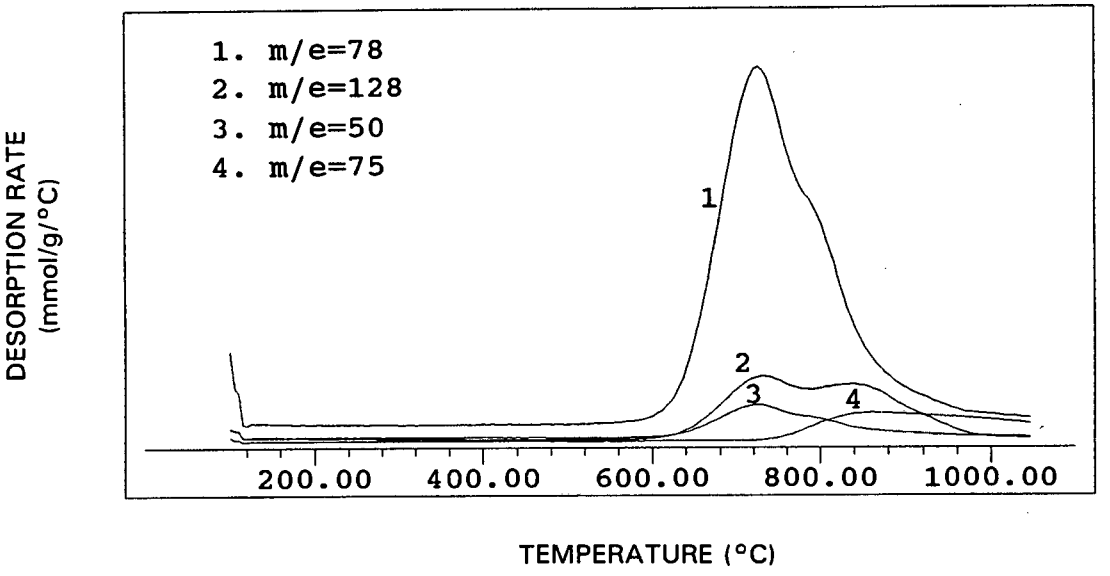

FIGURE 4.9: TPD spectrum of 4-methyl quinoline mass fractions from HZSM-5 (sample Z, 1.0 g, 40 ml/min helium, 10°C/min)

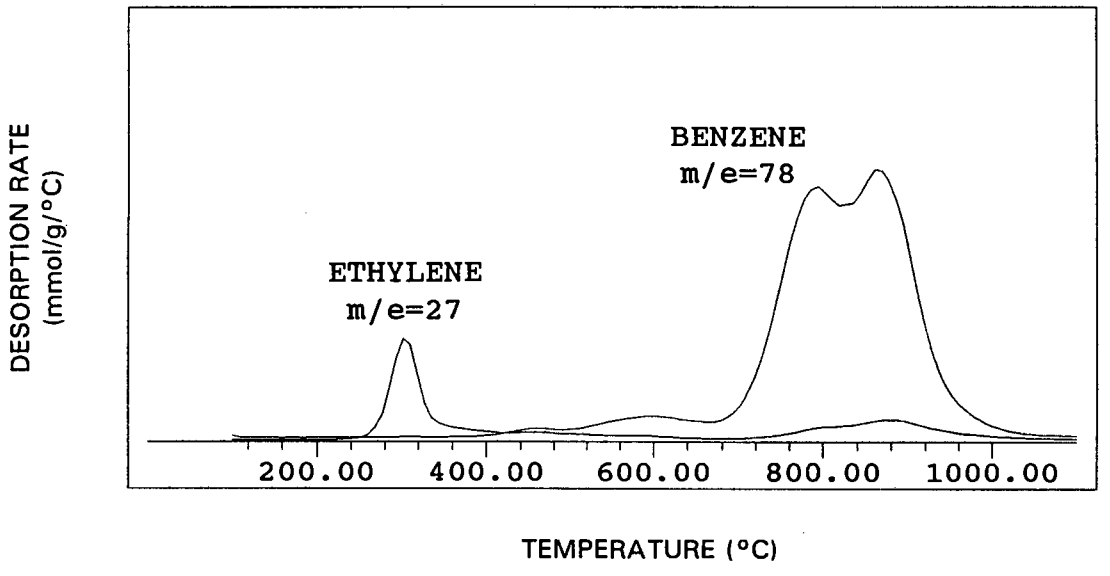

FIGURE 4.10: 4-Methyl quinoline dissociation on HZSM-5 (sample Z, 1.0 g, 30 ml/min helium, 20°C/min)

The parent ion of quinoline (*m/e* = 129) could not be detected, whereas a quinoline radical (*m/e* = 128) could indeed be observed, suggesting that dissociation of the methyl group took place (Figure 4.9). As *m/e* = 128 was detected, it was clear that at least a fraction of the quinoline radicals desorbed without undergoing further decomposition.

The most abundant ion in the spectrum of MQ-TPD was *m/e* = 78 (Figure 4.9), which can be ascribed to benzene formed from the decomposition of the quinoline radical. It is likely that HCN (*m/e* = 27) was also formed on decomposition of the quinoline radical above 700°C (Figure 4.10). It may be possible that the remaining decomposition fractions formed coke or that these reacted with H_2O of dehydroxylation, although no direct evidence for either possibility could be found. Spectra for dehydroxylation can be found in Appendix VIII. These decomposition products could be small enough to enter the channels, thus possibly further complicating the MQ-TPD spectrum.

In the case of ZSM-5, any material detected must have originated from the external surface of the catalyst, because (i) the critical diameter of 4MQ is ~7.3 Å [Rollmann, 1991] whereas the value of the largest kinetic pore diameter of ZSM-5 is 5.4 x 5.3 Å [Haag and Chen, 1987], (ii) only very small amounts of desorbing material were detected, even after prolonged (24 h) adsorption periods (Appendix VIII), and (iii) the dissociation of the methyl group (300°C) and decomposition of the quinoline radical (> 700°C) occurred well above the adsorption temperature (100°C).

In the case of Mordenite and Beta, with channel sizes of 7.0 x 6.5 Å and 7.6 x 6.4 Å respectively [Meier *et al.*, 1996], it appeared that 4MQ was able to enter the channels because the respective MQ-TPD desorption peaks observed after a 24 h adsorption period were ± 4 times larger than the peaks observed after a 3 h adsorption period (Appendix VIII). However, even for Mordenite and Beta samples, MQ-TPD spectra provided useful information on the relative changes in the external surface acidity after modification.

Because 4MQ decomposed during desorption, MQ-TPD data are reported as relative values. All MQ-TPD peak areas of the parent samples were normalized and MQ-TPD peak areas of modified samples are reported as relative values compared to their respective parent samples (based on the response signal of the most abundant fraction, viz. benzene, *m/e* = 78).

4.2.1.3 TPD reproducibility studies

The reproducibility of the pyridine and 4-methyl quinoline TPD studies on ZSM-5 are given in Figures 4.11 and 4.12 respectively.

Figure 4.11 shows that the reproducibility of the Py-TPD spectra was good. The peak maximum temperatures of the two spectra were 667 and 672°C and the number of acid sites were 0.45 and 0.46 mmol/g respectively.

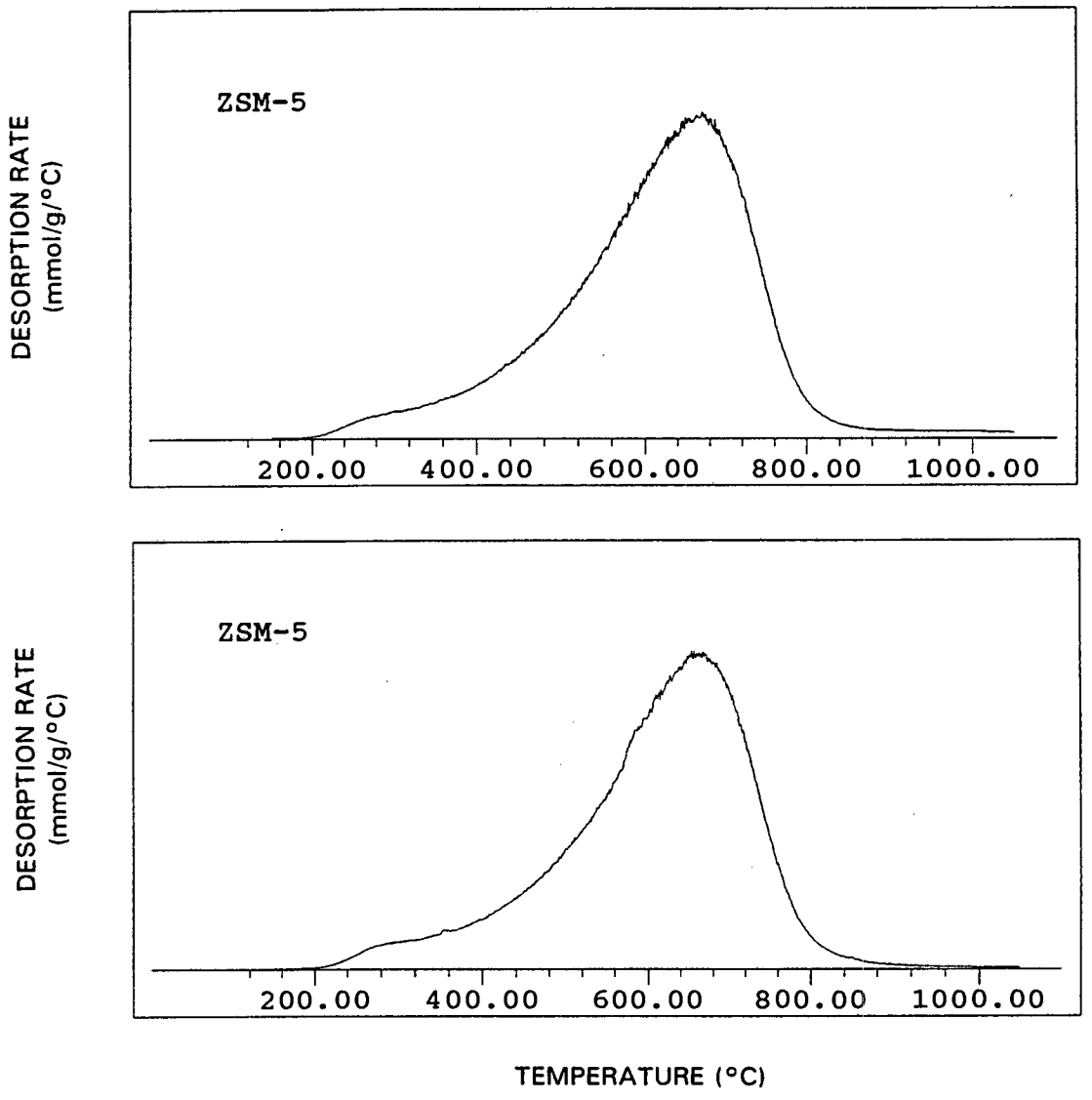

FIGURE 4.11: Reproducibility of Py-TPD spectra of sample Z, (0.10 g, 100 ml/min helium, 10°C/min, *m/e* = 79)

Figure 4.12 shows the reproducibility of the MQ-TPD spectra. The peak maximum temperatures of the two spectra were 803 and 820°C, and the relative external surface acidity values of the two spectra were 100% and 91% respectively. The first spectrum shows a double peak, whereas the second spectrum shows a classical bell-shaped curve. The desorption of the benzene fraction resulted from the decomposition of 4-methyl quinoline (Section 4.2.1.2) and the incomplete decomposition of 4MQ into benzene may have affected the reproducibility of the MQ-TPD measurements. However, the MQ-TPD measurements could still provide useful information of relatively large changes in the external surface acidity of the modified samples.

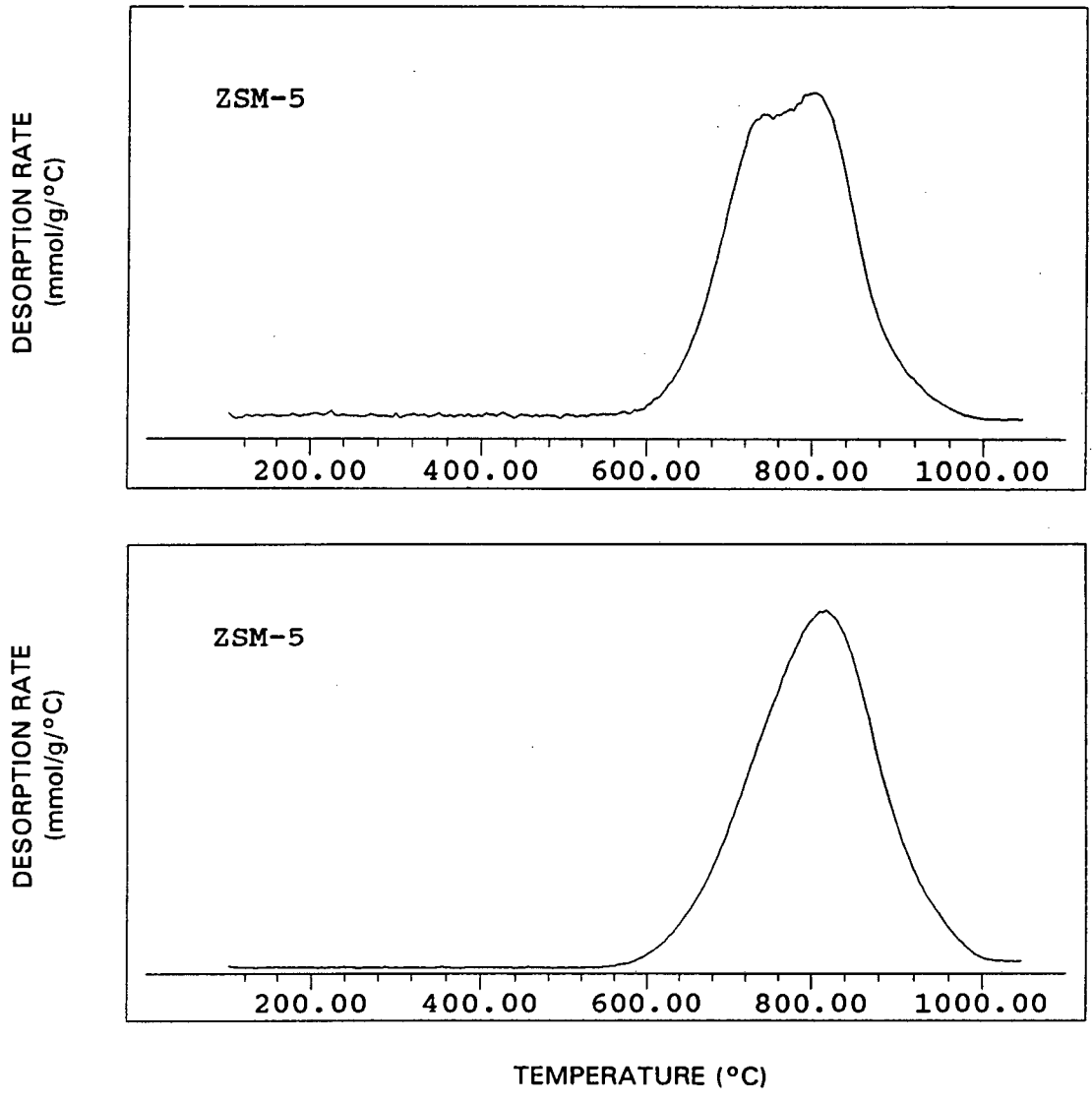

FIGURE 4.12: Reproducibility of MQ-TPD spectra of sample Z, (1.0 g, 40 ml/min helium, 10°C/min, *m/e* = 78)

4.2.2 TPD SPECTRA OF PARENT SAMPLES

4.2.2.1 NH_3-TPD spectra

The NH_3-TPD spectra were obtained using the apparatus described in Section 3.2.3.3. The TPD spectra for ZSM-5, Mordenite and Beta are shown in Figure 4.13. The number of acid sites per gram of catalyst and the peak maximum temperatures are given in Table 4.4.

Only one peak was observed for each sample in the NH_3-TPD studies under the conditions used (0.25 g, 70 ml/min helium, 10°C/min). The peak maximum temperature, T_{max}, of Beta was the lowest (346°C) whereas the peak maximum temperature of Mordenite occurred at 568°C (Figure 4.13). Both the ZSM-5 and Mordenite samples showed a leading edge in the NH_3-TPD spectra, whereas Beta showed a trailing edge. The number of acid sites obtained by NH_3-TPD of the Silicalite-I, ZSM-5, Mordenite and Beta samples were 0.01, 0.43, 1.15 and 0.65 mmol/g respectively (Table 4.4).

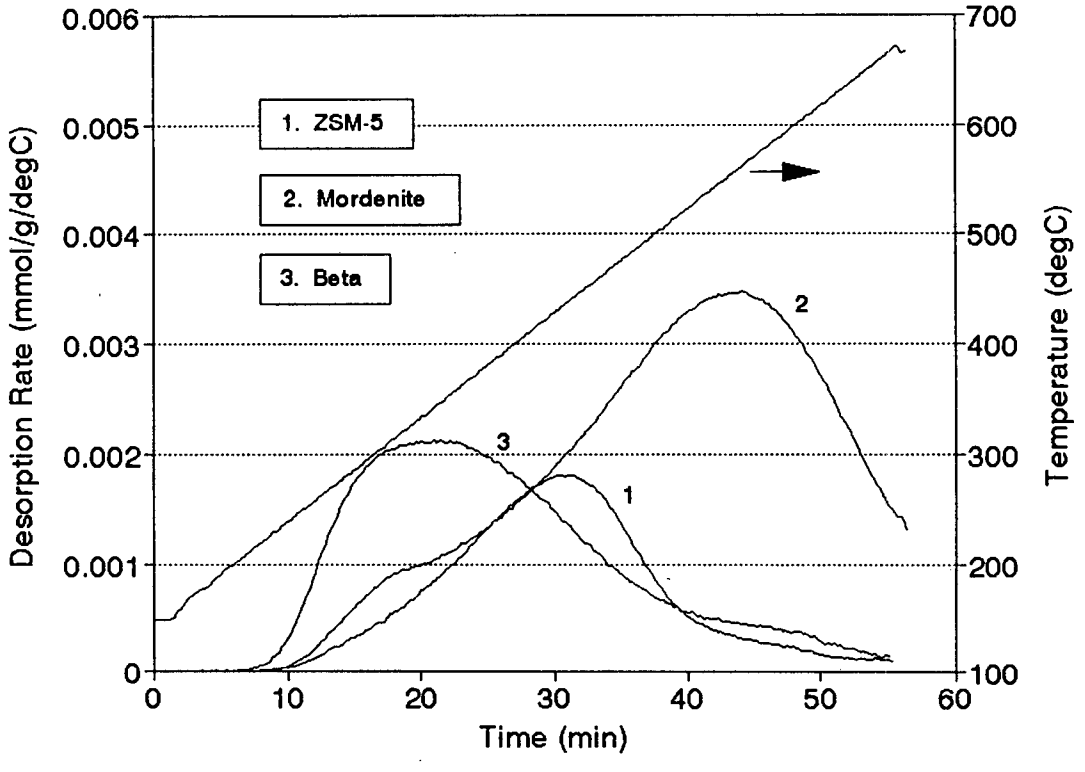

FIGURE 4.13: NH_3-TPD spectra of ZSM-5 (sample Z), Mordenite (sample M) and Beta (sample B) (0.25 g, 70 ml/min helium, 10°C/min)

Even though blank run TPD spectra were subtracted from the NH_3-TPD spectra, the Mordenite NH_3-TPD spectrum did not return to the baseline (Figure 4.13). Therefore the value of 1.15 mmol/g NH_3 desorption from Mordenite may have been underestimated slightly (Table 4.4). Blank run TPD spectra were obtained to monitor the H_2O loss due to dehydroxylation above the calcination temperature (500°C).

TABLE 4.4: Temperature programmed desorption data of Silicalite-I (sample S), ZSM-5 (sample Z), Mordenite (sample M) and Beta (sample B)

Catalyst	NH_3-TPD (mmol/g)	NH_3-TPD T_{max} (°C)	Py-TPD (mmol/g)	Py-TPD T_{max} (°C)	MQ-TPD (%)	MQ-TPD T_{max} (°C)
S	0.01	--	0.02	290	2	821
Z	0.43	440	0.46	667	100	820
M	1.15	568	1.03	637	76	807
B	0.65	346	0.72	630	276	818

4.2.2.2 Py-TPD spectra

The Py-TPD spectra were obtained using the apparatus described in Section 3.2.3.2. The Py-TPD spectra for Silicalite-I, ZSM-5, Mordenite and Beta are shown in Figure 4.14 (0.10 g, 100 ml/min helium, 10°C/min). The number of acid sites per gram of catalyst and the peak maximum temperatures are given in Table 4.4.

Only a small peak was observed for Silicalite-I. The peak shape of the Py-TPD spectrum of ZSM-5 (Figure 4.14) showed a leading edge similar to what was observed for the NH_3-TPD spectrum (Figure 4.13). Both Mordenite and Beta showed Py-TPD spectra that were broad (Figure 4.14), possibly suggesting the presence of several overlapping peaks, contrary to the single peaks observed in the NH_3-TPD spectra for these samples (Figure 4.13). The peak maximum temperature, T_{max}, of Silicalite-I was the lowest (290°C) whereas the peak maximum temperatures of ZSM-5, Mordenite and Beta ranged between 630 - 667°C (Table 4.4). The number of acid sites obtained by Py-TPD of the Silicalite-I, ZSM-5, Mordenite and Beta samples was 0.02, 0.46, 1.03 and 0.72 mmol/g respectively (Table 4.4).

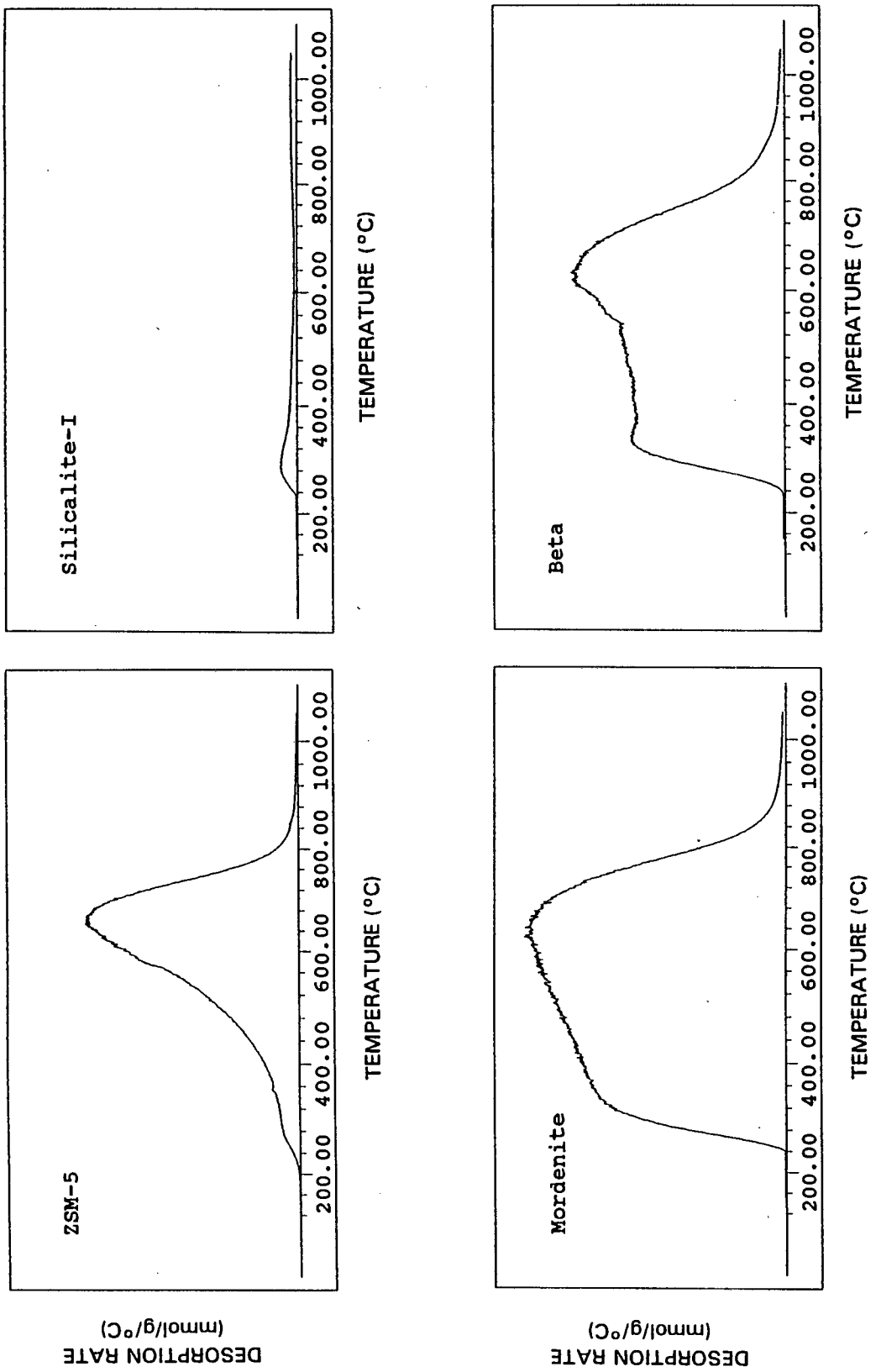

FIGURE 4.14: Py-TPD spectra of ZSM-5 (sample Z), Silicalite-I (sample S), Mordenite (sample M) and Beta (sample B) (0.10 g, 100 ml/min helium, 10°C/min, *m/e* = 79)

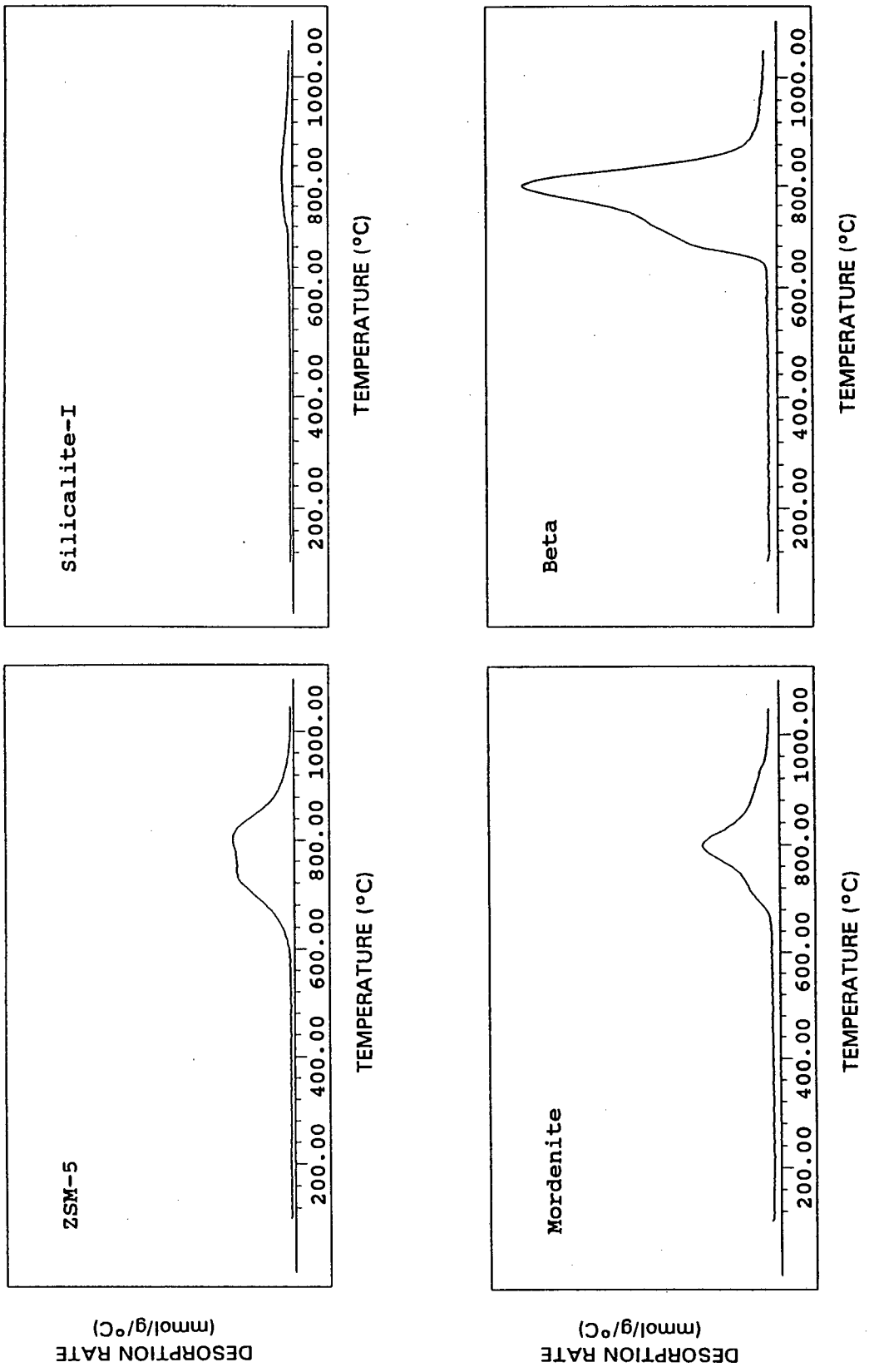

FIGURE 4.15: MQ-TPD spectra of ZSM-5 (sample Z), Silicalite-I (sample S), Mordenite (sample M) and Beta (sample B) (1.0 g, 40 ml/min helium, 10°C/min, *m/e* = 78)

4.2.2.3 MQ-TPD spectra

The MQ-TPD spectra were obtained using the apparatus described in Section 3.2.3.2. The MQ-TPD spectra for Silicalite-I, ZSM-5, Mordenite and Beta are shown in Figure 4.15 (1.0 g, 40 ml/min helium, 10°C/min). The relative external surface acidity values per gram of catalyst and the MQ-TPD peak maximum temperatures are given in Table 4.4.

Virtually no 4-methyl quinoline desorbed from Silicalite-I (Figure 4.15). The peak shape of the MQ-TPD spectra of the ZSM-5, Mordenite and Beta samples and their respective modified samples typically showed shoulders or even double peaks (Figure 4.15 and Appendix VII), although single, bell-shaped peaks were occasionally observed in the MQ-TPD spectra. The peak maximum temperatures of Silicalite-I (sample S), ZSM-5 (sample Z), Mordenite (sample M) and Beta (sample B) ranged between 807 - 821°C (Table 4.4) although a larger variation in T_{max} values for MQ-TPD spectra was typically observed compared to variations in T_{max} values for Py-TPD spectra.

ZSM-5 (sample Z) was assigned an external surface acidity value of 100%. The relative external surface acidity values of Silicalite-I (sample S), Mordenite (sample M) and Beta (sample B) were found to be 2, 76 and 276% respectively compared to ZSM-5 after a 3 h adsorption period (Table 4.4). However, for comparison of modified samples with their respective parent samples, each parent sample will be assigned a relative external surface acidity value of 100% in subsequent sections.

4.2.3 CHEMICAL VAPOUR AND LIQUID DEPOSITION

4.2.3.1 ZSM-5 temperature programmed desorption data

(i) Pyridine TPD studies

The number of acid sites measured by Py-TPD for ZSM-5 (sample Z) was 0.46 mmol/g and the peak maximum temperature was 660°C (Table 4.5). The Py-TPD spectrum of ZSM-5 is shown in Figure 4.14. The Py-TPD spectra and area counts of ZSM-5 samples modified by chemical vapour and liquid deposition methods are given in Appendix VI (0.10 g, 100 ml/min helium, 10°C/min).

The number of acid sites measured by Py-TPD of ZSM-5 samples modified using a static vacuum system (Z-V-*/* series) was 0.41 - 0.43 mmol/g (Table 4.5), indicating a slight decrease in total number of acid sites as a result of the chemical vapour deposition process, although changes were within the error margin. Neither the peak shapes nor the peak maximum temperatures, T_{max}, of the Py-TPD spectra changed significantly for ZSM-5 samples modified in a static vacuum system (Table 4.5).

Py-TPD studies showed that the overall number of acid sites of samples modified using a vapour phase flow system (Z-F-*/* series) had been reduced, especially for samples Z-F-50/4x10 and Z-F-400/4x5 (0.19 and 0.32 mmol/g respectively) (Table 4.5). The peak maximum temperatures, T_{max}, for samples Z-F-50/4x10 and Z-F-400/4x5 were found to be 602 and 688°C respectively. These samples were both subjected to deposition for longer times than their equivalents on which deposition occurred for 8 hours and which had T_{max} values of 664 and 660°C respectively (Table 4.5). The peak shape of the Py-TPD spectrum of sample Z-F-50/4x10 was found to be distorted due to the deposition of silica on the external surface (Figure A-VI.3 in Appendix VI). The effect of the deposition time for samples modified in a vapour phase flow system was found to be more pronounced than for samples modified in a static vacuum system because even relatively short deposition times (8 h) resulted in significant decreases in the number of acid sites measured by Py-TPD (Table 4.5).

ZSM-5 samples modified by CLD methods (Z-L-*/* series) showed a slight decrease from 0.46 to 0.40 - 0.44 mmol/g in the amount of pyridine desorption, although these changes were within the error margin (Table 4.5). The peak maximum temperature increased from 660°C to 677 and 685°C for samples Z-L-100/- and Z-L-5/H respectively. The Py-TPD peak shapes of the modified samples were not changed (Figure A-VI.4 in Appendix VI).

TABLE 4.5: Temperature programmed desorption data of ZSM-5 and modified ZSM-5 samples

Catalyst	Py-TPD (mmol/g)	Py-TPD T_{max} (°C)	MQ-TPD (%)	MQ-TPD T_{max} (°C)
Z	0.46	660	100	820
Z-V-100/60	0.42	660	97	783
Z-V-200/60	0.41	663	55	799
Z-V-300/60	0.43	660	40	801
Z-V-400/60	0.43	662	35	807
Z-V-400/4x4	0.43	662	3	790
Z-V-400/6x10	0.41	661	0	--
Z-F-50/8	0.39	664	42	819
Z-F-50/4x10	0.19	602	--	--
Z-F-400/8	0.41	660	20	794
Z-F-400/4x5	0.32	688	--	--
Z-L-100/-	0.40	677	77	808
Z-L-0.5/W	0.41	653	81	808
Z-L-5/W	0.40	660	53	808
Z-L-5/E	0.42	670	41	819
Z-L-5/H	0.44	685	29	823
error	± 5%	± 5°C	± 7%	--

NOTE: A statistical error analysis was not possible. The error listed in the table above is a non-statistical estimation, based on accuracy of the equipment and reproducibility of the measurements.

(ii) 4-Methyl quinoline TPD studies

The relative external surface acidity measured by MQ-TPD for ZSM-5 (sample Z) was assigned to be 100% (Table 4.5). The MQ-TPD spectrum of ZSM-5 is shown in Figure 4.15. The MQ-TPD spectra and area counts of ZSM-5 samples

modified by chemical vapour and liquid deposition methods are given in Appendix VII (1.0 g, 40 ml/min helium, 10°C/min).

Table 4.6 shows that the relative amount of external acidity as measured by MQ-TPD in samples modified using a static vacuum system decreased as the deposition temperature increased and, with some exceptions, as the deposition time increased. At 100°C no significant change was observed. A relative external acidity of 35% was obtained for a deposition time of 60 h at 400°C.

TABLE 4.6: Percentage relative external acidity of samples modified in a static vacuum system as measured by MQ-TPD

Deposition temperature (°C)	Percentage relative external acidity for a deposition time of 4 h	21 h	60 h
100	92	110	97
200	81	58	55
300	64	61	40
400	64	43	35

Table 4.5 shows MQ-TPD data for the more extensively modified ZSM-5 samples using a static vacuum system (Z-V-*/* series). Samples Z-V-400/4x4 and Z-V-400/6x10 showed relative external surface acidities of only 3% and 0% respectively compared to sample Z as measured by MQ-TPD (Table 4.5) indicating that repeated deposition cycles inertised the external surface of ZSM-5 more effectively than single deposition cycles (Tables 4.5 and 4.6) even though the total deposition time was shorter (sample Z-V-400/4x4).

The MQ-TPD results of ZSM-5 samples modified in a vapour phase flow system (Z-F-*/* series) showed that the relative external surface acidities of samples Z-F-50/8 and Z-F-400/8 were reduced to 42% and 20% respectively (Table 4.5). Unfortunately, insufficient sample was available to measure the relative external surface acidities of samples Z-F-50/4x10 and Z-F-400/4x5 by MQ-TPD, but it is likely that the relative reduction in external surface acidity for these samples would be at least similar if not more than those of samples Z-F-50/8 and Z-F-400/8.

The results of the MQ-TPD studies using ZSM-5 samples modified using chemical liquid deposition methods are shown in Table 4.5 (Z-L-*/* series). The sample where 5 vol% TEOS was added to *n*-hexane as diluent (sample Z-L-5/H) was found to have a relative external surface acidity of 29%. The relative external surface acidities of samples modified by adding 5 vol% TEOS to H_2O (sample Z-L-5/W) or to ethanol (sample Z-L-/5/E) decreased to 53% and 41% respectively. However, when pure TEOS was used (sample Z-L-100/-) the relative external surface acidity only decreased to 77%. The relative external surface acidities of samples Z-L-5/W and Z-L-0.5/W were 53% and 81% respectively, indicating that when using the same diluent a higher concentration of TEOS resulted in a greater decrease in external surface acidity (Table 4.5).

4.2.3.2 Mordenite temperature programmed desorption data

(i) Pyridine TPD studies

The number of acid sites measured by Py-TPD for Mordenite (sample M) was found to be 1.03 mmol/g, and the number of acid sites of the modified Mordenite samples ranged from 0.94 - 1.03 mmol/g. The peak maximum temperature of sample M occurred at 637°C (Table 4.7). The Py-TPD spectrum of Mordenite (sample M) is shown in Figure 4.14, and the Py-TPD spectra of the modified Mordenite samples are shown in Figure A-VI.6 of Appendix VI (0.10 g, 100 ml/min helium, 10°C/min). No significant changes in the Py-TPD peak shapes were observed, although the peak maximum temperatures of samples M-V-400/6x10 and M-L-5/H increased to 655 and 660°C respectively (Table 4.7).

(ii) 4-Methyl quinoline TPD studies

The relative external surface acidity measured by MQ-TPD for Mordenite (sample M) was assigned to be 100% (Table 4.7). The MQ-TPD spectrum of Mordenite is shown in Figure 4.15. The MQ-TPD spectra of Mordenite samples modified by chemical vapour and liquid deposition methods are given in Figure A-VII.6 of Appendix VII (1.0 g, 40 ml/min helium, 10°C/min).

The relative external acidities of both samples modified using a static vacuum system, viz. samples M-V-400/60 and M-V-400/6x10, were reduced to 1% and 0% respectively. Therefore the chemical vapour deposition was extremely effective for these samples. The relative external acidities of samples M-F-400/8 and M-L-5/H were reduced to 30% and 18% respectively.

TABLE 4.7: Temperature programmed desorption data of Mordenite and modified Mordenite samples

Catalyst	Py-TPD (mmol/g)	Py-TPD T_{max} (°C)	MQ-TPD (%)	MQ-TPD T_{max} (°C)
M	1.03	637	100	807
M-V-400/60	1.03	635	1	809
M-V-400/6x10	0.94	655	± 0	--
M-F-400/8	0.95	630	30	788
M-L-5/H	0.99	660	18	728
error	± 5%	± 5°C	± 7%	--

NOTE: A statistical error analysis was not possible. The error listed in the table above is a non-statistical estimation, based on accuracy of the equipment and reproducibility of the measurements.

4.2.3.3 Beta temperature programmed desorption data

(i) Pyridine TPD studies

The number of acid sites measured by Py-TPD for Beta (sample B) was found to be 0.72 mmol/g and the number of acid sites of the modified Beta samples ranged from 0.53 - 0.75 mmol/g. The number of acid sites had decreased significantly for samples B-F-400/8 and B-L-5/H (Table 4.8). The peak maximum temperature of sample B occurred at 630°C. The Py-TPD spectrum of Beta (sample B) is shown in Figure 4.14, and the Py-TPD spectra of the modified Beta samples are shown in Figure A-VI.7 of Appendix VI (0.10 g, 100 ml/min helium, 10°C/min). No significant changes were observed in the peak

shapes of the Py-TPD spectra and peak maximum temperatures of these samples, with the possible exception of sample B-V-400/60, which showed a large desorption peak at low temperatures compared to sample B (Table 4.8 and Figure A-VI.7 in Appendix VI).

TABLE 4.8: Temperature programmed desorption data of Beta and modified Beta samples

Catalyst	Py-TPD (mmol/g)	Py-TPD T_{max} (°C)	MQ-TPD (%)	MQ-TPD T_{max} (°C)
B	0.72	630	100	818
B-V-400/60	0.75	625	1	810
B-V-400/6x10	0.67	630	3	807
B-F-400/8	0.53	630	22	824
B-L-5/H	0.61	640	31	684
error	± 5%	± 5°C	± 7%	--

NOTE: A statistical error analysis was not possible. The error listed in the table above is a non-statistical estimation, based on accuracy of the equipment and reproducibility of the measurements.

(ii) 4-Methyl quinoline TPD studies

The relative external surface acidity measured by MQ-TPD for Beta (sample B) was assigned to be 100% (Table 4.8). The MQ-TPD spectrum of Beta is shown in Figure 4.15. The MQ-TPD spectra of Mordenite samples modified by chemical vapour and liquid deposition methods are given in Figure A-VII.7 of Appendix VII (1.0 g, 40 ml/min helium, 10°C/min).

The relative external acidities of both samples modified using a static vacuum system, viz. samples B-V-400/60 and B-V-400/6x10, were reduced to 1% and 3% respectively, suggesting effective inertisation of the external surface acidity of these samples (Table 4.8). The relative external acidities of samples B-F-400/8 and B-L-5/H were found to be 22% and 31% respectively.

4.2.3.4 The effect of post-modification treatment

Post-modification treatment consisted of grinding the sample in a mortar and pestle prior to performing the MQ-TPD experiments, to determine whether the silica layer was permanently attached to the external surface. Only samples M-V-400/6x10 and B-V-400/6x10 were investigated. To indicate that the sample had been subjected to post-modification treatment or grinding the term "(crushed)" is added after the sample name.

The relative external surface acidity of sample M-V-400/6x10 (crushed) was 57% compared to 0% for sample M-V-400/6x10. Similarly, the relative external surface acidity of sample B-V-400/6x10 (crushed) was 95% compared to 0% for sample B-V-400/6x10. This indicated that external surface acid sites inertised during CVD treatment, or acid sites not previously accessible to 4-methyl quinoline, were exposed after the sample had been subjected to grinding.

The MQ-TPD spectra of these samples are shown in Appendix VIII.

4.2.4 ZSM-5 COATED WITH SILICALITE SHELLS

The NH_3-TPD spectra (0.25 g, 70 ml/min helium, 10°C/min) of samples modified by coating with Silicalite shells all showed a decrease in the number of acid sites per gram of material from 0.49 to 0.18 - 0.22 mmol/g, and a decrease in T_{max} from 450 to 415 - 420°C (Table 4.9) because the Silicalite shell effectively reduced the mass of ZSM-5 in the sample and hence the number of acid sites in the sample.

Similarly, for the Py-TPD spectra (50 mg, 150 ml/min helium, 10°C/min) the number of acid sites per gram of material decreased from 0.49 to 0.21 - 0.23 mmol/g and T_{max} decreased from 615 to 585 - 590°C (Table 4.9 and Figure A-VI.5 in Appendix VI). The Py-TPD spectra of samples Z_9-C-Na and Z_9-C-NH_4 showed a shoulder in the region 320 - 480°C (Figure A-VI.5). Samples Z_9-C-Na and Z_9-C-NH_4 were both detemplated prior to modification. In order to

investigate whether the shoulder at lower temperatures was due to residual physisorbed pyridine "trapped" in the channels as a result of pore blockage, possibly caused by the deposition of silicon rich deposits during the coating procedure, sample Z_9-C-NH_4 was evacuated for 34 h. The Py-TPD spectrum of sample Z_9-C-NH_4 was not affected, and therefore the material desorbed at lower temperatures was chemisorbed pyridine.

TABLE 4.9: Temperature programmed desorption data of ZSM-5 and ZSM-5 modified by coating with Silicalite shells

Catalyst	NH_3-TPD (mmol/g)	NH_3-TPD T_{max} (°C)	Py-TPD (mmol/g)	Py-TPD T_{max} (°C)	MQ-TPD (%)	MQ-TPD T_{max} (°C)
Z_9	0.49	450	0.49	615	100	730
Z_9-C-templ	0.22	420	0.22	590	56	780
Z_9-C-Na	0.19	420	0.23	585	59	780
Z_9-C-NH_4	0.18	415	0.21	585	7	790

MQ-TPD spectra of the modified samples (1.0 g, 40 ml/min helium, 10°C/min) show that sample Z_9-C-NH_4 had a relative external surface acidity which was 7% of that of the parent sample Z_9 (Table 4.9 and Figure A-VII.5 in Appendix VII). This indicated that the external surface acidity had been essentially removed by the coating without seriously affecting the internal acidity of the catalyst as shown by the Py-TPD spectrum. Samples Z_9-C-templ and Z_9-C-Na still showed a significant amount of relative external surface acidity, viz. 56% and 59% of the parent sample respectively, and because these samples were not inertised completely they were not modified successfully (Table 4.9).

4.3 ADSORPTION STUDIES

4.3.1 PORE VOLUME ANALYSIS

4.3.1.1 Pore volume analysis of the parent samples

The pore volumes of ZSM-5 (sample Z), Mordenite (sample M) and Beta (sample B) were analyzed using nitrogen adsorption (N_2-BET) as described in Section 3.2.2.2. Micropore and mesopore surface areas were also obtained (Table 4.10). Because N_2-BET cannot measure pore sizes below ± 17 Å, the micropore surface areas and pore volumes were taken as being obtained from pores less than 17 Å, and the mesopore surface areas and pore volumes as being obtained from pores larger than 17 Å. Therefore, the mesopore surface area gave an indication of the external surface area of the sample.

Beta was found to have the largest total surface area (518.6 m^2/g) and Mordenite the smallest (137.7 m^2/g) (Table 4.10). Similarly, the mesopore surface area of Beta was found to be the largest (186.1 m^2/g) and that of Mordenite the smallest (58.7 m^2/g) (Table 4.10).

TABLE 4.10: Surface area and pore volume data for ZSM-5 (sample Z), Mordenite (sample M) and Beta (sample B)

		ZSM-5	Mordenite	Beta
BET surface area	(m^2/g)	395.2 ± 9.2	137.7 ± 2.6	518.6 ± 10.5
Micropore surface area	(m^2/g)	275.8	79.0	332.5
Mesopore surface area	(m^2/g)	119.4	58.7	186.1
Monolayer volume	(cc/g STP)	90.8	31.6	119.1
Micropore volume	(cc/g)	0.133	0.038	0.160
Mesopore volume	(cc/g)	0.128	0.113	0.459

Figure 4.16 shows the nitrogen adsorption isotherms for these samples. A hysteresis can be seen in all three samples, especially for Beta (sample B), indicating that mesopores are present.

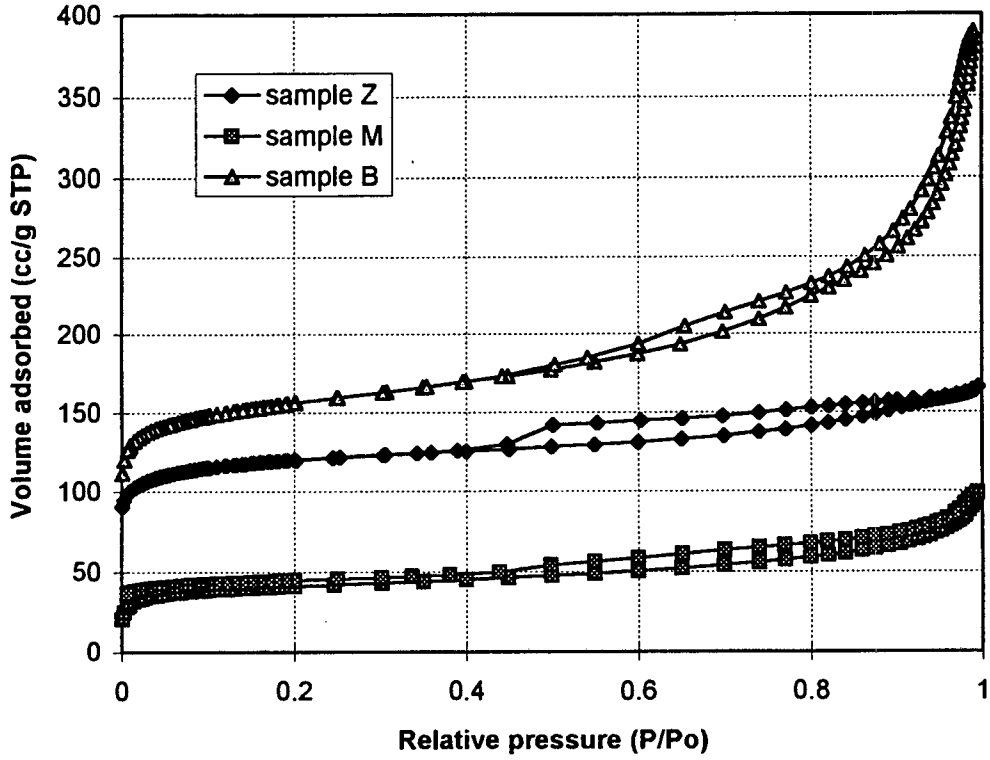

FIGURE 4.16: Nitrogen adsorption isotherms for ZSM-5 (sample Z), Mordenite (sample M) and Beta (sample B)

Figure 4.17 also clearly shows a wide pore size distribution for Beta. In contrast, ZSM-5 shows a narrow distribution in the mesopore range around 40 Å. Although few data points were taken in this region, reproducibility of the nitrogen adsorption experiments was good.

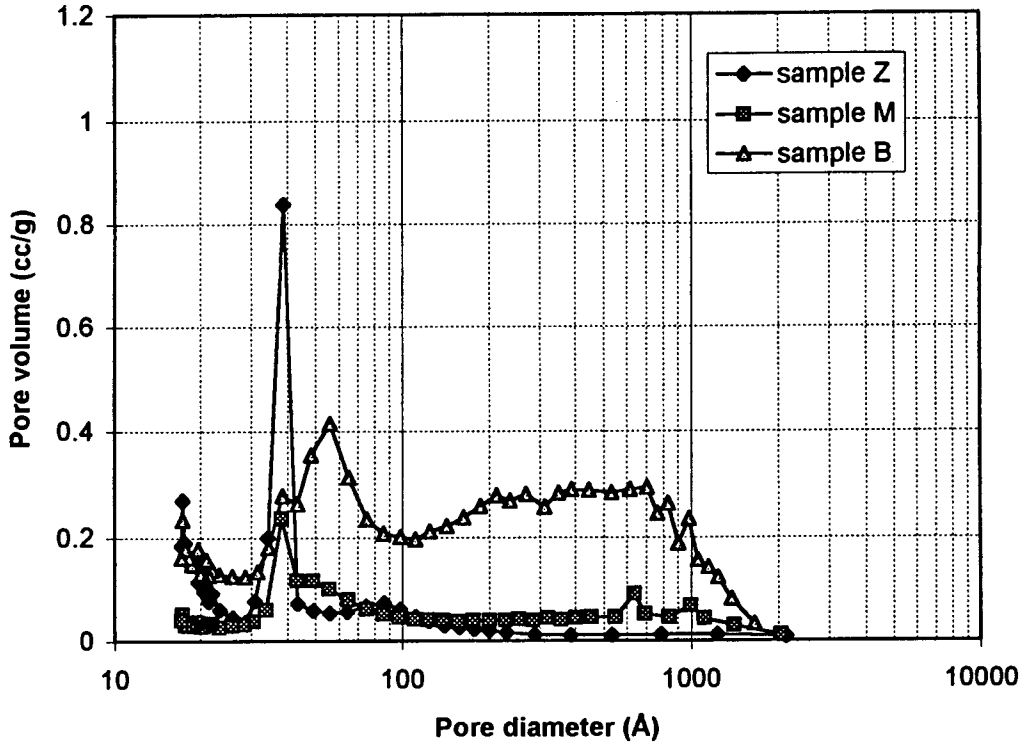

FIGURE 4.17: Pore size distribution of ZSM-5 (sample Z), Mordenite (sample M) and Beta (sample B)

3.3.1.2 Pore volume analysis of the ZSM-5 coated with Silicalite shells

The pore volumes of ZSM-5 (sample Z_9) and ZSM-5 modified by coating with Silicalite shells were analyzed using nitrogen adsorption (N_2-BET) as described in Section 3.2.2.2. Micropore and mesopore surface areas were also obtained (Table 4.11).

Sample Z_9 was found to have a total surface area of 395.4 m^2/g (Table 4.11). The total surface area of sample Z_9-C-templ (337.6 m^2/g) was significantly smaller than that of the parent sample. The micropore surface areas of samples Z_9-C-templ and Z_9-C-Na decreased while their mesopore surface areas increased

(Table 4.11). Changes to sample Z_9-C-NH_4 were less severe than for the other modified samples (Table 4.11).

TABLE 4.11: Surface area and pore volume data for ZSM-5 (sample Z_9) and ZSM-5 modified by coating with Silicalite shells

		Z_9	Z_9-C-templ	Z_9-C-Na	Z_9-C-NH_4
BET surface area	(m^2/g)	395.4 ± 8.3	337.6 ± 4.4	379.5 ± 2.0	404.1 ± 3.9
Micropore surface area	(m^2/g)	289.7	161.9	173.7	241.9
Mesopore surface area	(m^2/g)	105.7	175.7	205.8	162.2
Monolayer volume	(cc/g STP)	90.8	77.6	82.2	92.8

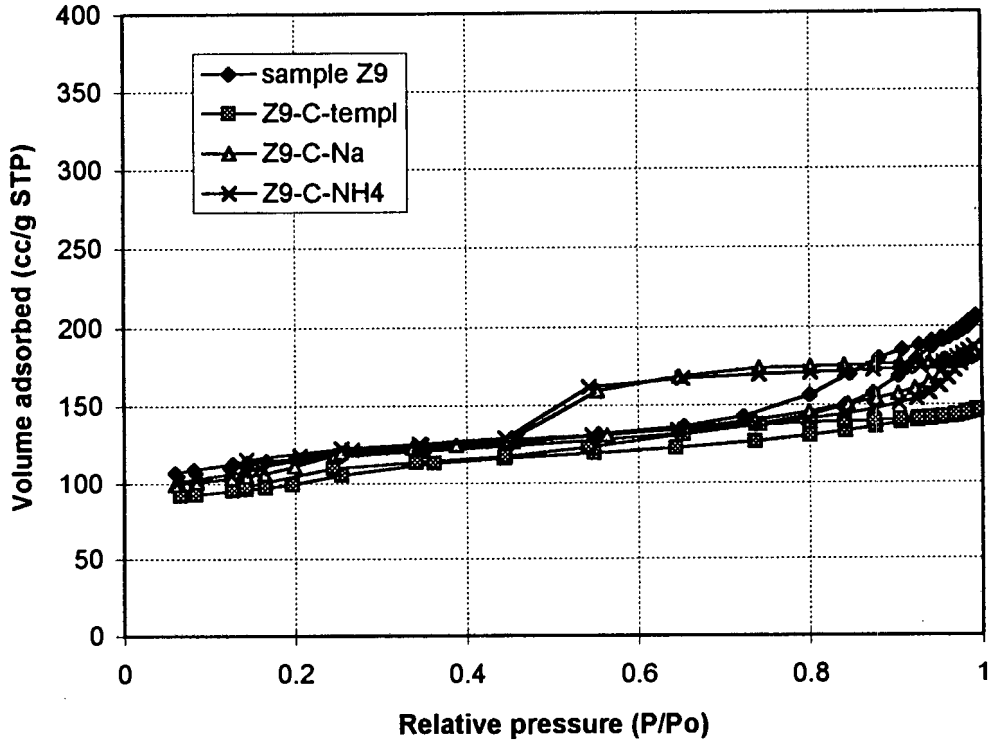

FIGURE 4.18: Nitrogen adsorption isotherms for ZSM-5 (sample Z_9) and samples modified by coating with Silicalite shells

Figure 4.18 shows the nitrogen adsorption isotherms for these samples. A hysteresis can be seen in all samples, but the desorption branch of samples Z_9-C-templ and Z_9-C-Na indicated a large change in the mesoporosity of these samples compared to the parent sample.

Figure 4.19 shows the pore size distribution for sample Z_9 and samples modified by coating with Silicalite shells. Sample Z_9 showed a significant portion of mesopores ranging from 50 - 200 Å. For sample Z_9-C-templ the mesopores in this range were no longer evident. Samples Z_9-C-Na and Z_9-C-NH_4 showed a narrow pore size distribution around 40 Å.

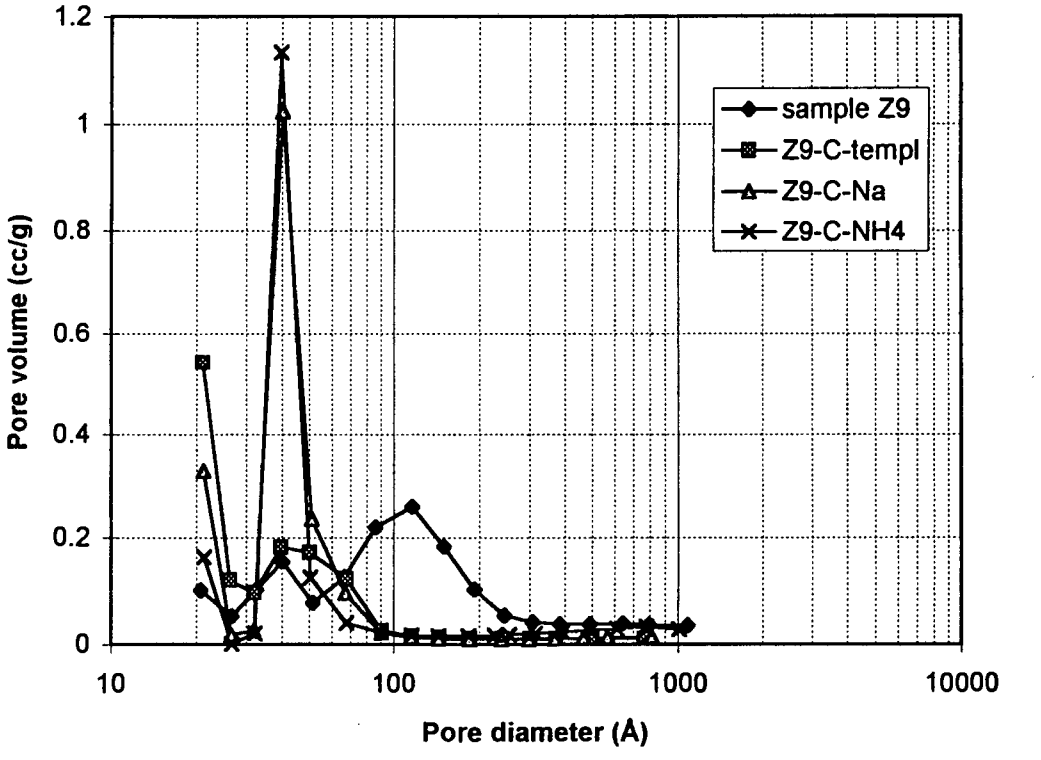

FIGURE 4.19: Pore size distribution of ZSM-5 (sample Z_9) and samples modified by coating with Silicalite shells

4.3.2 ADSORPTION CAPACITY DATA

The moisture contents and adsorption capacities of samples modified by chemical vapour and liquid deposition methods were measured by thermogravimetric analysis, as described in Section 3.2.2.1. The adsorbates used were *n*-hexane, *p*-xylene, *o*-xylene and 1,2,4-trimethyl benzene.

Figures 4.20 shows a typical calcination and *n*-hexane adsorption profile, using a 60 min adsorption period at 80°C. A small amount of mass was lost from the sample during the initial temperature ramp prior to the commencement of data logging at 40°C. The moisture content of each sample was calculated taking into account this initial mass loss. In this case, the mass loss recorded prior to the *n*-hexane adsorption was used to obtain the moisture content for this sample (4.3 wt%). Adsorption capacities were calculated on a dry basis (*n*-hexane adsorption capacity = 10.3 wt%).

Similarly, Figure 4.21 shows a typical calcination and *p*-xylene adsorption profile, using a 300 min adsorption period at 150°C. The mass lost during calcination (9.8 wt%) was due to *n*-hexane remaining in the sample after having been adsorbed in the previous adsorption experiment shown Figure 4.20. The *p*-xylene adsorption capacity was 3.0 wt%. The calcination and adsorption profiles for *o*-xylene and 1,2,4-trimethyl benzene were obtained similarly to that of *p*-xylene.

Other than in Figures 4.20 and 4.21 the calcination step will be omitted, and only the adsorption profile will be shown. The adsorption profiles of the samples modified by chemical vapour and liquid deposition methods are given in Appendix IX. The adsorption profiles in Figures 4.22, 4.23 and 4.24 and in Appendix IX are labelled as follows (kinetic diameters given in brackets):

1	*n*-hexane	(4.3 Å)
2	*p*-xylene	(5.85 Å)
3	*o*-xylene	(6.6 Å)
4	1,2,4-trimethyl benzene	(6.6 Å)

Note that the moisture content was probably largely dependent on atmospheric conditions, and in the case of liquid phase deposition on the diluent used in the modification step, and therefore the moisture content differed considerably from sample to sample.

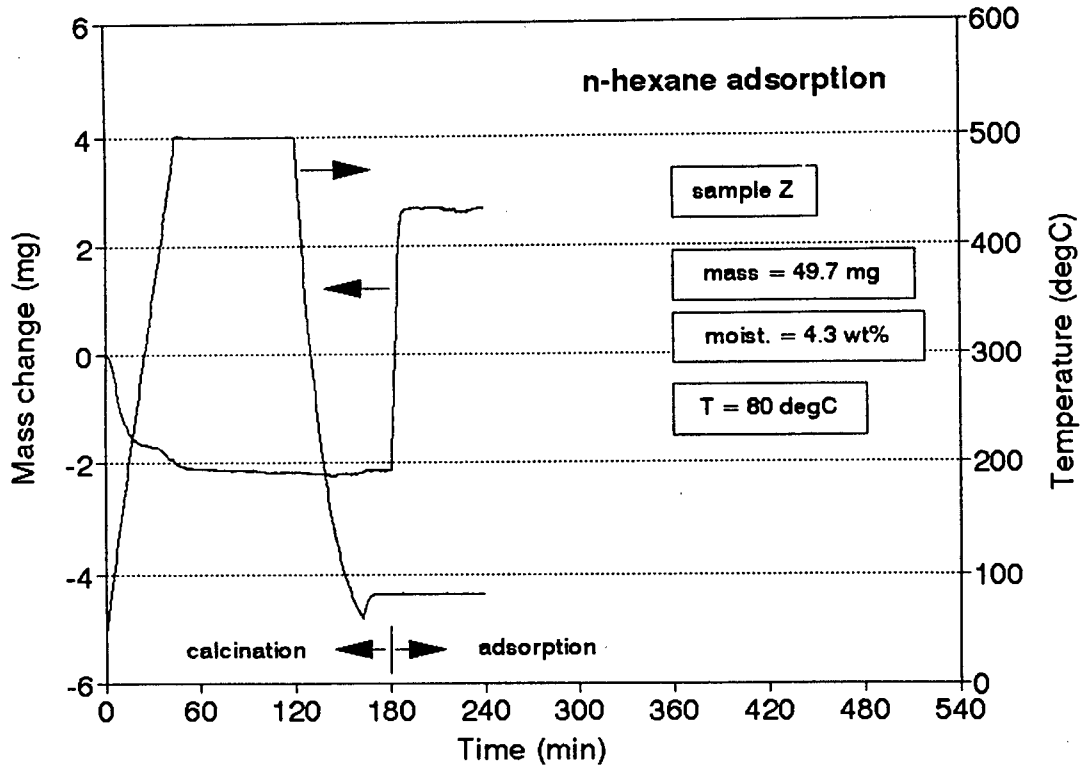

FIGURE 4.20: Typical calcination and *n*-hexane adsorption profile

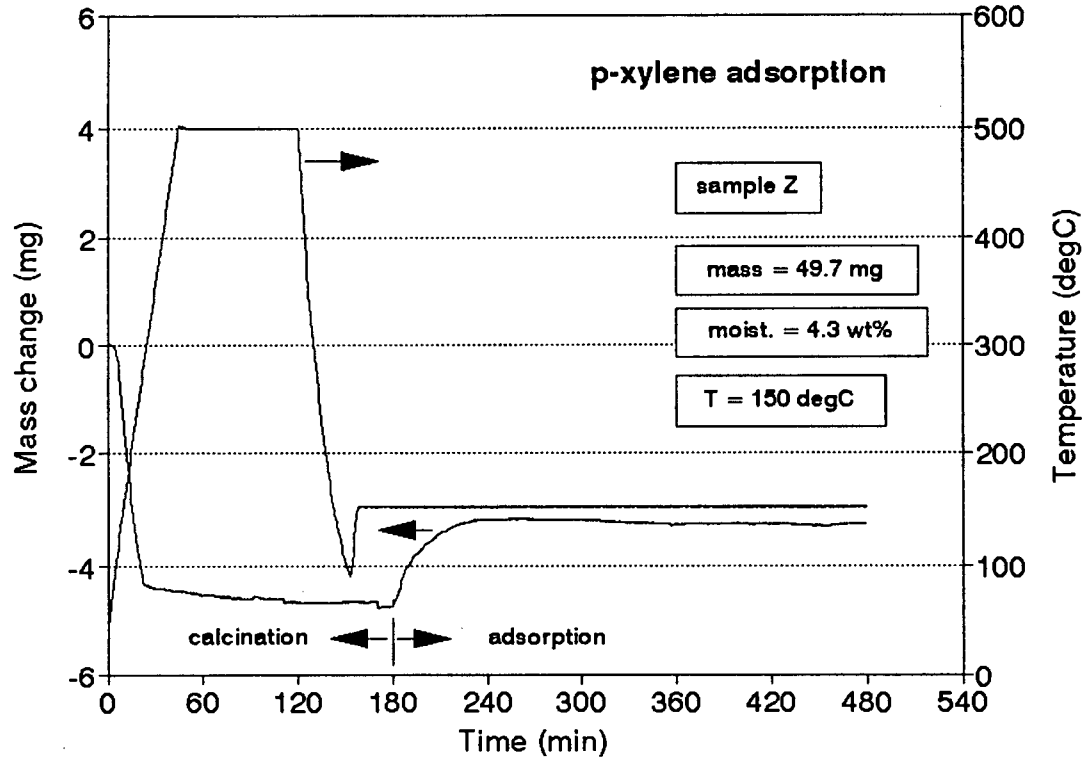

FIGURE 4.21: Typical calcination and *p*-xylene adsorption profile

4.3.2.1 ZSM-5 adsorption capacity data

Figure 4.22 shows the adsorption profiles of *n*-hexane, *p*-xylene, *o*-xylene and 1,2,4-trimethyl benzene on ZSM-5 (sample Z). The ZSM-5 sample was saturated with *n*-hexane within ± 10 - 15 min (*n*-hexane adsorption capacity = 10.3 wt%). Saturation with *p*-xylene (3.0 wt%) and *o*-xylene (2.7 wt%) occurred within ± 75 and 100 min respectively. When 1,2,4-trimethyl benzene was used the sample was not completely saturated after 300 min, although a weight increase of 2.8 wt% was similar to those obtained using *p*-xylene and *o*-xylene. Although no reproducible adsorption rate data was obtainable with the apparatus, it appeared that the adsorption rates (as observed from the initial slope for each adsorption profile) increased in the following order:

1,2,4-TMB < *o*-xylene < *p*-xylene < *n*-hexane

Adsorption profiles of the ZSM-5 samples modified by chemical vapour and liquid deposition methods are given in Appendix IX. The moisture content and adsorption capacities of the ZSM-5 and modified ZSM-5 samples are given in Table 4.12.

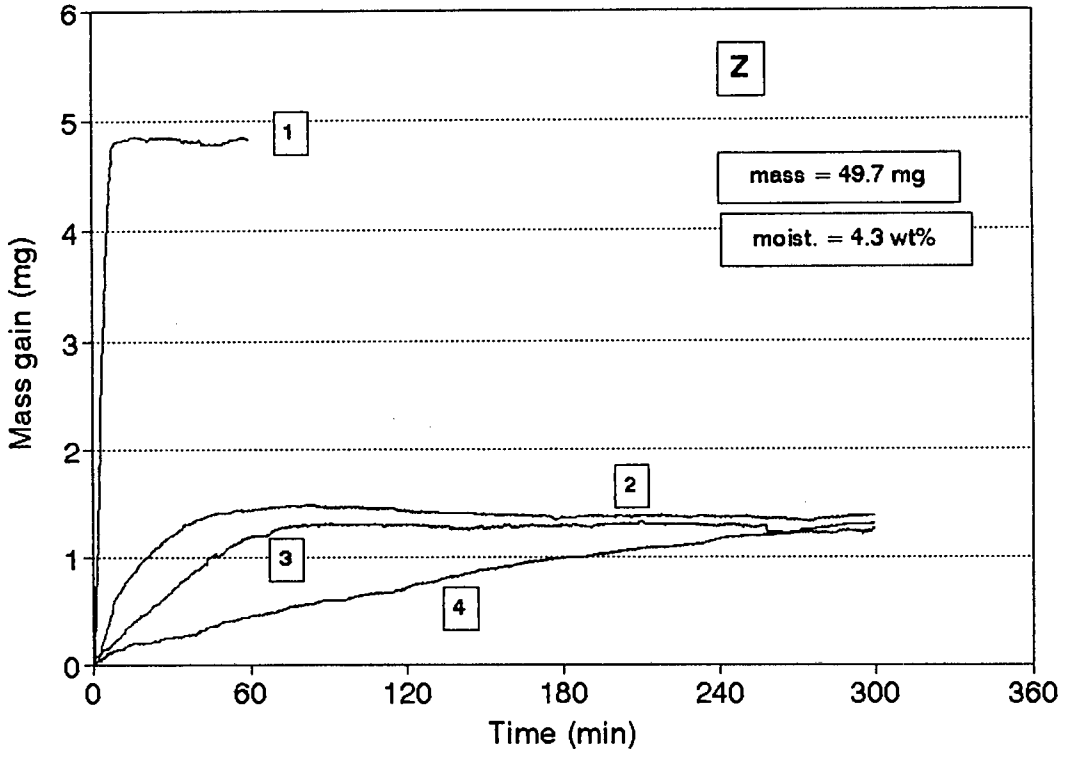

FIGURE 4.22: *n*-Hexane (1), *p*-xylene (2), *o*-xylene (3) and 1,2,4-TMB (4) adsorption profiles on ZSM-5 (sample Z)

TABLE 4.12: Adsorption capacity data of ZSM-5 and modified ZSM-5 samples

Catalyst	Sample mass (mg)	Moisture content (wt%)	Adsorption capacity *n*-hexane (wt%)	*p*-xylene (wt%)	*o*-xylene (wt%)	1,2,4-TMB (wt%)
Z	49.7	4.3	10.3	3.0	2.7	2.8
Z-V-100/60	49.7	7.6	10.3	2.9	2.7	2.5
Z-V-200/60	50.3	7.5	10.3	3.0	2.7	2.9
Z-V-300/60	50.0	7.7	10.4	3.0	2.6	2.7
Z-V-400/60	49.7	6.0	10.2	3.0	2.8	3.0
Z-V-400/4x4	49.7	6.5	10.3	2.9	2.6	3.0
Z-V-400/6x10	50.0	8.6	10.4	2.7	2.6	2.6
Z-F-50/8	49.9	3.0	10.3	2.2	2.1	1.9
Z-F-50/4x10	50.1	3.8	5.7	0.7	0.3	0.1
Z-F-400/8	50.1	7.5	9.6	2.9	0.7	0.6
Z-F-400/4x5	50.0	4.5	7.5	2.1	0.3	0.0
Z-L-100/-	49.7	7.3	9.6	2.9	2.2	1.6
Z-L-100/- (60h)	49.9	8.5	9.8	3.0	2.4	1.7
Z-L-0.5/W	50.1	7.2	10.2	2.9	2.8	2.9
Z-L-5/W	50.1	7.7	10.5	2.8	2.7	2.9
Z-L-5/E	49.7	8.2	10.0	2.4	2.4	2.3
Z-L-5/H	50.1	8.0	9.7	3.3	2.3	0.3
error	± 0.15 mg in the capacity measurements for each of the adsorbates					

NOTE: A statistical error analysis was not possible. The error listed in the table above is a non-statistical estimation, based on accuracy of the equipment and reproducibility of the measurements.

The adsorption data for ZSM-5 samples modified by CVD in a static vacuum system (Z-V-*/* series) showed little change in adsorption capacity from the parent batch (sample Z) for any of the four adsorbates used (Table 4.12). The adsorption profiles of these samples did not show significant changes (Figures A-IX.2 to A-IX.7 in Appendix IX).

The adsorption data for ZSM-5 samples modified by CVD in a vapour phase flow system (Z-F-*/* series) showed significant changes in virtually all adsorption capacity measurements compared to the parent batch (Table 4.12). The adsorption profiles are given in Figures A-IX.8 to A-IX.11 of Appendix IX. The greatest decreases in adsorption capacities were observed for sample

Z-F-50/4x10 (Table 4.12). The *n*-hexane adsorption capacity decreased from 10.3 wt% for sample Z to 5.7 wt% for sample Z-F-50/4x10. Virtually no *o*-xylene (0.3 wt%) or 1,2,4-TMB (0.1 wt%) was adsorbed by sample Z-F-50/4x10 (Table 4.12). Sample Z-F-400/4x5 showed similar adsorption capacities for *o*-xylene and 1,2,4-TMB to those obtained for sample Z-F-50/4x10, although the decrease in *n*-hexane and *p*-xylene adsorption capacities was not as severe as for sample Z-F-50/4x10 when compared to the parent sample (Table 4.12). Both samples Z-F-50/8 and Z-F-400/8 showed decreases in adsorption capacities compared to sample Z, especially for the larger adsorbates such as *o*-xylene and 1,2,4-TMB (Table 4.12).

The adsorption data for ZSM-5 samples modified by CLD in a liquid phase system (Z-L-*/* series) showed significant changes in the adsorption capacities for several samples, mainly when larger adsorbates were used (Table 4.12). The adsorption profiles are shown in Figures A-IX.12 to A-IX.17 of Appendix IX. When pure TEOS was used (samples Z-L-100/- and Z-L-100/-(60h)) the adsorption capacities generally decreased for each of the adsorbates (Table 4.12). When water was used as diluent (samples Z-L-0.5/W and Z-L-5/W) no significant change in any of the adsorption capacities could be observed. The adsorption capacities of sample Z-L-5/E were slightly lower than the corresponding values for sample Z. However, the adsorption capacity for 1,2,4-TMB decreased from 2.8 wt% for sample Z to 0.3 wt% for sample Z-L-5/H, while the other adsorption capacity values for sample Z-L-5/H generally decreased slightly (Table 4.12).

4.3.2.2 Mordenite adsorption capacity data

Figure 4.23 shows the adsorption profiles of *n*-hexane, *p*-xylene, *o*-xylene and 1,2,4-trimethyl benzene on Mordenite (sample M). The Mordenite sample was virtually completely saturated with *n*-hexane after 60 min (*n*-hexane adsorption capacity = 5.7 wt% after 60 min). The adsorption capacities and profiles for *p*-xylene (1.7 wt%) and *o*-xylene (1.7 wt%) on sample M were essentially identical, and the adsorption capacity of 1,2,4-trimethyl benzene was 1.2 wt%. Adsorption profiles of the Mordenite samples modified by chemical vapour and liquid deposition methods are shown in Appendix IX. The moisture content and

adsorption capacities of the Mordenite and modified Mordenite samples are given in Table 4.13.

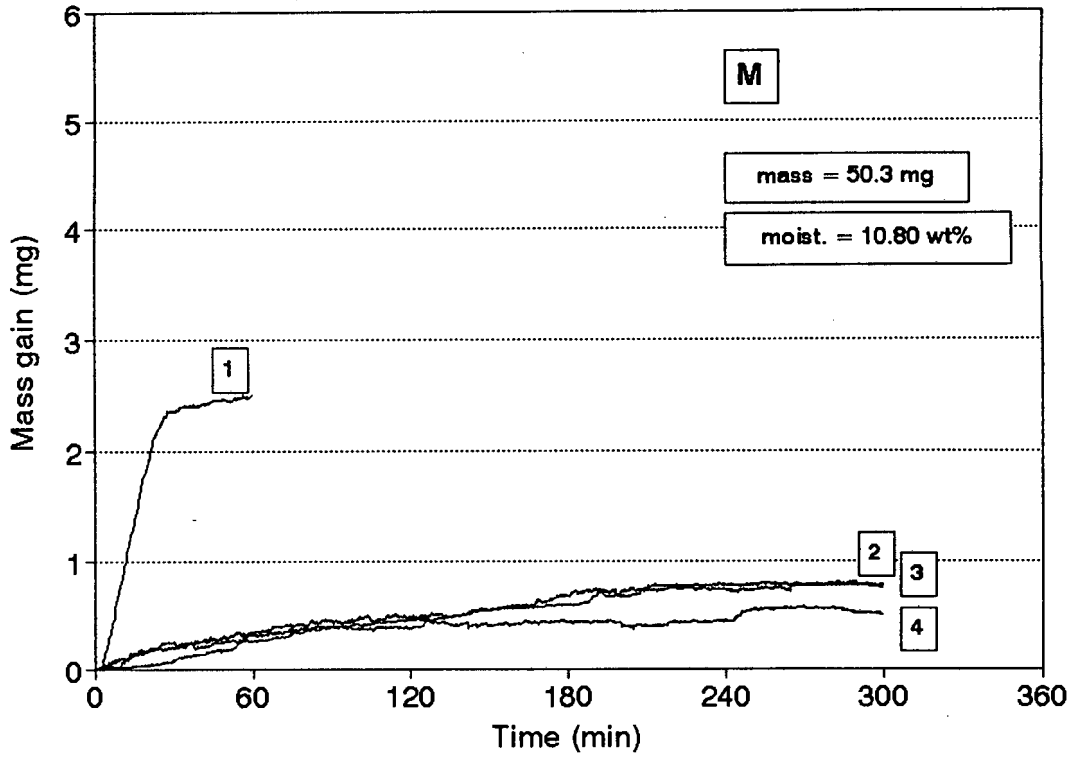

FIGURE 4.23: *n*-Hexane (1), *p*-xylene (2), *o*-xylene (3) and 1,2,4-TMB (4) adsorption profiles on Mordenite (sample M)

The greatest changes in adsorption data for the modified Mordenite samples was observed for *n*-hexane (Table 4.13). The *p*-xylene and *o*-xylene adsorption capacities of all samples were similar, although the adsorption capacity of 1,2,4-trimethyl benzene was typically slightly lower than adsorption capacities for the xylene isomers (Table 4.13). The *n*-hexane adsorption "capacities" decreased from 5.7 wt% for sample M to 4.7, 2.6 and 1.4 wt% for samples M-L-5/H, M-V-400/6x10 and M-F-400/8 respectively (Table 4.13). The adsorption profiles shown in Appendix IX showed that *n*-hexane equilibrium adsorption had in fact not been reached within the 60 min adsorption period for the experiment due to slow adsorption rates, especially for samples M-V-400/6x10 and M-F-400/8 (Figures A-IX.20 and A-IX.21). For both of these samples the *p*-xylene, *o*-xylene and 1,2,4-TMB adsorption capacities were similar, but lower than those of sample M (Table 4.13).

TABLE 4.13: Adsorption capacity data of Mordenite and modified Mordenite samples

Catalyst	Sample mass (mg)	Moisture content (wt%)	Adsorption capacity *n*-hexane (wt%)	*p*-xylene (wt%)	*o*-xylene (wt%)	1,2,4-TMB (wt%)
M	50.3	10.8	5.7	1.7	1.7	1.2
M-V-400/60	49.9	11.4	5.5	1.2	1.3	0.6
M-V-400/6x10	50.1	9.9	2.6	1.0	1.0	1.0
M-F-400/8	50.2	7.5	1.4	0.9	0.9	0.8
M-L-5/H	49.6	13.2	4.7	1.6	1.6	1.1
error	± 0.15 mg in the capacity measurements for each of the adsorbates					

NOTE: A statistical error analysis was not possible. The error listed in the table above is a non-statistical estimation, based on accuracy of the equipment and reproducibility of the measurements.

4.3.2.3 Beta adsorption capacity data

Figure 4.24 shows the adsorption profiles of *n*-hexane, *p*-xylene, *o*-xylene and 1,2,4-trimethyl benzene on Beta (sample B). The Beta sample was virtually saturated with *n*-hexane after 60 min (*n*-hexane adsorption capacity = 11.1 wt% after 60 min). The adsorption levels of *p*-xylene (3.2 wt%) and *o*-xylene (3.1 wt%) were similar after 300 min. The amount of 1,2,4-trimethyl benzene adsorbed (0.8 wt%) after 300 min was significantly less than the amount of *p*-xylene or *o*-xylene adsorbed by sample B. Adsorption profiles of the Beta samples modified by chemical vapour and liquid deposition methods are shown in Appendix IX. The moisture content and adsorption capacities of the Beta and modified Beta samples are given in Table 4.14.

The most noticeable change in adsorption data on modified Beta samples was observed for sample B-F-400/8 (Table 4.14). Essentially no *p*-xylene, *o*-xylene or 1,2,4-TMB was adsorbed (0.2 wt% max.) and the *n*-hexane adsorption "capacity" was reduced from 11.1 wt% for sample B to 2.1 wt% for sample B-F-400/8 (Table 4.14). However, sample B-F-400/8 was not saturated with *n*-hexane within the 60 min duration of the adsorption experiment (Figure A-IX.26 of Appendix IX). With some exceptions, reductions in adsorption

capacities for *n*-hexane, the xylene isomers and 1,2,4-TMB could be observed for all modified Beta samples (Table 4.14).

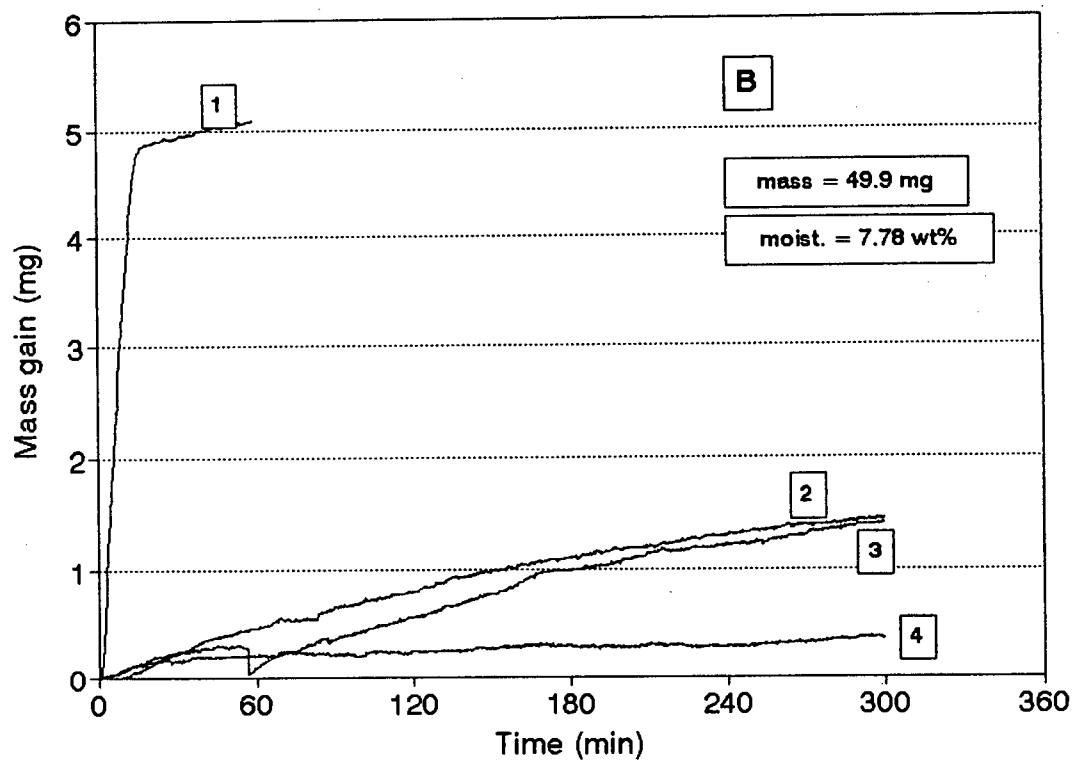

FIGURE 4.24: *n*-Hexane (1), *p*-xylene (2), *o*-xylene (3) and 1,2,4-TMB (4) adsorption profiles on Beta (sample B)

TABLE 4.14: Adsorption capacity data of Beta and modified Beta samples

Catalyst	Sample mass (mg)	Moisture content (wt%)	Adsorption capacity *n*-hexane (wt%)	*p*-xylene (wt%)	*o*-xylene (wt%)	1,2,4-TMB (wt%)
B	49.9	7.8	11.1	3.2	3.1	0.8
B-V-400/60	50.0	5.6	10.7	2.5	2.5	0.7
B-V-400/6x10	50.0	5.2	10.0	2.5	2.4	0.3
B-F-400/8	50.3	4.5	2.1	0.2	0.2	0.1
B-L-5/H	50.0	11.3	9.8	1.3	1.6	0.3
error	± 0.15 mg in the capacity measurements for each of the adsorbates					

NOTE: A statistical error analysis was not possible. The error listed in the table above is a non-statistical estimation, based on accuracy of the equipment and reproducibility of the measurements.

4.4 TETRAETHOXYSILANE DEPOSITION STUDIES

4.4.1 TEMPERATURE PROGRAMMED REACTION STUDIES

The deposition of tetraethoxysilane (TEOS) was studied during a temperature ramp from 50°C to 500°C at 5°C/min on HZSM-5 and Silicalite-I as described in Section 3.3.1. A blank run without catalyst showed that TEOS did not crack thermally at temperatures up to 500°C.

Figure 4.25 shows the main decomposition products detected during the temperature ramp on HZSM-5. Ethanol (*m/e* = 31) was observed at temperatures below ± 200°C (T_{max} = 175°C), whereas ethylene (*m/e* = 27) and H_2O were observed at temperatures higher than ± 200°C (T_{max} = 245°C) when passed over HZSM-5. No TEOS was observed during the course of the experiment. At temperatures above ± 300°C higher hydrocarbons were observed, although these could not be identified. Although both ethanol and ethylene were observed when TEOS was passed over Silicalite-I, TEOS was partly unconverted at all temperatures.

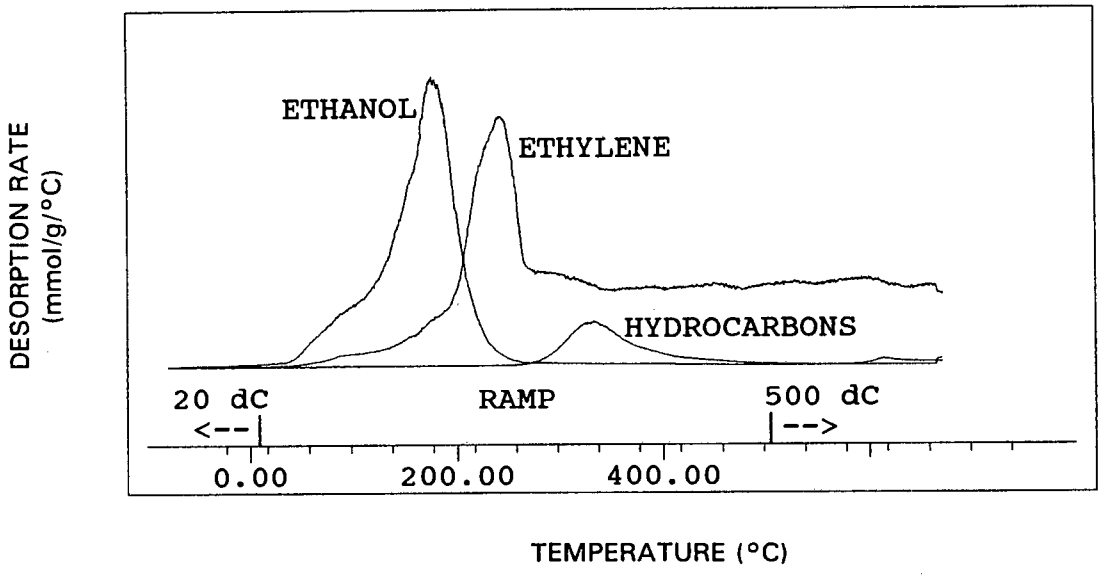

FIGURE 4.25: TEOS deposition on ZSM-5 during temperature ramp from 20 - 500°C (sample Z, 0.2 g, 30 ml/min helium carrier gas, TEOS part. press. ± 2.1 mbar)

4.4.2 ISOTHERMAL REACTION STUDIES

The deposition of tetraethoxysilane (TEOS) was studied at 50°C and at 400°C on HZSM-5, Silicalite-I and silica, as described in Section 3.3.2. TEOS was fed by saturator (30 ml/min helium carrier gas). The product stream was analyzed by mass spectrometer during the course of each deposition cycle. When steady state was reached the catalyst was regenerated (30 ml/min air, 500°C, 2 h) after which the deposition cycle was repeated.

4.4.2.1 Low temperature

Figure 4.26 shows breakthrough curves for TEOS passed over 0.2 g HZSM-5, Silicalite-I and silica at 50°C. During the first 100 min of the first deposition cycle on HZSM-5 no TEOS was detected, suggesting that all the TEOS decomposed. The major decomposition product detected by the mass spectrometer during TEOS deposition on HZSM-5 at 50°C was ethanol (Figure 4.27).

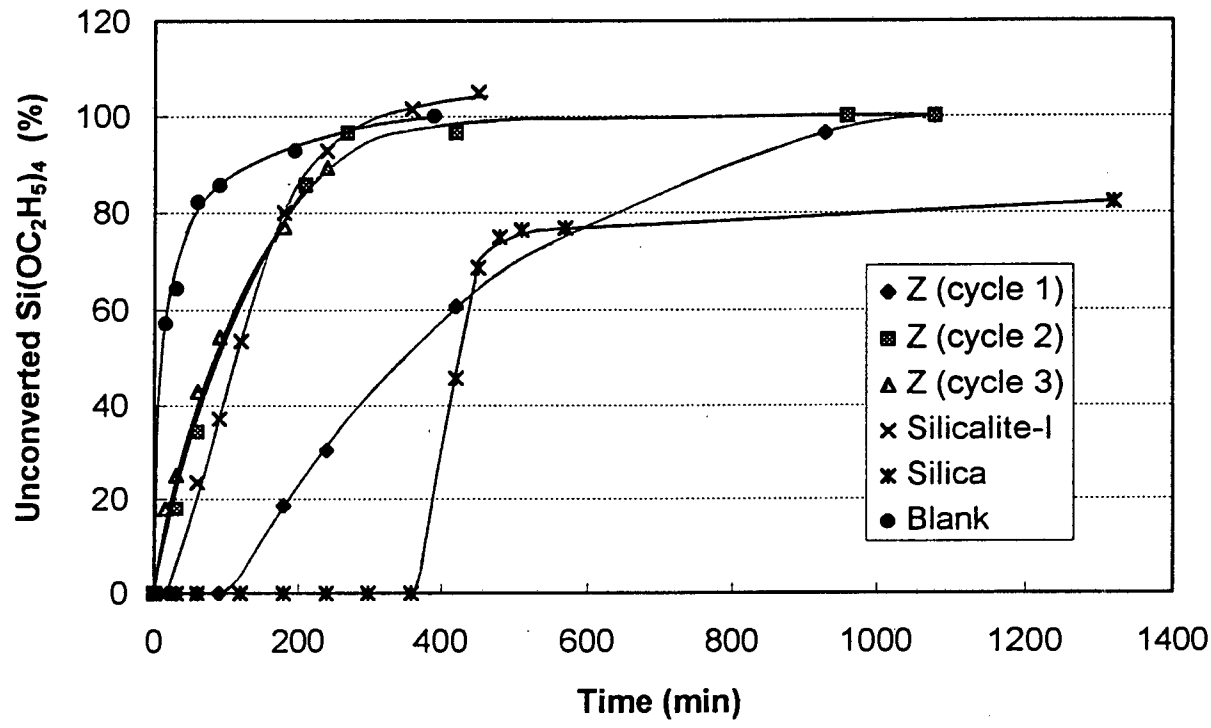

FIGURE 4.26: TEOS deposition at 50°C (0.2 g, 30 ml/min helium carrier gas, TEOS part. press. ± 2.1 mbar)

After the first 100 min the amount of TEOS decomposed decreased until no more TEOS was decomposed from about 1000 min onwards. After successive regenerations, during the second and third cycles respectively, progressively less TEOS was decomposed after any given time period compared to the first cycle (Figure 4.26). In fact, the amount of TEOS which decomposed on HZSM-5 during the second and third cycles was comparable to the amount which decomposed when TEOS was deposited on Silicalite-I at 50°C (Figure 4.26). When TEOS was deposited on SiO_2 at 50°C, no TEOS was detected during the first 360 min (Figure 4.26). TEOS did not decompose on SiO_2 at 50°C because no ethanol, or any other decomposition products, were present in the product stream (Figure 4.27). Hence TEOS was able to be physisorbed but not decomposed by SiO_2 at 50°C.

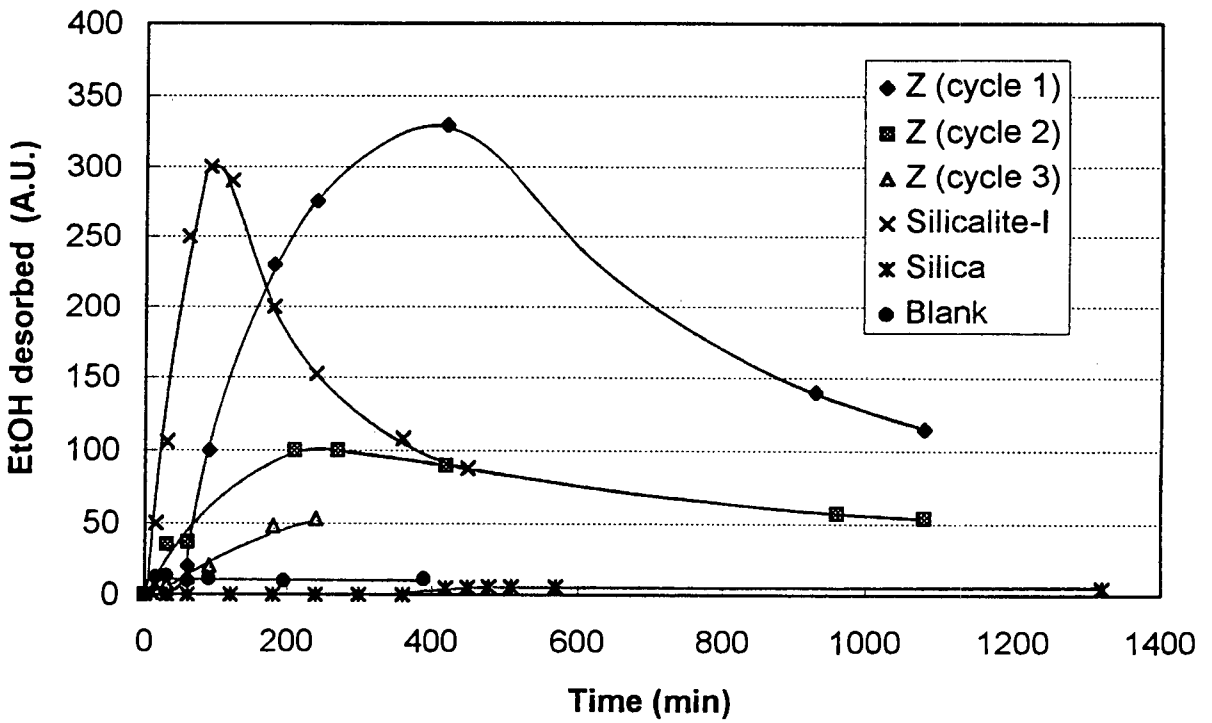

FIGURE 4.27: Ethanol formation during TEOS deposition at 50°C (0.2 g, 30 ml/min helium carrier gas, TEOS part. press. ± 2.1 mbar)

The major decomposition product on HZSM-5 at 50°C was found to be ethanol and the corresponding breakthrough curves for ethanol are shown in Figure 4.27. During the initial stages of TEOS deposition at 50°C, the ethanol formed was adsorbed by both HZSM-5 and Silicalite-I, because during this time no ethanol was detected while TEOS was being deposited on the catalyst. As the

catalyst became saturated, the ethanol peak rose to a maximum (t_{max} = 400 min), but decreased when no more TEOS was decomposed, and ethanol was desorbed from the catalyst by the carrier gas (Figure 4.27). During subsequent deposition cycles less ethanol was detected, and the ethanol peak reached a maximum more quickly (t_{max} = 240 min) than what was observed in the previous cycle (Figure 4.27) because less TEOS was converted (Figures 4.26). Whereas similar amounts of TEOS seemed to be decomposed on Silicalite-I and during the second deposition cycle on HZSM-5 (Figure 4.26), the ethanol breakthrough curve for Silicalite-I (t_{max} = 90 min) was quite different to that of the second deposition cycle on HZSM-5 (t_{max} = 240 min) (Figure 4.27). Because Silicalite-I is more hydrophobic than HZSM-5, ethanol was weakly adsorbed by Silicalite-I, and hence it was removed more easily from Silicalite-I. No ethanol was detected when TEOS was passed over SiO_2 at 50°C (Figure 4.27).

Figure 4.28 shows that little or no ethylene was detected when TEOS was passed over HZSM-5, Silicalite-I or silica at 50°C. Figure 4.29 shows some desorption of H_2O from Silicalite-I and during the first cycle of TEOS decomposition from HZSM-5.

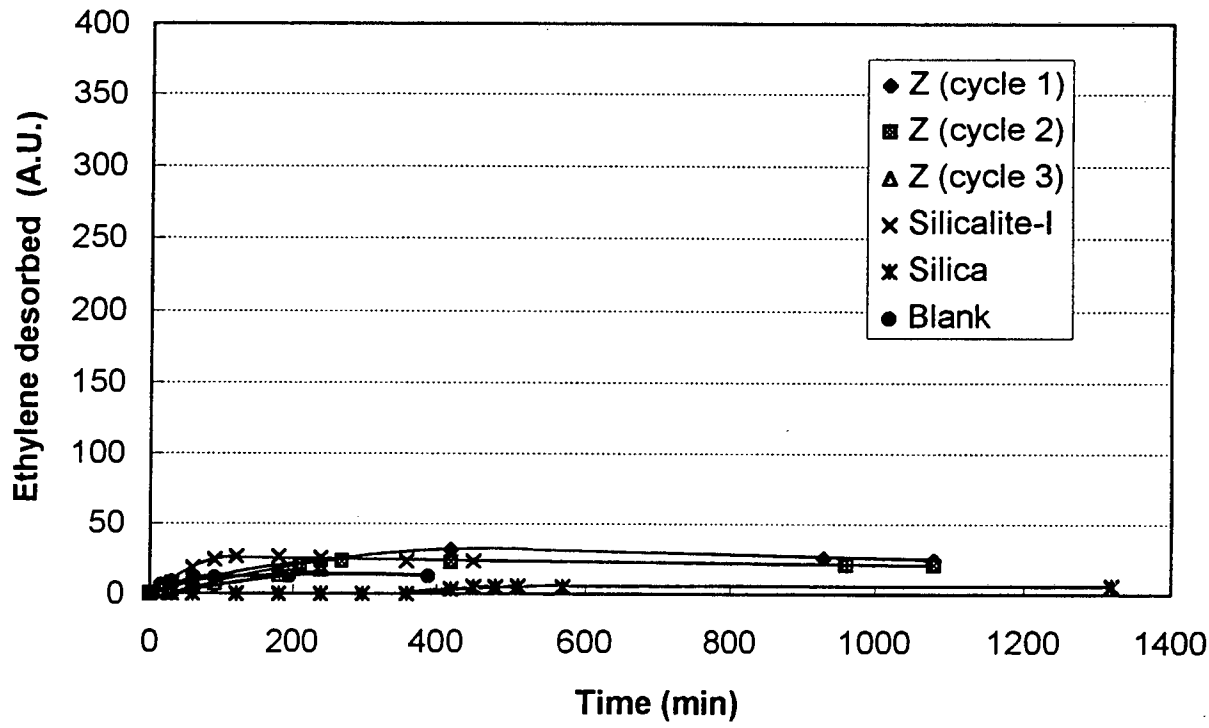

FIGURE 4.28: Ethylene formation during TEOS deposition at 50°C (0.2 g, 30 ml/min helium carrier gas, TEOS part. press. ± 2.1 mbar)

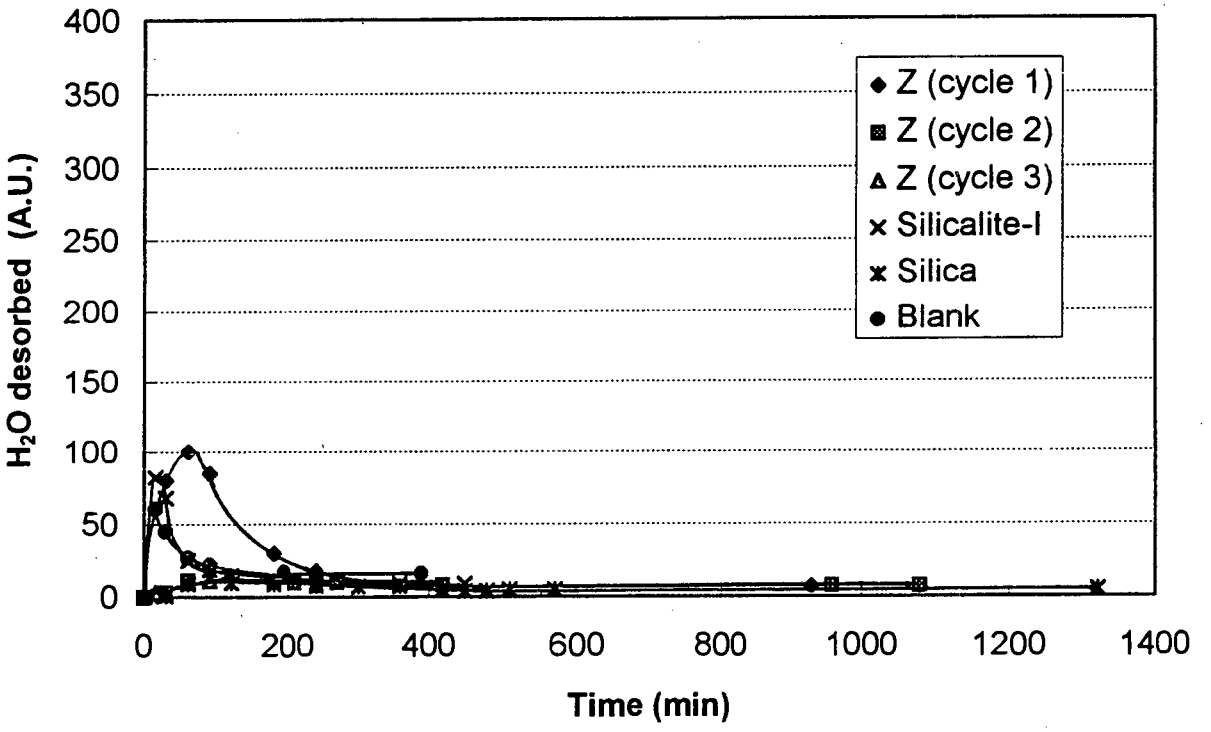

FIGURE 4.29: H_2O formation during TEOS deposition at 50°C (0.2 g, 30 ml/min helium carrier gas, TEOS part. press. ± 2.1 mbar)

4.4.2.2 High temperature

When the deposition of TEOS was carried out on HZSM-5 at 400°C, TEOS was completely decomposed during the first 70 min of cycle 1 (Figure 4.30) and even after 800 min approximately 60% of TEOS was converted to ethylene and H_2O by HZSM-5. No ethanol was detected for HZSM-5 and Silicalite-I at 400°C (Figure 4.31) but the corresponding ethylene and H_2O breakthrough curves are shown in Figures 4.32 and 4.33 respectively. After regeneration at the end of each cycle, subsequent cycles indicated that TEOS was still partially converted when the deposition was carried out at 400°C (Figure 4.30).

In contrast to the sample kept at 50°C, the active sites on HZSM-5 remained strong enough for the decomposition of TEOS at 400°C and a steady state conversion of 60% was obtained. When TEOS was passed over Silicalite-I at 400°C, TEOS was decomposed into ethylene and H_2O during the first 200 min, after which no more TEOS was decomposed (Figures 4.30, 4.32 and 4.33).

When TEOS was deposited on SiO_2 at 400°C ethylene and H_2O were formed during the first 30 - 45 min (Figures 4.32 and 4.33), but thereafter only ethanol was formed (Figure 4.31).

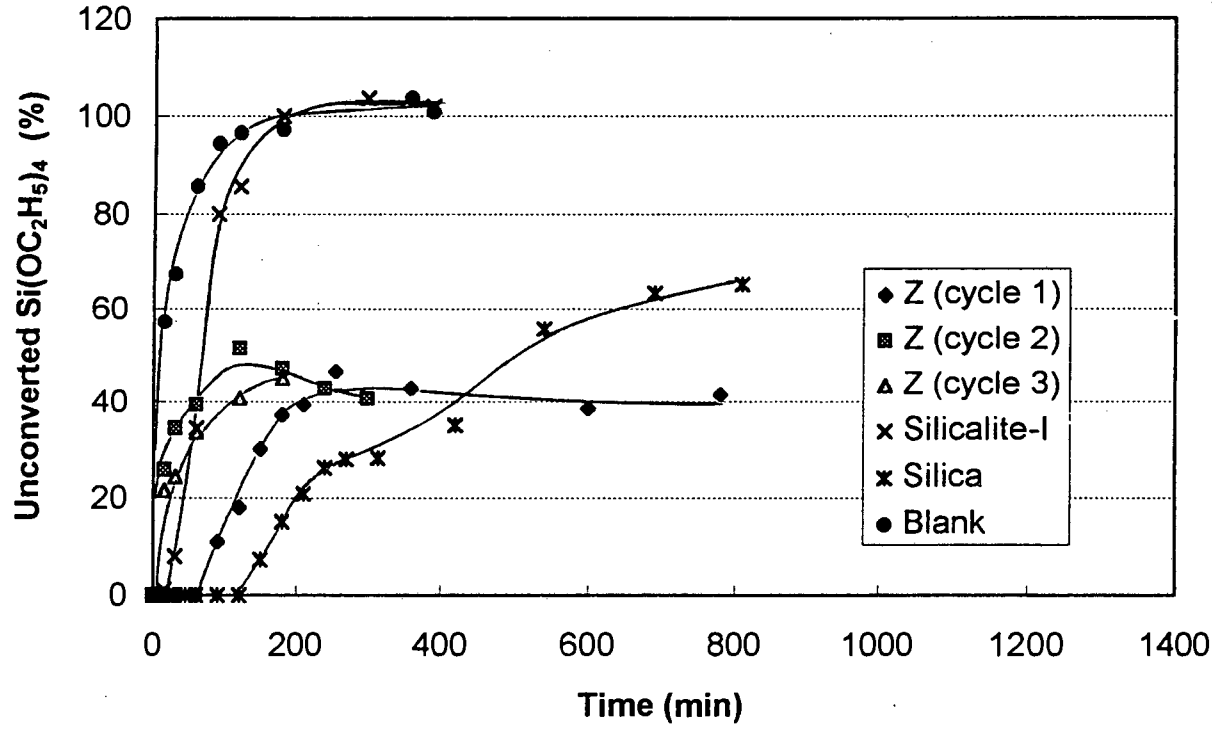

FIGURE 4.30: TEOS deposition at 400°C (0.2 g, 30 ml/min helium carrier gas, TEOS part. press. ± 2.1 mbar)

Figure 4.32 shows that the ethylene breakthrough curve for the first deposition cycle on HZSM-5 at 400°C reached a constant value after about 200 min. This time corresponded approximately to the TEOS conversion reaching a steady state value on HZSM-5 at 400°C (Figure 4.30). During deposition cycles 2 and 3 less ethylene was detected than during cycle 1, corresponding to a slightly lower TEOS conversion during cycles 2 and 3 (Figure 4.30). However, the amounts of ethylene detected in cycles 2 and 3 were very similar, suggesting that the external surface was hardly altered between the second and third cycle (Figure 4.32). Trends similar to ethylene were observed for H_2O (Figure 4.33). The amount of ethylene formed on Silicalite-I at 400°C was small (Figure 4.32).

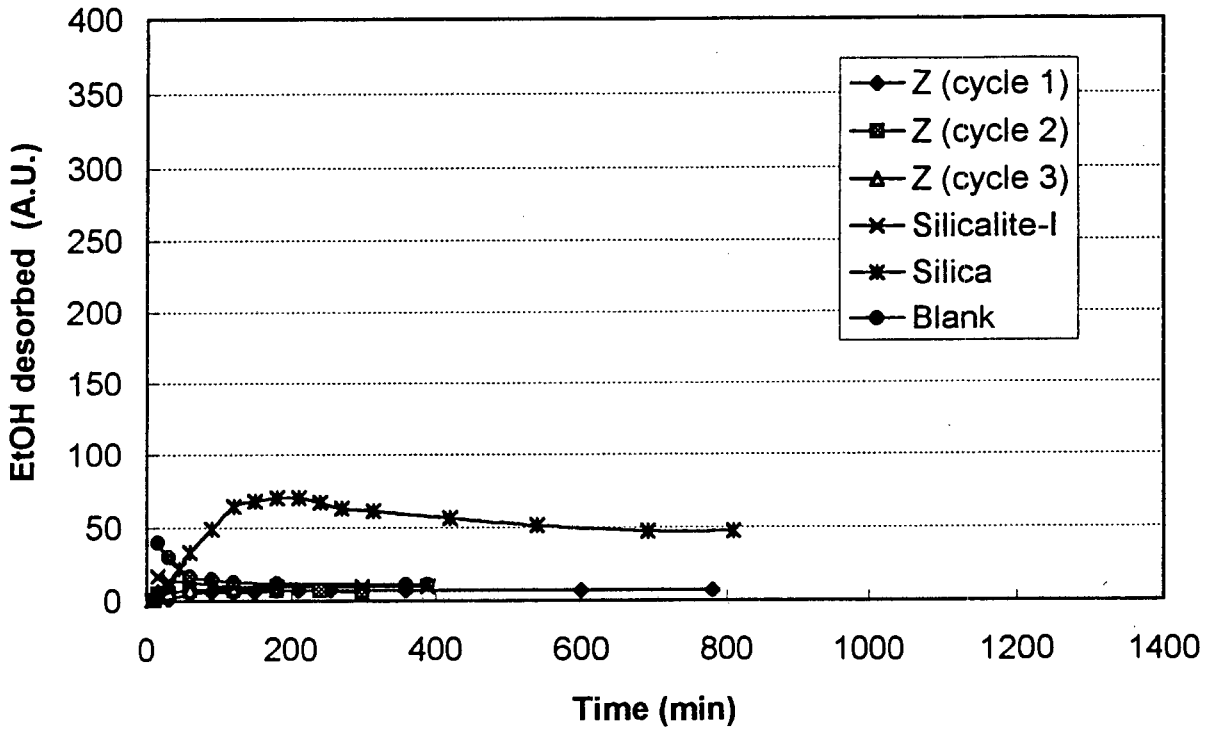

FIGURE 4.31: Ethanol formation during TEOS deposition at 400°C (0.2 g, 30 ml/min helium carrier gas, TEOS part. press. ± 2.1 mbar)

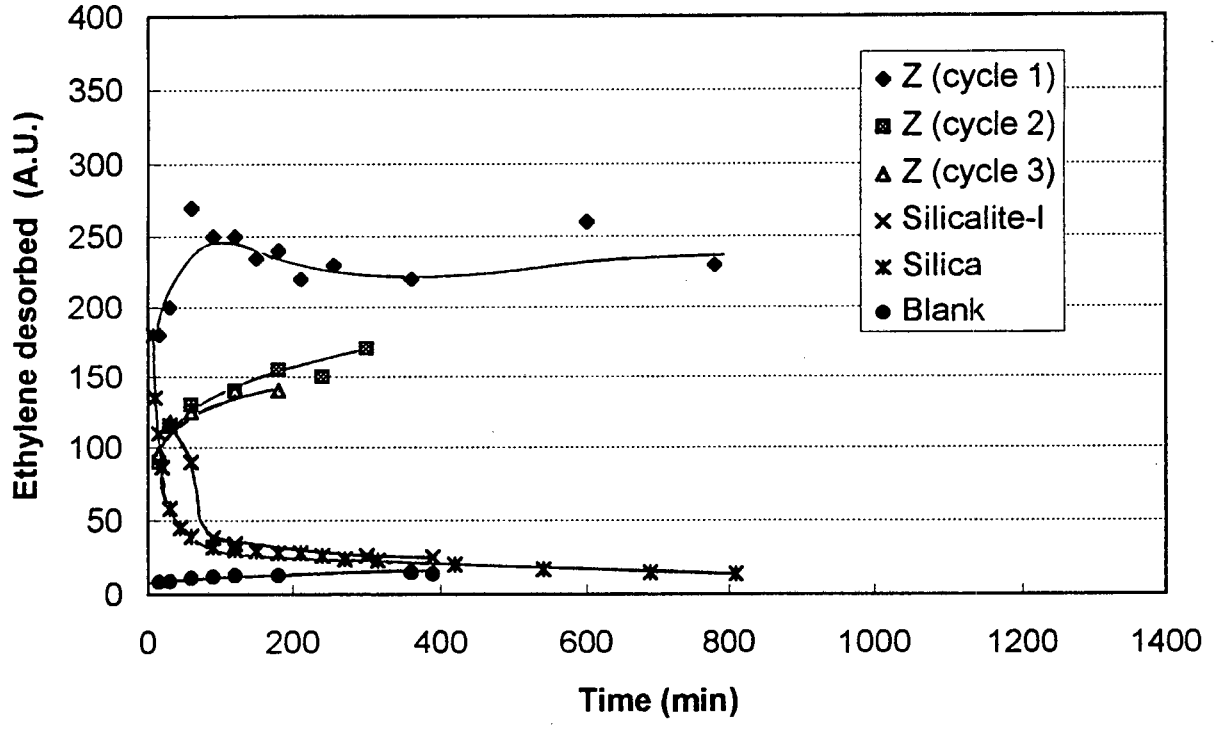

FIGURE 4.32: Ethylene formation during TEOS deposition at 400°C (0.2 g, 30 ml/min helium carrier gas, TEOS part. press. ± 2.1 mbar)

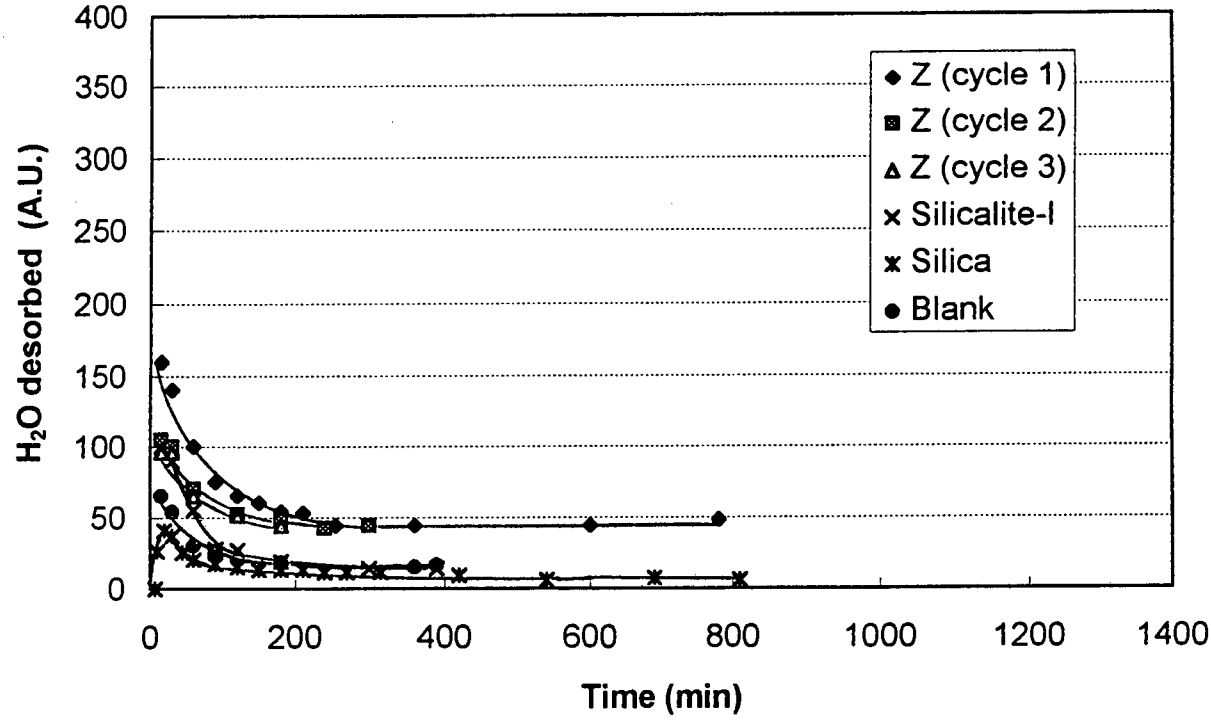

FIGURE 4.33: H_2O formation during TEOS deposition at 400°C (0.2 g, 30 ml/min helium carrier gas, TEOS part. press. ± 2.1 mbar)

4.4.3 THERMOGRAVIMETRIC ANALYSIS

The weight gain upon deposition of TEOS was measured by TGA for HZSM-5 samples kept at different temperatures as described in Section 3.3.3. TEOS was fed by saturator (50 mg catalyst, 30 ml/min N_2 carrier gas, 10 h).

Figure 4.34 and Table 4.15 clearly show that the higher the deposition temperature the greater the weight gain. The weight gain reached a constant value of 3.2 wt% after 600 min at 100°C, indicating that no more deposition of TEOS occurred (Figure 4.34). At 450°C the sample was still gaining weight steadily after 600 min, suggesting that at higher temperatures the deposition of TEOS continued (Figure 4.34). However, the sample modified at 100°C lost 75% of the mass gained by the deposition after calcination, whereas the sample modified at 450°C only lost 3% of the mass originally gained (Table 4.15).

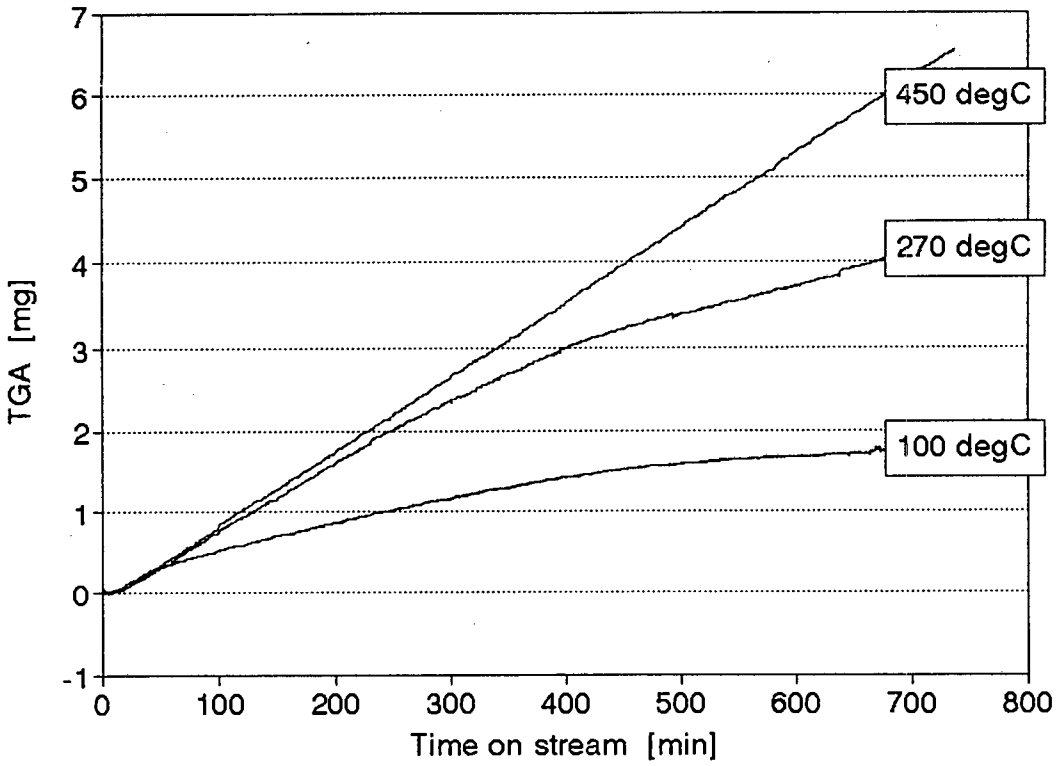

FIGURE 4.34: Weight gain during TEOS deposition on HZSM-5 (50 mg, 30 ml/min nitrogen carrier gas, TEOS part. press. ± 0.5 mbar)

TABLE 4.15: Comparison of HZSM-5 weight gain during TEOS deposition with deposition temperature after 10 h

Deposition temperature (°C)	weight gain (%)	weight gain after calcination (%)	weight loss during calcination (%)
100	3.2	0.8	75
270	7.5	6.6	12
450	10.6	10.3	3

NOTE: The weight lost during calcination is expressed as a percentage of the total weight gained during the TEOS deposition.

4.5 THE CONVERSION OF 1,3,5-TRIISOPROPYL BENZENE

The conversion of 1,3,5-triisopropyl (TiPB) benzene was studied to investigate the external surface activity of selected samples. Only modified samples showing inertised external surface acidities as measured by MQ-TPD were used as comparison with their respective parent samples. Post-modification treatment was used to determine whether the silica layer was irreversibly attached to the external surface. Post-modification treatment consisted of grinding the sample in a mortar and pestle prior to loading the catalyst as described in Section 3.4. To indicate that the sample had been subjected to post-modification treatment or grinding the term "(crushed)" is added after the sample name.

4.5.1 ZSM-5

The conversion of TiPB was carried out on sample Z (crushed), sample Z-V-400/6x10 (crushed) and sample Z-V-400/6x10 (Figure 4.35).

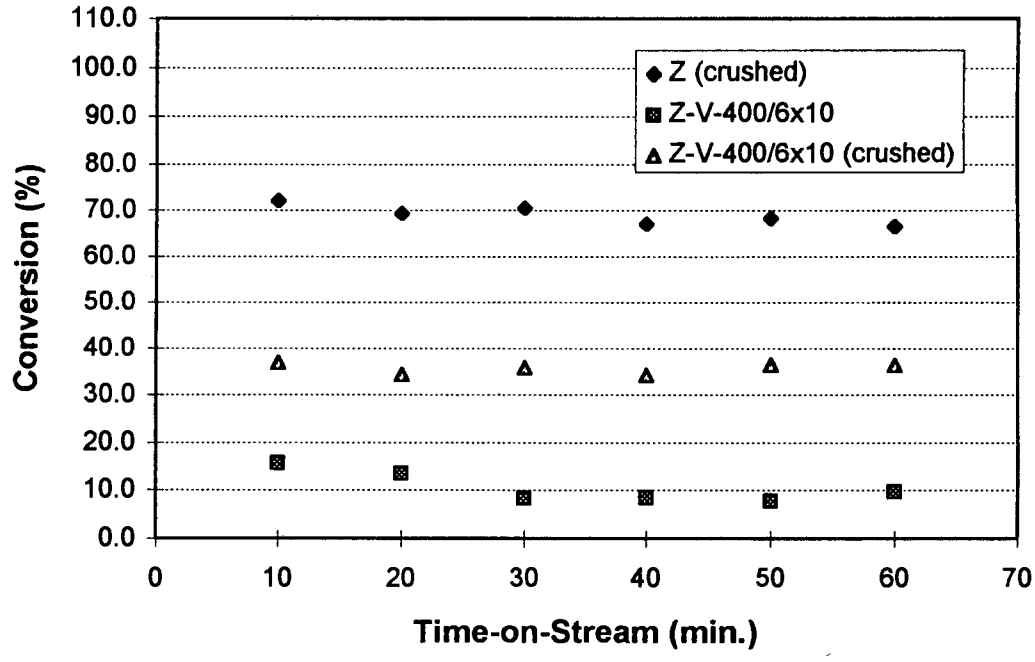

FIGURE 4.35: The conversion of TiPB on ZSM-5 and modified ZSM-5 samples (0.1 g, WHSV = 0.6 h^{-1}, 270°C)

The conversion for sample Z (crushed) was found to be ± 70%. Although sample Z was not tested, Mordenite samples showed that the conversion on sample M was slightly lower than on sample M (crushed) (Section 4.5.2). The conversion for sample Z-V-400/6x10 was found to be ± 15-8%, indicating that chemical vapour deposition using TEOS had significantly decreased the external surface activity of the modified sample. Grinding the modified sample resulted in a conversion of ± 35% for sample Z-V-400/6x10 (crushed), indicating that grinding may have partly destroyed the silica layer deposited during CVD on sample Z-V-400/6x10, thus resulting in a higher conversion for sample Z-V-400/6x10 (crushed) than for sample Z-V-400/6x10. Figure 4.36 shows that the mass balances for the conversion of TiPB over the samples shown in Figure 4.35 were within ± 5%.

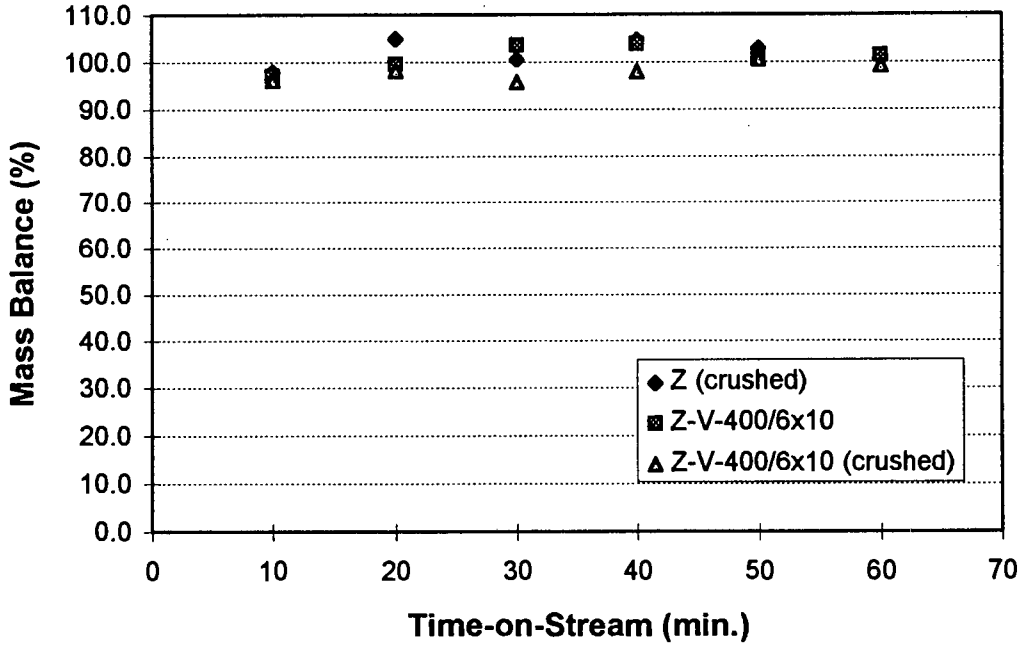

FIGURE 4.36: Mass balances for the conversion of TiPB on ZSM-5 and modified ZSM-5 samples

4.5.2 MORDENITE

The conversion of TiPB benzene was carried out on sample M, sample M (crushed), sample M-V-400/6x10 and sample M-V-400/6x10 (crushed) (Figure 4.37). The conversion on the Mordenite samples decreased with time. The conversion for sample M (crushed) was higher than that of sample M throughout the experiment, indicating that grinding the parent sample resulted in a greater external surface activity, possibly due to a greater external surface area. The conversion of sample M-V-400/6x10 was less than 20% throughout the experiment, indicating that the modification was successful. However, the conversion of sample M-V-400/6x10 (crushed) ranged from 95% after 10 min to 65% after 60 min. Similar to observations for ZSM-5, grinding may have partly destroyed the silica layer deposited during CVD on sample M-V-400/6x10, thus resulting in a much higher conversion for sample M-V-400/6x10 (crushed) than for sample M-V-400/6x10.

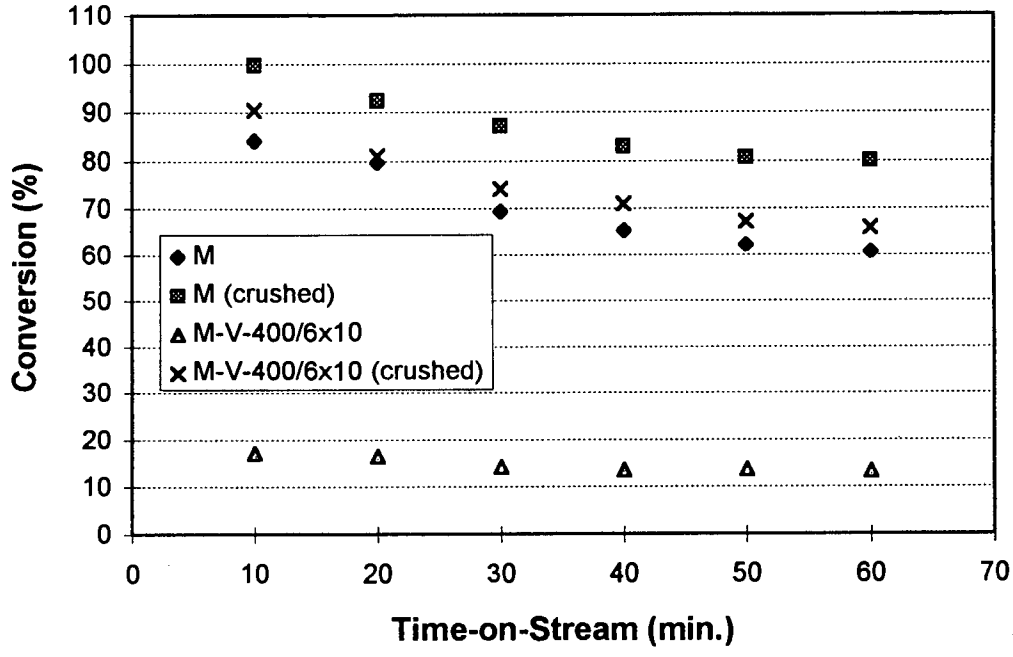

FIGURE 4.37: The conversion of TiPB on Mordenite and modified Mordenite samples (0.1 g, WHSV = 0.6 h^{-1}, 200°C)

Figure 4.38 shows the mass balances for the conversion of TiPB over the samples shown in Figure 4.37. The cracking products of 1,3,5-triisopropyl benzene are able to enter the channels of Mordenite (6.5 x 7.0 Å), and therefore the mass balance was as low as 20% after 10 min. on stream. The mass balances improved with time-on-stream, presumably because less products were adsorbed by the samples. However, because of the successful inertisation of sample M-V-400/6x10 the conversion on sample M-V-400/6x10 was low (Figure 4.37) and therefore there were few cracking products that could be adsorbed by this sample, resulting in the mass balances that were close to 100% (Figure 4.38).

By-pass samples were taken prior to the experiment to ensure that the apparatus was operating at steady state and that there were no fluctuations in the flows through the saturators. In addition, the ampoule sampling system allowed the user to take several samples at quick intervals, and hence the reproducibility of the samples could easily be determined. Therefore, even though adsorption of reaction products by the samples resulted in "poor" mass balances, the conversions were assumed to be accurate provided the reproducibility of the by-pass samples and gas samples was established.

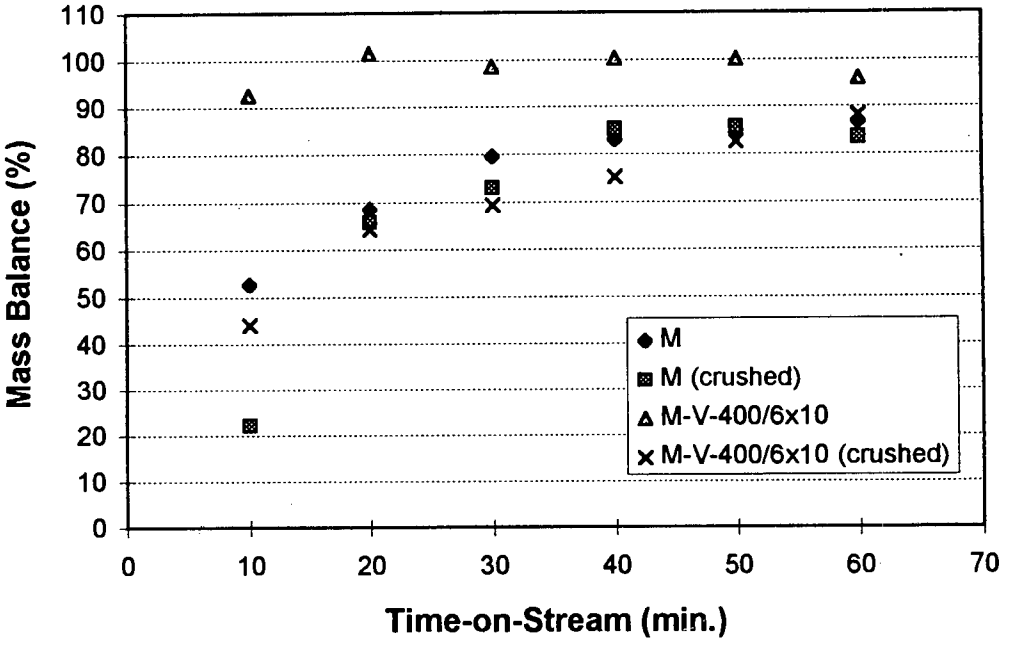

FIGURE 4.38: Mass balances for the conversion of TiPB on Mordenite and modified Mordenite samples

4.5.3 BETA

The conversion of TiPB benzene was carried out on sample B (crushed), sample B-V-400/6x10 (crushed) and sample B-V-400/6x10 (Figure 4.39). The conversion on the Beta samples decreased relatively rapidly with time. Although the conversion of the Beta samples decreased in the order

B (crushed) > B-V-400/6x10 (crushed) > B-V-400/6x10

little difference was observed between the samples, and the CVD process did not seem to have inertised the external surface of sample B-V-400/6x10 successfully according to TiPB conversion measurements.

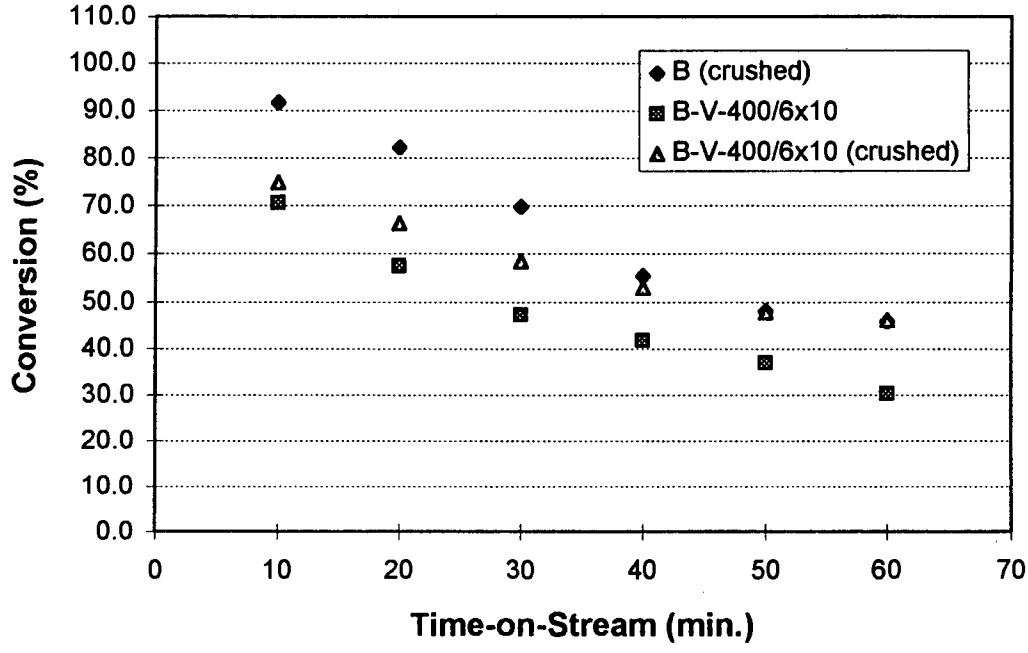

FIGURE 4.39: The conversion of TiPB on Beta and modified Beta samples (0.1 g, WHSV = 0.6 h^{-1}, 160°C)

Figure 4.40 shows the mass balances for the conversion of TiPB over the samples shown in Figure 4.39. The cracking products of 1,3,5-triisopropyl benzene are able to enter the channels of Beta (7.6 x 6.4 Å), and therefore the mass balance was as low as 25% after only 10 min. on stream. As was observed for Mordenite, the mass balances improved with time-on-stream, presumably because less products were adsorbed by the samples. Even though adsorption of reaction products by the samples resulted in "poor" mass balances, the conversions were assumed to be accurate provided the reproducibility of the by-pass samples and gas samples was established.

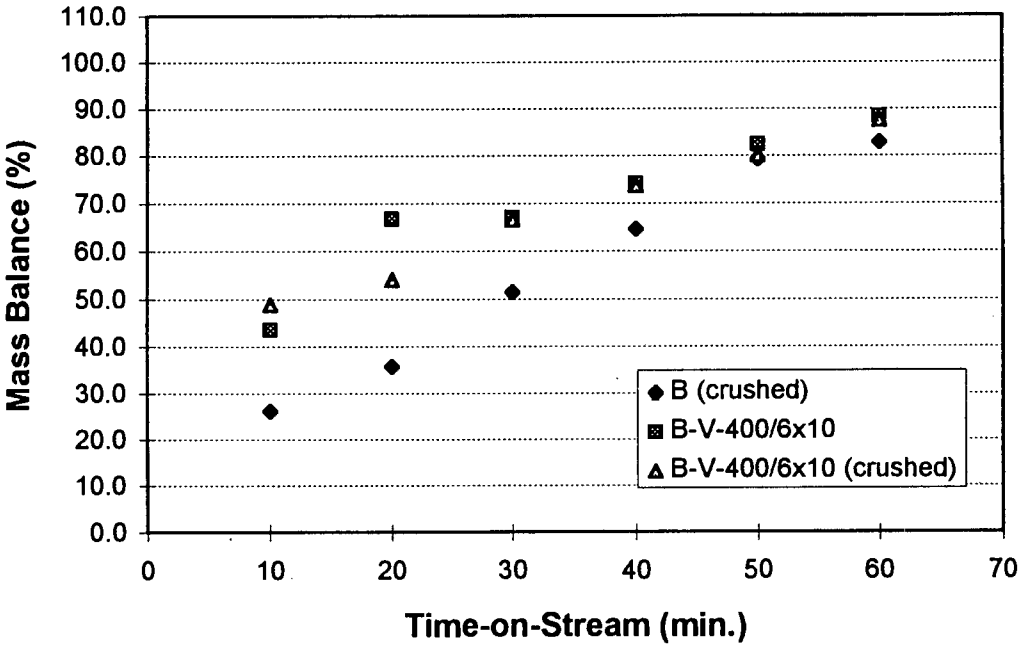

FIGURE 4.40: Mass balances for the conversion of TiPB on Beta and modified Beta samples

CHAPTER 5

DISCUSSION

"If we don't stand for something, we will fall for anything"

John Cougar Mellencamp, *on the album* **'Scarecrow'**

5.1 EVALUATION OF CHARACTERIZATION TECHNIQUES

5.1.1 PHYSICO-CHEMICAL CHARACTERIZATION OF ZSM-5

The Si/Al ratio obtained by AA for sample Z (Si/Al = 34) corresponded well to the Si/Al ratio in the synthesis gel (Si/Al = 35). The aluminium content obtained by AA for sample Z (0.42 mmol/g) also corresponded well to the theoretical aluminium content calculated from the unit cell formula for ZSM-5 with a Si/Al ratio of 35 (0.44 mmol/g) (Appendix III), indicating that the final ZSM-5 obtained from the synthesis had a composition close to the desired composition. Furthermore, the number of acid sites obtained by NH_3-TPD and Py-TPD were 0.43 and 0.46 mmol/g respectively (Table 4.4). Therefore the results obtained with both TPD apparatus were in good agreement with each other, and the number of acid sites obtained by TPD corresponded to the aluminium content obtained by AA and to the theoretical aluminium content.

The average yield of zeolite was 8.16 g as-synthesized NaZSM-5 per 100 g synthesis gel which, based on either aluminium or silicon, corresponded to ± 89% of the theoretical maximum yield (Appendix III). The Na/Al ratio of the as-synthesized NaZSM-5 was found to be less than 1 (typically 0.5 - 0.75), suggesting that the TPA^+ ion also acted as charge balancing ion [Flanigen *et al.*, 1978; Zones, 1989]. The weight loss due to detemplation was estimated to be 9.8 wt% (Appendix III).

The pH of the supernatant liquor decreased from 12.9 to 12.15 within the first 6 h, after which the pH increased again to a steady value of 12.3 - 12.4 from about 16 h onwards (Appendix III). Brinker and Scherer [1990] reported that particles 1 - 2 nm in diameter are rapidly formed at pH values greater than 7 for aqueous silicates, and that polymerization occurs via a nucleophilic mechanism:

$$\equiv Si\text{-}OH + OH^- \xrightarrow[fast]{} \equiv Si\text{-}O^- + H_2O \quad (1)$$

$$\equiv Si\text{-}O^- + HO\text{-}Si\equiv \xrightarrow[slow]{} \equiv Si\text{-}O\text{-}Si\equiv + OH^- \quad (2)$$

Step 1 is fast and may have caused a decrease in pH shortly after the start of the synthesis, whereas the pH may have increased when Step 2 occurred. Zones [1989] suggested that the pH increased as the hydroxide was transported from the gel into the solution as siloxane bonds were formed. An

increase in pH of the supernatant liquor reflects changes in the mass of zeolite recovered from the gel [Camblor and Pérez-Pariente, 1991].

A decrease in pH with time may be indicative of hydroxide consumption during Hoffmann degradation of certain organocations that have not been incorporated into the zeolite [Zones, 1989]. However, the TPA^+ ions used in the synthesis of the parent ZSM-5 do not experience Hoffmann degradation to any great extent, and the constant final pH value of 12.3 - 12.4 obtained here was similar to a constant final pH value of 12 reported by Zones [1989] for ZSM-5.

It has been reported that aluminium zoning may occur in ZSM-5 crystals [Suib *et al.*, 1980; Derouane *et al.*, 1981; Von Ballmoos and Meier, 1981; Hughes *et al.*, 1983; Chao and Chern, 1988]. Aluminium incorporation increases with increasing pH. The incorporation of aluminium into the zeolite structure is disruptive and may therefore retard crystallization, thus resulting in an aluminium enrichment on the outer edge of the growing crystals [Zones, 1989]. If aluminium zoning occurred in the parent ZSM-5 crystals this was only likely to have taken place early on in the synthesis, because the pH remained constant after the first 16 h. This was confirmed by the fact that during the entire course of the timed synthesis study the bulk Si/Al ratios of the solids remained constant (Appendix III).

5.1.2 TEMPERATURE PROGRAMMED DESORPTION SPECTRA

Blank runs indicated no adsorption/desorption of ammonia, pyridine or 4-methyl quinoline from equipment lines. NH_3-TPD data was obtained for the parent HZSM-5 (sample Z), Mordenite (sample M) and Beta (sample B) batches to cross-calibrate the total number of acid sites with results obtained using Py-TPD. The NH_3-TPD, Py-TPD and MQ-TPD spectra of the three parent zeolites are discussed in sections 5.1.2.1 - 5.1.2.3 and the number of acid sites measured by NH_3-TPD and Py-TPD are subsequently also compared quantitatively with the aluminium content obtained by AA for each parent zeolite (Section 5.1.2.4).

5.1.2.1 NH_3-TPD spectra of ZSM-5, Mordenite and Beta

A single high temperature desorption (HTD) peak was observed for ammonia desorption from ZSM-5 (sample Z), Mordenite (sample M) and Beta (sample B), indicating that the samples contained no physisorbed ammonia (Figure 4.13). The peak shape of the NH_3-TPD spectra from both ZSM-5 and Mordenite were skewed towards higher desorption temperatures, thus showing a leading edge. These leading edges are indicative of the combined effects of diffusional restrictions and readsorption in the channels of ZSM-5 and Mordenite [Gorte, 1982; Herz *et al.*, 1982; Jones and Griffin, 1983; Demmin and Gorte, 1984]. The peak shape of the NH_3-TPD spectrum from Beta showed a trailing edge. Using identical experimental conditions (0.25 g, 70 ml/min, 10°C/min) but using different zeolite structures with different Si/Al ratios the peak maximum temperatures were found to increase in the order: Beta (346°C), ZSM-5 (440°C) and Mordenite (568°C) (Table 4.4). This data may therefore indicate that the diffusional restrictions and readsorption effects for ammonia desorption from the 3-dimensional large port Beta were less pronounced than for the medium port ZSM-5 or the 1-dimensional Mordenite [Rieck and Bell, 1984] (Section 2.3.1.2).

5.1.2.2 Py-TPD spectra of ZSM-5, Mordenite and Beta

Using identical experimental conditions (0.10 g, 100 ml/min, 10°C/min) the peak maximum temperatures in this work were found to increase in the order: Silicalite-I (290°C), Beta (630°C), Mordenite (637°C) and ZSM-5 (667°C) (Table 4.4). Direct comparisons of the peak maximum temperatures for the Py-TPD and NH_3-TPD spectra must be treated with caution, because of the different experimental conditions that were used (see Section 2.3.1). However, electrons can be delocalized by the resonance effect of the ring structure in pyridine, thereby stabilizing the adsorbed structure. Even though ammonia is the stronger base, the zeolite-pyridine complex is thought to be more stable than the zeolite-ammonia complex. Furthermore, the diffusional resistances in the channels are greater for pyridine than for ammonia, thereby resulting in a higher peak maximum temperature for pyridine than for ammonia [Sharma *et al.*, 1993].

Similar to the NH_3-TPD spectrum from ZSM-5 (Figure 4.13), a single high temperature desorption (HTD) peak was observed for pyridine desorption from ZSM-5 (sample Z), indicating that because the experimental method was designed to prevent this, the ZSM-5 sample contained no physisorbed pyridine. However, the peak was skewed to higher desorption temperatures (Figure 4.14), indicating that diffusional restrictions and readsorption effects were present [Rieck and Bell, 1984]. On the other hand, only a small desorption peak was obtained for Silicalite-I (Figure 4.14) because Silicalite-I has a crystalline structure with little acidity (0.02 mmol/g).

Contrary to the NH_3-TPD spectra, the Py-TPD peaks from Mordenite (sample M) and Beta (sample B) were broad and irregular (Figure 4.14). TPD spectra from dealuminated Mordenite presented by Karge and Dondur [1990] also showed a broader TPD peak for pyridine than for ammonia. Their spectra were obtained under vacuum (10 mg, 20°C/min). Peak maximum temperatures of 402 and 397°C were reported by Karge and Dondur [1990] for ammonia and pyridine TPD spectra respectively, although shoulders were observed at 502 and 652°C in the Py-TPD spectrum. In fact, it was proposed that their TPD spectra could be deconvoluted to show desorption from 4 different types of acid sites from the Mordenite samples, viz. weak and strong Brönsted and Lewis acidity. Hence the broadness of the Py-TPD peaks for Mordenite and Beta presented in Figure 4.14 may be due to the existence of different types of acid sites on these samples, resulting in the overlapping of desorption peaks similar to results presented by Karge and Dondur [1990].

5.1.2.3 MQ-TPD spectra of ZSM-5, Mordenite and Beta

A single high temperature desorption (HTD) peak was observed for 4-methyl quinoline desorption from ZSM-5 (sample Z), Mordenite (sample M) and Beta (sample B), suggesting that the samples contained no physisorbed 4-methyl quinoline (Figure 4.15). Using identical experimental conditions (1.0 g, 40 ml/min, 10°C/min) the peak temperatures were found to be similar: ZSM-5 (820°C), Mordenite (807°C) and Beta (818°C) (Table 4.4). Silicalite-I showed no desorption of 4-methyl quinoline (Figure 4.15) due to the almost complete absence of acid sites (Si/Al ~ 500). Similar to the stabilizing effect of the ring structure of the pyridine-zeolite complex discussed in Section 5.1.2.2 [Sharma

et al., 1993], the stabilizing effect of the double ring structure of 4MQ may explain the high desorption temperatures of 4MQ. Indeed, Anderson *et al.* [1979] reported that the desorption of 4MQ from ZSM-5 was extremely slow under reaction conditions at 450°C.

4-Methyl quinoline was chosen because it was not expected to enter the channels of ZSM-5. The critical diameter of 4MQ is 7.3 Å [Rollmann, 1991], whereas the largest pore diameter of ZSM-5 is 5.4 x 5.3 Å [Haag and Chen, 1987]. Changing the catalyst mass or the carrier gas flowrate showed no change in T_{max}, suggesting the absence of diffusion and readsorption effects [Rieck and Bell, 1984]. Furthermore, the 4MQ desorption spectra of ZSM-5 were not affected by prolonged adsorption times or by long evacuation times after the adsorption of 4MQ. These observations are consistent with the proposal that 4MQ did not enter the channels of HZSM-5, and that 4MQ was chemisorbed onto the external acid sites of ZSM-5 (Section 2.3.1.3).

4-Methyl quinoline was probably able to enter the channels of Mordenite (6.5 x 7.0 Å) and Beta (6.4 x 7.6 Å) [Meier *et al.*, 1996], because for both zeolites an increase in the adsorption time from 3 to 24 h resulted in approximately a 4-fold increase in the desorption peak area (Table A-VII.1 and Appendix VIII). Furthermore, when 4MQ was adsorbed for 24 h on Beta, a low temperature desorption peak was observed at 550°C (Appendix VIII). However, changes in the external surface acidity could still be observed when using constant adsorption times.

5.1.2.4 Comparison and evaluation of NH_3-TPD, Py-TPD and AA results

(i) ZSM-5

To compare the NH_3-TPD and Py-TPD spectra from ZSM-5, identical conditions were used (Si/Al = 34, 0.10 g, 100 ml/min, 10°C/min). The T_{max} value of the NH_3-TPD occurred at a lower temperature (390°C) than that of the Py-TPD peak (667°C). This is in agreement with TPD studies of Parrillo *et al.* [1990] and Sharma *et al.* [1993]. Sharma *et al.* [1993] have reported T_{max} values of 347 and 624°C for ammonia and pyridine TPD studies on HZSM-5 respectively (Si/Al = 34, 5-25 mg, 75 ml/min). Heats of adsorption for ammonia and

pyridine on HZSM-5 were found to be approximately 145 and 200 kJ/mol respectively [Parrillo and Gorte, 1993; Sharma *et al.*, 1993]. As explained in Section 5.1.2.2, the zeolite-pyridine complex is thought to be more stable than the zeolite-ammonia complex and the diffusional resistances in the channels of HZSM-5 are greater for pyridine than for ammonia, thus resulting in a higher peak maximum temperature for the former [Sharma *et al.*, 1993].

As mentioned in Section 5.1.1, the number of acid sites obtained by NH_3-TPD and Py-TPD from ZSM-5 (sample Z) were 0.43 and 0.46 mmol/g respectively (Table 4.4), and the aluminium content measured by AA was 0.42 mmol/g (Table 4.1). Therefore the results obtained with both TPD systems were in very good agreement with each other, and the number of acid sites obtained by TPD corresponded to the aluminium content obtained by AA for ZSM-5. The differences were less than the standard deviation for each method.

(ii) Mordenite

As for ZSM-5, the T_{max} value of the NH_3-TPD spectrum (568°C) of Mordenite occurred at a lower value than that of the Py-TPD spectrum (637°C), due to the stability of the zeolite-pyridine complex and the greater diffusional resistances for pyridine in the Mordenite channels [Sharma *et al.*, 1993]. Parrillo and Gorte [1993] have reported heats of adsorption of 160 and ±200 kJ/mol for ammonia and pyridine respectively on Mordenite. Besides the difference in the heat of adsorption for ammonia for ZSM-5 and Mordenite, the T_{max} values are also strong functions of zeolite structure, diffusion and Si/Al ratio [Kapustin *et al.*, 1988, Forni *et al.*, 1992 and 1995]. Therefore the difference in T_{max} values of NH_3-TPD and Py-TPD spectra for Mordenite and ZSM-5 could be due to any one of the above factors, and they need to be interpreted with great caution (refer to Section 2.3.2.2 for discussion).

The aluminium content measured by AA was 1.29 mmol/g (Table 4.2) and corresponded to the theoretical aluminium content calculated from the unit cell formula for Mordenite with a Si/Al ratio of 10 (1.32 mmol/g). The number of acid sites obtained by NH_3-TPD and Py-TPD from Mordenite (sample M) were 1.15 and 1.03 mmol/g respectively (Table 4.4). The NH_3-TPD value may have been underestimated slightly, because the spectrum did not return to the

baseline (Figure 4.13). In their studies, Karge and Dondur [1990] proposed that the bulkier pyridine could not reach all the acid sites that could be probed by ammonia. In light of the above and the close compatibility of the NH_3-TPD, Py-TPD and AA results for ZSM-5, it can be said that the results obtained were accurate, although the number of acid sites measured by TPD did not correspond to the aluminium content for Mordenite as measured by AA, probably for reasons proposed by Karge and Dondur [1990] as described above.

(iii) Beta

The aluminium content measured by AA was 0.82 mmol/g (Table 4.3). This value was slightly lower than the theoretical aluminium content calculated from the unit cell formula for Beta (0.88 mmol/g). The number of acid sites obtained by NH_3-TPD and Py-TPD from Beta (sample B) were 0.65 and 0.72 mmol/g respectively (Table 4.4). Similar to NH_3-TPD and Py-TPD results obtained here, it has been reported previously that the number of acid sites measured by NH_3-TPD would be less than the aluminium content measured by AA for Beta [Leu *et al.*, 1991; Moon, 1995]. As observed for both ZSM-5 and Mordenite, the T_{max} value of the NH_3-TPD spectrum (346°C) of Beta occurred at a lower value than that of the Py-TPD spectrum (630°C). The heat of adsorption of ammonia onto Beta is estimated to be ± 107 kJ/mol [Moon, 1995].

Due to the limited availability of the NH_3-TPD apparatus, the TPD studies of the modified samples were carried out mostly using Py-TPD. Even though pyridine was not always able to access all the aluminium atoms in the zeolite (i.e. in Mordenite and Beta), any changes in the Py-TPD data of the modified samples could be compared to the parent sample of that zeolite type.

5.1.3 ADSORPTION CAPACITY DATA

In these studies the adsorption temperature and time used were 80°C and 60 min respectively for *n*-hexane, with a partial pressure of 60.4 mbar. The adsorption temperature and time used for *p*-xylene, *o*-xylene and 1,2,4-trimethyl benzene were 150°C and 300 min respectively, with partial pressures of 2.36, 1.72 and 0.52 mbar respectively. In the following discussion literature data is given in some cases as a comparison, although the adsorption capacity may be strongly dependent on temperature, partial pressure and Si/Al ratio.

5.1.3.1 ZSM-5

In these studies the adsorption capacities for ZSM-5 using *n*-hexane, *p*-xylene, *o*-xylene and 1,2,4-trimethyl benzene were 10.3, 3.0, 2.7 and 2.8 wt% respectively (Table 4.12). Adsorption capacities measured at 120°C and 5.3 mbar for *p*-xylene and *o*-xylene were approximately 2.8 and 2.7 wt% respectively [Kim *et al.*, 1996]. Adsorption capacities for *n*-hexane (20 mbar) at 50 and 100°C were 11.0 and 9.0 wt% respectively [Szostak, 1992]. Therefore, allowing for differences in experimental conditions, the adsorption capacities obtained in these studies were similar to those reported in the literature.

5.1.3.2 Mordenite

In these studies the adsorption capacities for Mordenite using *n*-hexane, *p*-xylene, *o*-xylene and 1,2,4-trimethyl benzene were 5.7, 1.7, 1.7 and 1.2 wt% respectively (Table 4.13), although the samples were not completely saturated under the conditions used. Adsorption capacities measured at 20°C and using adsorbate partial pressures at 20°C for *n*-hexane, *p*-xylene and *o*-xylene were approximately 6.0, 7.0 and 5.3 wt% respectively [Niwa *et al.*, 1984a]. The lower adsorption capacities observed in these studies are probably largely due to the higher adsorption temperatures used here and because saturation was not completely reached in these studies.

5.1.3.3 Beta

In these studies the adsorption capacities for Beta using *n*-hexane, *p*-xylene, *o*-xylene and 1,2,4-trimethyl benzene were 11.1, 3.2, 3.1 and 0.8 wt% respectively (Table 4.14), although the samples were not completely saturated under the conditions used. Indeed, adsorption capacities measured at 25°C and P/P_o = 0.5 for *n*-hexane, *o*-xylene and 1,2,4-trimethyl benzene were much greater, viz. 19.0, 21.8 and 24.0 wt% respectively [Szostak, 1992]. Because the lower adsorption temperature and much higher partial pressures used by Szostak [1992], much greater adsorption capacities were obtained compared to these studies.

5.2 CHEMICAL VAPOUR AND LIQUID DEPOSITION

5.2.1 TEOS DEPOSITION ON ZSM-5 USING A VAPOUR PHASE FLOW SYSTEM

5.2.1.1 Decomposition species formed during TEOS deposition on ZSM-5

A blank run without catalyst showed that TEOS did not thermally crack at temperatures up to 500°C. In section 4.4.1 it was shown that during a temperature programmed reaction of TEOS on HZSM-5 in a vapour phase flow system, ethanol was formed at temperatures below ± 200°C, whereas ethylene and H_2O were formed above ± 200°C. Although in Figure 4.25 it appears that ethylene was also formed below 200°C, $m/e = 27$ is a characteristic ion for both ethanol and ethylene. Therefore it cannot be conclusively said that ethylene was formed below 200°C. However, at higher temperatures it would be possible for the acid sites on the internal or external surfaces to dehydrate ethanol to ethylene and H_2O. This reaction has been shown to occur above about 200°C [Aronson *et al.*, 1986; Li-feng *et al.*, 1989]. Furthermore, above ± 300°C higher hydrocarbons were observed in the product stream. Ethylene conversion to higher hydrocarbons may have occurred at these temperatures [Bessel and Seddon, 1987].

5.2.1.2 TEOS deposition at relatively low temperatures on ZSM-5

In Section 4.4.2.1 it has been shown by isothermal reaction studies of TEOS deposition that initially all the TEOS decomposed on HZSM-5 at 50°C, the major decomposition product being ethanol. After the initial deposition, the amount of TEOS decomposed decreased until no more TEOS decomposed. After successive regenerations progressively less TEOS decomposed after any given time period compared to the first cycle. The amount of TEOS which decomposed on HZSM-5 during the second and third cycles was comparable to the amount which decomposed when TEOS was deposited on Silicalite-I at 50°C.

When TEOS was deposited on SiO_2 at 50°C, no ethanol was present in the product stream (Figure 4.27). However, no TEOS was detected at the start of

the deposition (Figure 4.26), indicating that the silanol groups on SiO_2 were able to physisorb but not decompose TEOS at 50°C. This agrees with the TGA data obtained at 100°C which suggested that some physisorption of TEOS occurred on HZSM-5, possibly after inertisation of the external surface acidity. This will be discussed in more detail in Section 5.2.1.4.

As the critical diameter of TEOS is 10.3 Å, it cannot enter the channels of HZSM-5 or Silicalite-I (5.3 x 5.4 Å). Bearing in mind that Silicalite-I possessed trace aluminium (<0.02 mmol/g), with a relative external surface acidity of about 2% of that of HZSM-5 (Table 4.4), these experiments suggested that acid sites on or near the external surface of the HZSM-5 or Silicalite-I samples were needed to decompose TEOS at 50°C. After the first deposition cycle of TEOS on HZSM-5, the external surface of HZSM-5 behaved more like Silicalite-I (few acid sites) than like SiO_2 (no acid sites). When the acid sites on the external surface were inertised, possibly by a layer of partially decomposed alkoxy silanes, the deposition of TEOS at 50°C was inhibited. The HZSM-5 sample was regenerated after no more TEOS decomposed at the end of the each deposition cycle. Figures 4.26 and 4.27 show that TEOS decomposed and ethanol was formed at the start of the subsequent deposition cycles on HZSM-5, indicating that regeneration of the catalyst (re-)exposed some active sites allowing further deposition of TEOS.

During the initial stages of TEOS deposition at 50°C, any ethanol formed was adsorbed by both the HZSM-5 sample and the Silicalite-I sample, because during this time no ethanol was detected while TEOS was being deposited on either of these catalysts. As the catalyst became saturated, the ethanol peak rose to a maximum (t_{max} = 400 min), but decreased when no more TEOS was decomposed, and ethanol was desorbed from the catalyst by the carrier gas (Figure 4.27). During subsequent deposition cycles on HZSM-5 less ethanol was detected, and the ethanol peak reached a maximum more quickly (t_{max} = 240 min for cycle 2) than what was observed in the previous cycle because less TEOS was converted (Figures 4.26 and 4.27). Whereas similar amounts of TEOS seemed to be decomposed on Silicalite-I and during the second deposition cycle on HZSM-5 (Figure 4.26), the ethanol breakthrough curve for Silicalite-I (t_{max} = 90 min) was quite different to that of the second deposition cycle on HZSM-5 (t_{max} = 240 min) (Figure 4.27). Because Silicalite-I is more hydrophobic than HZSM-5, ethanol was weakly adsorbed by Silicalite-I, and hence it was removed more easily from Silicalite-I.

However, it is clear that the deposition of TEOS on HZSM-5 at relatively low temperatures was accompanied by substantial amounts of adsorption / desorption of decomposition products such as ethanol by the sample. The adsorbed species may prevent further deposition of TEOS. Regeneration (re-)exposed some of the active sites, allowing further deposition to take place. The influence of adsorbed species on TEOS deposition will be discussed in more detail in Section 5.2.2.

5.2.1.3 TEOS deposition at relatively high temperatures on ZSM-5

When the deposition of TEOS was carried out at 400°C on HZSM-5, it was initially completely decomposed to ethylene, H_2O and the deposited silane species, after which a steady state conversion of approximately 60% was observed (Section 4.4.2.2). After regeneration at the end of each cycle, subsequent cycles indicated that TEOS was still partially converted when the deposition was carried out at 400°C.

Therefore, in contrast to the sample kept at 50°C, the active sites on ZSM-5 remained strong enough for the decomposition of TEOS at 400°C and a steady state conversion of 60% was obtained. Wang *et al.* [1988] have reported that the conversion of TEOS on HZSM-5 between 180 - 230°C decreased with deposition time and reached a steady state value of approximately 10% when using a vapour phase flow system. Similar findings have been reported by Niwa *et al.* [1984a] at 320°C using a static vacuum system. Furthermore, Niwa *et al.* [1988a] proposed that H_2O may react with the surface alkoxy silane species, thereby forming a surface SiOH group and alcohol. The surface SiOH group could then further react with TEOS, thus propagating the reaction. H_2O could be formed by ethanol dehydration on the internal or external acid sites at temperatures above about 200°C [Aronson *et al.*, 1986; Li-feng *et al.*, 1989], thereby forming ethylene and providing H_2O for further reaction with surface alkoxy silane species. In this manner a "continuous" deposition of TEOS could be obtained.

The TGA data showed that the amount of SiO_2 deposited on HZSM-5 at relatively high temperatures was in excess of the aluminium content, indicating that TEOS must have been deposited on silanol groups as well as acid sites

(Section 5.2.1.4). Indeed, when TEOS was deposited on SiO_2 at 400°C ethylene and H_2O were formed initially, but thereafter only ethanol was formed (Figures 4.31, 4.32 and 4.33). Thus the silanol groups on SiO_2 were able to decompose TEOS at 400°C. However, the external surface area of the SiO_2 sample (± 0.007 μm) was 5 orders of magnitude larger than the HZSM-5 and Silicalite-I samples (1 - 5 μm) used here. For this reason, the conversion of TEOS on Silicalite-I at 400°C was relatively low (Figure 4.30). The initial conversion on Silicalite-I may be largely ascribed to the presence of trace aluminium rather than to the external surface silanol groups.

By varying the temperature to obtain 50% conversion over HZSM-5, SiO_2-Al_2O_3, γ-Al_2O_3 and kieselguhr, Wang *et al.* [1988] concluded that the rate of decomposition strongly depended on the strength of the acid sites. These results have shown that the acid sites on the external surface were more active for the decomposition of TEOS than the silanol groups, although it was shown to be possible to deposit TEOS on silanol groups at relatively high temperatures. Contrary to these results and the results reported by Wang *et al.* [1988], Hibino *et al.* [1993] reported that the silicon alkoxide reacted equivalently with both terminal silanol and acidic hydroxyl groups, because varying the Si/Al ratio of Mordenite samples had no effect on the amount of silane deposition required to reduce the conversion of 1,3,5-triisopropyl benzene by the same degree (Section 2.2.1.5).

Figures 4.32 and 4.33 show that the ethylene and H_2O breakthrough curves for the first deposition cycle on HZSM-5 at 400°C reached constant values after about 200 min. This time corresponded approximately to the TEOS conversion reaching a steady state value (Figure 4.30). During deposition cycles 2 and 3 less ethylene and H_2O were detected than during cycle 1, corresponding to a slightly lower TEOS conversion during cycles 2 and 3 (Figure 4.30). However, the amounts of ethylene and H_2O detected in cycles 2 and 3 were very similar, suggesting that the external surface was hardly altered between the second and third cycle (Figures 4.32 and 4.33). Initially small amounts of ethylene and H_2O were formed on Silicalite-I at 400°C, probably because of the conversion of TEOS on the relatively few acid sites of Silicalite-I as discussed in the paragraphs above.

5.2.1.4 The weight gain during TEOS deposition on ZSM-5

It was shown by thermogravimetric analysis that the higher the TEOS deposition temperature the greater the weight gain observed on HZSM-5 (sample Z) using a vapour phase flow system (Section 4.4.3). The weight gain could be due to either partially decomposed alkoxy silane species bonded to the external surface or adsorbed decomposition products. The sample modified at 100°C lost 75% of the mass gained by the deposition after calcination, whereas the sample modified at 450°C only lost 3% of the mass originally gained (Table 4.15). This indicated that at low temperatures TEOS and/or decomposition products were reversibly adsorbed by the catalyst, whereas at high temperatures little physisorption took place. At 100°C the weight gain reached an almost constant value of 3.2 wt% after 600 min, whereas at 450°C the sample was still gaining weight steadily after 600 min. This showed that at higher temperatures the decomposition of TEOS continued, whereas decomposition virtually stopped at relatively lower temperatures (Table 4.15 and Figure 4.34), which is consistent with the observations described in Sections 5.2.1.2 and 5.2.1.3.

Assuming that TEOS completely decomposed to SiO_2 during calcination, a weight gain after calcination of 0.8, 6.6 and 10.3% corresponded to 0.13, 1.10 and 1.72 mmol SiO_2 being deposited per gram of HZSM-5 at 100, 270 and 450°C respectively (Table 4.15). The bulk aluminium content of sample Z measured by AA was 0.42 mmol/g. Hence the amount of SiO_2 deposited on samples modified at 270 and 450°C was in excess of the total aluminium content. Therefore TEOS must have been deposited on silanol groups as well as the acid sites on the external surface at these temperatures. The amount of SiO_2 deposited at 100°C was ± 30% of the total aluminium content in the sample. Therefore, either ± 30% of the acid sites were situated on the external surface, or TEOS was also deposited on silanol groups as well as the acid sites after long deposition times at relatively low temperatures.

The mass of TEOS required to decompose to 0.13 mmol SiO_2 is 0.028 g (2.8 wt%). The original weight gain at 100°C (3.2 wt%) was greater than the mass of TEOS required to decompose to 0.13 mmol SiO_2, even if all the decomposition products were adsorbed by the sample at 100°C. Therefore the "additional" weight gain (at least 0.4 wt%) at 100°C was most likely due to

physisorbed TEOS which was subsequently removed unreacted during calcination.

5.2.1.5 Summary

The extent of TEOS deposition was found to be strongly dependent on temperature in a vapour phase flow system. At relatively low temperatures acid sites readily decomposed TEOS to ethanol, leaving a residual partially decomposed alkoxy silane species on the external surface, although TEOS may be physisorbed on the silanol groups. At low temperatures H_2O, which catalyses the deposition reaction at high temperatures [Niwa *et al.*, 1988a], was not formed via ethanol dehydration. In addition, competitive adsorption onto acid sites of decomposition products such as ethanol may have inhibited the deposition of TEOS. At relatively high temperatures the acid sites on both the internal and external surfaces were able to dehydrate ethanol, thereby forming ethylene and providing H_2O to catalyse the decomposition of surface alkoxy silane species to SiOH, creating active sites for further TEOS deposition and thereby enabling a greater extent of deposition to occur.

5.2.2 CHARACTERIZATION OF CVD AND CLD MODIFIED ZSM-5 SAMPLES

5.2.2.1 Chemical vapour deposition using a vapour phase flow system

The relative external surface acidities of samples Z-F-50/8 and Z-F-400/8 as measured by MQ-TPD were reduced by 58% and 80% respectively (Table 4.5). Unfortunately, insufficient sample was available to measure the relative external surface acidities of samples Z-F-50/4x10 and Z-F-400/4x5 by MQ-TPD, but it is likely that the relative reduction in external surface acidity for these samples would be at least similar if not greater that those of samples Z-F-50/8 and Z-F-400/8, because samples Z-F-50/4x10 and Z-F-400/4x5 were calcined between deposition cycles and were exposed to TEOS for longer periods than samples Z-F-50/8 and Z-F-400/8.

All samples modified in a vapour phase flow system showed decreased adsorption capacities and increased deposition times and temperatures resulted in a greater decrease in adsorption capacity (Table 4.12 and Appendix IX), ultimately resulting in significant reductions in pore mouth openings on samples Z-F-50/4x10 and Z-F-400/4x5. For these samples *n*-hexane adsorption capacities were reduced from 10.3 wt% for the parent sample to 5.7 and 7.5 wt% respectively. Py-TPD studies showed that the overall number of acid sites of all samples in which this method was used had been reduced, especially for samples Z-F-50/4x10 and Z-F-400/4x5 (from 0.46 to 0.19 and 0.32 mmol/g respectively) (Table 4.5). The peak shape of the Py-TPD spectrum of sample Z-F-50/4x10 was found to be distorted due to TEOS deposition on the external surface (Figure A-VI.3 in Appendix VI). These changes were probably not only due to a SiO_2 layer coating the external surface acid sites but also to reduced access of probe molecules to the internal acid sites as a result of pore mouth narrowing and blocking.

The Si/Al ratio increased from 34 for the parent sample to 43 and 42 for samples Z-F-50/8 and Z-F-400/8 respectively, indicating that significant amounts of silicon were deposited on these samples. The aluminium content of the above samples measured by AA (0.39 and 0.40 mmol/g) corresponded well to the number of acid sites measured by Py-TPD (0.39 and 0.41 mmol/g).

Although pore mouth narrowing and pore blocking occurred for samples Z-F-50/8 and Z-F-400/8, MQ-TPD results still indicated a relative external surface acidity for these samples of 42 and 20% respectively (Table 4.5). These results may indicate that the SiO_2 layer was not deposited uniformly on the external surfaces of these samples because not all the external surface sites were inertised, and that not all the external surface acid sites were necessarily silanised before pore mouth narrowing was observable. Niwa and co-workers have reported that increases in shape selectivity were ascribed mainly to narrowing of the pore openings rather than to the actual inertisation of the external surface acid sites themselves [Niwa *et al.*, 1984b and 1986a; Hibino *et al.*, 1991; Kim *et al.*, 1996].

Thiart and Hlavacek [1995] simulated interface evolution during CVD for long deposition times from various initial interface shapes. Their model was based on film formation on a solid interface using mainly CVD data for micro-electronic applications rather than zeolite catalysts, but several analogous observations

were made. They presented simulations of film growth under kinetic control and diffusional control. Under kinetic control the formation of the film was uniform (Figure 5.1a), whereas under diffusional control protrusions were formed (Figure 5.1b). These finger-like protrusions have been observed in practice by Van den Brekel [1977] for film growth using CVD for coating applications in the micro-electronics industry.

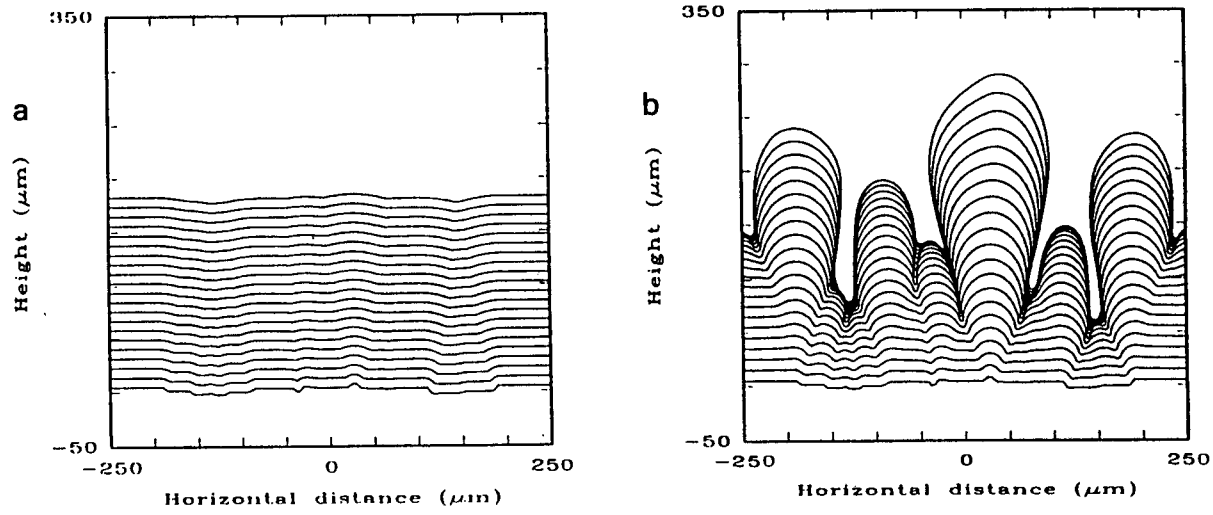

FIGURE 5.1: Film growth under kinetic control (a) and diffusional control (b) [from Thiart and Hlavacek, 1995]

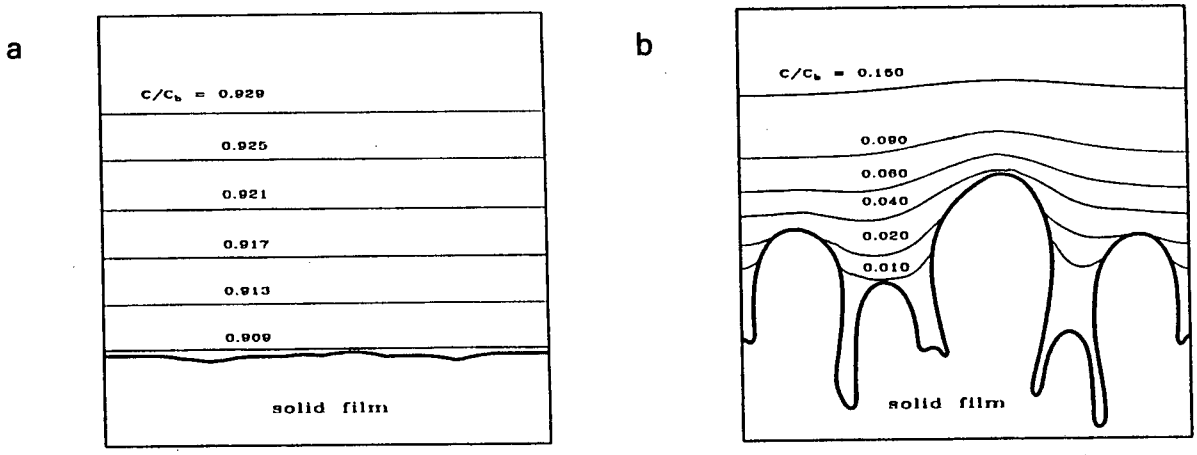

FIGURE 5.2: Isoconcentration lines in the gas boundary layer for deposition conditions in Figure 5.1a and 5.1b [from Thiart and Hlavacek, 1995]

Figure 5.2a shows that the reactant concentration at the interface for the cases studied in Figure 5.1 was similar to the bulk concentration for kinetic control, whereas a large concentration gradient existed for diffusional control (Figure 5.2b).

When a rough surface was used as starting point, it was shown that under kinetic control the grooves or depressions were filled relative to the protrusions due to capillarity, as reactant tended to be adsorbed in the grooves rather than on the protrusions, thereby obtaining a uniform coating (Figures 5.3a and 5.3b). Under diffusional control, more reactant was adsorbed on the protrusions than in the depressions, thereby enhancing non-uniform growth (Figures 5.3c and 5.3d).

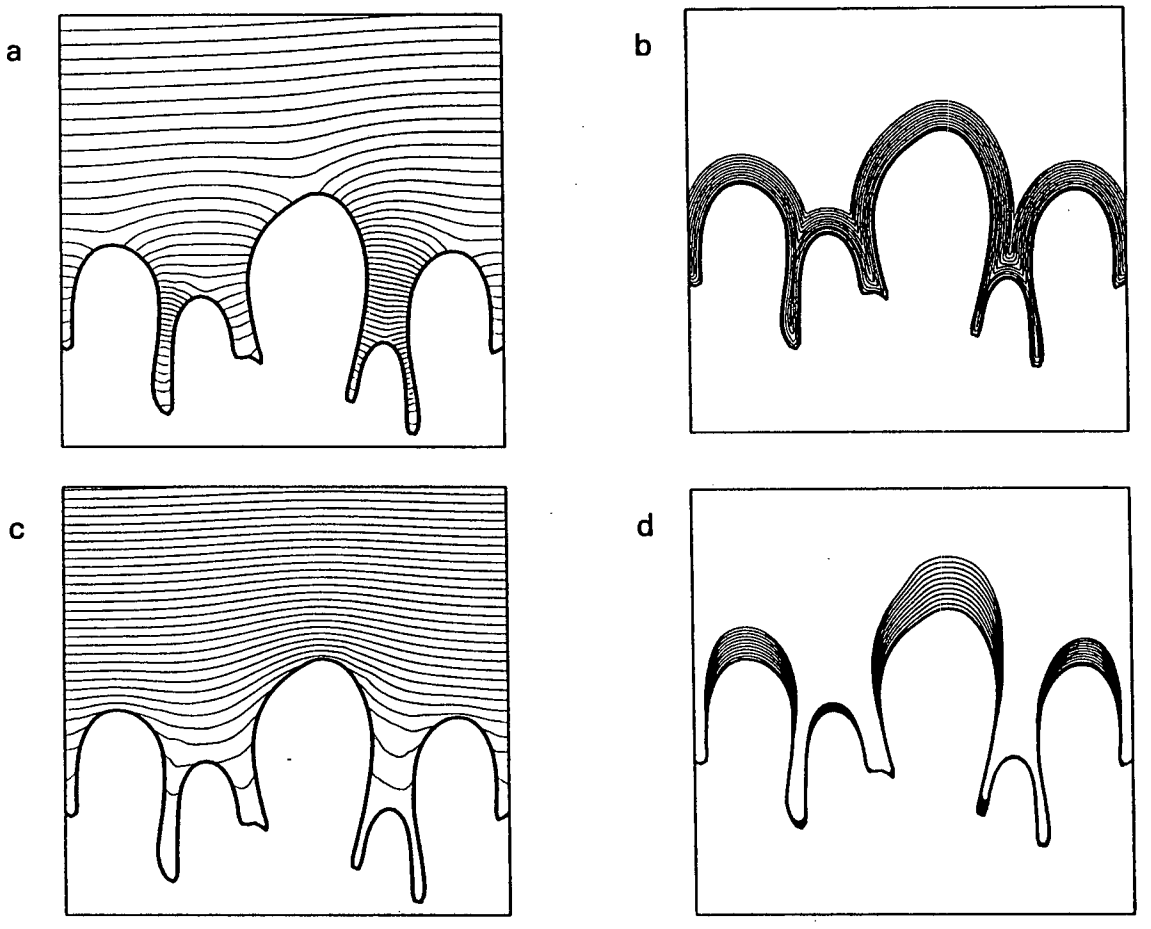

FIGURE 5.3: Isoconcentration lines (a and c) and film growth conditions (b and d) from finger-like initial conditions under kinetic control (a and b) and diffusional control (c and d) [from Thiart and Hlavacek, 1995]

It was predicted that film uniformity could be improved by using lower temperatures and pressures and that under similar conditions a smooth surface gave a more uniform coating than a rough surface [Thiart and Hlavacek, 1995]. With an increase in temperature the kinetics become faster and the interface concentration decreases to a point where the process becomes controlled by diffusion in the gas phase.

Differing physical properties and impurities can enhance the creation of irregularities and protrusions on the surface [Thiart and Hlavacek, 1995]. Zeolite acid sites can be viewed as irregularities in the surface, as it has been shown in Section 5.2.1 that the acid sites were more active for TEOS deposition than silanol groups. In addition, decomposition products formed during CVD may further magnify non-uniform growth behaviour because they may be viewed as impurities when adsorbed on the external surface acid sites.

It has been shown by Koegler *et al.* [1997] that the external surface of ZSM-5 is rough, caused by the formation of hillocks and dendritic crystallites. Heat of crystallization is transported from the crystal to the solution, which is facilitated at the extremities of the crystal, resulting in maximization of the external surface. The distance between hillocks is a few hundred nanometers [Koegler *et al.*, 1997]. The distance between top and bottom of the hillocks was estimated to be ± 20 - 50 nm [Jansen, 1998]. Channel openings are likely to be found both on the hillocks or in the valleys of the surface. The deposition may be further affected in a vapour phase flow system by the flow patterns of the carrier gas, because the flow may be relatively turbulent at the top of hillock compared to the base of the hillock.

Therefore, the irregular zeolite surface may promote non-uniform deposition. In addition, especially at high temperatures, there may be large concentration gradients in the catalyst bed and between the bulk gas phase and the external surface of the zeolite particles when TEOS deposition is carried out in a vapour phase flow system. Because the ZSM-5 samples modified in a vapour phase flow system generally showed significant amounts of pore mouth narrowing and blocking, while the external surface acidity had not been completely inertised, a non-uniform deposition process was apparent. Therefore it may be postulated that diffusional control dominated the deposition process for the samples modified in a vapour phase flow system.

This data shows that extreme care must be taken to ensure that pore mouth blocking does not occur. It is likely that channel openings are obtained with different degrees of pore mouth narrowing or blocking. However, by carefully controlling the extent of deposition excellent shape-selectivities can be obtained. Röger *et al.* [1998] used a number of deposition-calcination-reaction cycles. After each deposition-calcination cycle the *p*-selectivity in toluene disproportionation was monitored. Hence, by carefully depositing small amounts of silica on ZSM-5, a gradual increase in *p*-selectivity was obtained after each deposition-calcination cycle, with the *p*-xylene isomer reaching 98% after repeated cycles.

5.2.2.2 Chemical vapour deposition using a static vacuum system

Table 4.6 shows that the relative amount of external acidity as measured by MQ-TPD in samples modified using a static vacuum method decreased as the deposition temperature increased and, with some exceptions, as the deposition time increased. At 100°C no significant change was observed, possibly because no H_2O was available to catalyse the deposition reaction [Niwa *et al.*, 1988a]. A relative external acidity of 35% was obtained for a deposition time of 60 h at 400°C. Using several deposition cycles, the relative external surface acidities of samples Z-V-400/4x4 and Z-V-400/6x10 decreased by 97 and 100% respectively compared to sample Z as measured by MQ-TPD (Table 4.5).

The decrease in conversion of 1,3,5-triisopropyl benzene from ± 70% for sample Z to 10% for sample Z-V-400/6x10 confirmed the MQ-TPD results in that a significant reduction in external surface activity was observed, similar to results obtained by Hibino *et al.* [1991] and Cejka *et al.* [1996]. However, the probe reaction indicated that at least some activity remained whereas MQ-TPD results indicated that complete inertisation had been achieved. Hibino *et al.* [1993] have reported that approximately four silica layers were required to completely eliminate the conversion of 1,3,5-triisopropyl benzene over both ZSM-5 and Mordenite, assuming that these layers are deposited uniformly. A possible explanation for the apparent discrepancy between the MQ-TPD and 1,3,5-triisopropyl benzene results will be put forward in Section 5.2.5, which

deals with the robustness of the silica layer and the breaking up of agglomerate particles when subjected to grinding, thereby exposing new surfaces.

The number of acid sites determined by Py-TPD possibly showed a slight decrease from 0.46 mmol/g for the parent sample to 0.41 - 0.43 mmol/g for the modified samples (Table 4.5). The peak maximum temperatures, T_{max}, in the Py-TPD spectra did not change, indicating that there were no changes in acid site strength. The Si/Al ratios for the modified samples increased slightly from 34 for the parent sample to 36 - 42 for the modified samples. There was no measurable change in the relative crystallinities of these samples (Table 4.1). Therefore inertisation using a static vacuum system hardly affected the total number of acid sites, although the relative external surface acidities of samples Z-V-400/4x4 and Z-V-400/6x10 were reduced by 97 and 100% respectively as measured by MQ-TPD. These results were consistent with the findings of Niwa *et al.* [1984a and 1986a], who showed that in their NH_3-TPD studies neither the strength nor the amount of acidity changed due to the deposition of TMOS in a vacuum system on HZSM-5 and HM.

There was also no significant change in the adsorption capacities and profiles of samples treated for 60 h in the temperature range 100 - 400°C (Table 4.12 and Appendix IX) indicating that for these samples no measurable pore mouth narrowing had occurred. Niwa *et al.* [1986a] have also reported in their studies referred to above that the adsorption capacity of *p*- and *o*-xylene remained unchanged, although pore mouth narrowing was observed because the adsorption rates of *p*- and *o*-xylene decreased with increasing TEOS deposition [Niwa *et al.*, 1986a; Hibino *et al.*, 1991].

The decomposition products formed upon deposition of TEOS would virtually all be adsorbed by the sample in a static system. Indeed, flushing the samples after CVD (100 - 500°C, 60 ml/min He) showed that ethylene as well as some higher hydrocarbons desorbed from samples modified in a static vacuum system. During the deposition the partial pressure of TEOS over the catalyst was kept constant, whereas the partial pressures of decomposition products increased. This may have resulted in competitive adsorption between TEOS and decomposition products. These decomposition products may have inhibited further deposition of the silane, by directly adsorbing onto external surface acid sites, thus preventing TEOS from bonding to that site, or by inhibiting the

ethanol dehydration reaction and thus the formation of H_2O required for propagation of the deposition reaction [Niwa *et al.*, 1988a].

The effect of the deposition time for samples modified in a static vacuum system was found to be less pronounced than for samples modified in a vapour phase flow system. In a vapour phase flow system, the decomposition products were continuously flushed from the sample, especially at higher temperatures (see Sections 5.2.1.2 and 5.2.1.3), preventing an increase in partial pressure of the decomposition products. Hence a smaller amount of decomposition products would be adsorbed by the sample than in a static vacuum system. This would increase the adsorption of TEOS onto active sites, ultimately resulting in a greater amount of deposition and thus a greater extent in pore mouth narrowing or blocking for a vapour phase flow system than for a static vacuum system, as shown by the adsorption capacity data in Table 4.12. The static environment of the vacuum system would be more conducive to smaller TEOS concentration gradients between the bulk and the zeolite surface compared to the relatively turbulent environment of the vapour phase flow system, thereby possibly favouring a kinetically controlled process and obtaining a more uniform deposition.

Repeated deposition cycles have been employed by Niwa *et al.* [1986a] and Hibino *et al.* [1991] to increase TMOS deposition. The effects of evacuating samples Z-V-400/4x4 and Z-V-400/6x10 were that the decomposition species were removed, thereby reducing the partial pressures of the decomposition species and (re-)exposing external surface acid sites on which TEOS could be deposited during the subsequent cycle. Thus it was possible to deposit significant amounts of TEOS using several deposition cycles even though a much shorter total deposition time was used (viz. sample Z-V-400/4x4). The static vacuum system, therefore, probably enabled the decomposition products to adsorb preferentially onto active sites, thus inhibiting further deposition. Evacuation or calcination between deposition cycles would overcome this problem.

5.2.2.3 Chemical liquid deposition

The diluents chosen for this study were ethanol and H_2O, because they were decomposition products formed at either low or high temperatures. The presence of these diluents could provide information on their behaviour as inhibiting species during TEOS deposition. *n*-Hexane was chosen as a liquid phase, non-polar molecule similar to ethylene.

Samples modified by chemical liquid deposition possibly showed a slight decrease from 0.46 to 0.40 - 0.44 mmol/g in the amount of pyridine desorption (Table 4.5). These values were in good agreement with the aluminium content found by AA (Table 4.1). Cejka *et al.* [1996] and Yue *et al.* [1996] also reported no change in NH_3-TPD studies in liquid phase modification of ZSM-5. The relative crystallinities of these samples showed no significant change from the parent HZSM-5 (Table 4.1).

The sample showing the most significant changes was the sample where 5 vol% TEOS was added to *n*-hexane as diluent (sample Z-L-5/H). The relative external surface acidity of sample Z-L-5/H decreased by 71% (Table 4.5), and showed a decrease from 2.8 to 0.3 wt% in the adsorption capacity of 1,2,4-TMB (Table 4.12). The adsorption capacities of smaller adsorbates were slightly lower than sample Z, indicating that the pore openings had experienced slight narrowing.

When pure TEOS was used (sample Z-L-100/-), the relative external surface acidity only decreased by 23%, even though 36 mmol TEOS were available per gram of HZSM-5, where 1 gram HZSM-5 contained 0.42 mmol aluminium. In the case where 5 vol% TEOS was added to the diluent, the amount of TEOS available corresponded to 1.8 mmol TEOS per gram of HZSM-5, but complete inertisation was not achieved. The adsorption capacities of sample Z-L-100/- generally decreased slightly, suggesting pore mouth narrowing and/or blocking had occurred. Increasing the deposition time to 60 h with pure TEOS did not decrease the adsorption capacities further. Similar to observations made for samples Z-F-50/8 and Z-F-400/8 modified in a vapour phase flow system, when pure TEOS was used in chemical liquid deposition, pore narrowing was observed for sample Z-L-100/- while 77% of the relative external surface acidity remained as measured by MQ-TPD, indicating that the external surface of sample Z-V-100/- was neither inertised uniformly nor completely.

The relative external acidities of samples modified by adding 5 vol% TEOS to H_2O (sample Z-L-5/W) or to ethanol (sample Z-L-5/E) decreased by 47 and 59% respectively as measured by MQ-TPD, and the adsorption capacities of these samples showed little change from the parent sample, especially for sample Z-L-5/W. However, the relative external surface acidities of samples Z-L-0.5/W and Z-L-5/W decreased by 19 and 47% respectively, suggesting that higher concentrations of TEOS resulted in a greater decrease in external surface acidity. Indeed, Yue *et al.* [1996 and 1997] used non-polar cyclohexane as a diluent for TEOS in their liquid phase deposition experiments, and reported more extensive TEOS deposition at higher concentrations.

The use of a diluent affected the inertisation of the external surface. Using HZSM-5 with a Si/Al ratio of 35, the polar ethanol and H_2O molecules would be more strongly adsorbed onto the acid sites on the external surface than the non-polar *n*-hexane molecules. Hence TEOS would have to compete more strongly with ethanol or H_2O molecules than with *n*-hexane molecules for adsorption onto acid sites due to competitive adsorption. Therefore the presence of polar molecules inhibited the decomposition of TEOS due to competitive adsorption on the external surface acid sites. Furthermore, the ternary-phase diagram shows that the miscibility of TEOS in alcohol is much greater than in H_2O (Figure 5.4), providing even greater resistance to diffusion of TEOS through H_2O layers covering the surface of the catalyst.

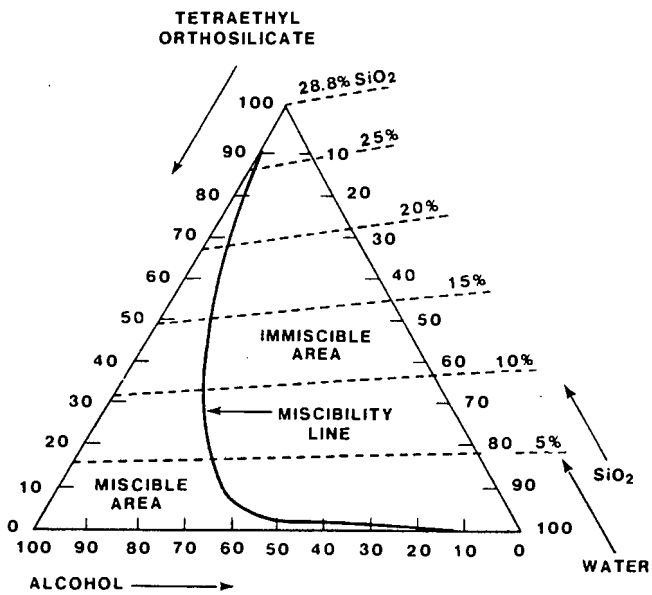

FIGURE 5.4: TEOS, H_2O, alcohol ternary-phase diagram at 25°C [from Brinker and Scherer, 1990]

Similar to the behaviour of the diluents used in the liquid phase deposition studies described above, it is possible that the decomposition products, such as ethanol, were adsorbed onto acid sites as soon as they had been formed. This may have been a contributing factor in the incomplete inertisation of the external surface acidity for all samples modified by CLD, similar to incomplete inertisation of samples modified using a single deposition cycle in a static vacuum system.

It will be shown in Section 5.2.5 that when agglomerates present in the sample are broken up, new surfaces are exposed requiring further inertisation. It is possible that the non-polar *n*-hexane molecules acted as a better dispersant than the polar ethanol and H_2O molecules, resulting in a more extensive inertisation of sample Z-L-5/H than samples Z-L-5/E and Z-L-5/W. No dispersion of particles was possible prior to the addition of pure TEOS to the parent sample to obtain sample Z-L-100/-. The sudden exposure of the sample to large amounts of pure TEOS resulted in an incomplete and non-uniform silane deposition. The presence of a diluent would require the diffusion of TEOS through the diluent to the surface, resulting in a more gradual and therefore possibly more uniform covering than observed for samples where pure TEOS was used, especially when the diluent is non-polar and therefore less strongly adsorbed onto active sites.

Wang *et al.* [1988], Bhat and Halgeri [1993] and Bhat *et al.* [1994] used toluene/methanol mixtures as a diluent in vapour phase flow systems. Wang *et al.* [1988] claimed that H_2O, formed by *in-situ* dehydration of methanol, would catalyse the deposition reaction, thereby giving a more uniform coating. The presence of H_2O may indeed result in "continuous" deposition at high temperatures in a vapour phase flow system as discussed in Section 5.2.1.3, but the more uniform coating reported by Wang *et al.* [1988] may have been due to the presence of toluene.

5.2.3 COMPARISON OF OTHER ZEOLITE TYPES WITH ZSM-5

Mordenite and Beta samples were modified using a static vacuum system, a vapour phase flow system and by liquid phase deposition. The modified Mordenite and Beta samples were compared to ZSM-5 samples modified using similar modification procedures.

5.2.3.1 Characterization of CVD and CLD modified Mordenite samples

The Si/Al ratios increased from 10 for the parent sample (sample M) to 11-13 for the modified Mordenite samples (Table 4.2), indicating that silica was deposited on the Mordenite samples. The aluminium content decreased from 1.29 mmol/g for the parent sample to 1.15 - 1.23 mmol/g for the modified Mordenite samples (Table 4.2). The number of acid sites measured by Py-TPD was 1.03 mmol/g for sample M and 0.94 - 1.03 mmol/g for the modified Mordenite samples (Table 4.7). As discussed in Section 5.1.2.4, the number of acid sites measured by Py-TPD were all slightly lower than the aluminium content measured by AA for the Mordenite samples, but these data show that the majority (>90%) of the acid sites were still accessible to pyridine.

Although it has been shown that 4-methyl quinoline was able to enter the Mordenite channels after relatively long adsorption times (Table A-VII.1), the relative external surface acidities of both Mordenite samples modified in a static vacuum system (samples M-V-400/60 and M-V-400/6x10) were reduced by 99 and ± 100% respectively as measured by MQ-TPD (Table 4.7). This indicated that the acid sites on the external surface were not only inertised completely, but also that the pore openings may have been narrowed to prevent 4-methyl quinoline from entering the Mordenite channels. In the case of Mordenite one deposition cycle was sufficient to inertise the external surface of Mordenite, whereas several cycles were needed for ZSM-5. As expected from the ZSM-5 work, adsorption studies showed that when several deposition cycles were used (sample M-V-400/6x10) pore narrowing occurred more extensively than for a single cycle (sample M-V-400/60) (Table 4.13 and Figures A-IX.19 and A-IX.20 in Appendix IX).

The conversion of 1,3,5-triisopropyl benzene on sample M-V-400/6x10 confirmed that the external surface activity had been reduced by 50 - 70% to ± 15% for this sample (Figure 4.37). As for ZSM-5, the probe reaction indicated that at least some activity remained whereas MQ-TPD results indicated that complete inertisation had been achieved. It is possible that approximately four silica layers are required to completely eliminate the conversion of 1,3,5-triisopropyl benzene over both ZSM-5 and Mordenite [Hibino *et al.*, 1993]. As mentioned in Section 5.2.2.2, the apparent discrepancy between the MQ-TPD and 1,3,5-triisopropyl benzene results will be discussed further in Section 5.2.5 w.r.t. the robustness of the silica layer.

The greatest changes in Si/Al ratio, Py-TPD and adsorption capacity were observed when TEOS was deposited on Mordenite using a vapour phase flow system (Tables 4.2, 4.7 and 4.13). However, the relative external surface acidity of sample M-F-400/8 was reduced only by 70% as measured by MQ-TPD (Table 4.7). This indicated that the acid sites on the external surface were not inertised completely and/or that 4-methyl quinoline was able to enter the Mordenite channels. In Section 5.2.2.1 it was argued that a "continuous" but possibly non-uniform silica deposition was obtained for ZSM-5 when TEOS was deposited under these conditions using a vapour phase flow system. The results obtained for Mordenite are therefore similar to those obtained for ZSM-5.

The *n*-hexane adsorption profiles for samples M-V-400/6x10 and M-F-400/8 clearly show that the adsorption rates were reduced (Figures A-IX.20 and A-IX.21 in Appendix IX) and that the samples were not saturated at the end of the *n*-hexane adsorption period. However, Py-TPD studies showed that the acid sites were still accessible, and hence the pore mouths were narrowed but probably not completely blocked.

The deposition of TEOS on Mordenite using liquid phase deposition indicated that the relative external surface acidity of sample M-L-5/H was reduced by 82% (Table 4.7) and the adsorption studies indicated little change in adsorption capacity for this sample (Table 4.13). Hence 4-methyl quinoline was still adsorbed onto the external surface acid sites of the sample and/or 4-methyl quinoline was able to enter the Mordenite channels. For liquid phase deposition, the results obtained for Mordenite were also similar to those obtained for ZSM-5 in that several deposition-calcination cycles may be required to completely inertise Mordenite using CVD.

5.2.3.2 Characterization of CVD and CLD modified Beta samples

The Si/Al ratios increased from 18 for the parent sample (sample B) to 19-22 for the modified Beta samples (Table 4.3), indicating that silica was deposited on the Beta samples. The aluminium content decreased from 0.84 mmol/g for the parent sample to 0.72 - 0.81 mmol/g for the modified Beta samples (Table 4.3). The number of acid sites measured by Py-TPD was 0.72 mmol/g for sample B and 0.53 - 0.75 mmol/g for the modified Beta samples (Table 4.8). As discussed in Section 5.1.2.4, the number of acid sites measured by Py-TPD were all slightly lower than the aluminium content measured by AA for the Beta samples. Although a value of 0.75 mmol/g measured by Py-TPD for sample B-V-400/60 may be spuriously high, a significant loss in the number of acid sites occurred for sample B-F-400/8 (0.53 mmol/g).

4-Methyl quinoline was able to enter the Beta channels after relatively long adsorption times (Table A-VII.1). However, the relative external surface acidities of both Beta samples modified in a static vacuum system (samples B-V-400/60 and B-V-400/6x10) were reduced by 99 and 97% respectively (Table 4.8). As for the Mordenite samples, this indicated that the acid sites on the external surface of Beta were not only inertised completely, but also that the pore openings may have been narrowed to prevent 4-methyl quinoline from entering the Beta channels. As for Mordenite, one deposition cycle was sufficient to inertise the external surface of Beta, and adsorption studies showed that when several deposition cycles were used (sample B-V-400/6x10) the pore openings were altered slightly more extensively than for a single cycle (sample B-V-400/60) (Table 4.14 and Figures A-IX.24 and A-IX.25 in Appendix IX). However, the conversion of 1,3,5-triisopropyl benzene on sample B-V-400/6x10 was only slightly lower than that of the parent sample (Figure 4.39). It is possibly that agglomerates were broken up during reactor loading, resulting in higher conversions than expected. This will be discussed in more detail in Section 5.2.5.

As for ZSM-5 and Mordenite, the greatest changes in Si/Al ratio and adsorption capacity were observed when TEOS was deposited on Beta using a vapour phase flow system. The relative external surface acidities of sample B-F-400/8 was 22% (Table 4.8), indicating that the acid sites on the external surface were not inertised completely and/or that 4-methyl quinoline was able to enter the channels of Beta. The results obtained for Beta modified in a vapour phase flow

system were therefore similar to those obtained for ZSM-5 and Mordenite. Indeed, adsorption studies showed that pore narrowing occurred for sample B-F-400/8. The *n*-hexane adsorption profile for sample B-F-400/8 clearly shows that the adsorption rate was reduced (Figure A-IX.26 in Appendix IX) and that the sample was not saturated at the end of the *n*-hexane adsorption period. Py-TPD studies showed that only a portion of the acid sites were still accessible for sample B-F-400/8 (0.53 mmol/g), and hence the pore mouths were narrowed and pore mouth blocking probably occurred.

The deposition of TEOS on Beta using liquid phase deposition indicated that several deposition-calcination cycles may also be required to inertise Beta using CLD, as the relative external surface acidity of sample B-L-5/H was 31% compared to sample B. This indicated that the acid sites on the external surface were not inertised completely and/or that 4-methyl quinoline was able to enter the channels of Beta. For liquid phase deposition, the results obtained for Beta were also similar to those obtained for ZSM-5 and Mordenite.

5.2.3.3 Comparison of modified ZSM-5, Mordenite and Beta samples

The characterization data has indicated that the different zeolite types influenced the TEOS deposition only to a small extent. Using similar modification conditions, Mordenite and Beta samples modified in a static vacuum system, a vapour phase flow system or in liquid phase showed similar trends to their respective ZSM-5 counterparts. Therefore the factors affecting the uniformity and completeness of the inertisation of the external surface acidity of ZSM-5 described in Section 5.2.2 probably affect the zeolites Mordenite and Beta in similar ways.

Perhaps the most noticeable difference was that several cycles were necessary to completely inertise ZSM-5 in a static vacuum system, whereas only one cycle was required for Mordenite or Beta as measured by MQ-TPD. Niwa *et al.* [1986a] reported that the shape-selectivity of a relatively aluminium-rich Mordenite was improved with the deposition of one to three layers of silica, whereas four to six layers were required for a relatively siliceous HZSM-5. It

has been reported that crystallites with greater specific external surface areas required greater amounts of silane deposition than crystallites with relatively smaller specific surface areas [Wang *et al.*, 1988; Bhat *et al.*, 1996]. This could explain why Mordenite appeared to be inertised more easily, as it has the smallest external surface area (58.7 m^2/g), but not why Beta (186.1 m^2/g) appeared to be more easily inertised than ZSM-5 (119.4 m^2/g). The samples were not tested for extra-framework species, but their presence on the external surface would require greater amounts of silane deposition for complete inertisation [Hibino *et al.*, 1991 and 1993; Bhat *et al.*, 1996].

Adsorption studies seemed to indicate that pore mouth narrowing and blocking tended to occur to a greater extent on the Mordenite and Beta samples than on ZSM-5 samples. It has been claimed that the extent of pore-opening narrowing was dependent on the Si/Al ratio [Hibino *et al.*, 1993] (see Section 2.2.1.5). They proposed that the Si-O-Si bond of the silica layer protruded into the pore, narrowing the pore-opening size to a greater extent for zeolites with a low Si/Al ratio than for siliceous zeolites. The silica layer consists of Si-O-Si bonds, whereas the zeolite contains both Si-O-Si and Si-O-Al bonds, resulting in different bond lengths or bond angles between the silica layer and the zeolite, which become larger as the aluminium content of the zeolite increases. Therefore the apparently greater extent in pore mouth narrowing on the Mordenite and Beta samples could be due to the lower aluminium content of sample Z (Si/Al = 34) compared to Mordenite (Si/Al = 10) and Beta (Si/Al = 18). However, it was not possible to obtain reproducible rates of adsorption to quantify these results in more detail. If TEOS is deposited preferentially on acid sites, then zeolites with a lower Si/Al ratio, and specifically a greater acid site concentration near pore openings, may be more susceptible to pore mouth narrowing than zeolites with a high Si/Al ratio.

In addition, Mordenite has a one-dimensional channel structure, whereas ZSM-5 and Beta have three-dimensional channel structures. Hence the channel system of Mordenite would be more susceptible to reduced adsorption rates or capacities than ZSM-5 or Beta if pore mouth narrowing and blocking occurred.

5.2.4 ESTIMATE OF SILICA LAYER THICKNESS FOR UNIFORM DEPOSITION

In order to calculate the number of uniform mono-layers deposited on the external surface of the different zeolites, an estimate was made of the amount of SiO_2 required for a mono-layer. It was necessary to make the following assumptions:

(i) The diameter of the smallest circumscribing cylinder of a tetrahedral silica molecule was 2.6 Å, based on a Si-O bond length of 1.504 Å [CRC Handbook of Chemistry and Physics, 1982 - 1983], giving a circular area of 5.31×10^{-20} m^2 for each tetrahedral silica molecule.

(ii) The void spaces between three circular silica molecules spaced together as close as possible was 2.72×10^{-21} m^2. Two such void spaces exist per silica molecule.

(iii) The effective area covered (i.e. the area of a silica molecule plus its associated void space) is 5.31×10^{-20} m^2 + 2 (2.72×10^{-21}) m^2, which equals 5.85×10^{-20} m^2 per silica molecule.

(iv) The equivalent coverage is 1.71×10^{-19} SiO_2 molecules per m^2, or 0.0284 mmol SiO_2 per m^2.

Based on the external surface areas of zeolites ZSM-5 (119.4 m^2/g), Mordenite (58.7 m^2/g) and Beta (186.1 m^2/g), the amount of silica required for one mono-layer was estimated to be 3.39, 1.66 and 5.28 mmol SiO_2 / g respectively. If the external surfaces were covered in one monolayer, the Si/Al ratios would be expected to increase from 34 to 43, 10 to 11 and 18 to 24 for zeolites ZSM-5, Mordenite and Beta respectively.

In the case of the modified Mordenite samples the Si/Al ratio increased from 10 for sample M to 11 - 13 for the modified samples, indicating that one or more theoretical mono-layers were deposited. For both the modified ZSM-5 samples and the modified Beta samples the increase in Si/Al ratio was at most equal to the calculated increase required for a coverage of one complete mono-layer (ZSM-5 samples changed from 34 to 36 - 43, and Beta samples changed from 18 to 19 - 22). However, the adsorption studies have shown that pore mouth narrowing occurred on several of the samples (Tables 4.12, 4.13 and 4.14 for ZSM-5, Mordenite and Beta samples respectively). In the case of Mordenite

several uniform mono-layers may have resulted in the observed pore mouth narrowing [Niwa *et al.* 1984b and 1986a]. In the case of ZSM-5, pore mouth narrowing appeared to occur to the smallest extent, and this could be due to the surface being covered by not more than one uniform mono-layer [Niwa *et al.* 1986a]. However, it is unlikely that one uniform mono-layer would have resulted in the changes in pore mouth narrowing observed for Beta, especially for sample B-F-400/8.

Sample B-F-400/8, like the ZSM-5 and Mordenite samples modified in a vapour phase flow system, showed significant pore mouth narrowing or blocking, even though the external surface acidity had not been inertised completely. The Si/Al ratio for sample B-F-400/8 was 20, which is less than the expected amount for one uniform mono-layer. The acid sites on the external surface of sample B-V-400/60 were completely inertised, but the Si/Al ratio increased from 18 for sample B to 19 for sample B-V-400/60, indicating that complete inertisation was achieved with less than one mono-layer and thus that TEOS was deposited preferentially on the acid sites. This is in agreement with the TEOS deposition studies discussed in Section 5.2.1.3. Bearing in mind the error margins of the measurements, it does not appear that the silane is always deposited uniformly, as discussed in Section 5.2.2.1. Nevertheless, it is possible to increase selectivities for a number of reaction with chemical vapour and liquid deposition [e.g. Hibino *et al.*, 1991; Parikh *et al.*, 1992; Das *et al.*, 1993; Mirth *et al.*, 1994; Röger *et al.*, 1998]. The observed increases in selectivities may not necessarily be due to a uniform silica layer (i.e. a silica layer of equal thickness covering the whole of the surface) narrowing each of the pore mouths uniformly, but rather to a distribution in pore opening sizes resulting in increased diffusion resistances and hence in greater selectivities for smaller products. Clearly, the greater the control over the distribution of the pore opening sizes after CVD treatment, the better the control over selectivities.

5.2.5 ROBUSTNESS OF THE CVD TREATMENT

In order to test whether or not the silica layer deposited on the external surfaces of the samples was resistant to mechanical stresses, selected samples were subjected to grinding in a mortar and pestle. The Malvern particle size distributions shown in Figures 4.3a and 4.3b showed that the grinding of parent samples Z, M and B resulted in a smaller average particle size for the ZSM-5, Mordenite and Beta samples, although the changes were more pronounced for Mordenite and Beta than for ZSM-5. Although it is unlikely that the grinding would have broken individual crystals to expose new acid sites, agglomerates of particles were probably broken up, thereby exposing acid sites that were not inertised during the CVD treatment.

The conversion of 1,3,5-triisopropyl benzene on sample M (crushed) was approximately 10 - 15% higher than on sample M (Figure 4.37), indicating that a greater external surface activity was obtained by breaking up the agglomerates. The conversions of 1,3,5-triisopropyl benzene over samples Z-V-400/6x10 and M-V-400/6x10 were ± 10 and 15% respectively. However, after subjecting these samples to grinding the conversions of the above samples, viz. samples Z-V-400/6x10 (crushed) and M-V-400/6x10 (crushed), increased to ± 35 and greater than 65% respectively (Figures 4.35 and 4.37). Samples M-V-400/6x10 and M-V-400/6x10 (crushed) were analyzed by MQ-TPD and showed relative external surface acidities of 0 and 57% compared to sample M (Table A-VII.1), indicating that acid sites on the external surface were exposed by grinding the samples. Similarly, the relative external surface acidities of samples B-V-400/6x10 and B-V-400/6x10 (crushed) were 3 and 93% respectively as measured by MQ-TPD (Table A-VII.1), indicating that acid sites on the external surface were exposed by grinding the samples. However, the conversion of 1,3,5-triisopropyl benzene did not indicate that the external surface acidity of sample B-V-400/6x10 had been inertised effectively because the conversions on samples B (crushed), B-V-400/6x10 and B-V-400/6x10 (crushed) were very similar (Figure 4.39).

Possibly, the loading of sample B-V-400/6x10 into the reactor was not done carefully enough, resulting in mild "grinding". The catalyst sample was loaded together with quartz sand particles in the reactor for the probe reaction work, but the sample was not mixed with quartz sand particles when loaded into the

MQ-TPD reactor cell. Note that the conversion of 1,3,5-triisopropyl benzene on samples Z-V-400/6x10 and M-V-400/6x10 (± 10 and 15% respectively) were also slightly higher than the relative external surface acidity as measured by MQ-TPD (0% for both these samples). The apparent discrepancy in probe reaction and MQ-TPD results may have arisen from the catalyst loading procedure.

5.3 COATING WITH SILICALITE SHELLS

5.3.1 STRUCTURE OF THE RESULTING MATERIAL

To determine whether the phase formed in this modification was crystalline Silicalite-I grown epitaxially or some other (amorphous) phase, scanning electron micrographs and X-ray diffraction patterns were obtained. The electron micrographs showed no distinguishable deposits of amorphous material at the magnifications used here. The particle sizes of the parent samples ranged from 1 μm to 5 μm. Particle sizes of the modified samples were not measurably larger than the parent particles. However, a modified particle with a shell / core weight ratio of 1.5/1 is only expected to be 1.36 times larger in diameter than the seed particle.

None of the XRD patterns revealed any noticeable increase in the baseline indicating that no X-ray detectable amorphous phases were present. Furthermore, given that the relative crystallinities differed only minimally from the parent material (Table 4.1), it is likely that all samples studied were of good crystallinity. The XRD patterns of the three modified samples thus indicated that Silicalite-I (or possibly highly siliceous ZSM-5) phases were formed. It is, however, possible that separate Silicalite-I crystals were also formed. As expected, an increase in the bulk Si/Al ratio from 39 to 81-108 was observed for the modified samples (Table 4.1).

Thermogravimetric analysis has shown that the moisture contents of Silicalite-I (sample S) and HZSM-5 (sample Z) were 0.1 and 4.3 wt% respectively. Due to the presence of a Silicalite-I phase, the intensity of the peaks at 2θ values of 7.9° and 8.8° (Cu-Kα radiation) in the XRD patterns of the Silicalite shell modified samples increased in magnitude compared to sample Z_9 (Appendix V), because the above reflections increase in magnitude with increasing amounts of dehydration of the sample [Hardenberg *et al.*, 1992; Szostak, 1989]. Lee *et al.* [1993] reported a decrease in the intensities of the peaks at 2θ values of 7.9° and 23.1° for Silicalite shell modified ZSM-5. The findings reported by Lee *et al.* [1993] are contrary to what might be expected, possibly indicative of a loss in crystallinity for their samples, whereas the findings of this study are consistent with what may be expected to result from the catalyst preparation methods.

5.3.2 INTERNAL ACIDITY AND PORE VOLUME OF THE RESULTING MATERIAL

The NH_3-TPD spectra (0.25 g, 10°C/min, 70 ml/min) of samples modified by coating with Silicalite shells all showed a decrease in the number of acid sites per gram of material from 0.49 to 0.18-0.22 mmol/g, and a decrease in T_{max} from 450 to 415-420°C (Table 4.9), because the Silicalite shell effectively reduced the mass of ZSM-5 in the sample and hence the number of acid sites in the sample. Similarly, for the Py-TPD spectra (50 mg, 10°C/min, 150 ml/min) the number of acid sites per gram of material decreased from 0.49 to 0.21-0.23 mmol/g, and T_{max} decreased from 615 to 585-590°C (Table 4.9). Lee *et al.* [1993] have reported a reduction in intensity of the signal and a decrease in T_{max} from 480 to 430°C for NH_3-TPD spectra (0.1 g, 12°C/min) from ZSM-5 coated with Silicalite shells. It has been shown by several researchers that an increase in the Si/Al ratio lowers both the intensity of the signal and T_{max} [Hidalgo *et al.*, 1984; Kapustin *et al.*, 1988]. A reduction in catalyst mass results in similar observations [Rieck and Bell, 1984]. In both cases the number of acid sites are reduced. The Silicalite shell effectively reduced the mass of ZSM-5 in the sample and hence the specific number of acid sites. The overall reduced acid site density resulted in reduced gas phase concentrations and reduced readsorption effects, the result of which is the observed reduction of the intensity of the signal and the lowering of T_{max} (see Section 2.3.1.2).

Atomic absorption (AA) results confirmed the decrease in aluminium content of the modified samples (Table 4.1). The aluminium contents of modified samples Z_9-C-templ, Z_9-C-Na and Z_9-C-NH_4 were found to be 41, 41 and 30% respectively of the aluminium content of the parent crystals, which corresponded well with the expected value of 40% for these samples. The value of 40% was calculated from the secondary synthesis mixture yielding 1.5 gram Silicalite-I per gram ZSM-5 added. The aluminium content obtained from AA studies corresponded well with values of the number of acid sites obtained from NH_3-TPD and Py-TPD studies for these samples, again showing good agreement between the characterization techniques for ZSM-5 samples (Tables 4.1 and 4.9).

The Py-TPD spectra of samples Z_9-C-Na and Z_9-C-NH_4 showed a shoulder in the region 320-480°C (Figure A-VI.5 in Appendix VI). Both of these samples were detemplated prior to modification. In order to investigate whether the shoulder at lower temperatures was due to residual physisorbed pyridine "trapped" in the

channels as a result of pore blockage, possibly caused by the deposition of silicon-rich deposits during the coating procedure, sample Z_9-C-NH_4 was evacuated for 34 h instead of 1 h. The Py-TPD spectrum of sample Z_9-C-NH_4 was not affected and therefore the pyridine desorbing at lower temperatures was chemisorbed pyridine.

N_2-BET adsorption isotherms suggested significant changes in the porosity of samples Z_9-C-Na and Z_9-C-NH_4 (Figure 4.18). In the mesoporous range, pore size distributions of all the modified samples revealed a significant reduction in pore sizes ranging from 50 to 200 Å, while samples Z_9-C-Na and Z_9-C-NH_4 showed an increased pore size distribution at ± 40 Å compared to the parent sample (Figure 4.19). The micropore surface areas of the modified samples (i.e. the area of pores less than 17 Å) decreased whereas the mesopore surface areas (i.e. area of pores larger than 17 Å) increased compared to sample Z_9 (Table 4.11). It therefore appeared that the Silicalite-I synthesis gel penetrated the mesopore system of the parent ZSM-5 seed particles, and possibly the micropore system of seed particles in which removal of the template would also have allowed access to the channels (samples Z_9-C-Na and Z_9-C-NH_4). Handreck and Smith [1990] suggested that this modification method may result in the formation of (acidic) amorphous material. The deposition of such material in the mesopores may be the source of the observed reduction in average pore diameter (Figure 4.19), and of the shoulders seen in the Py-TPD spectra of samples Z_9-C-Na and Z_9-C-NH_4 (Figure A-VI.5 in Appendix VI).

5.3.3 EXTERNAL ACIDITY OF THE RESULTING MATERIAL

MQ-TPD spectra of the modified samples (Figure A-VII.5 in Appendix VII) showed that the relative external surface acidity of sample Z_9-C-NH_4 had been reduced by 93% compared to that of sample Z_9 (Table 4.9). This indicated that the external surface acidity had been essentially removed by the Silicalite shell coating without seriously affecting the internal acidity of the catalyst as shown by the Py-TPD results. The detemplated NH_4-form of ZSM-5 was used as seed material for the synthesis of Z_9-C-NH_4. Samples Z_9-C-templ and Z_9-C-Na still showed a significant amount of relative external surface acidity, viz. 56 and 59% respectively compared to the external surface acidity of the parent sample

(Table 4.9), and had therefore not been modified successfully because complete inertisation of the external surface acidity had not been achieved.

5.3.4 SUMMARY

In each of the Silicalite shell modified catalysts the internal acidity and micropore volume were still accessible to probe molecules such as ammonia and pyridine. The modification seems to have formed mostly Silicalite-I or at least siliceous ZSM-5 phases, but separate Silicalite-I particles may also have formed. It is possible that small amounts of (acidic) amorphous material were formed in the mesopores of the seed particles. However, sample Z_9-C-NH_4 was coated with an inert layer without a significant loss in either crystallinity or access to the internal acid sites.

The detemplated NH_4-form of ZSM-5 was used as seed material for the synthesis of Z_9-C-NH_4, whereas the Na-form of ZSM-5 was used in the synthesis of both Z_9-C-templ and Z_9-C-Na. Warzywoda *et al.* [1991] also reported more success when using the NH_4-form of ZSM-5 as seeds to initiate epitaxial growth than when using the Na-form, although Lee *et al.* [1993] used the Na-form.

Whereas from this work no proper explanation can be given why the NH_4-form of the seed particles would have been more successful than the Na-form, it has been found that the Silicalite-I gel was probably able to penetrate the mesopore system of the seed particles, thereby significantly changing the adsorption characteristics of the samples.

CHAPTER 6

CONCLUDING REMARKS

"Nothing is so difficult as a beginning, unless perhaps the end"

6.1 CONCLUDING REMARKS

These studies have confirmed that temperature programmed desorption can be used as an alternative method to the commonly used 1,3,5-triisopropyl benzene reaction for determining whether the inertisation of the external surface acidity of zeolites has been achieved. 4-Methyl quinoline has been shown to be suitable as a selective probe for the external acidity of ZSM-5, although its suitability may be limited to small and medium pore zeolites because it has been shown that 4-methyl quinoline was probably able to enter the channels of large pore Mordenite and Beta after prolonged adsorption times. Because 4-methyl quinoline decomposed during desorption it was not possible to accurately quantify the number of acid sites on the external surface using a mass selective detector, but semi-quantitative data could be obtained by determining the relative changes in the external surface acidity of ZSM-5, Mordenite and Beta.

The extent of TEOS deposition was found to be strongly dependent on temperature in both vapour phase flow and static vacuum systems. The amount of TEOS deposited at relatively low temperatures was shown to be small because acid sites were required to decompose TEOS to ethanol, leaving residual partially decomposed alkoxy silane species on the external surface. TEOS did not appear to decompose but was shown to physisorb onto the silanol groups on the external surface. At low temperatures water, which catalyses the deposition reaction at high temperatures [Niwa *et al.*, 1988a], was not formed via ethanol dehydration. In addition, competitive adsorption onto acid sites of decomposition products such as ethanol may inhibit the deposition of TEOS, resulting in an incomplete inertisation of the external surface acidity.

It was shown that both the acid sites and the SiOH groups were able to decompose TEOS at relatively high temperatures, although it appeared that the rate of decomposition was much greater on acid sites than on SiOH groups. This is in agreement with findings of Wang *et al.* [1988], but contrary to those of Hibino *et al.* [1993]. Ethylene, water and a residual partially decomposed alkoxy silane species were formed above 200°C. The acid sites on the internal and external surfaces would be able to dehydrate ethanol to ethylene and water at temperatures above about 200°C [Aronson *et al.*, 1986; Li-feng *et al.*, 1989]. As mentioned above, the water formed by ethanol dehydration catalyses the decomposition of surface alkoxy silane species to SiOH and

alcohol [Niwa *et al.*, 1988a]. This creates new active sites for further TEOS deposition, while ethanol can again be dehydrated to ethylene and water, thereby allowing the deposition to proceed "continuously".

However, it was observed that inertisation of the external acid sites was not complete at high deposition temperatures for samples modified using a single cycle in a vapour phase flow system, even though significant increases in Si/Al ratio were obtained. Similarly, inertisation of the external acid sites was not complete for ZSM-5 samples modified using a single cycle in a static vacuum system, although both the Mordenite (sample M-V-400/60) and Beta (sample B-V-400/60) samples were inertised completely using a single cycle in a static vacuum cycle. By comparing samples Z-V-400/60, Z-V-400/6x10 and Z-V-400/4x4 modified at 400°C in a static vacuum system it was shown that decomposition products had to be removed from the sample to ensure complete inertisation of the external surface acidity, and that with a deposition-evacuation procedure the total deposition time could be reduced (sample Z-V-400/4x4). The use of such repeated deposition-evacuation cycles to re-expose acid sites to fresh TEOS resulted in the relative external surface acidities of samples modified in a static vacuum system being reduced by 97% or more as measured by MQ-TPD regardless of zeolite type.

ZSM-5, Mordenite and Beta samples modified using a single deposition cycle in a vapour phase flow system showed significant pore mouth narrowing and increases in Si/Al ratio, while MQ-TPD results showed that inertisation of the external surface acidity was not complete (viz. 20% or more relative to the respective parent sample). Consequently, the silane was not deposited uniformly, and not all the external surface acid sites were necessarily inertised before pore mouth narrowing was observable. It is proposed here that the static environment of the vacuum system would be more conducive to smaller concentration gradients compared to the relatively turbulent environment of the vapour phase flow system, thereby possibly favouring a kinetically controlled process in a vacuum system. Therefore it was possible to obtain complete inertisation of the external surface acidity in a static vacuum system without significant pore mouth narrowing. On the other hand, TEOS concentration gradients through the catalyst bed, and possible concentration gradients near the catalyst surface, may have favoured a diffusion controlling process contributing to non-uniform TEOS deposition in a vapour phase flow system. Ensuring low TEOS conversion levels in a vapour phase flow system is likely to

improve the uniformity of the silica layer, but in a large or industrial scale operation unreacted TEOS will need to be recycled. The use of fluidised bed reactors for CVD may also be considered to obtain improved uniformity of the silane deposition.

The potential inhibiting effect of the decomposition products on the complete inertisation of the external surface acidity was highlighted by the liquid phase deposition studies. By using water, ethanol and *n*-hexane as diluents, being similar in nature to typical decomposition products formed at different temperatures, it was found that the polar water and ethanol molecules inhibited TEOS deposition due to competitive adsorption on the acid sites. The relative external surface acidities as measured by MQ-TPD of samples Z-L-5/W and Z-L-5/E were reduced by 47 and 59% respectively compared to sample Z. The non-polar *n*-hexane molecules were less strongly adsorbed by the acid sites, enabling a greater extent of inertisation of the external surface acidity to occur than for the polar diluents, viz a reduction of at least 69% in external surface acidity compared to the parent sample for each of the zeolite types used. The samples modified using *n*-hexane as diluent showed slight pore mouth narrowing. The presence of diluents may provide an environment in which a more gradual and therefore more uniform deposition occurs than when pure TEOS is used, and diluents may disperse agglomerate particles, thus improving both the uniformity and completeness of the deposition during CLD treatment. However, a liquid phase system may be prone to incomplete inertisation of the external surface acidity because decomposition products, such as ethanol, are likely to be adsorbed onto the acid sites as soon as they are formed. Repeated deposition-calcination cycles may overcome this problem, but large scale manufacturing of this nature would be expensive.

Toluene/methanol mixtures have been used as diluent in vapour phase flow systems [Wang *et al.*, 1988; Bhat and Halgeri, 1993; Bhat *et al.*, 1994]. Wang *et al.* [1988] claimed that water, formed by *in-situ* dehydration of methanol, would catalyse the deposition reaction, thereby giving a more uniform coating. The presence of water may indeed result in a "continuous" deposition at high temperatures in a vapour phase flow system as discussed in the paragraphs above, but the more uniform coating reported by Wang *et al.* [1988] may in fact have been due to the presence of toluene. The use of such mixtures at high temperatures in vapour phase flow systems may therefore provide the dual but opposing functions of having water present to allow a the deposition to

proceed, while a non-polar component is present to moderate the TEOS deposition ensuring uniformity of the coating. In this manner it may be possible to use longer deposition times, and possibly reduce the number of deposition-calcination cycles, to obtain both a complete and uniform inertisation of the external surface acidity and thus maintaining good control over pore mouth narrowing.

The robustness of the inertisation obtained by chemical vapour deposition was tested by grinding selected samples in a mortar and pestle. Particle size distributions showed that grinding caused agglomerates to break up, exposing new surfaces that would not have been inertised previously. Whereas before grinding MQ-TPD results and 1,3,5-triisopropyl benzene studies showed large decreases in the external surface acidities of these modified samples, the relative external surface acidity increased after grinding. For example, the relative external surface acidity of samples M-V-400/6x10 and B-V-400/6x10 increased from 0% and 3% respectively after CVD to 57% and 95% respectively after subsequently being subjected to grinding. Similarly, the conversion of 1,3,5-triisopropyl benzene increased from ± 10% to ± 35% after sample Z-V-400/6x10 had been subjected to grinding. Transport and handling of these catalysts when the powder form is modified may thus be detrimental to the effectiveness of the coating. For industrial applications it may therefore be necessary to consider *in-situ* chemical vapour deposition techniques, or modification of pellet or extrudate forms of the catalysts.

Inertisation of the external surface acidity using the Silicalite shell coating method on ZSM-5 seed particles was successful when the NH_4-form of the parent seed particles was used (sample Z_9-C-NH_4). The relative external surface acidity of this sample was reduced by 93%. No conclusive explanation is apparent as to why the NH_4-form of the seed particles would have been more successfully inertised than the Na-form. It has been found that the Silicalite-I gel was probably able to penetrate the mesopore system of the seed particles and therefore the use of undetemplated seed particles may be preferred, in that the deposition of amorphous species in the mesopores or even the channels can be prevented during the modification process.

A Silicalite-I (or possibly a highly siliceous ZSM-5) phase has been formed in samples modified using the Silicalite shell method, but separate Silicalite-I particles may also have been formed. The Silicalite-I phase has resulted in a

decrease in the specific number of acid sites (i.e. the number of acid sites per gram of resulting material), as shown by the aluminium content and by the NH_3-TPD and Py-TPD results. The channel structure and internal acid sites remained accessible to ammonia and pyridine because a good correlation was found between the NH_3-TPD and Py-TPD results and the aluminium content. The samples retained good crystallinities. It is possible that small amounts of amorphous material were formed in the mesopores of the parent seed particles, causing significant changes in the mesopore size distributions as measured by N_2-BET.

Obvious shortcomings of the Silicalite shell method of modification are that this method applies to ZSM-5 only, and that the presence of large amounts of Silicalite-I will add substantially to the reactor size. The amount of TEOS deposited during chemical vapour and liquid deposition at low temperatures is limited and therefore excessive pore mouth narrowing is prevented. Repeated deposition-calcination cycles may be needed to completely inertise the external surface acidity, and to increase the amount of silane deposited on the external surface. In this manner excellent control over pore mouth narrowing can be maintained, as is evident from results to be published by Röger *et al.* [1998]. Operating at relatively high temperatures will increase the amount of TEOS that can be deposited per cycle, but probably at the expense of controlled pore mouth narrowing. Co-feeding diluents or diluent mixtures at high temperatures and using fluidised bed reactors could be ways in which fewer deposition-calcination cycles are needed, while maintaining good control over pore mouth narrowing.

APPENDICES

"Patience is bitter but its fruit sweet"

APPENDIX I: CHEMICALS, EQUIPMENT AND EQUIPMENT TESTING

TABLE A-I.1: List of chemicals and reagents

REAGENT	SUPPLIER	PURITY
CHEMICALS		
$Al(OH)_3$	BDH	99.5 %
NaOH	Saarchem	97 %
Ludox HS40	Du Pont	40 % SiO_2
tetrapropylammonium bromide (TPA-Br)	Fluka Chemie A.G.	98 %
tetraethoxysilane (TEOS)	Fluka Chemie A.G.	98 %
NH_4NO_3	Saarchem	99 %
HF	Riedel-de-Haën A.G.	40 % HF
Al solution	Saarchem	1000 PPM
Si solution	Saarchem	1000 PPM
Na solution	Saarchem	1000 PPM
n-hexane	Saarchem	96 %
cyclo-hexane	ACE	98.5 %
p-xylene	Saarchem	99 %
o-xylene	Saarchem	99 %
1,2,4-trimethyl benzene (1,2,4-TMB)	Aldrich	98 %
1,3,5-triisopropyl benzene (TiPB)	Aldrich	97 %
ethanol	Merck	99.8 %
pyridine	Merck	99.7 %
4-methyl quinoline	Aldrich	99 %
NH_3/He	Air Products	1 mol% NH_3
CARRIER GASES		
air	Fedgas	99.99 %
helium	Fedgas	99.996 %
nitrogen	Fedgas	99.995 %
argon/helium	Fedgas	1 mol% Ar
OTHER		
SiO_2	Aldrich	99.8 %
N_2 (liquid)	Air Products	
molecular sieve (3A)	Merck	>2.5 mm 5% <1.6 mm 2%
Quartz wool	Supelco	
Quartz sand particles	BDH	
Chromosorb P	Supelco	60/80 mesh

TABLE A-I.2: List of equipment

DESCRIPTION	MANUFACTURER	MODEL
VACUUM PUMPS		
rotary pump	Edwards	ED100
air-cooled oil diffusion pump	Edwards	EO50/60
oil for rotary pump	Edwards	No 16
oil for diffusion pump	Dow Corning	Silicone 705
accessories	Edwards	
VACUUM GAUGES		
Pirani vacuum gauge	Edwards	PRH10K
Penning vacuum gauge	Edwards	CP25K
vacuum display unit	Edwards	1005
accessories	Edwards	
FURNACES and TEMPERATURE CONTROLLERS		
TPD furnace	Kiln Contracts	
reactor kiln	Kiln Contracts	
temp. programmer (TPD)	RKC Instruments	REX-P9
temp. controllers	RKC Instruments	REX-C10
temp. display indicator	RKC Instruments	DP-4
temp. selector unit	RKC Instruments	SP-4
thermocouples	ElectroHeat	
heating tape	ElectroHeat	
FLOWMETERS		
mass flow controllers	Brooks	5850TR
4-channel display unit	Brooks	5878
QUARTZ and GLASSWARE		
quartz tubing and frits	Heraeus	
glass stopcocks	J.Young Glassware	
glass male/female joints	J.Young Glassware	
glass ball joints	J.Young Glassware	
o-rings and accessories	J.Young Glassware	
GAS CHROMATOGRAPHS and MASS SPECTROMETER		
gas chromatographs	Hewlett Packard	5890 Series II
	Varian	3300
mass spectrometer	Hewlett Packard	5971A
GC columns (polyimide deactivated fused silica)	Scientific Glass Eng.	062447
RH-1		RP/N 01-0532
MISCELLANEOUS		
valves, fittings, filters	The Swagelok Companies	
regulators	Air Products	1001

THE VACUUM SYSTEM

(i) LEAK TESTING

The vacuum line was leak tested prior to operation. Results of the pressure obtained in various parts of the vacuum line are given in the table below. The pressure in certain parts of the vacuum line was checked periodically, especially after maintenance tasks had been performed, and compared to the values given in the table below.

TABLE A-I.3: Leak testing data

VALVE		PRESSURE
open	closed	(mbar)
V1 - V12		1.0×10^{-5}
V1 - V10	V11, V12	7.6×10^{-6}
V9 - V12	V1 - V8	9.0×10^{-6}
V9 - V11	V12	7.8×10^{-6}
V9 - V10	V11, V12	6.0×10^{-6}

NOTE: The pressure indicated is the pressure in the vacuum line with the valves (as given in Figure 3.6) opened or closed as indicated. Valves V13 and V14 are closed in each case.

These results indicate that the pressure in the clean line is less than 1×10^{-5} mbar after pumping down for two days. Under normal operating conditions the vacuum line is pumped down to less than 1×10^{-4} mbar prior to the adsorption stage. The pressures in the vacuum line during pyridine and 4-methyl quinoline adsorption are approximately 5.2 and 0.5 mbar. An estimate of the leak rate showed that, during the adsorption step, the pressure increase due to "leaks" in the vacuum line was negligible compared to the partial pressure of the adsorbates.

(ii) FURNACE CONFIGURATION AND TEMPERATURE RAMP

The furnace shown below has been designed for this project. The heating element is *alferon super*, which is wound around twelve ceramic tubes. This is housed in a well insulated chamber. The TPD cell can be inserted through openings at the top and bottom of the furnace. Deflector shields above and below the furnace prevent heat losses from the top and bottom of the furnace, thus preventing the Cajon fittings from being heated excessively.

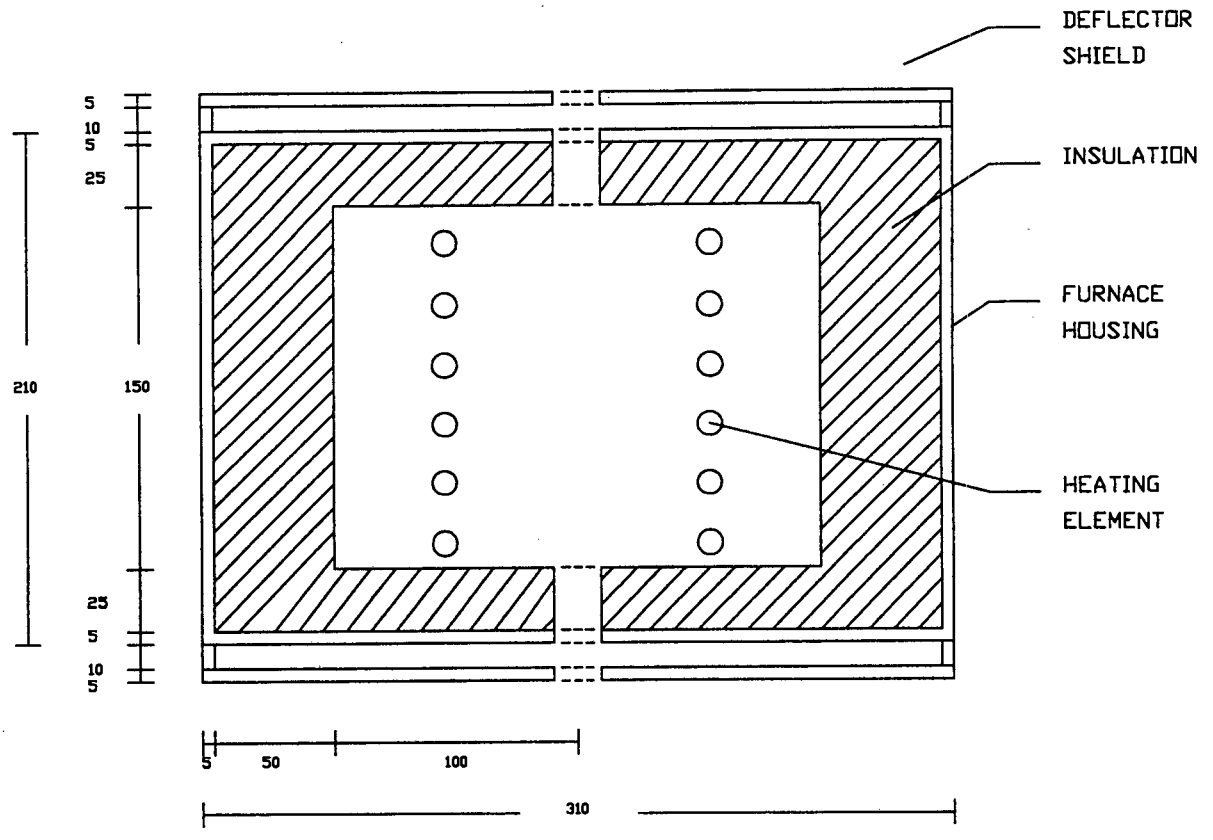

FIGURE A-I.1: The TPD furnace

The figure below shows the linearity of the temperature ramp for different heating rates from 50-1050°C. The slope of the temperature ramp is calculated by linear regression. In each case the correlation coefficient (based on 101 data points) is better than 0.99999.

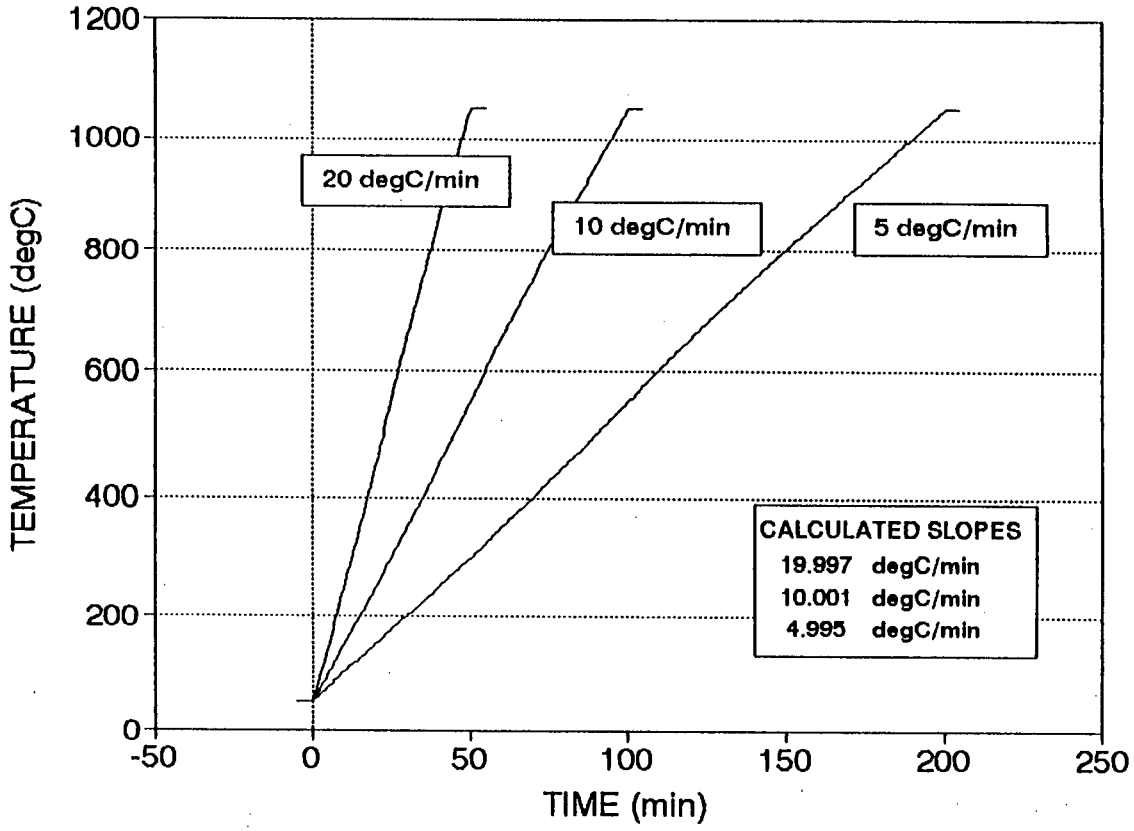

FIGURE A-I.2: Profiles of the temperature ramps in the TPD furnace.

APPENDIX II: CATALYST NOMENCLATURE

The catalysts are named according to the following code:

ZEOLITE - MODIFICATION - PARAMETERS

e.g. X_n - Y - T/t/c/d

where

- **X** is the zeolite type.
  - **Z** ZSM-5 (a mixture of several smaller ZSM-5 batches)
  - **M** Mordenite
  - **B** Beta
  - **S** Silicalite-I
  - **n** included when referring to a particular parent ZSM-5 batch
- **Y** is the modification type.
  - **V** modified with TEOS using a static vacuum system
  - **F** modified with TEOS using a vapour phase flow system
  - **L** modified with TEOS using a liquid phase system
  - **C** modified by coating with Silicalite shells (ZSM-5 only)

Nomenclature for samples modified by chemical vapour and liquid deposition methods

T	the deposition temperature (°C)	(not CLD samples)
t	the deposition time (h)	(not CLD samples)
c	the volume % TEOS in the liquid phase system	(CLD samples only)
d	the diluent used in the liquid phase system, where	(CLD samples only)
	W Water	
	E Ethanol	
	H *n*-Hexane	
	- pure TEOS was used without diluent	

Nomenclature for ZSM-5 samples modified by coating with Silicalite shells

templ sample prepared using the as-synthesized material (i.e. not detemplated and not ion-exchanged parent crystals)

Na sample prepared using detemplated but not ion-exchanged parent crystals (Na-form)

NH_4 sample prepared using detemplated and ion-exchanged parent crystals (NH_4-form)

A separate "bookmark" can be used as further reference guide.

Examples and Miscellaneous Nomenclature are given overleaf.

examples

1. Z — This is unmodified ZSM-5, batch Z.

2. Z_9-C-Na — This sample was modified by coating with Silicalite shells, using primary ZSM-5 batch Z_9 which was detemplated but not ion-exchanged during the preparatory treatment.

3. Z-V-400/60 — This sample was modified by chemical vapour deposition (static vacuum system), using primary batch Z (parent ZSM-5 sample), modified at 400°C for 60 h.

4. M-V-400/6x10 — This sample was modified by chemical vapour deposition (static vacuum system), using primary batch M (parent Mordenite sample), modified at 400°C for 6 cycles of 10 h each.

5. B-F-400/8 — This sample was modified by chemical vapour deposition (vapour phase flow system), using primary batch B (parent Beta sample), modified at 400°C for 8 h.

6. Z-L-100/- — This sample was modified by chemical liquid deposition, using primary batch Z (parent ZSM-5 sample), modified in pure TEOS (100 vol%).

7. M-L-5/H — This sample was modified by chemical liquid deposition, using primary batch M (parent Mordenite sample), modified using a 5 vol% TEOS in *n*-hexane mixture.

<u>Miscellaneous:</u>

Z-L-100/-(60h) — This sample was modified by chemical liquid deposition, using primary batch Z (parent ZSM-5 sample), modified in pure TEOS (100 vol%) for 60 h.

"(crushed)" — this term follows the sample name when the sample was subjected to grinding

APPENDIX III: ZSM-5 CHARACTERIZATION

The unit cell formula for ZSM-5 is:

$$Na_n\ Al_n\ Si_{96-n}\ O_{192}\ .\ 16H_2O$$
$$H_n\ Al_n\ Si_{96-n}\ O_{192}\ .\ 16H_2O$$

(i) Theoretical aluminium and silicon content

For a Si/Al ratio of 35, $Si_{96-n} / Al_n = 35$

therefore $n = 2.67$

The molecular weight of NaZSM-5 = 6106.27 $g.mol^{-1}$

and HZSM-5 = 6048.0 $g.mol^{-1}$

Per gram of HZSM-5,

no. mmol HZSM-5	=	0.1653 mmol
no. mmol Al	=	0.4409 mmol
no. mmol Si	=	15.432 mmol
mass of Al	=	0.0119 g
mass of Si	=	0.4321 g

(ii) Theoretical maximum yield of ZSM-5 synthesis

Using the reagents and quantities described in Section 3.1.1 to synthesize ZSM-5 with a Si/Al ratio of 35:

H_2O	100.0	g
Ludox (40% SiO_2)	31.84	g
TPA-Br (98% pure)	25.18	g
NaOH (97% pure)	1.87	g
$Al(OH)_3$ (99.5% pure)	0.4751	g
total mass of synthesis mixture	159.3651	g

No. mol Si in synthesis mixture = 31.84 x [28/60] x [1/28] x 0.40

= 0.2123 mol Si

No. mol Al in synthesis mixture = 0.4751 x [27/78] x [1/27] x 0.995

= 0.006061 mol Al

Based on the number of moles Si in the synthesis mixture, the number of moles NaZSM-5 that can be formed with a Si/Al ratio of 35 equals

$$0.2123 / [96 - 2.67] = 0.002274 \text{ mol}$$

Based on the number of moles Al in the synthesis mixture, the number of moles NaZSM-5 that can be formed with a Si/Al ratio of 35 equals

0.006061 / 2.67 = 0.002273 mol

The theoretical maximum yield = 0.002273 x 6106.67
= 13.88 g (per 159.37 g synthesis gel)
= 8.71 g (per 100 g synthesis gel)

(iv) Estimate of actual yield of ZSM-5 synthesis

Based on the average as-synthesized yields of washed, dried and undetemplated batches Z_1-Z_8, the following estimates were made:

Average mass of as-synthesized batch = 39.0 ± 1.28 g (per 478.1 g batch)
= 8.16 g (per 100 g synthesis gel)

The weight loss during detemplation determined from TGA measurements (see figure below) was found to be 9.8 wt%.

The catalyst lost during washing and drying before detemplation (Section 3.1.2.1) was estimated to be ± 5 wt%.

Therefore the actual yield per 100 g synthesis gel = 8.16 x [0.902 / 0.95]
= 7.75 g

The *Percentage Yield* = 7.75 / 8.71 x 100
= 89 %

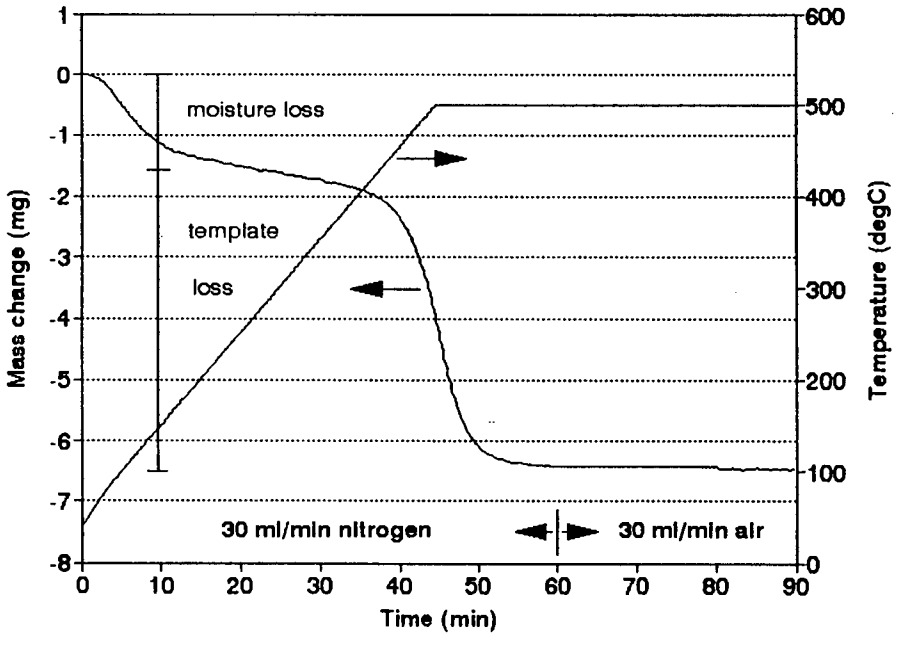

FIGURE A-III.1: Moisture and template loss from sample Z (50.0 mg, not detemplated, not ion-exchanged)

(v) Timed ZSM-5 synthesis study

The ZSM-5 synthesis mixture as described in Section 3.1.1 was placed in 8 Parr bombs, and the Parr bombs were placed in an oven at 160°C. Each Parr bomb was removed from the oven after having spent different times in the oven, viz. 6, 16, 28, 41, 54, 62, 66 and 87 h. The pH of the supernatant liquor was measured, and Si/Al ratios were obtained from atomic absorption spectrometry (AA) measurements for each of the samples.

The Si/Al ratios for the timed-synthesis samples were found to be 37.3 ± 3.0. No decrease or increase in Si/Al ratio with synthesis time was apparent. As the Si/Al ratios of ZSM-5 batches Z_1 - Z_8 synthesized as described in Section 3.1.1 at 160°C for 72 h were found to be 36.6 ± 2.6, no significant difference in Si/Al ratio could be observed during a timed-synthesis study from parent ZSM-5 samples.

The pH of the synthesis mixture was found to be 12.9. The pH of the supernatant liquor after 6 h was 12.15, after which the pH remained steady at about 12.3 - 12.4 for the remainder of the timed-synthesis study, as shown below.

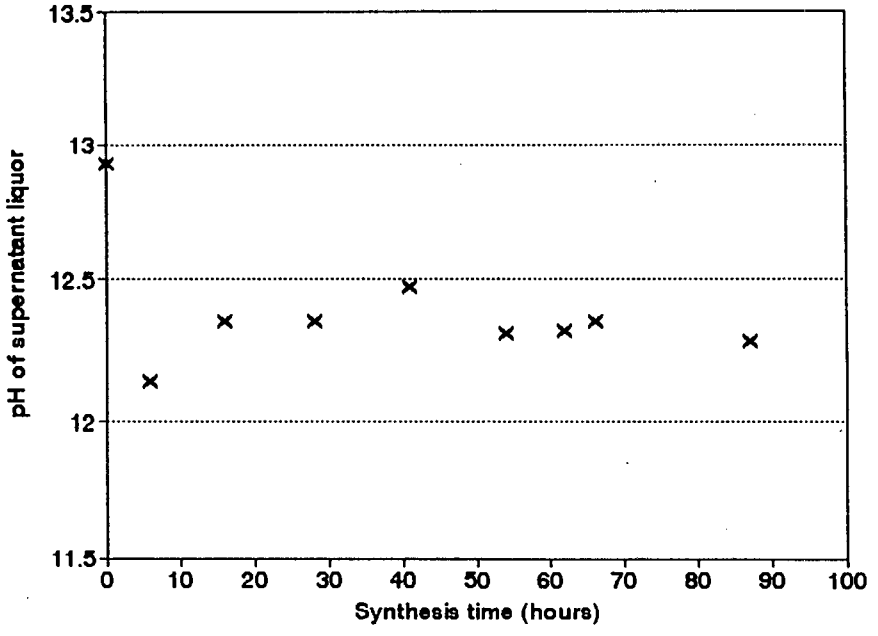

FIGURE A-III.2: pH values of timed-synthesis samples

APPENDIX IV: SAMPLE CALCULATION OF AA RESULTS

The sample calculation of the aluminium content in sample Z, as determined by AA, is shown below. The silicon and sodium contents can be calculated similarly. The values given in brackets are those for silicon. As no sodium was detected no values are given for sodium.

Al reading:	22.0 PPM	(dilution = 1)
Si reading:	39.4 PPM	(dilution = 20)
Na reading:	0.0 PPM	
wet mass:	100.1 mg	
moist. cont.:	4.3 wt%	

(i) mass% Al_2O_3 = $\frac{\text{Al reading (PPM) x final vol. (ml) x dilution x MW}(Al_2O_3) \text{ x } 100}{\text{wet mass (mg) x MW}(Al_2) \text{ x } 1000}$

= $\frac{22.0 \text{ x } 50 \text{ x } 1 \text{ x } 101.96 \text{ x } 100}{100.1 \text{ x } 53.96 \text{ x } 1000}$

= 2.08 % (84.2) .....A

(ii) mass Al_2O_3 in sample = mass% Al_2O_3 x wet mass (mg) / 100

= 2.08 x 100.1 / 100

= 2.08 mg (84.3) .....B

(iii) mmol Al / g sample = $\frac{\text{Al reading (PPM) x final vol. (ml) x dilution}}{\text{wet mass (mg) x MW(Al)}}$

= $\frac{22.0 \text{ x } 50 \text{ x } 1}{100.1 \text{ x } 26.982}$

= 0.407 mmol (14.01) C

(iv) theor. dry mass = mass Al_2O_3 + mass SiO_2 + mass Na_2O in sample

= 2.08 + 84.3 + 0.0

= 86.4 mg .....D

theor. % moisture = $\frac{[\text{ wet mass (mg) - theor. dry mass (mg) }] \text{ x } 100}{\text{wet mass (mg)}}$

= $\frac{[\ 100.1 - 86.4\ ] \text{ x } 100}{100.1}$

= 13.68 % .....E

(v) actual dry mass = wet mass (mg) - [wet mass (mg) x moist. cont. / 100]

= 100.1 - [100.1 x 4.3 / 100]

= 95.8 mg .....F

(vi) mass% Al_2O_3 per g dry sample = $\frac{\text{mass } Al_2O_3 \text{ in sample (mg) x 100}}{\text{actual dry mass (mg)}}$

= $\frac{2.08 \times 100}{95.8}$

= 2.17 % (88.0) .....G

(vii) mmol Al_2O_3 per g dry sample = $\frac{\text{mass\% } Al_2O_3 \times 1000}{MW(Al_2O_3) \times 100}$

= $\frac{2.17 \times 1000}{101.96 \times 100}$

= 0.213 mmol (14.65) .....H

(viii) mol% Al_2O_3 = $\frac{\text{mmol } Al_2O_3 \times 100}{\text{mmol TOTAL}}$

= $\frac{0.213 \times 100}{14.863}$

= 1.43 % (98.67) I

(ix) Si/Al = $\frac{\text{mmol } SiO_2}{\text{mmol } Al_2O_3 \times 2}$

= $\frac{14.65}{0.213 \times 2}$

= 34.4 .....J

APPENDIX V: XRD PATTERNS

XRD spectra of Silicalite-I, ZSM-5 and modified ZSM-5 samples were obtained using either Cu-Kα radiation (wavelength = 1.542 Å) or Co-Kα radiation (wavelength = 1.769 Å). All Mordenite, Beta and their respective modified samples were obtained using Co-Kα radiation. Table A-V.1 shows the peak positions used to obtain relative crystallinities.

TABLE A-V.1: Peak positions (2θ values) for relative crystallinity calculations

ZSM-5 / Silicalite-I		Mordenite	Beta
Cu-Kα	Co-Kα	Co-Kα	Co-Kα
23.1°	27.2°	23.1°	26.3°
23.9°	28.1°	26.2°	
24.4°	28.7°	30.2°	
		31.0°	
		32.5°	

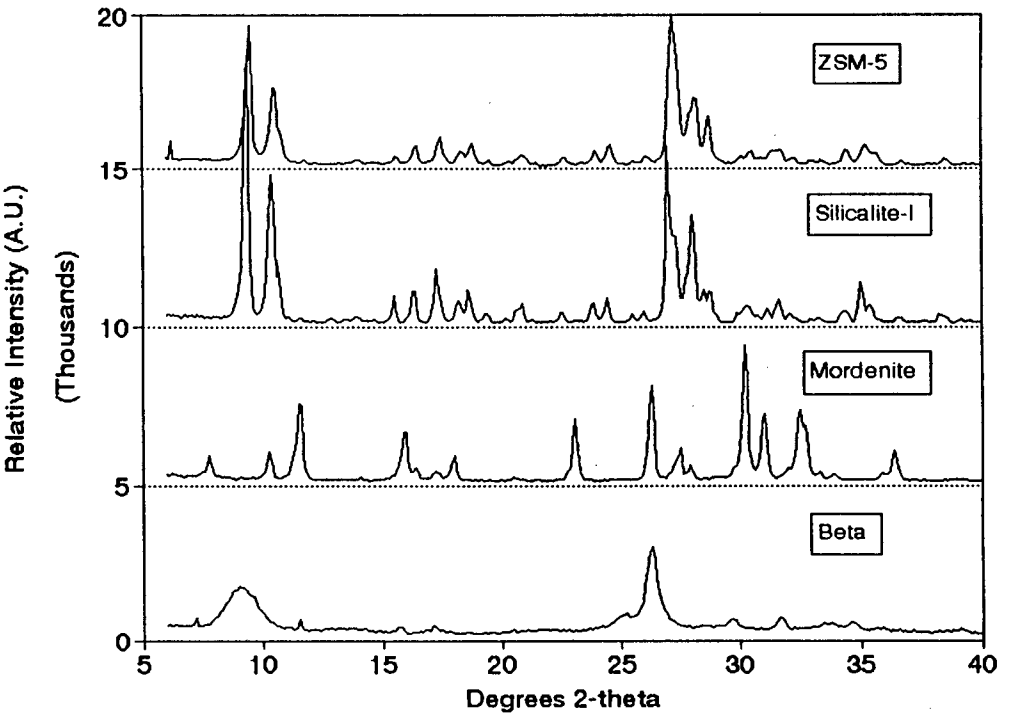

FIGURE A-V.1: XRD spectra of parent samples (Co-Kα radiation)

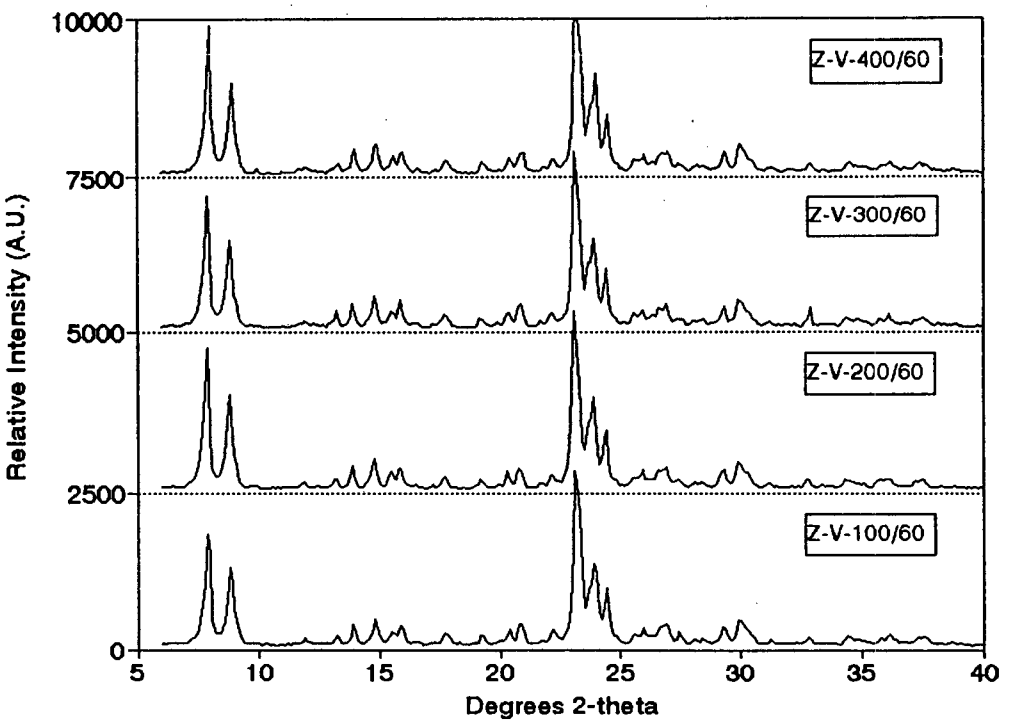

FIGURE A-V.2: XRD spectra of ZSM-5 samples modified by CVD using a static vacuum system (Cu-Kα radiation)

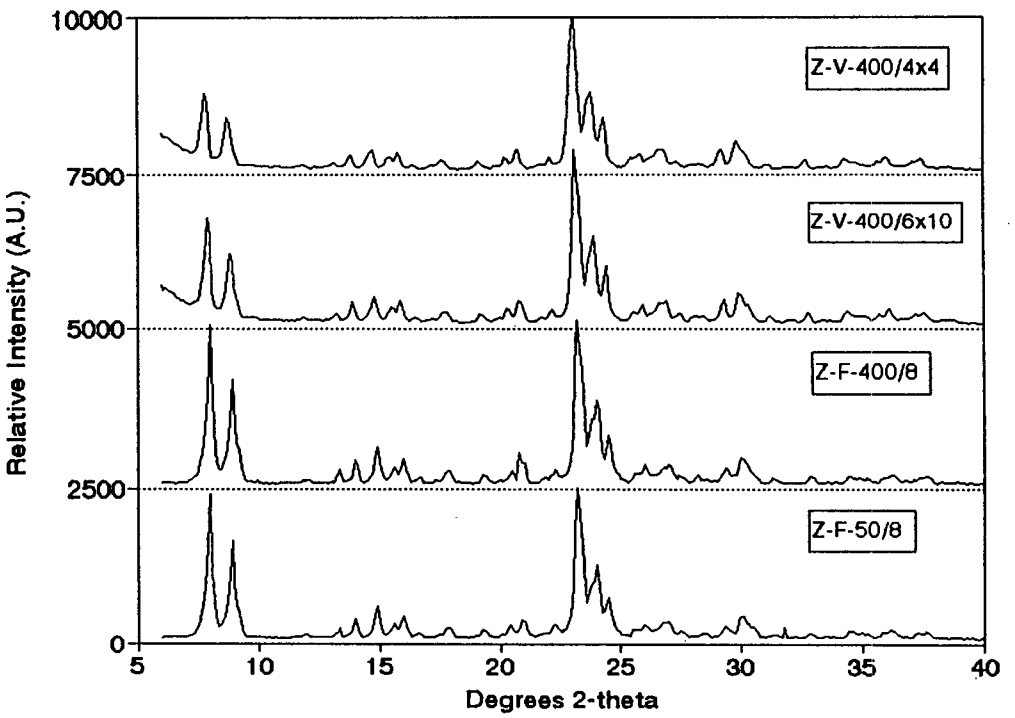

FIGURE A-V.3: XRD spectra of ZSM-5 samples modified by CVD using a static vacuum and a vapour phase flow system (Cu-Kα radiation)

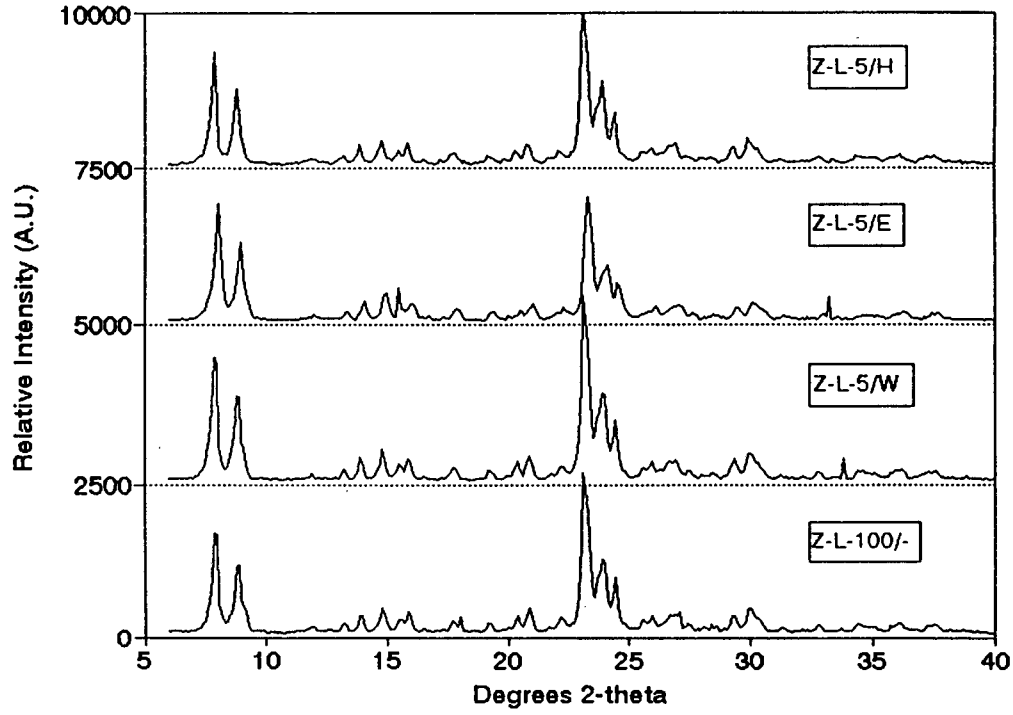

FIGURE A-V.4: XRD spectra of ZSM-5 samples modified by CLD (Cu-Kα radiation)

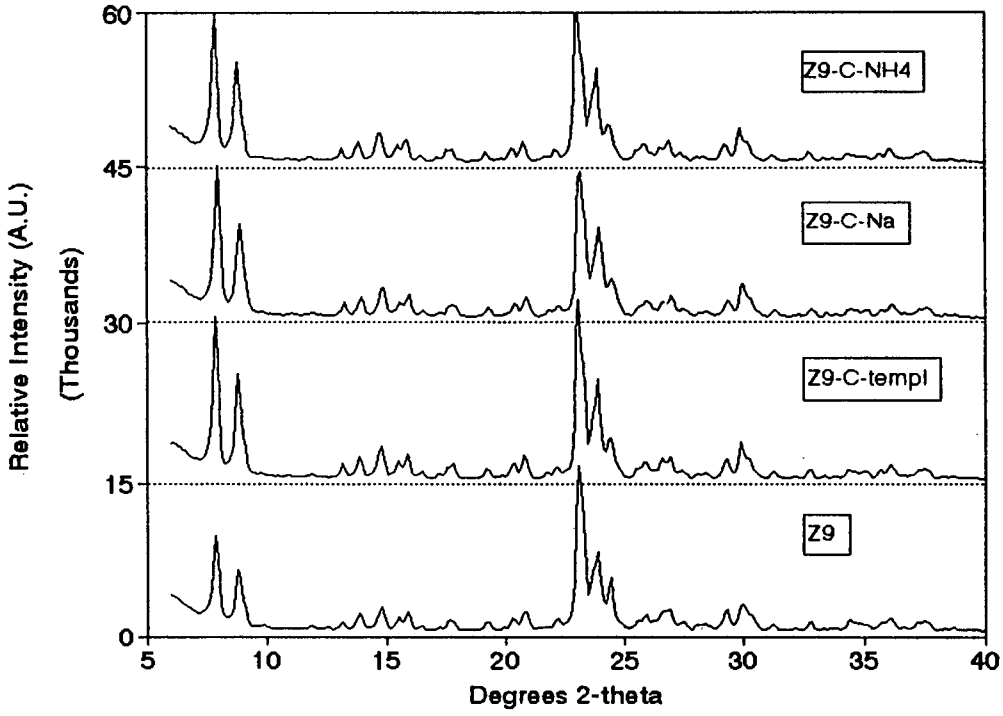

FIGURE A-V.5: XRD spectra of ZSM-5 samples coated with Silicalite shells (Cu-Kα radiation)

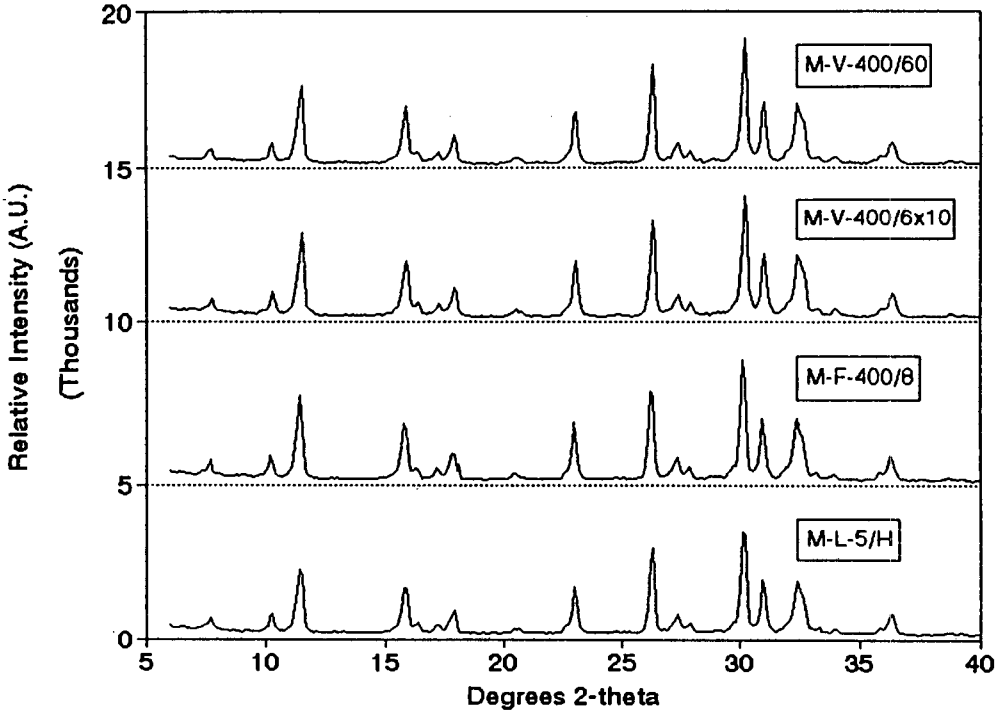

FIGURE A-V.6: XRD spectra of modified Mordenite samples (Co-Kα radiation)

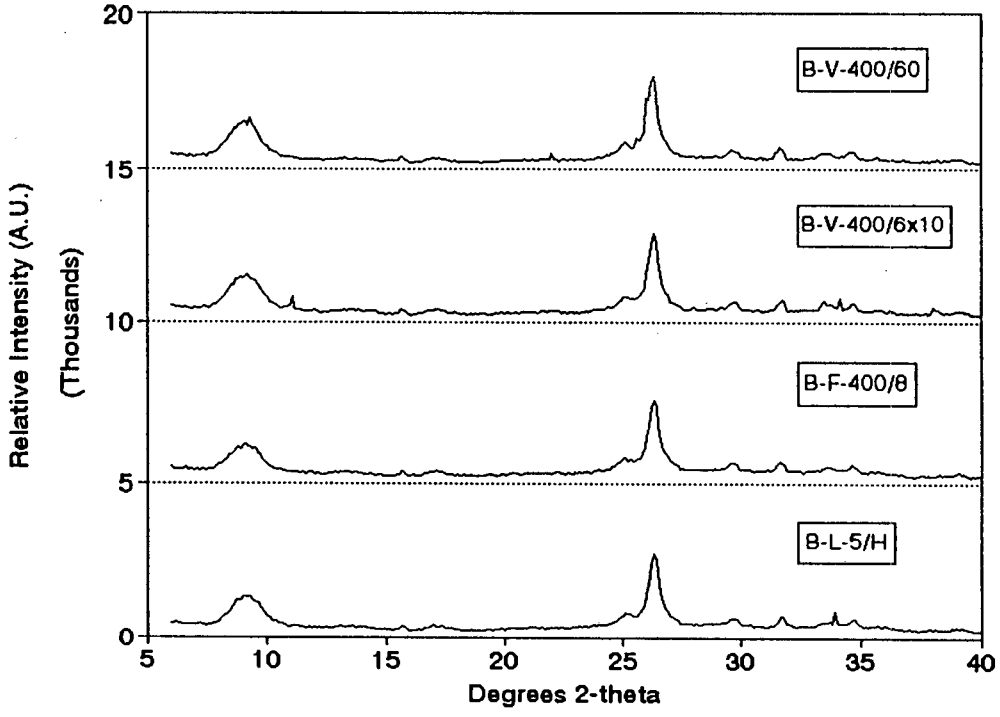

FIGURE A-V.7: XRD spectra of modified Beta samples (Co-Kα radiation)

APPENDIX VI: Py-TPD SPECTRA OF MODIFIED SAMPLES

The Py-TPD spectra of modified samples are shown in this Appendix. For comparison, the Py-TPD spectra of the parent samples Z, M and B are shown in a fold-out at the end of this Appendix. All spectra of modified and parent samples are scaled relative to each other. The number of acid sites measured by Py-TPD was calculated as follows (see Section 3.2.3.2):

[mmol/g] = Area Count x Internal Std. Ratio / Calibration Factor

TABLE A-VI.1: Py-TPD area count data

Catalyst	Calibration Factor ($x10^{-9}$)	Internal Std. Ratio	Area Count ($x10^{-9}$)	Py-TPD (mmol/g)	Figures
S	47.25	0.9624	0.97	0.02	4.14
Z	47.25	1.0465	20.29	0.45	4.11
Z	47.25	0.9574	22.61	0.46	4.14, A-VI.8
Z-V-100/60	29.46	1.0060	12.29	0.42	A-VI.2
Z-V-200/60	29.46	1.0727	11.30	0.41	A-VI.2
Z-V-300/60	29.46	1.0012	12.77	0.43	A-VI.2
Z-V-400/60	49.93	0.8881	24.24	0.43	A-VI.2
Z-V-400/4x4	49.93	1.0101	21.20	0.43	A-VI.1
Z-V-400/6x10	29.46	0.9005	13.73	0.42	A-VI.1
Z-F-50/8	29.46	1.0102	11.31	0.39	A-VI.3
Z-F-50/4x10	29.46	1.1055	5.03	0.19	A-VI.3
Z-F-400/8	29.46	0.7132	17.02	0.41	A-VI.3
Z-F-400/4x5	29.46	1.0413	9.17	0.32	A-VI.3
Z-L-100/-	30.09	0.9375	12.68	0.40	A-VI.4
Z-L-5/W	30.09	1.0017	12.03	0.40	A-VI.4
Z-L-5/E	30.09	0.8082	15.74	0.42	A-VI.4
Z-L-5/H	30.09	1.0526	12.50	0.44	A-VI.4
Z_9	32.33	1.0723	14.71	0.49	A-VI.5
Z_9-C-templ	32.33	0.9546	7.54	0.22	A-VI.5
Z_9-C-Na	32.33	1.1573	6.50	0.23	A-VI.5
Z_9-C-NH_4	32.33	0.9549	7.26	0.21	A-VI.5
M	45.02	1.0417	44.60	1.03	4.14, A-VI.8
M-V-400/60	45.02	1.1710	39.60	1.03	A-VI.6
M-V-400/6x10	45.02	0.9709	43.41	0.94	A-VI.6
M-F-400/8	45.02	0.8850	48.38	0.95	A-VI.6
M-L-5/H	45.02	1.0526	42.22	0.99	A-VI.6
B	42.89	0.9207	33.55	0.72	4.14, A-VI.8
B-V-400/60	42.89	0.9707	33.22	0.75	A-VI.7
B-V-400/6x10	42.89	1.0238	28.03	0.67	A-VI.7
B-F-400/8	42.89	0.9753	23.54	0.53	A-VI.7
B-L-5/H	42.89	0.9389	27.96	0.61	A-VI.7

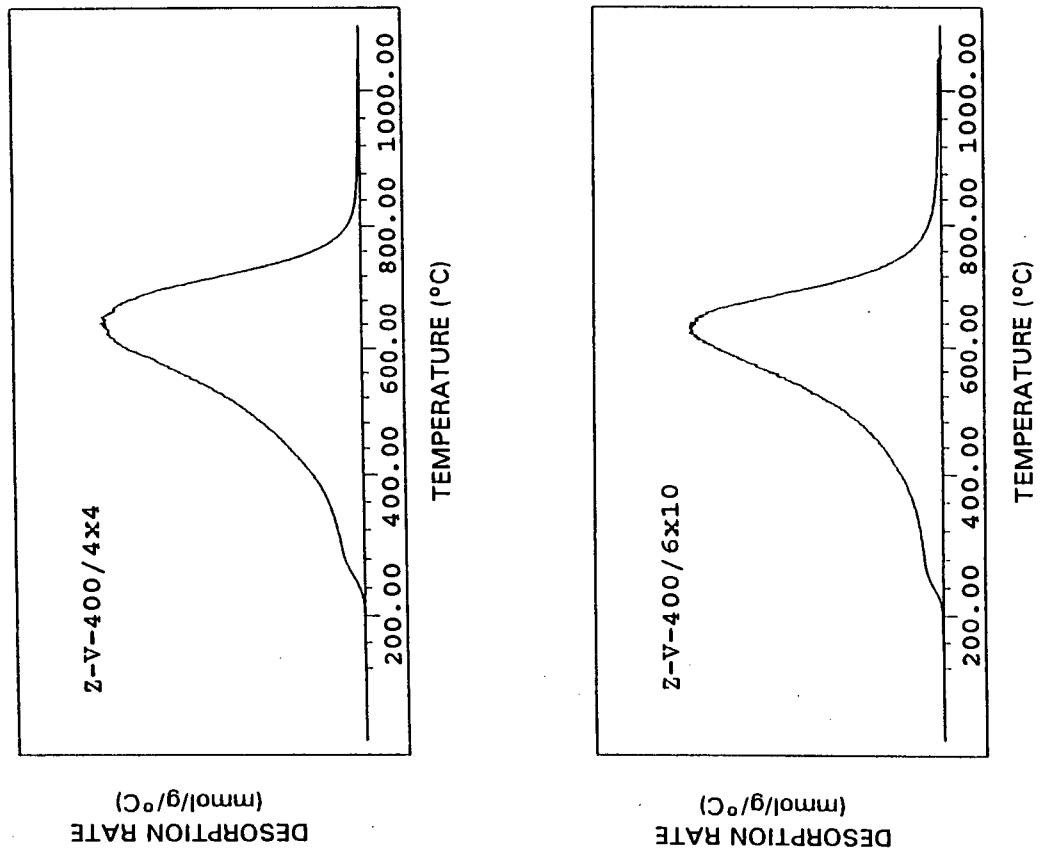

FIGURE A-VI.1: Py-TPD spectra of ZSM-5 samples modified by CVD using multiple deposition cycles in a static vacuum system

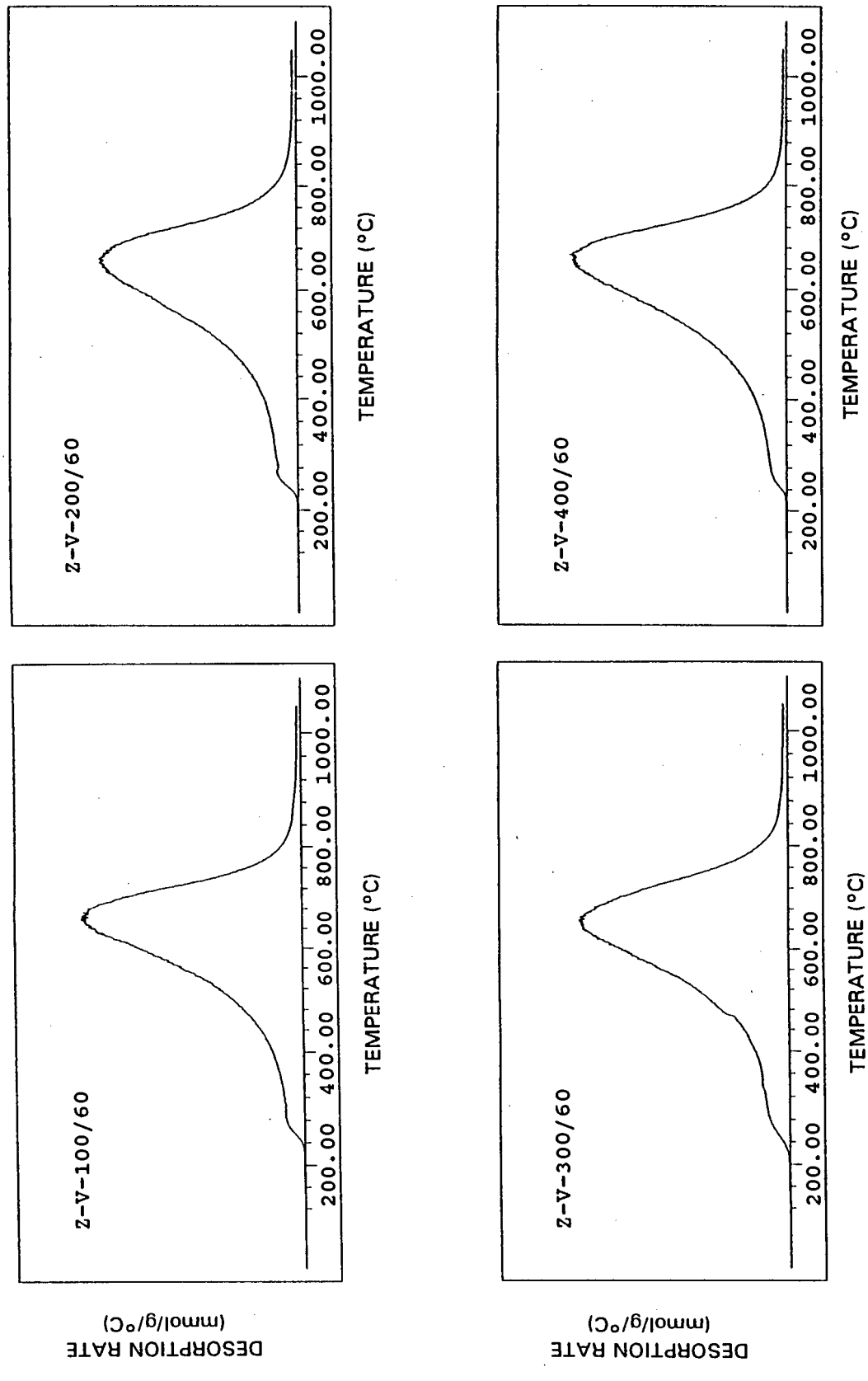

FIGURE A-VI.2: Py-TPD spectra of ZSM-5 samples modified by CVD using a single deposition cycle in a static vacuum system

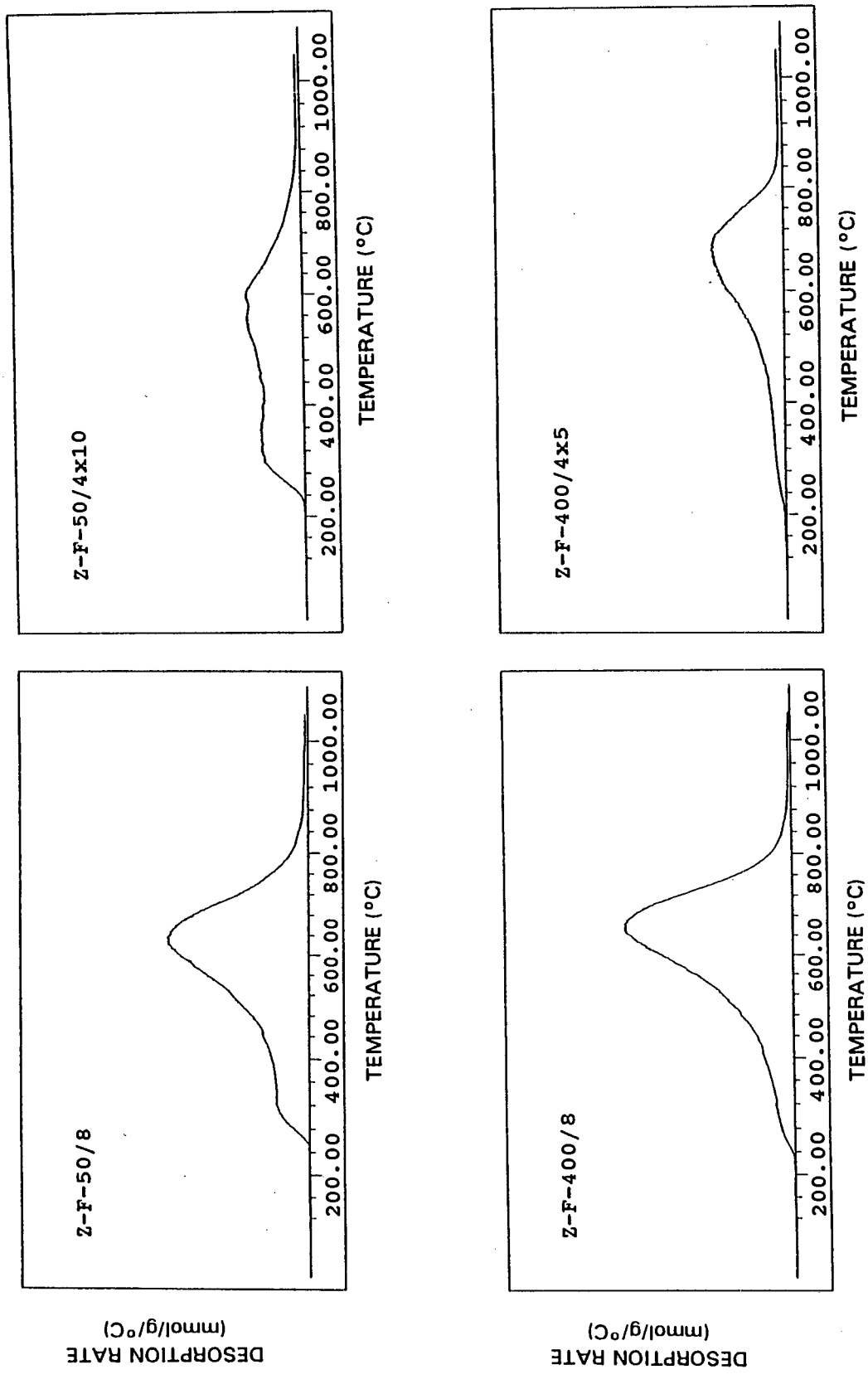

FIGURE A-VI.3: Py-TPD spectra of ZSM-5 samples modified by CVD using a vapour phase flow system

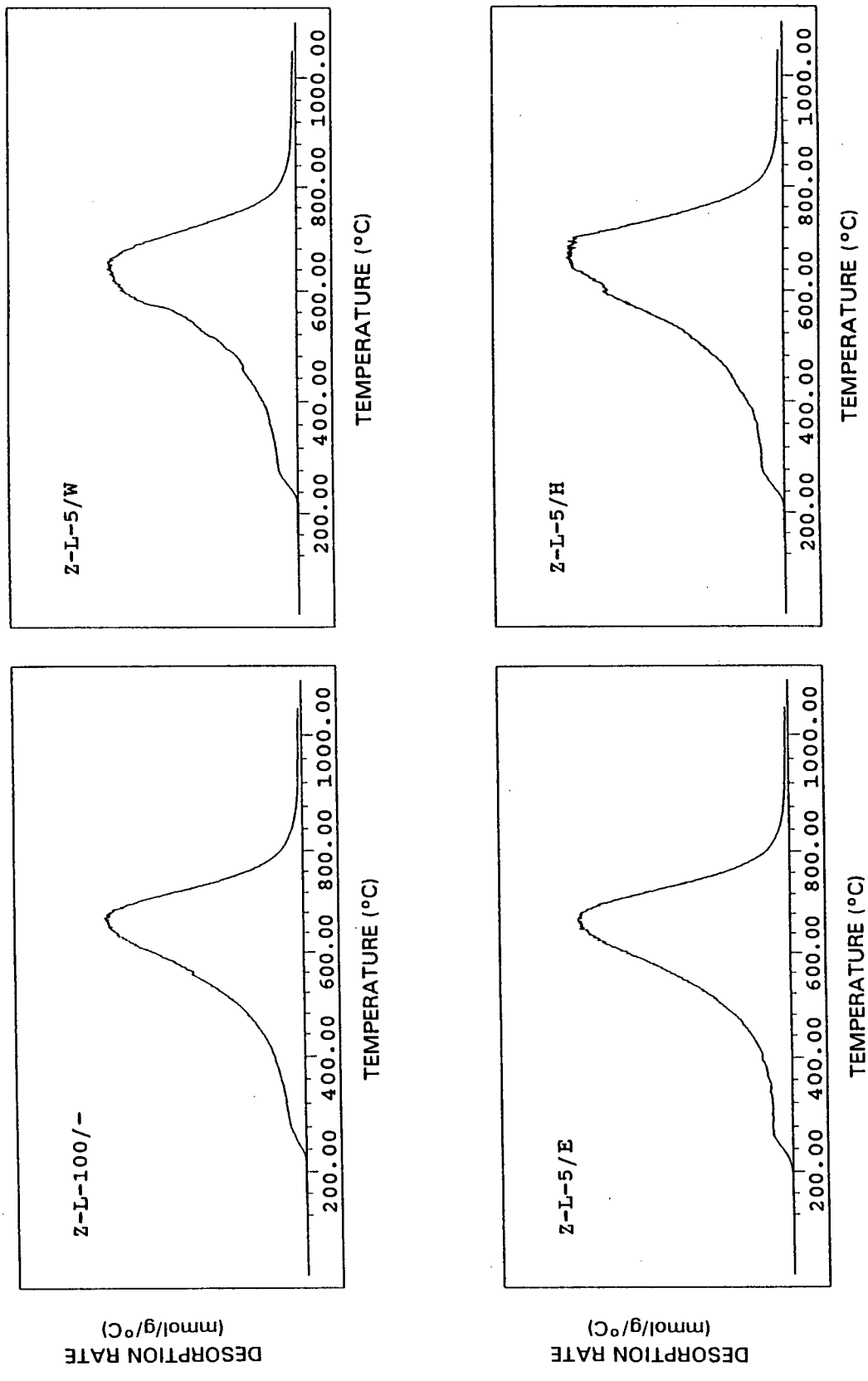

FIGURE A-VI.4: Py-TPD spectra of ZSM-5 samples modified by CLD

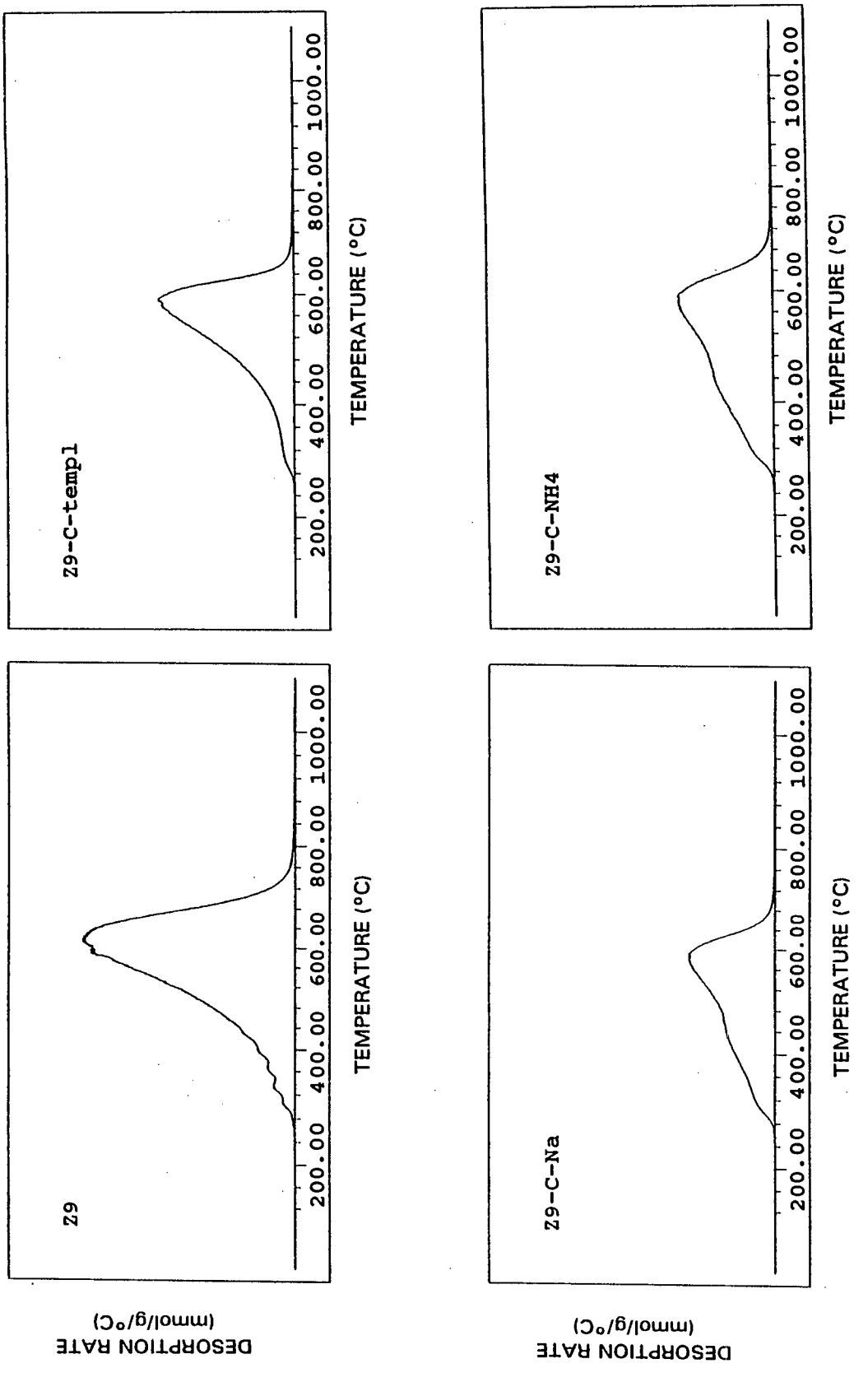

FIGURE A-VI.5: Py-TPD spectra of ZSM-5 samples coated with Silicalite shells

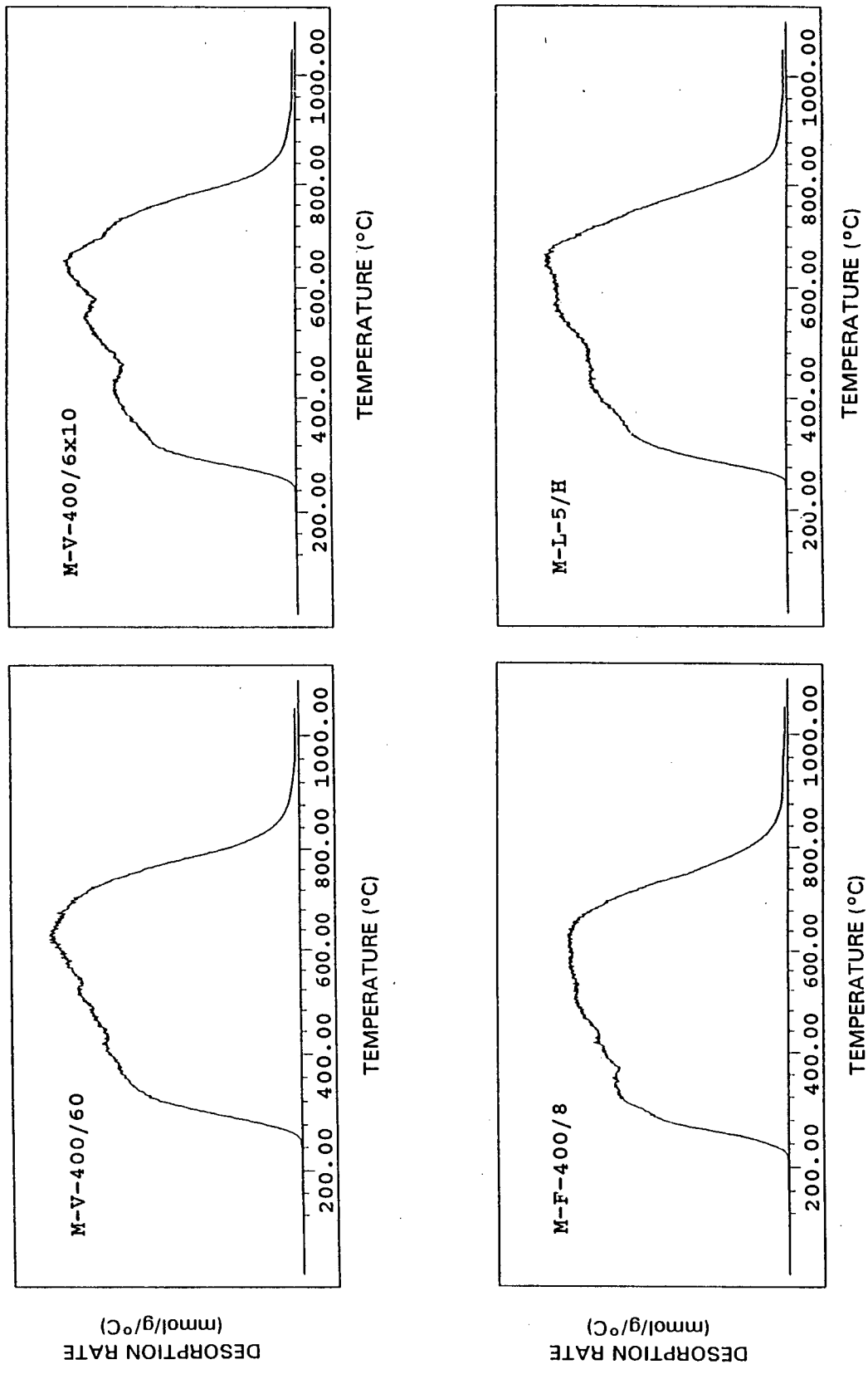

FIGURE A-VI.6: Py-TPD spectra of modified Mordenite samples

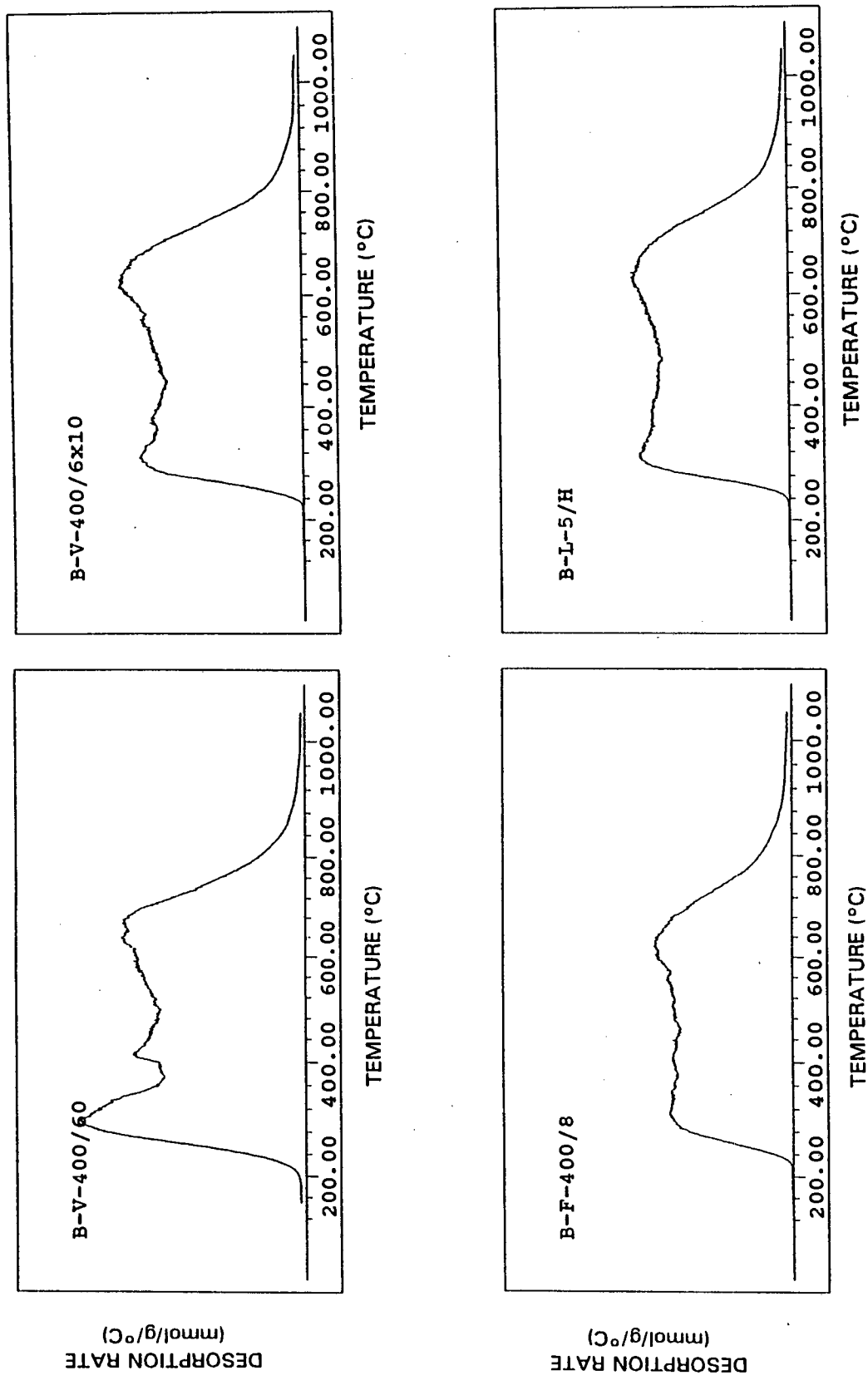

FIGURE A-VI.7: Py-TPD spectra of modified Beta samples

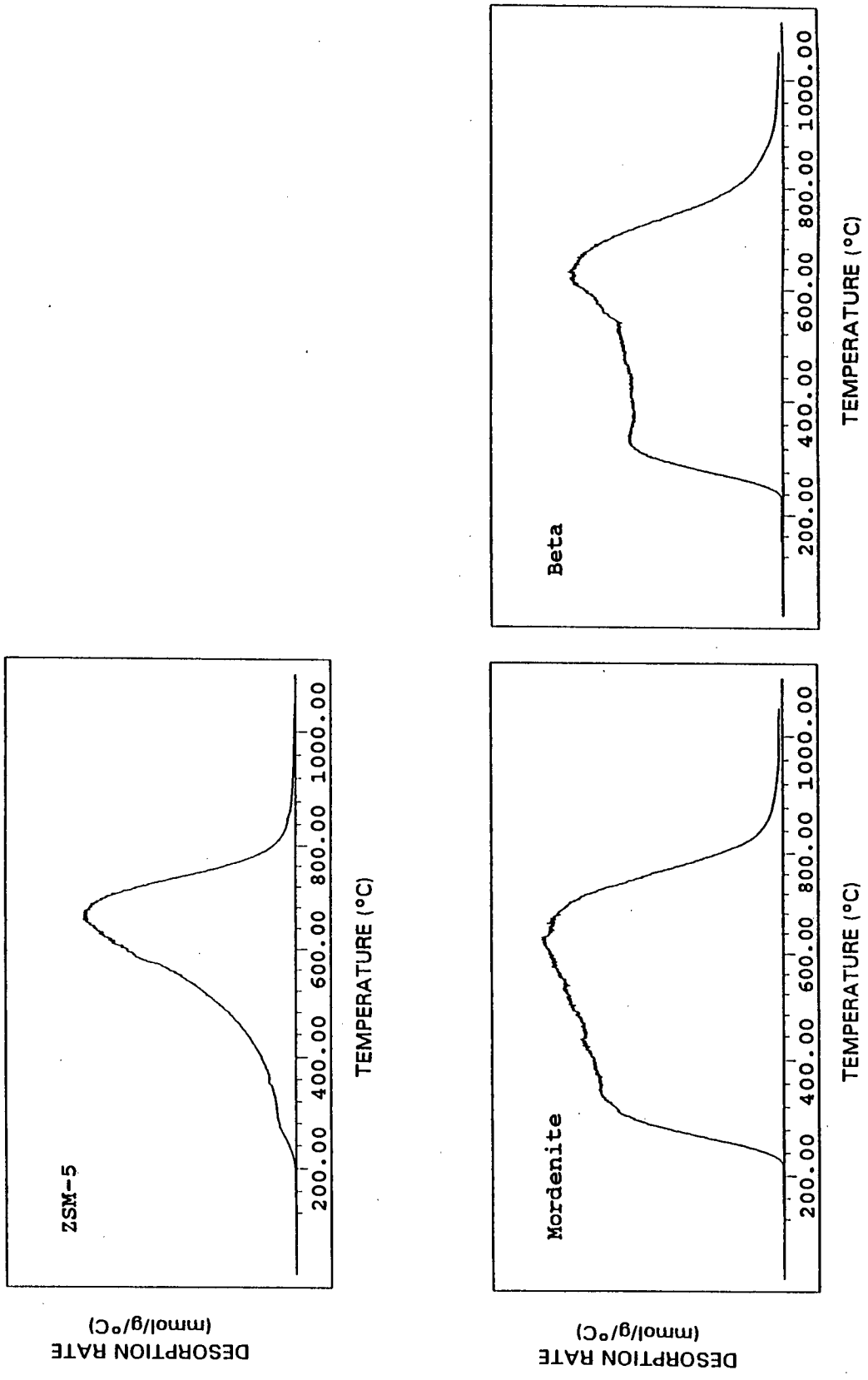

FIGURE A-VI.8: Py-TPD spectra of parent samples (to scale w.r.t. each other and the respective modified samples)

APPENDIX VII: MQ-TPD SPECTRA OF MODIFIED SAMPLES

The MQ-TPD spectra of modified samples are shown in this Appendix. For comparison, the MQ-TPD spectra of the parent samples Z, M and B are shown in a fold-out at the end of this Appendix. All spectra are scaled to their respective parent sample. The percentage relative external surface acidity (RESA) measured by MQ-TPD was calculated as follows (see Section 3.2.3.2):

$$\% \text{ RESA} = 100 \times \text{Area Count} \times \text{Internal Std. Ratio} / \text{Area Count of Reference}$$

TABLE A-VII.1: MQ-TPD area count data

Catalyst	Area Count Reference ($x10^{-6}$)	Internal Std. Ratio	Area Count ($x10^{-6}$)	MQ-TPD (%)	Figures
S	1270	0.9536	32	2	4.15
Z	1270	0.9829	1169	91	4.12
Z	1270	1.0000	1270	100	4.15, A-VII.8
Z (24 h ads)	1270	1.0101	1302	104	A-VIII.3
Z-V-100/60	475	0.9778	469	97	A-VII.2
Z-V-200/60	475	0.8727	299	55	A-VII.2
Z-V-300/60	475	1.0536	181	40	A-VII.2
Z-V-400/60	475	1.1639	142	35	A-VII.2
Z-V-400/4x4	475	0.9740	13	3	A-VII.1
Z-V-400/6x10	475	0.9633	1	0	A-VII.1
Z-F-50/8	313	0.9187	141	42	A-VII.3
Z-F-400/8	313	1.0659	58	20	A-VII.3
Z-L-100/-	313	1.0936	222	77	A-VII.4
Z-L-5/W	313	1.0187	159	53	A-VII.4
Z-L-5/E	1250	0.9178	562	41	A-VII.4
Z-L-5/H	1250	0.8802	417	29	A-VII.4
Z_9	486	1.0000	486	100	A-VII.5
Z_9-C-templ	486	0.8429	321	56	A-VII.5
Z_9-C-Na	486	0.9919	287	59	A-VII.5
Z_9-C-NH_4	486	1.0937	30	7	A-VII.5
M	240	1.0000	240	100	4.15, A-VII.8
M (24 h ads)	240	1.1250	886	416	A-VIII.3
M-V-400/60	240	1.0112	2	1	A-VII.6
M-V-400/6x10	240	1.0465	0	0	A-VII.6
M-V-400/6x10 (crush.)	240	1.3636	100	57	A-VIII.4
M-F-400/8	240	0.7692	71	30	A-VII.6
M-L-5/H	240	1.0227	43	18	A-VII.6
B	966	1.0000	966	100	4.15, A-VII.8
B (24 h ads)	966	1.2500	3180	411	A-VIII.3
B-V-400/60	966	0.9804	12	1	A-VII.7
B-V-400/6x10	966	0.9709	31	3	A-VII.7
B-V-400/6x10 (crush.)	966	1.0433	880	95	A-VIII.4
B-F-400/8	966	0.9524	218	22	A-VII.7
B-L-5/H	966	0.9434	315	31	A-VII.7

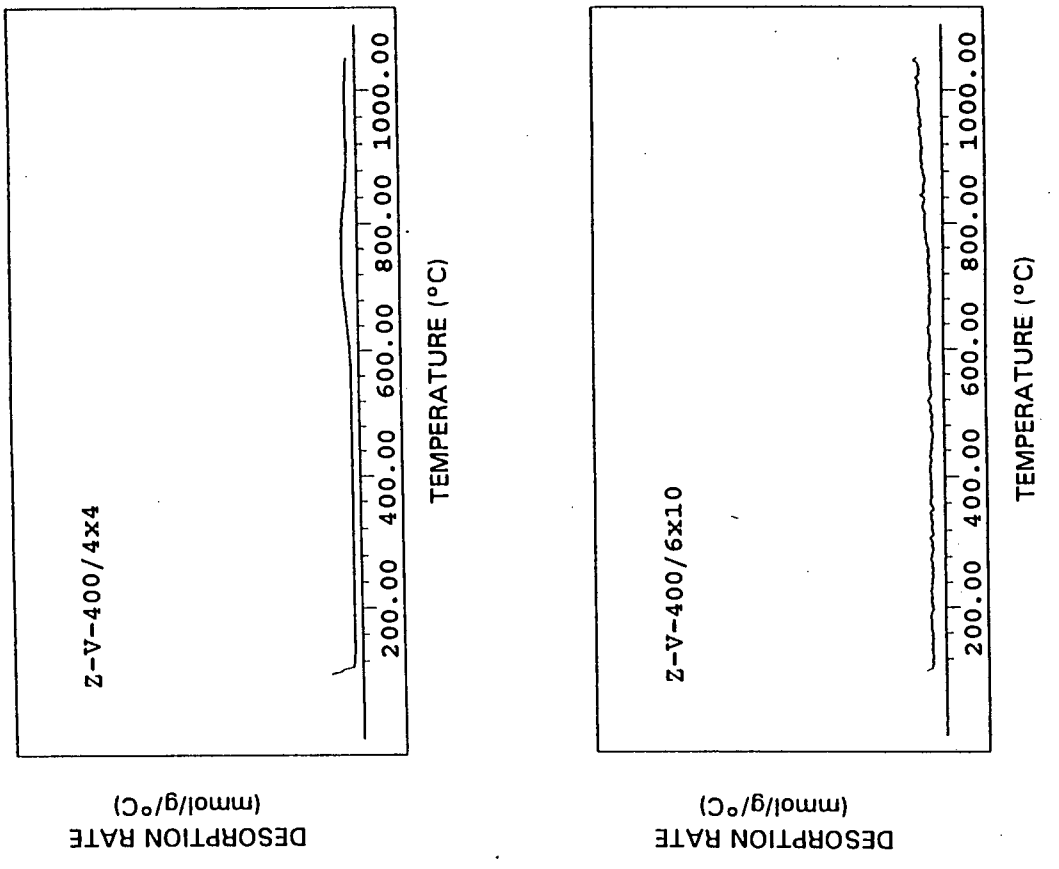

FIGURE A-VII.1: MQ-TPD spectra of ZSM-5 samples modified by CVD using multiple deposition cycles in a static vacuum system

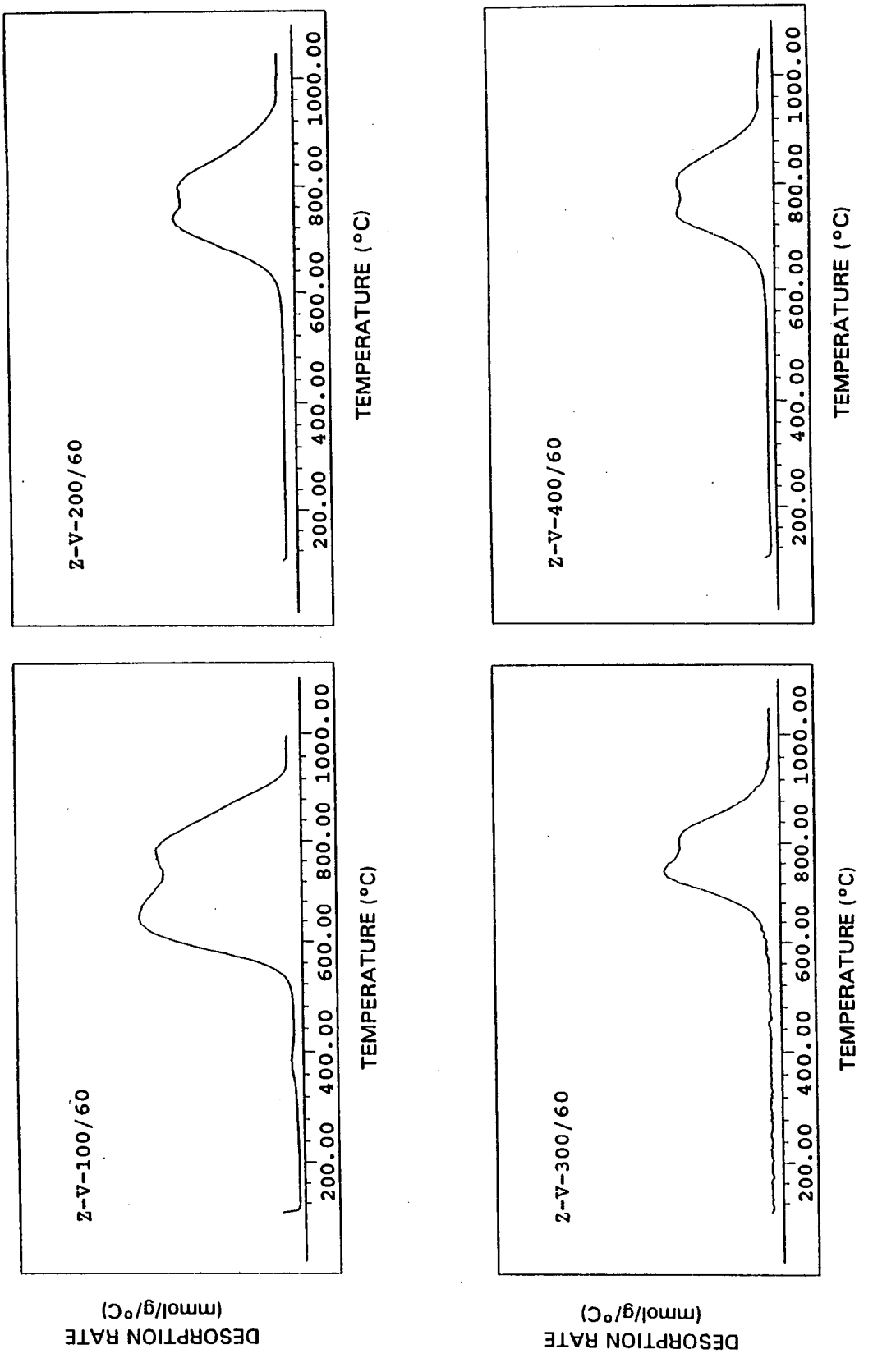

FIGURE A-VII.2: MQ-TPD spectra of ZSM-5 samples modified by CVD using a single deposition cycle in a static vacuum system

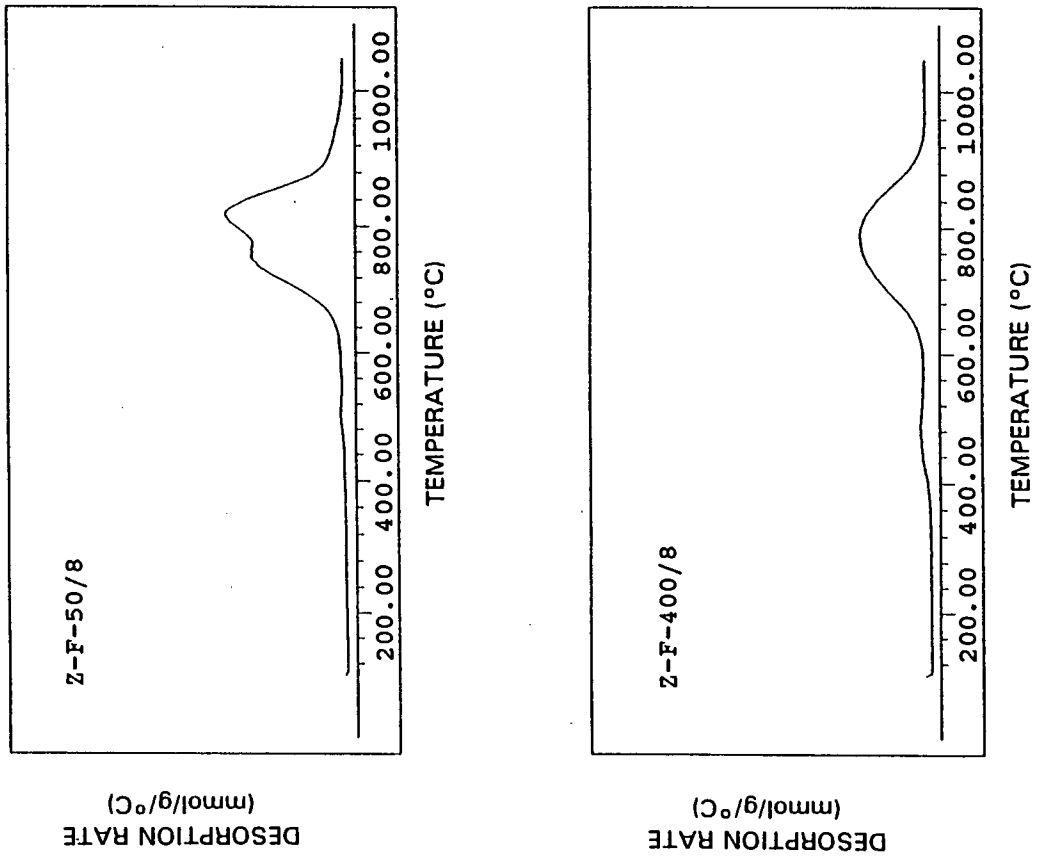

FIGURE A-VII.3: MQ-TPD spectra of ZSM-5 samples modified by CVD using a vapour phase flow system

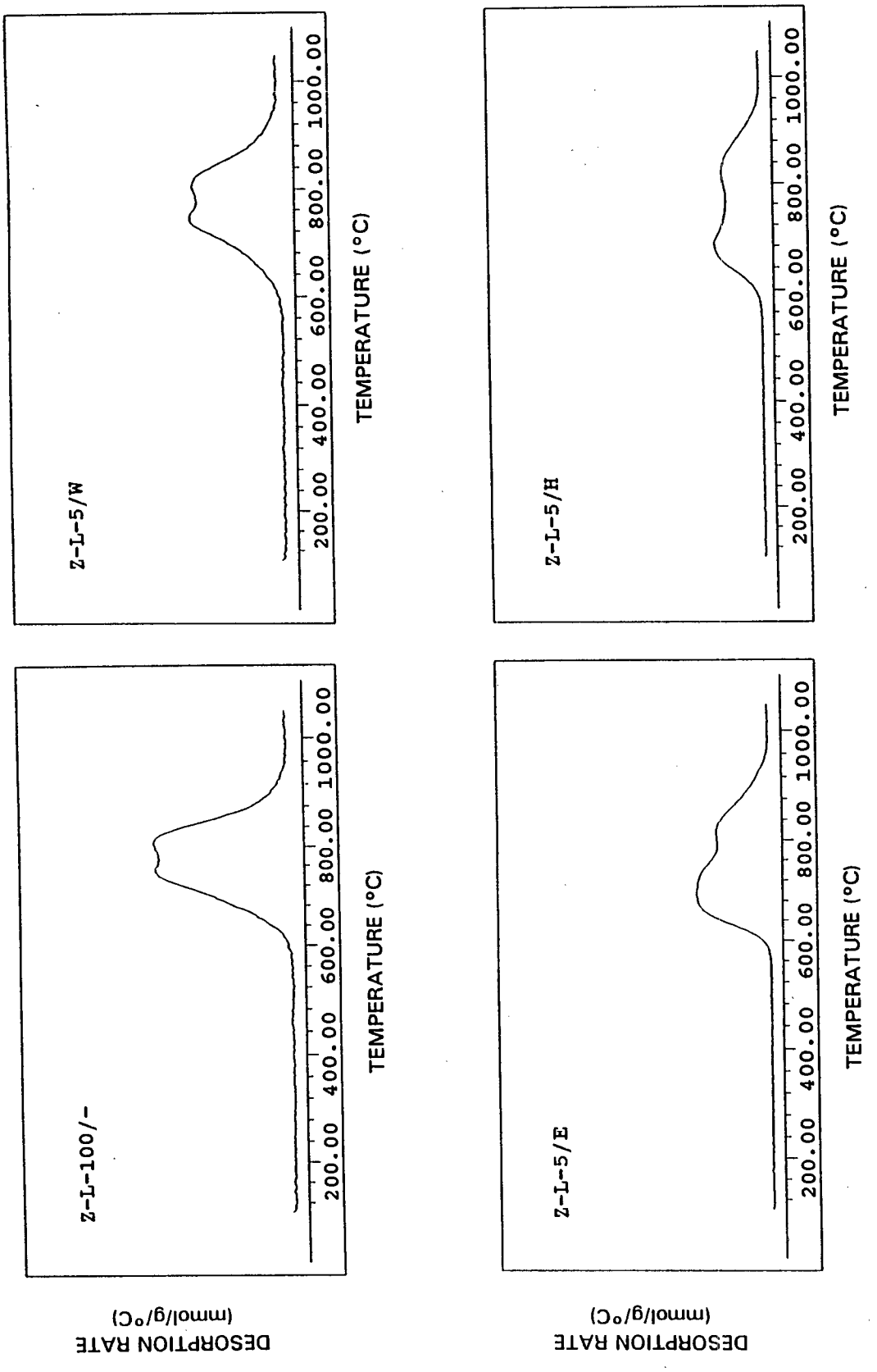

FIGURE A-VII.4: MQ-TPD spectra of ZSM-5 samples modified by CLD

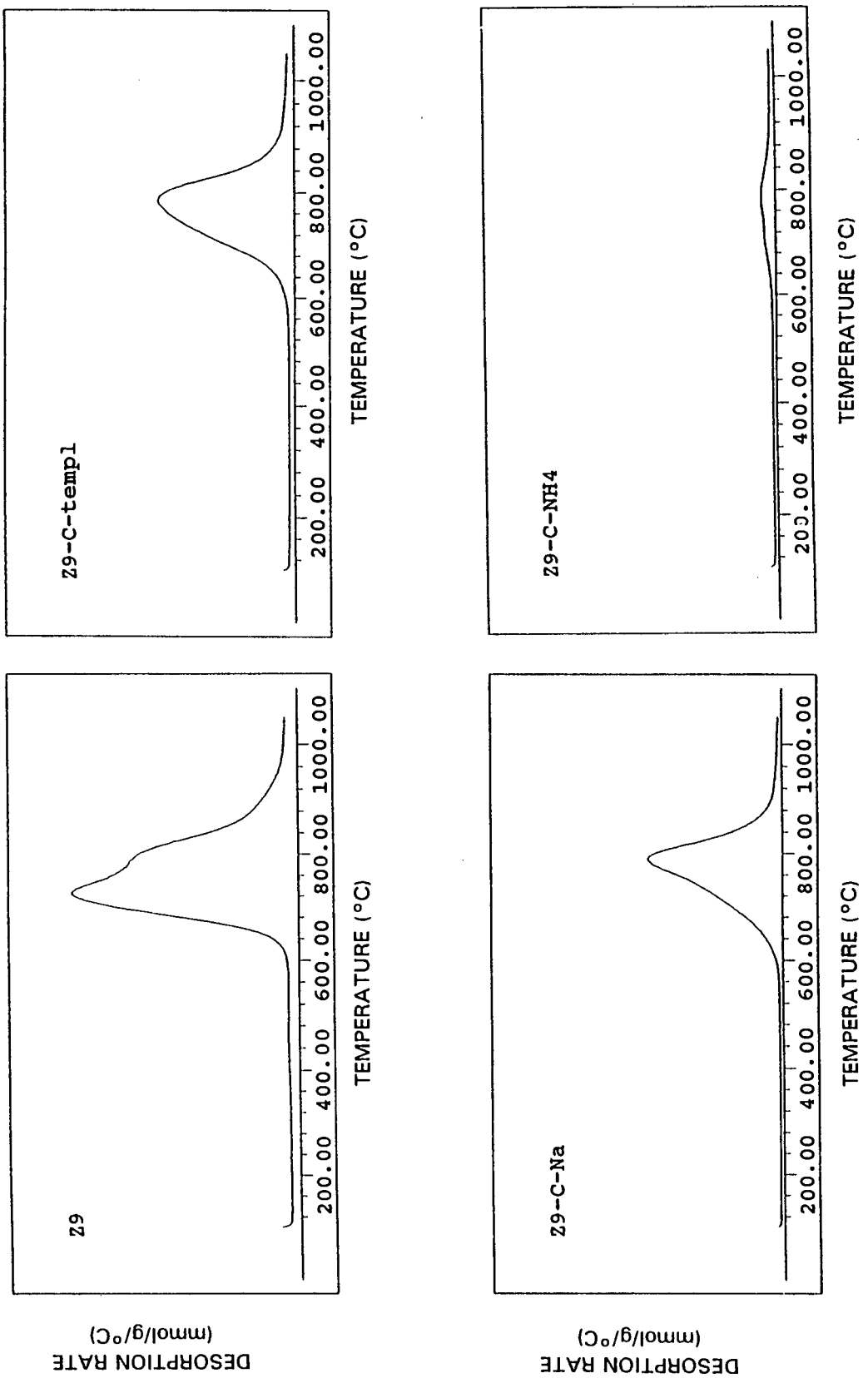

FIGURE A-VII.5: MQ-TPD spectra of ZSM-5 samples coated with Silicalite shells

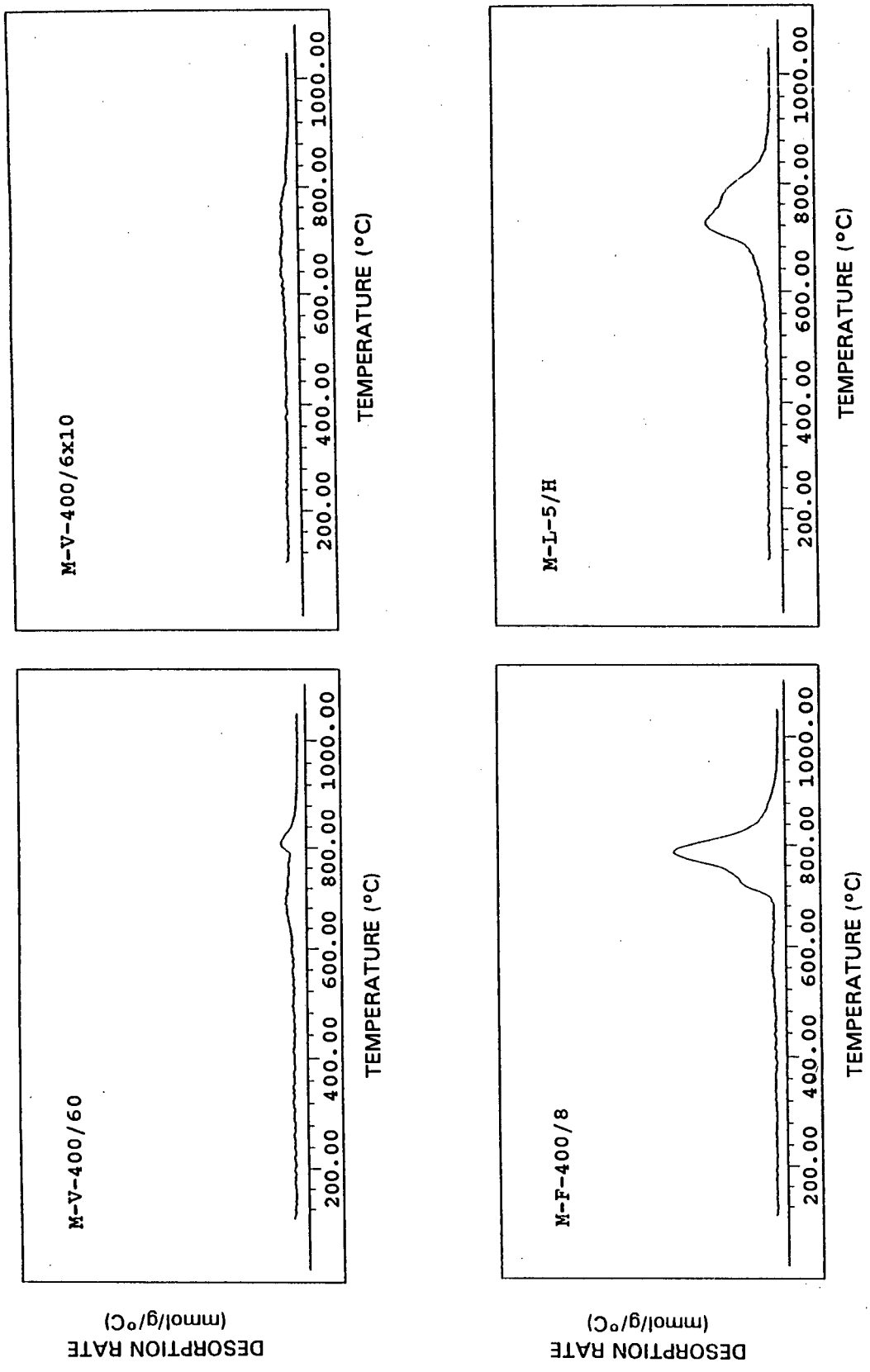

FIGURE A-VII.6: MQ-TPD spectra of modified Mordenite samples

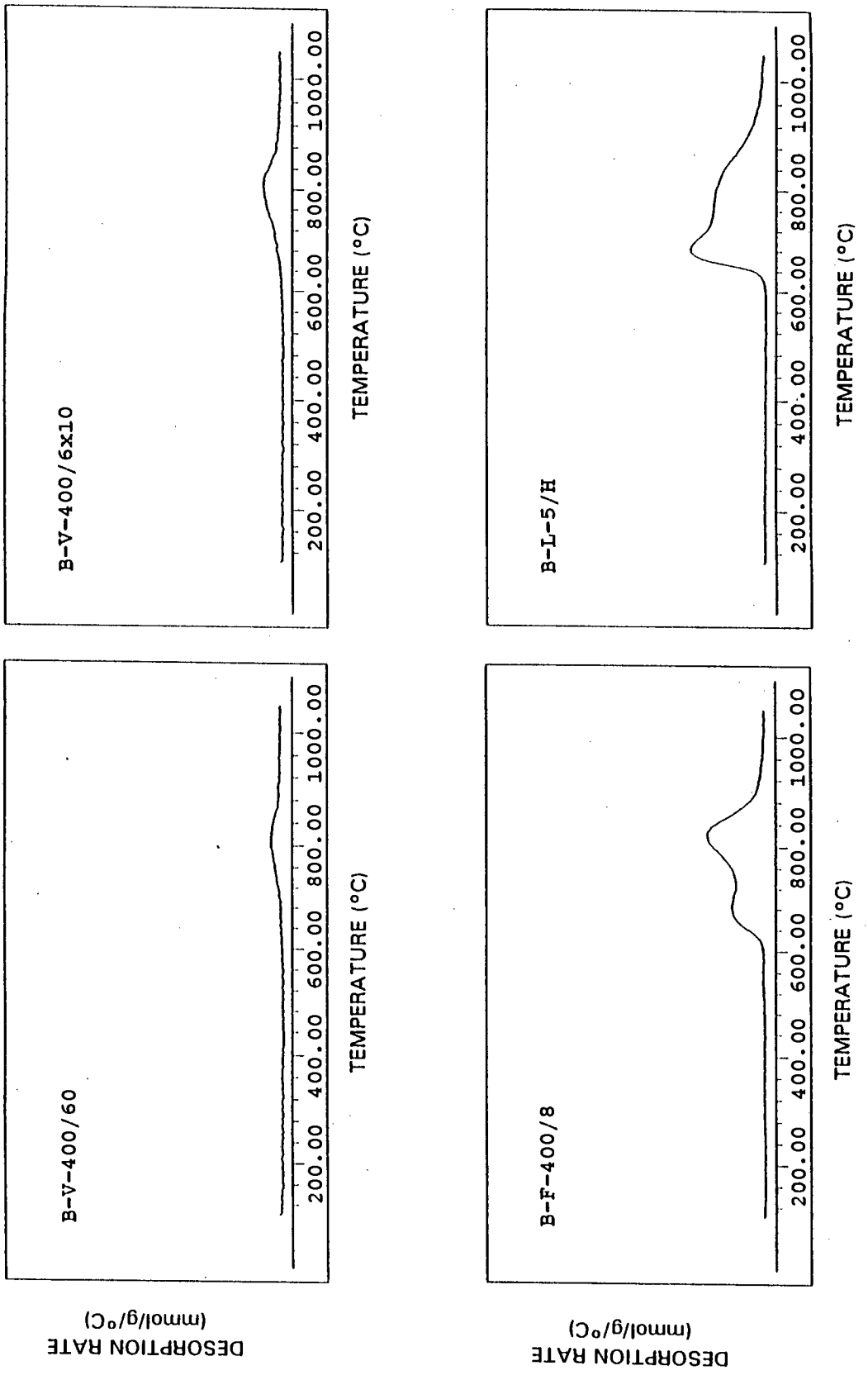

FIGURE A-VII.7: MQ-TPD spectra of modified Beta samples

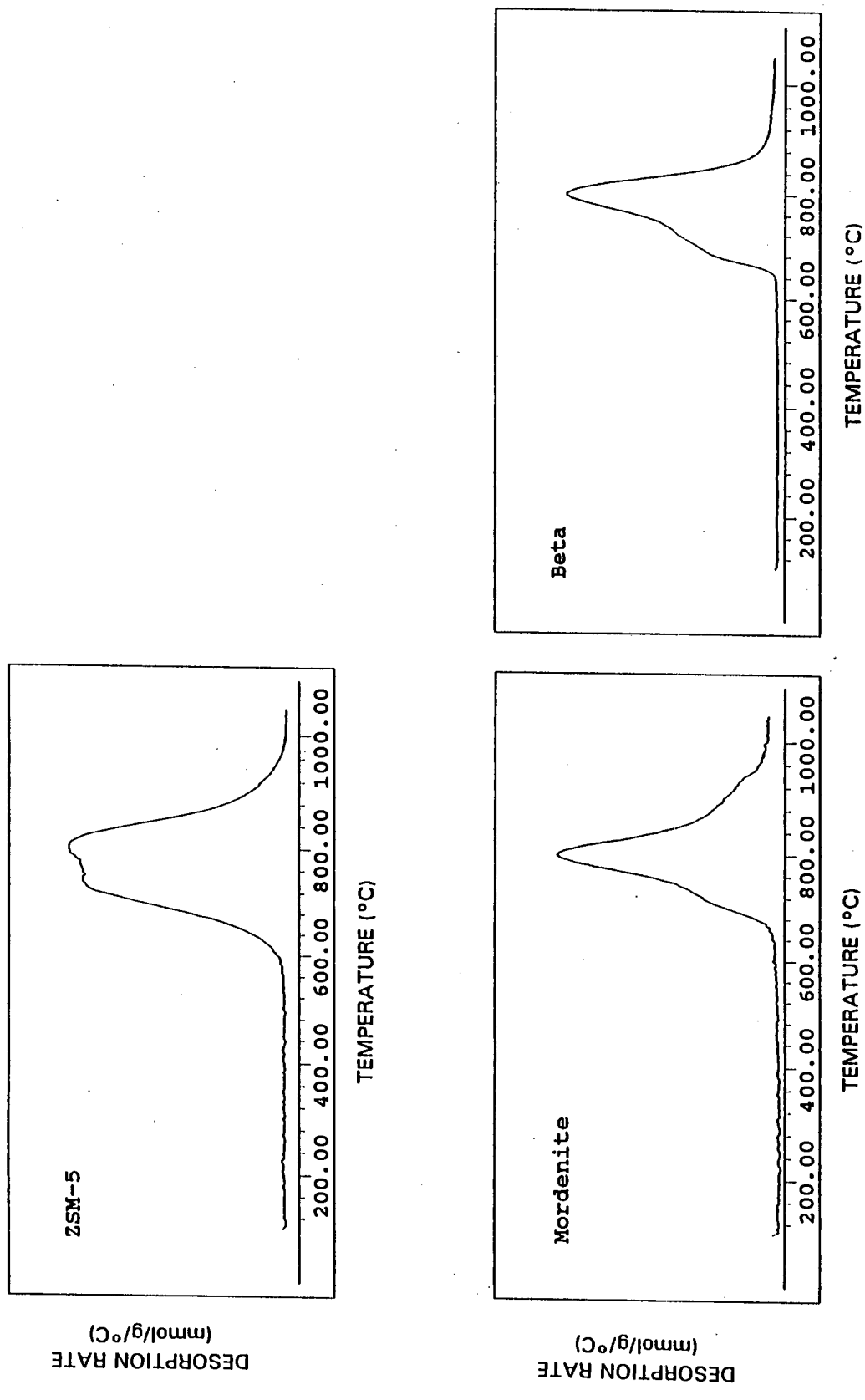

FIGURE A-VII.8: MQ-TPD spectra of parent samples (to scale w.r.t. the respective modified samples)

APPENDIX VIII: MISCELLANEOUS TPD SPECTRA

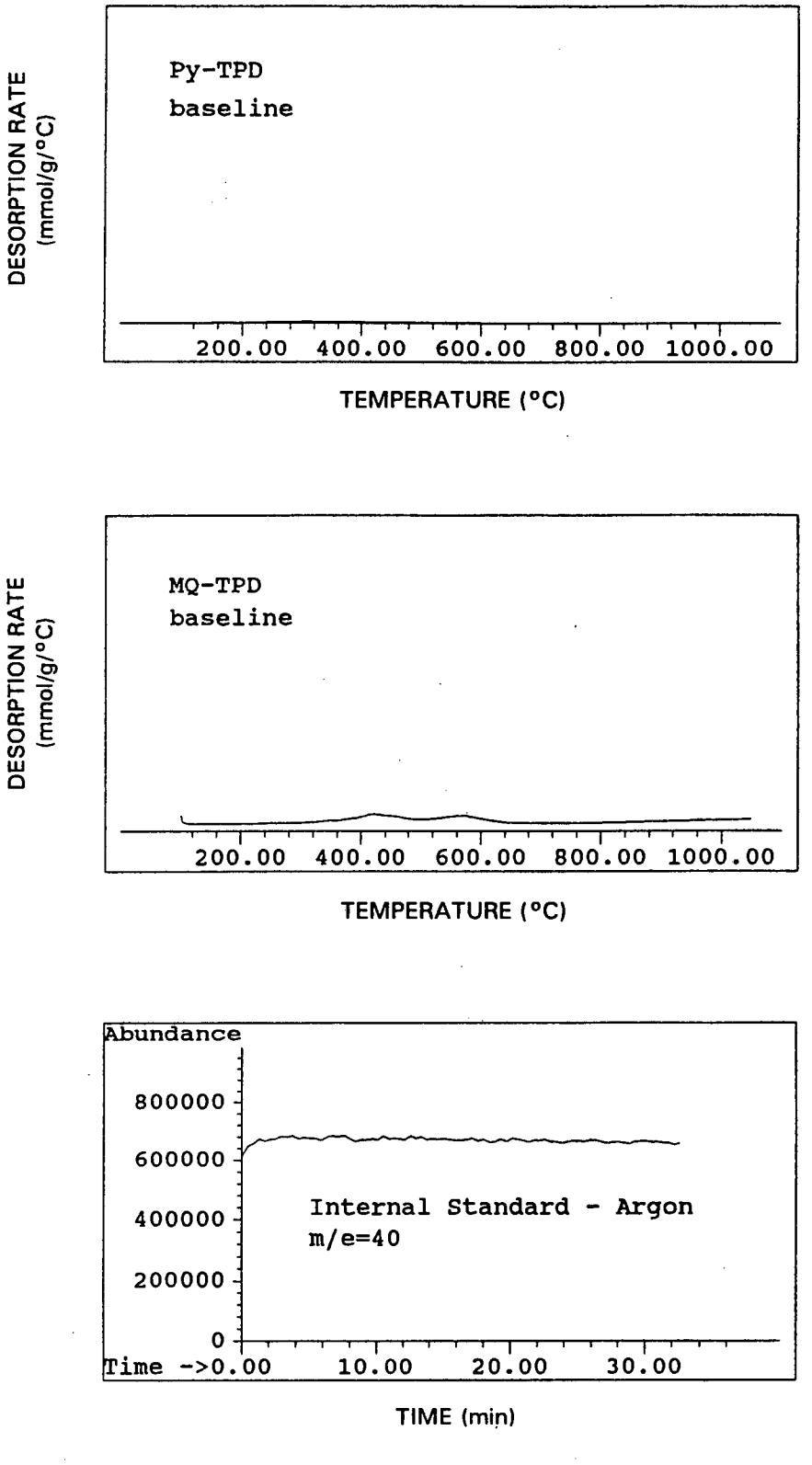

FIGURE A-VIII.1: Py-TPD and MQ-TPD baseline spectra and internal standard response-line

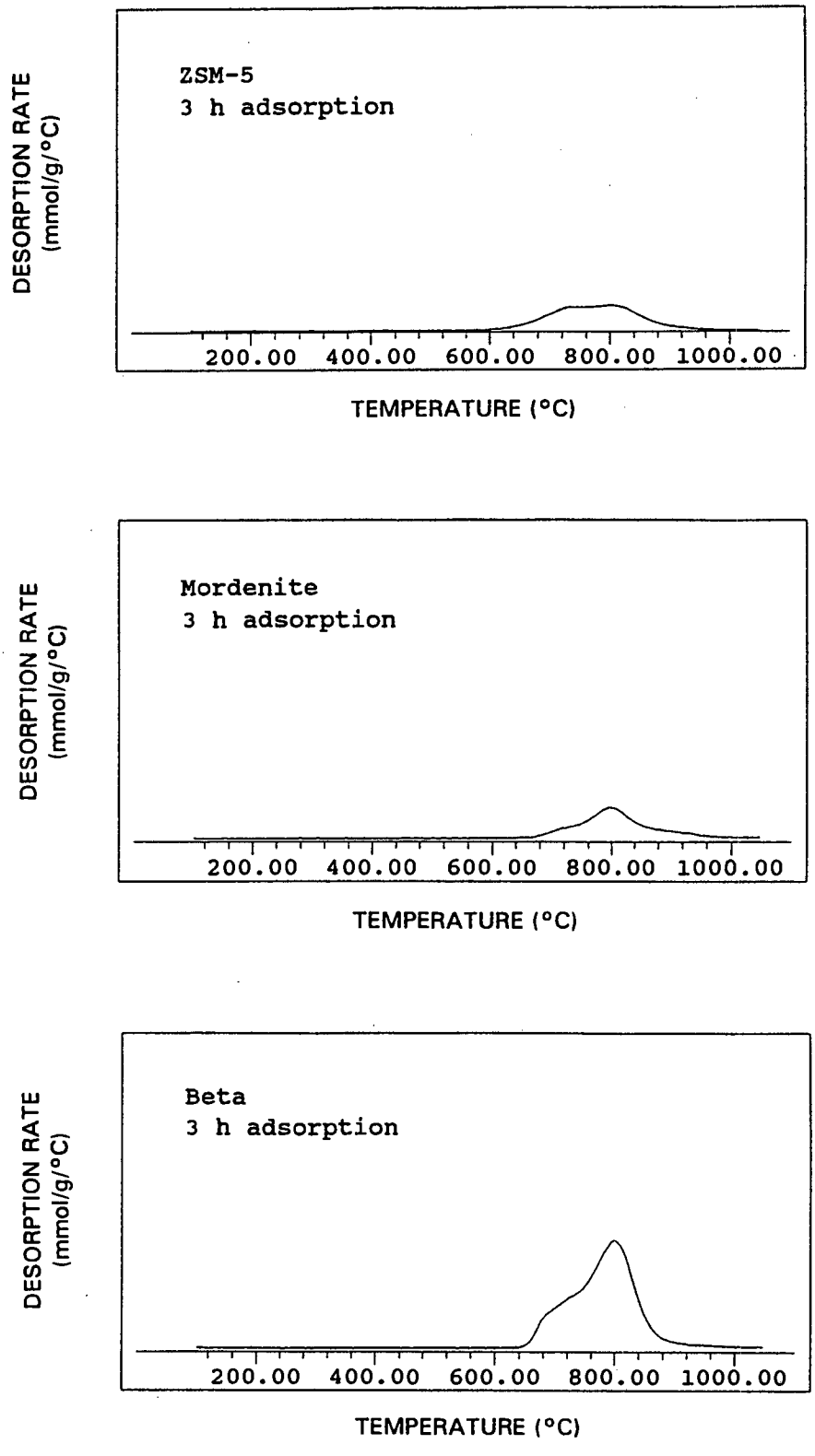

FIGURE A-VIII.2: MQ-TPD spectra of 3 h adsorption periods of 4-methyl quinoline on ZSM-5 (sample Z), Mordenite (sample M) and Beta (sample B)

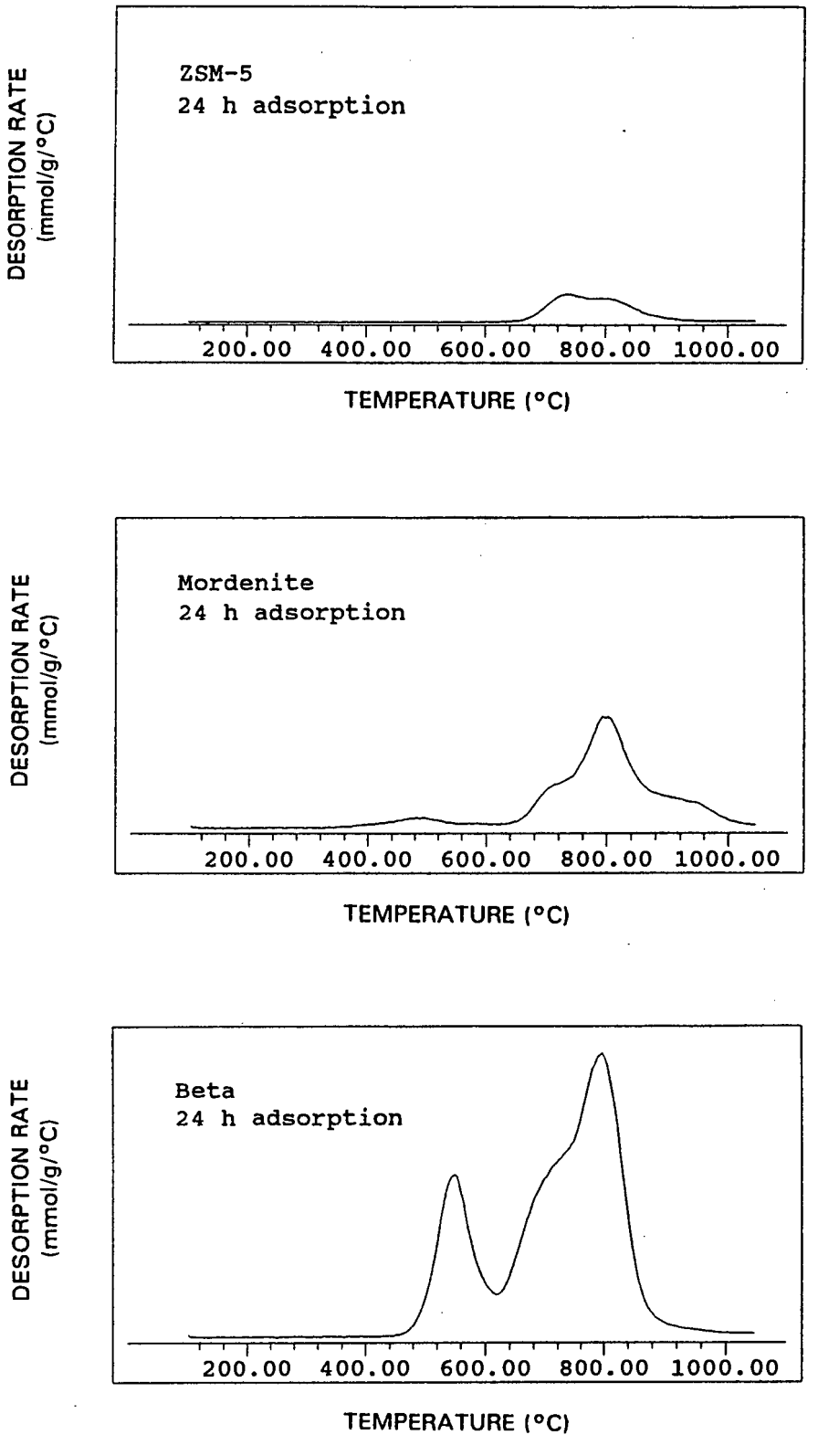

FIGURE A-VIII.3: MQ-TPD spectra of 24 h adsorption periods of 4-methyl quinoline on ZSM-5 (sample Z), Mordenite (sample M) and Beta (sample B)

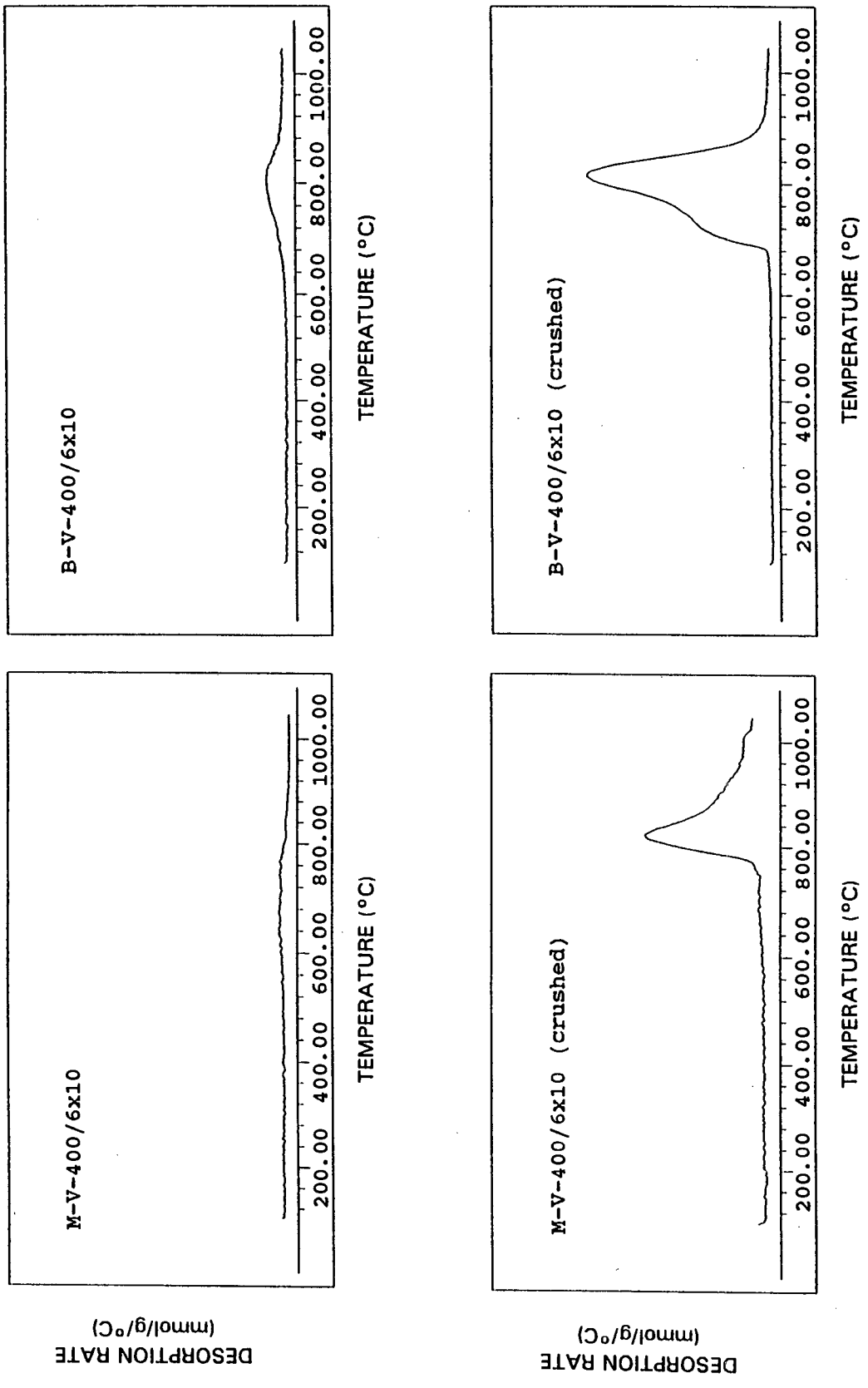

FIGURE A-VIII.4: MQ-TPD spectra of samples M-V-400/6x10 and M-V-400/6x10 (crushed) and samples B-V-400/6x10 and B-V-400/6x10 (crushed)

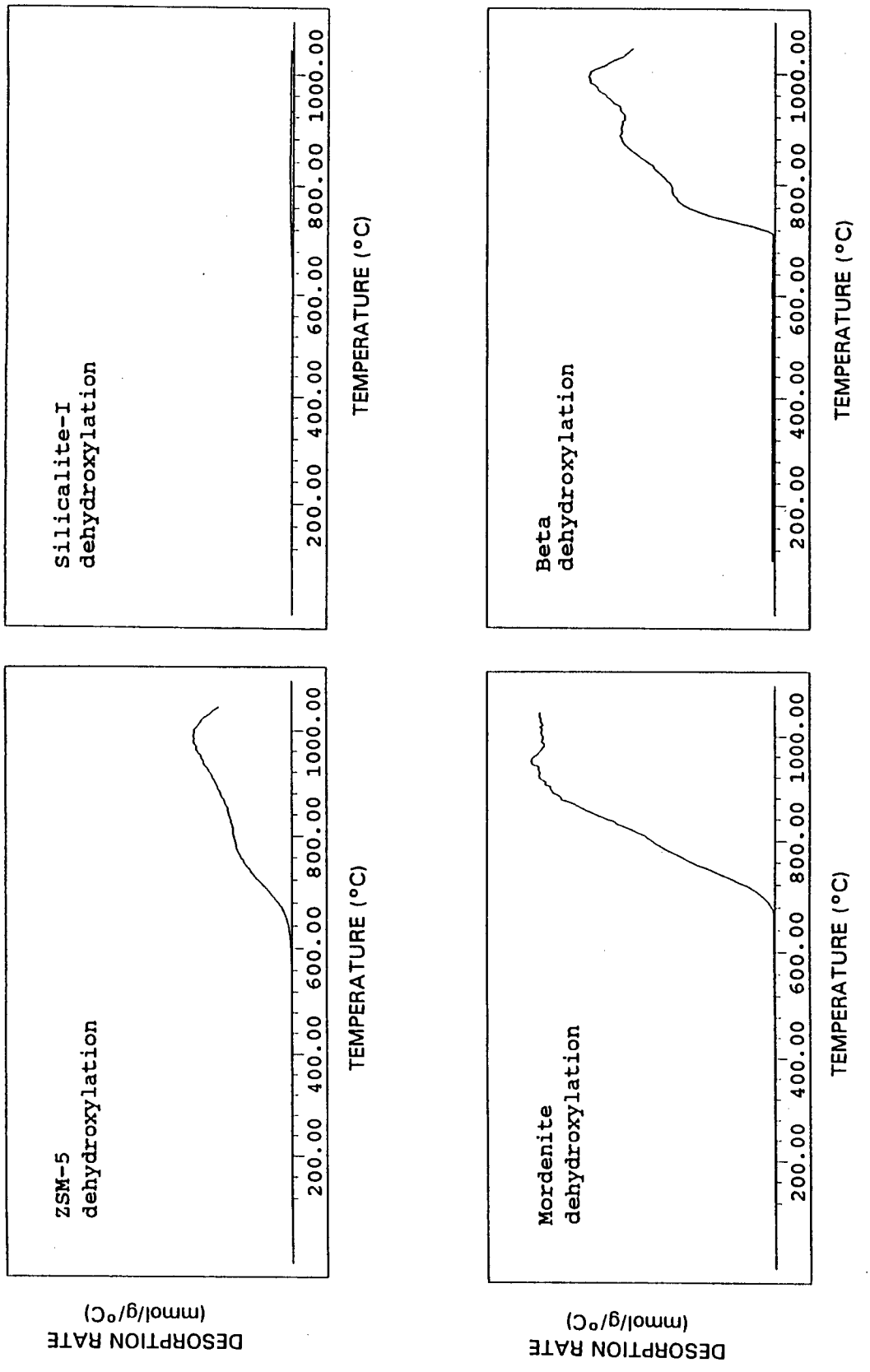

FIGURE A-VIII.5: Dehydroxylation spectra of ZSM-5 (sample Z), Silicalite-I (sample S), Mordenite (sample M) and Beta (sample B)

APPENDIX IX: ADSORPTION PROFILES OF MODIFIED SAMPLES

The adsorption profiles shown in Appendix IX are labelled as follows:

1 *n*-hexane
2 *p*-xylene
3 *o*-xylene
4 1,2,4-trimethyl benzene

The mass indicated on each figure is the sample mass. Note that the sample moisture content was probably largely dependent on atmospheric conditions, and in the case of liquid phase deposition on the diluent used in the modification step, and therefore the moisture content differed considerably from sample to sample.

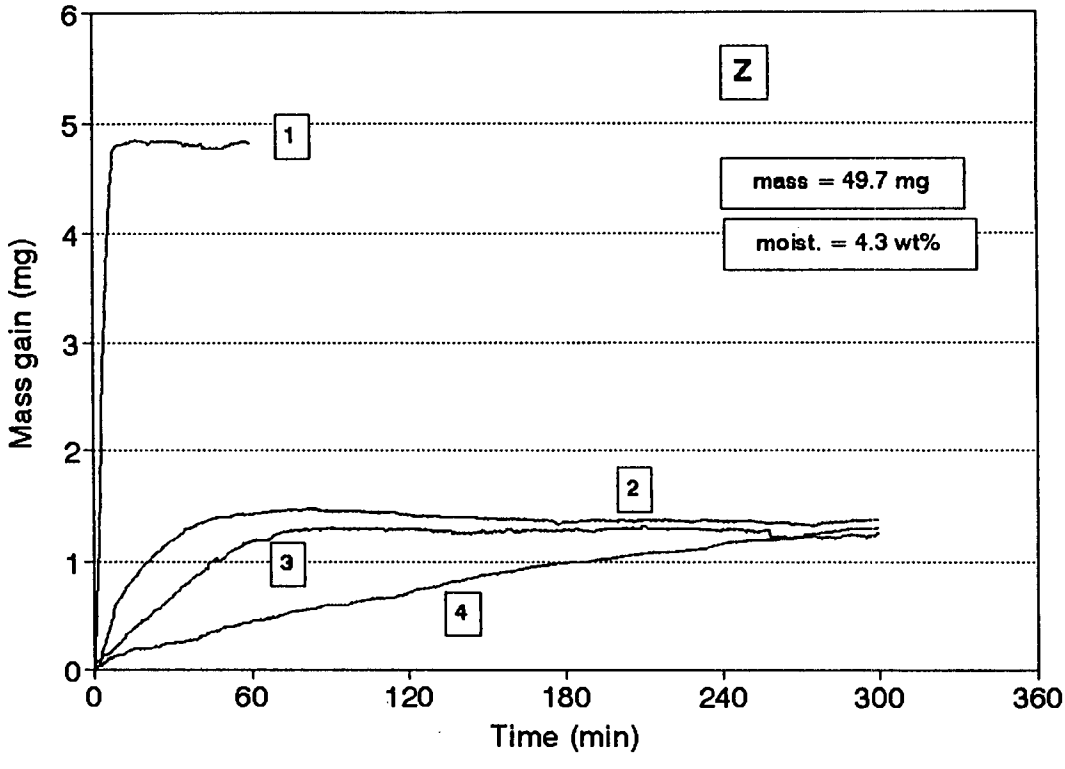

FIGURE A-IX.1: Adsorption profiles of sample Z

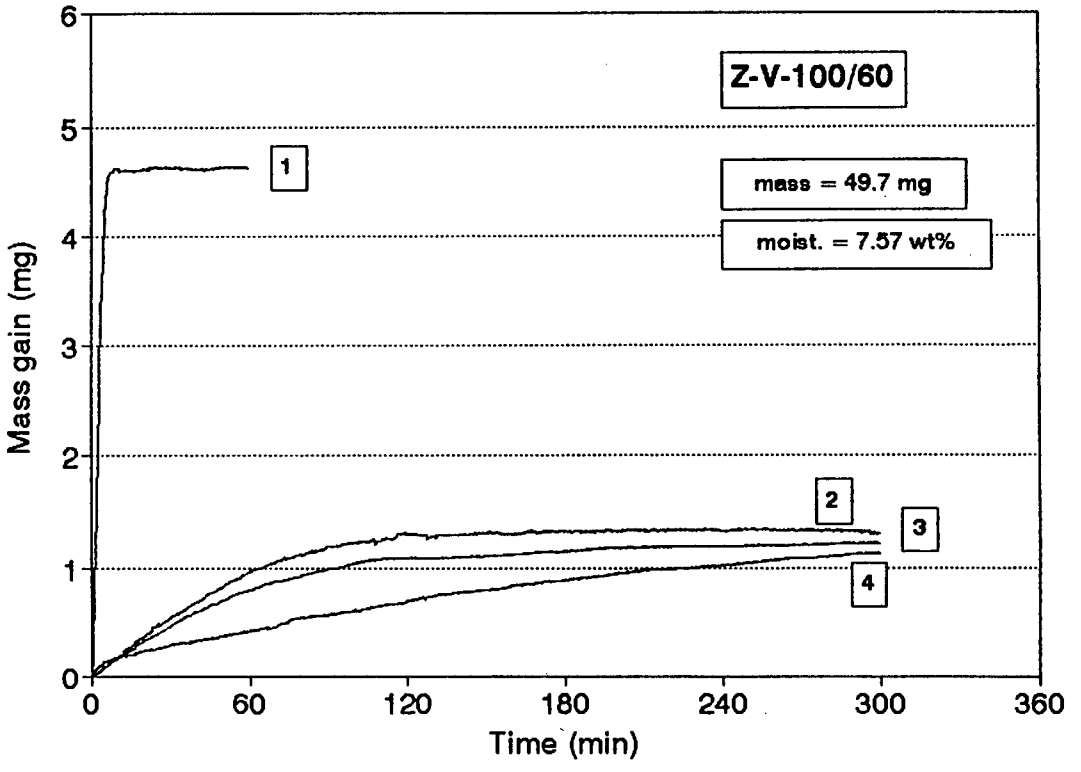

FIGURE A-IX.2: Adsorption profiles of sample Z-V-100/60

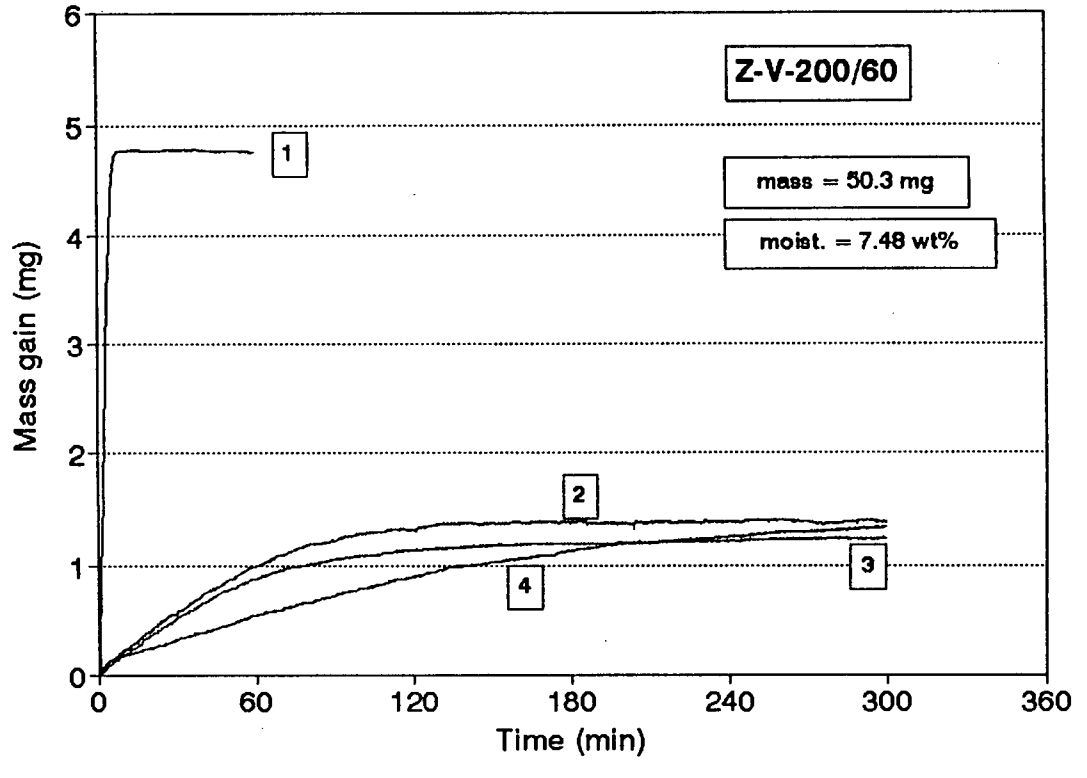

FIGURE A-IX.3: Adsorption profiles of sample Z-V-200/60

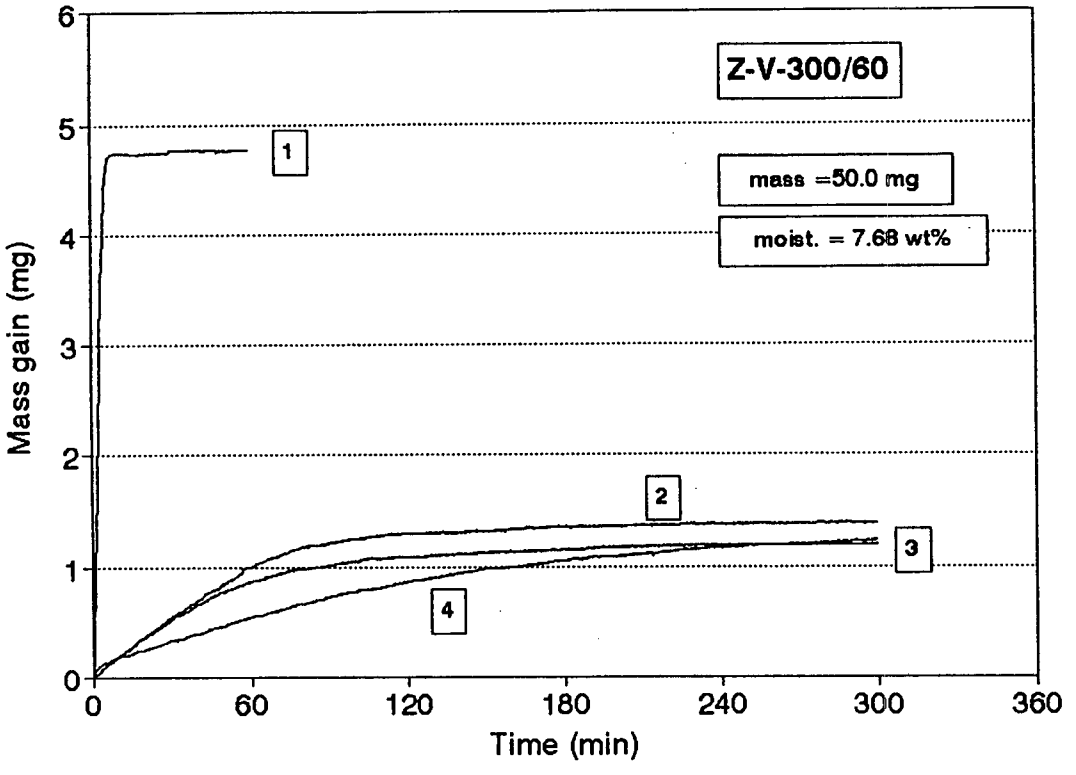

FIGURE A-IX.4: Adsorption profiles of sample Z-V-300/60

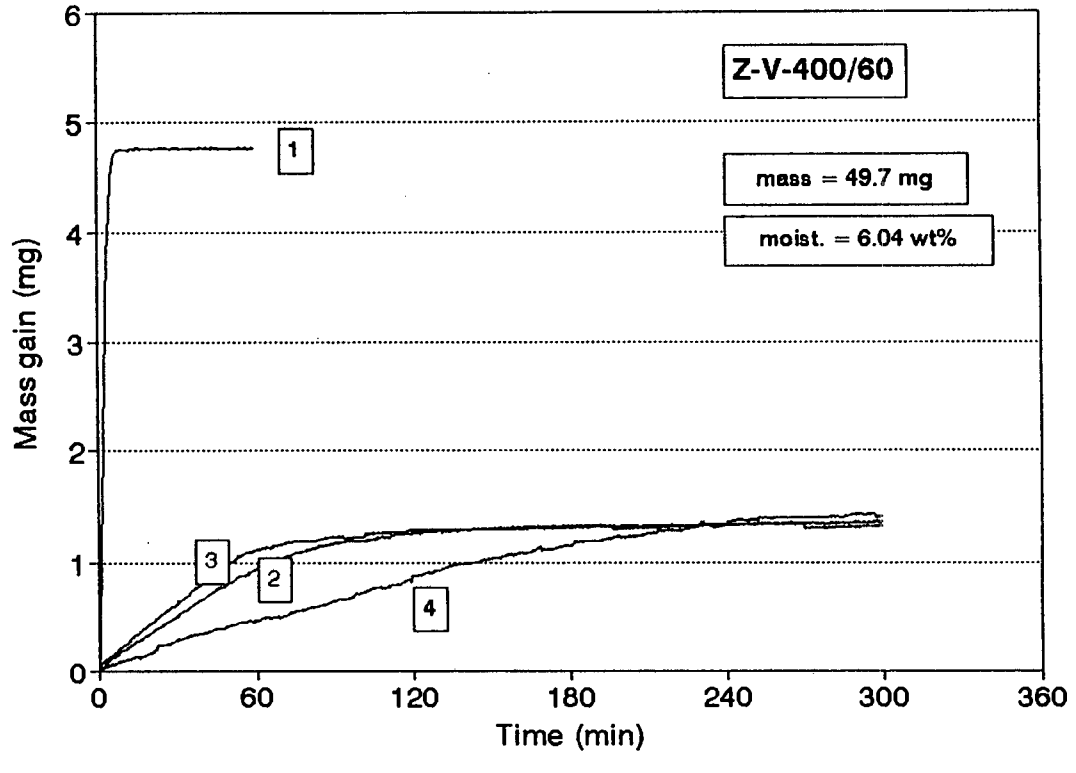

FIGURE A-IX.5: Adsorption profiles of sample Z-V-400/60

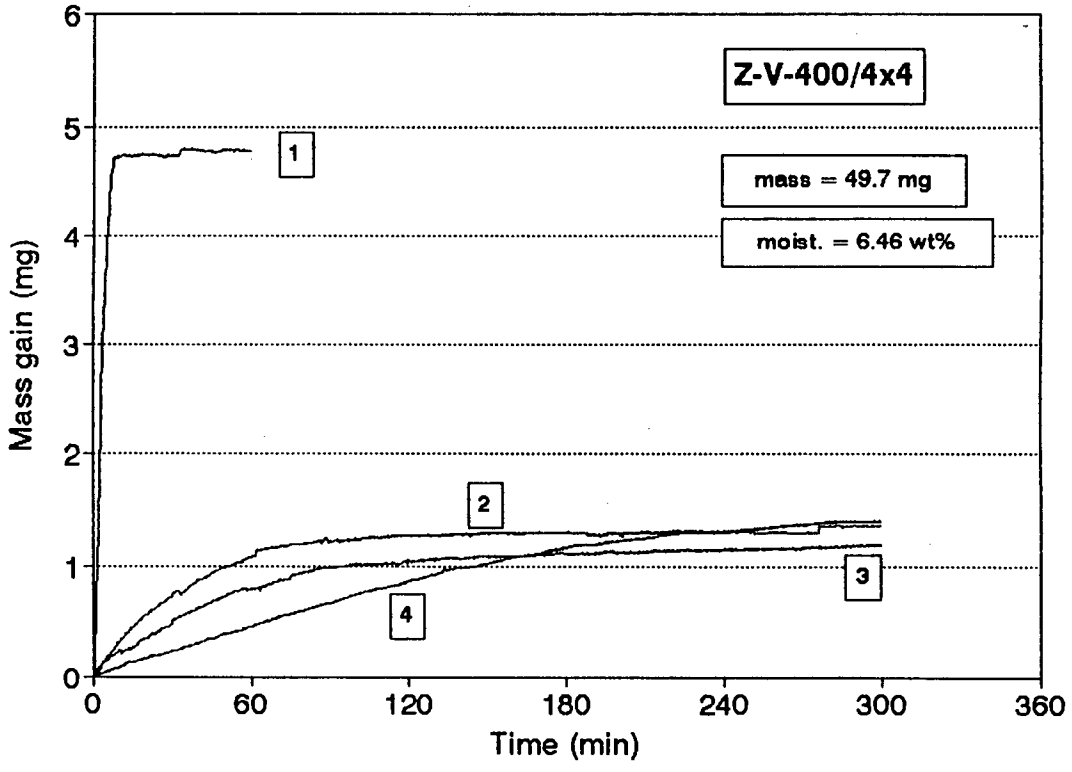

FIGURE A-IX.6: Adsorption profiles of sample Z-V-400/4x4

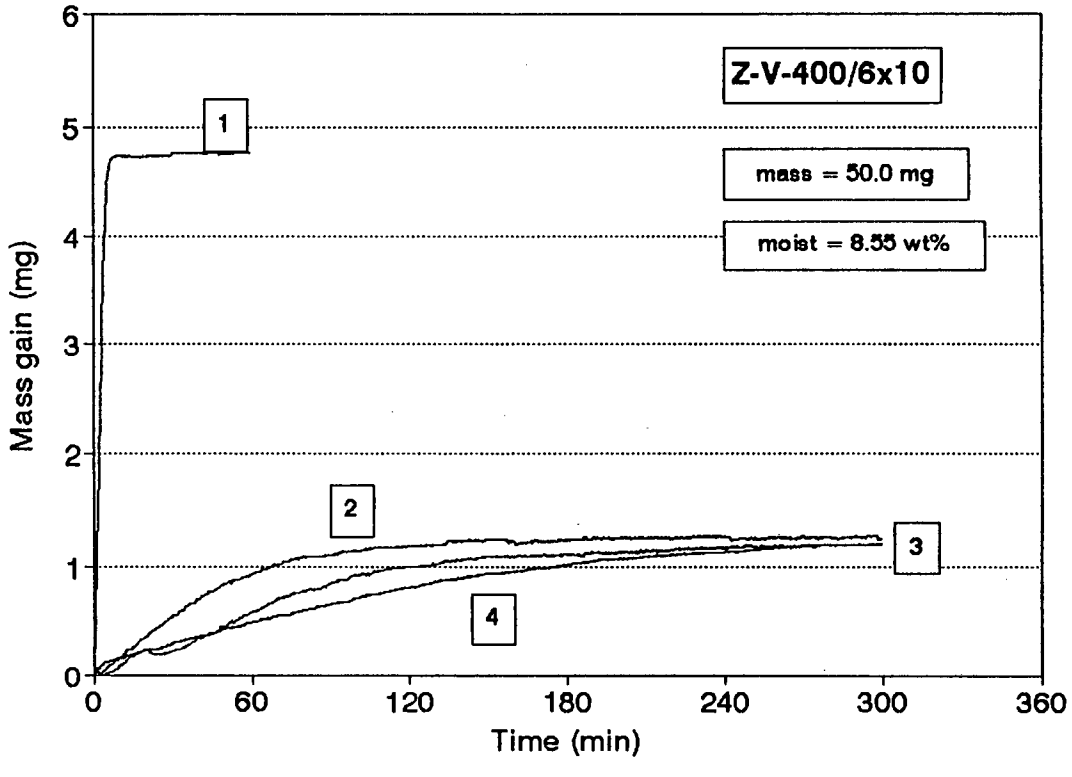

FIGURE A-IX.7: Adsorption profiles of sample Z-V-400/6x10

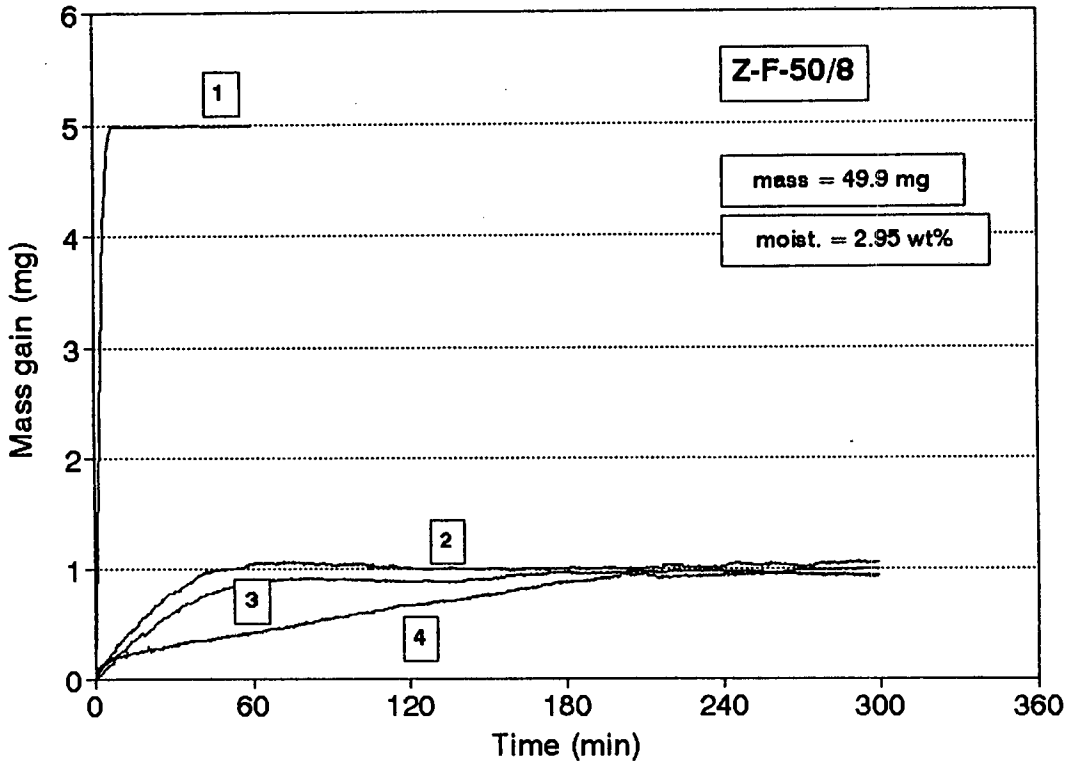

FIGURE A-IX.8: Adsorption profiles of sample Z-F-50/8

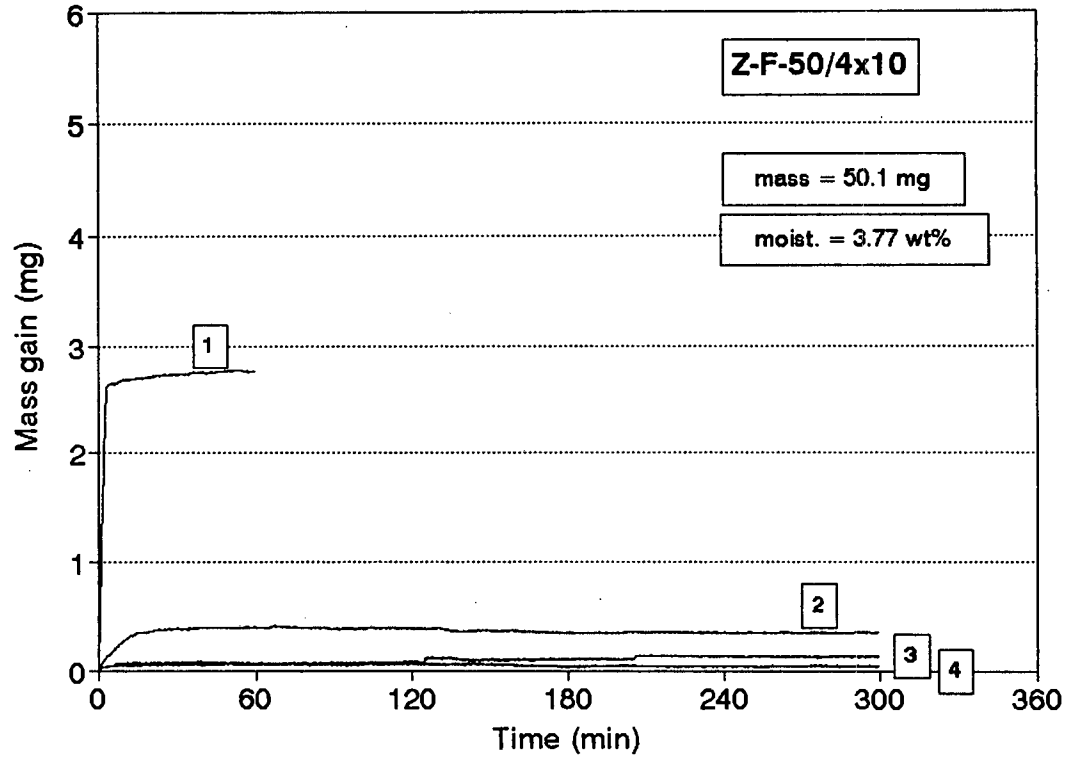

FIGURE A-IX.9: Adsorption profiles of sample Z-F-50/4x10

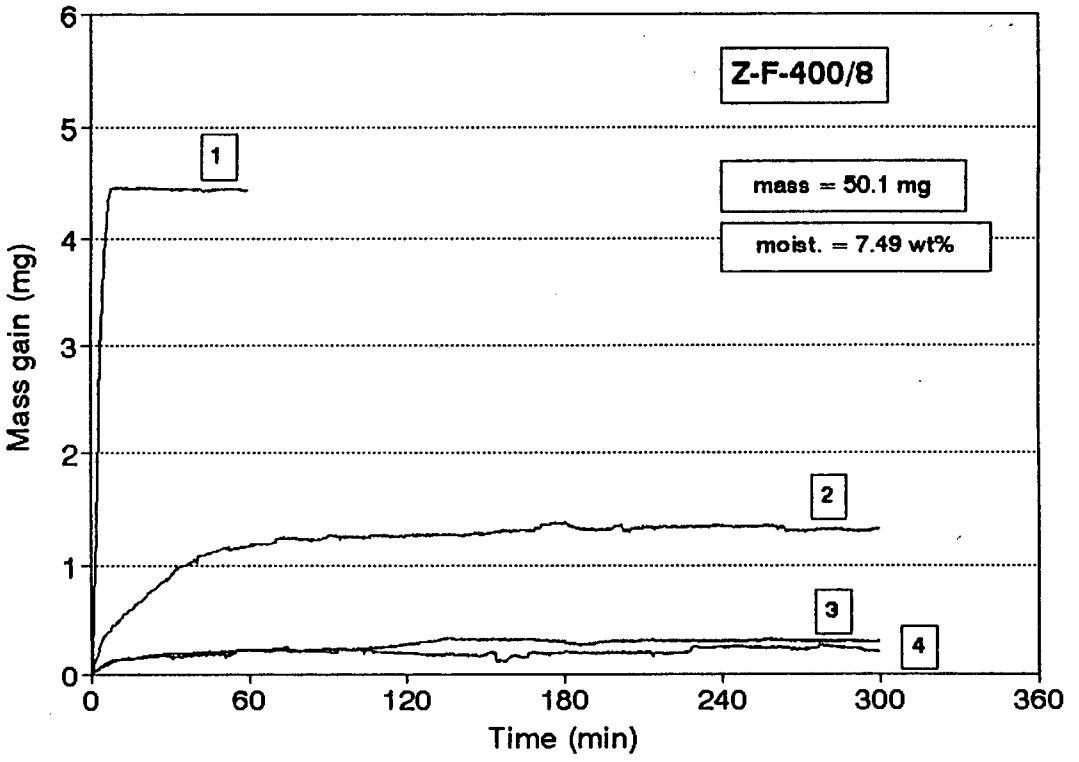

FIGURE A-IX.10: Adsorption profiles of sample Z-F-400/8

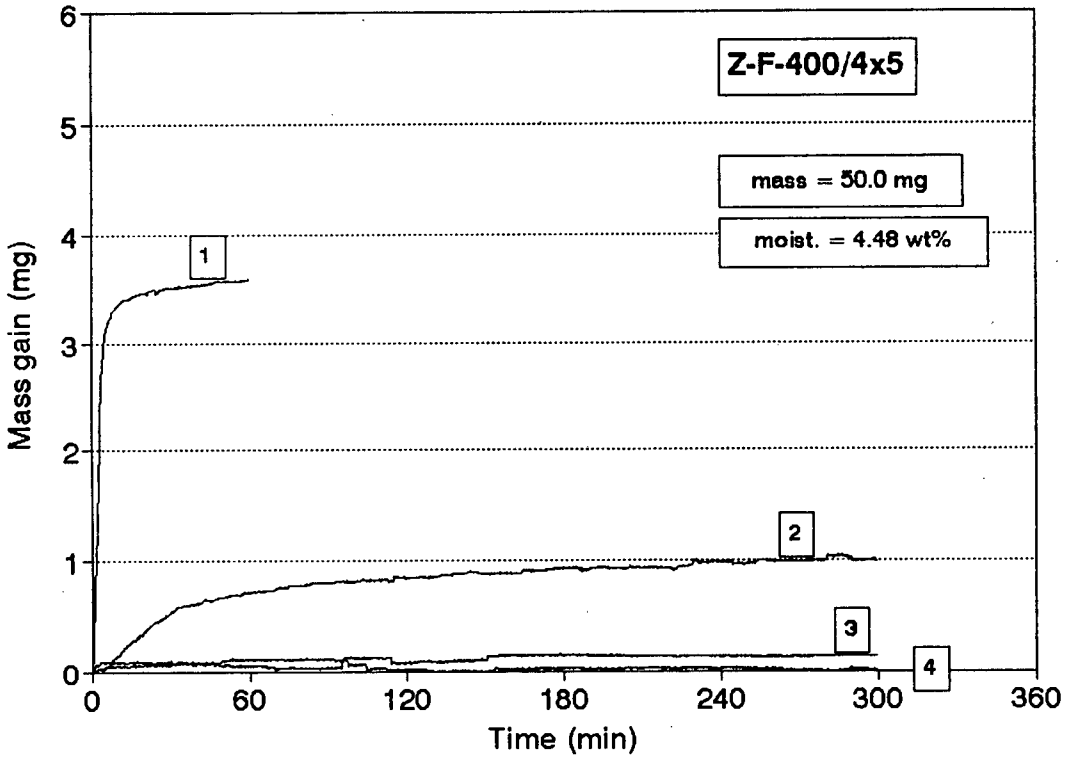

FIGURE A-IX.11: Adsorption profiles of sample Z-F-400/4x5

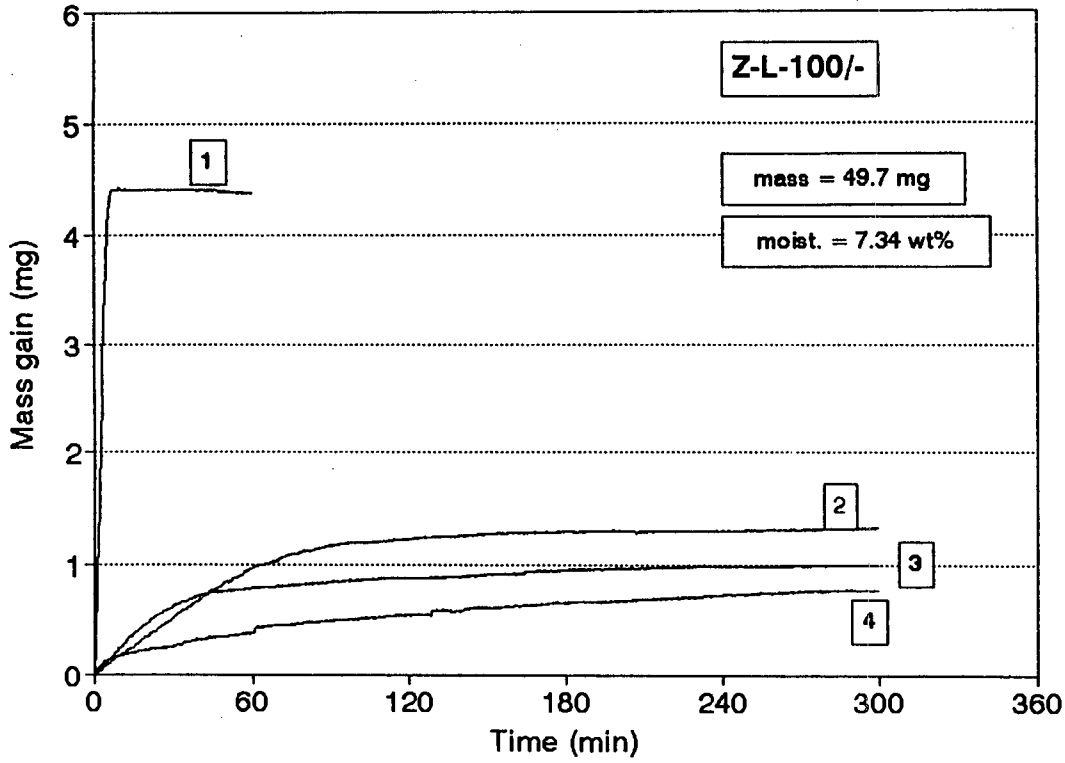

FIGURE A-IX.12: Adsorption profiles of sample Z-L-100/-

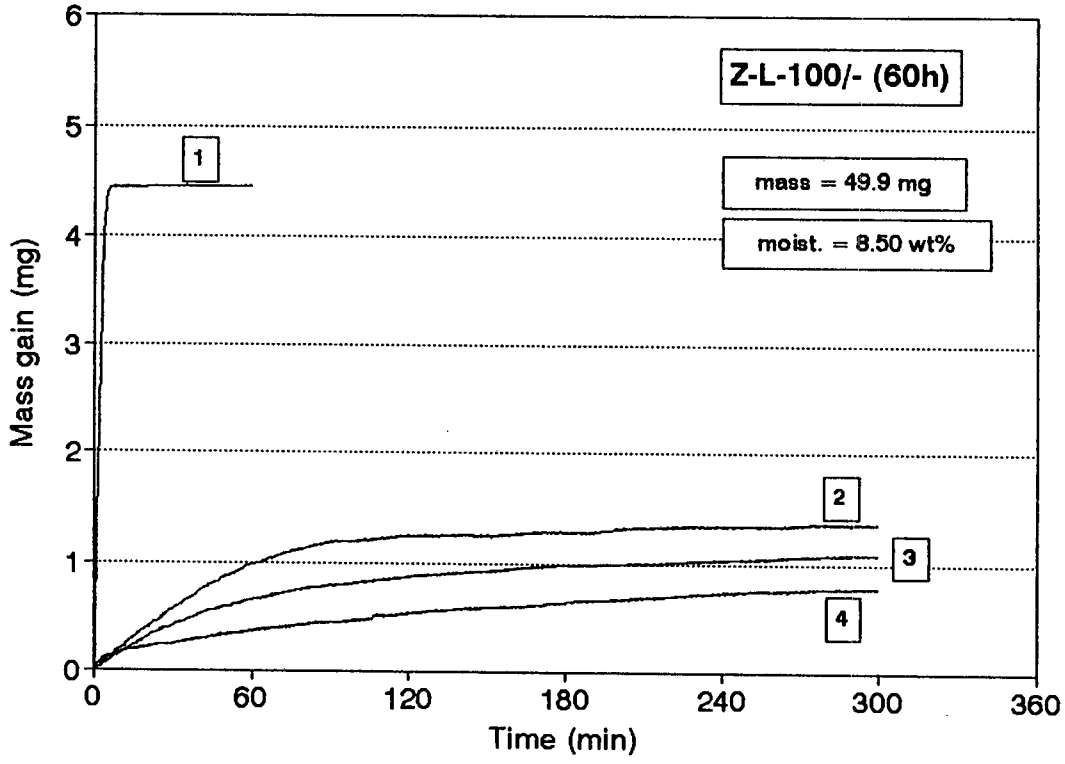

FIGURE A-IX.13: Adsorption profiles of sample Z-L-100/-(60h)

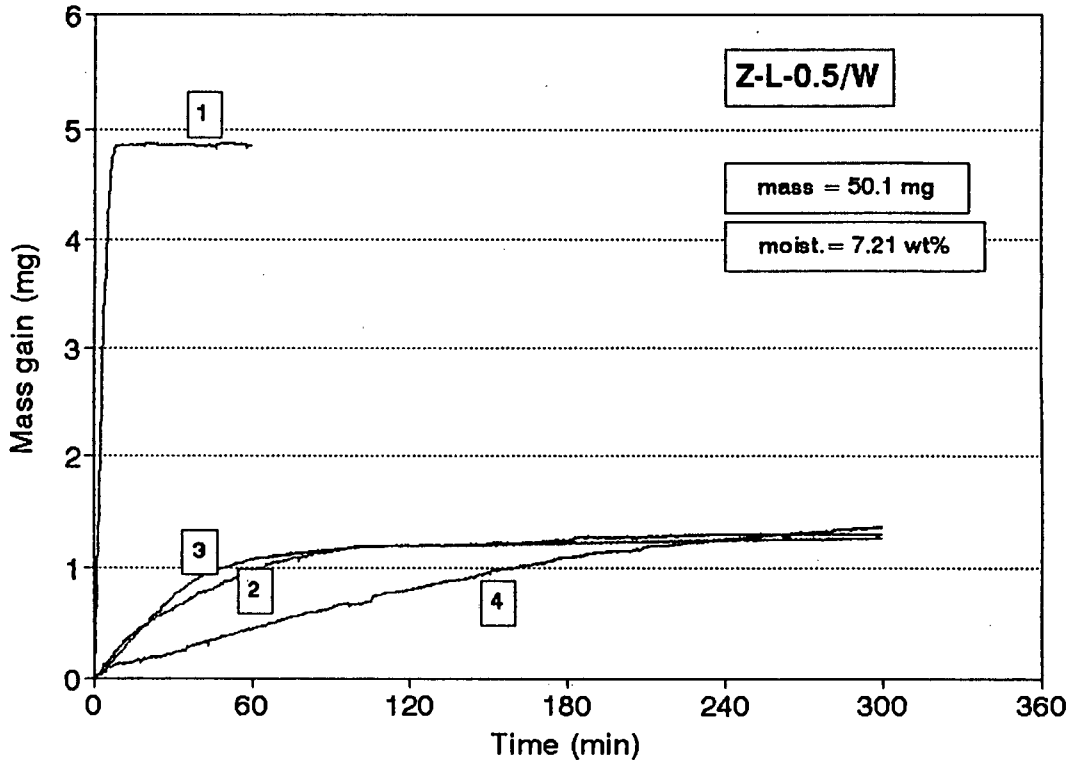

FIGURE A-IX.14: Adsorption profiles of sample Z-L-0.5/W

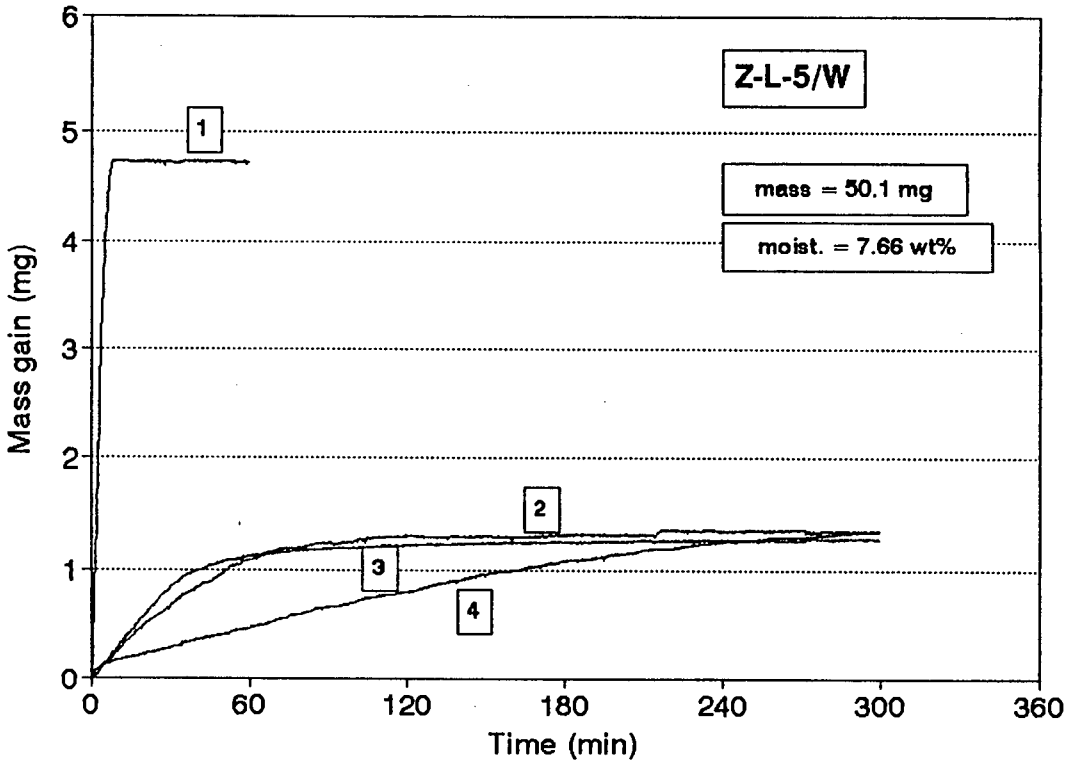

FIGURE A-IX.15: Adsorption profiles of sample Z-L-5/W

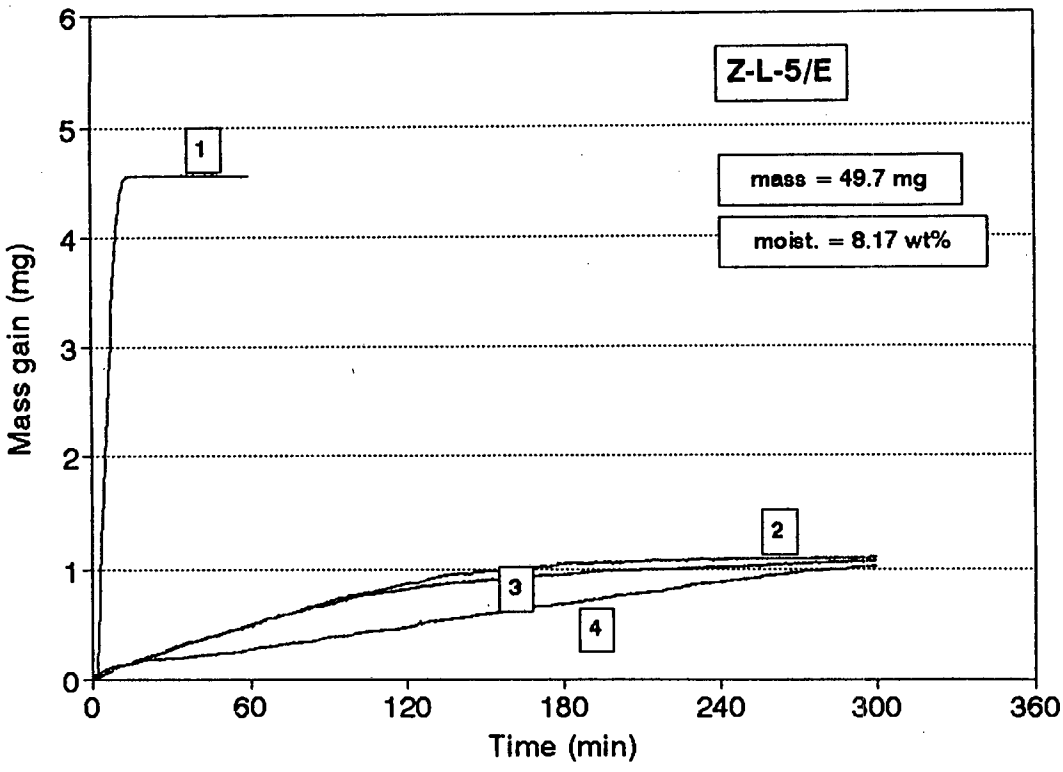

FIGURE A-IX.16: Adsorption profiles of sample Z-L-5/E

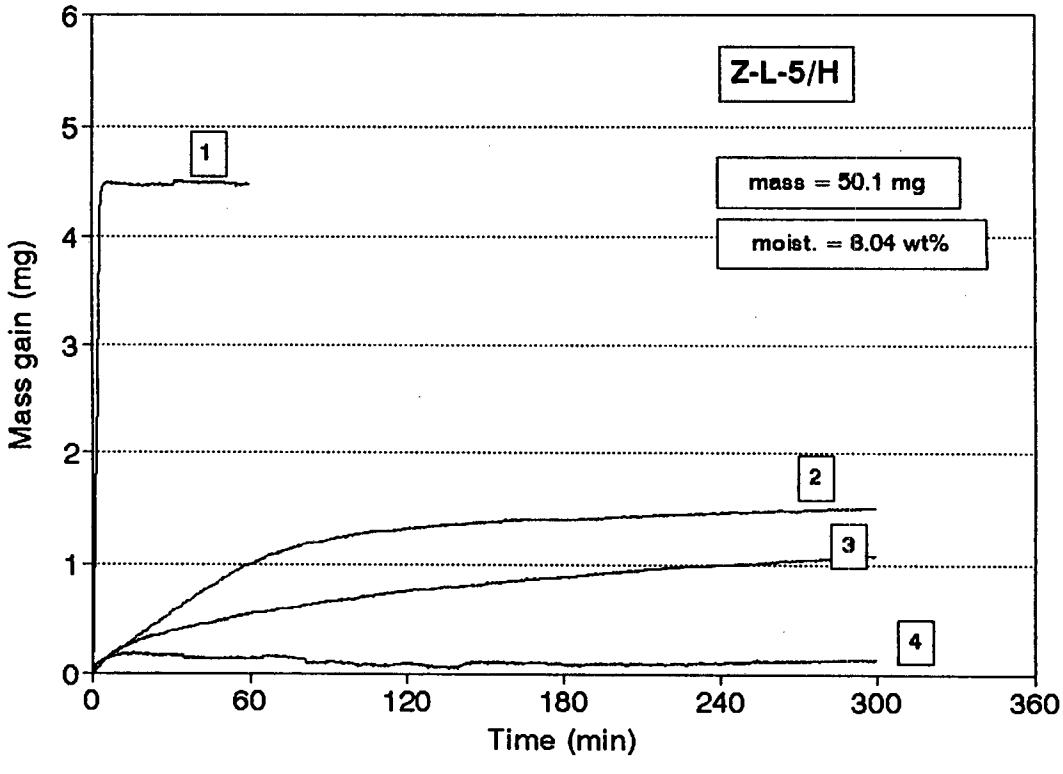

FIGURE A-IX.17: Adsorption profiles of sample Z-L-5/H

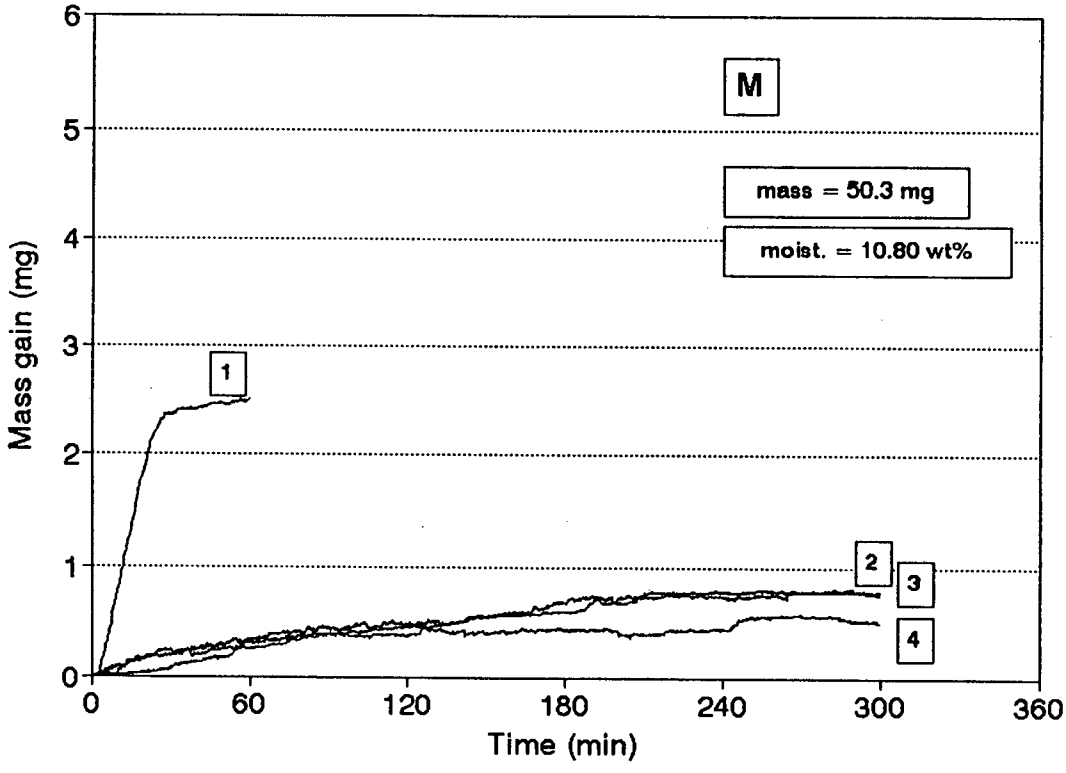

FIGURE A-IX.18: Adsorption profiles of sample M

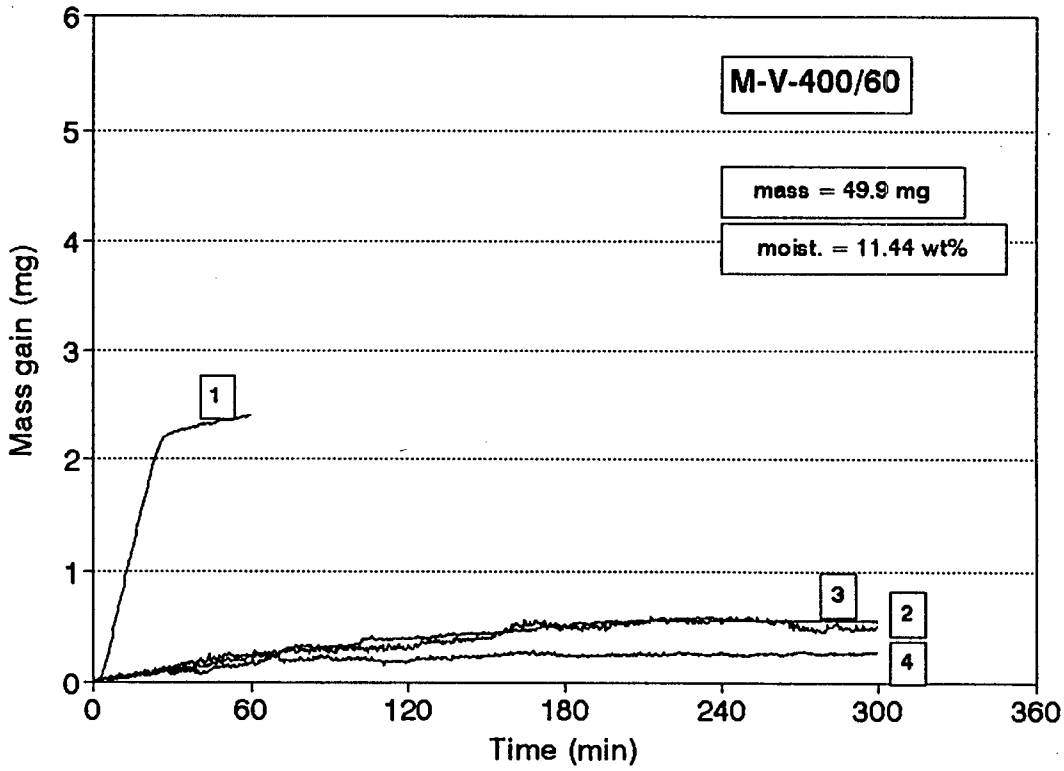

FIGURE A-IX.19: Adsorption profiles of sample M-V-400/60

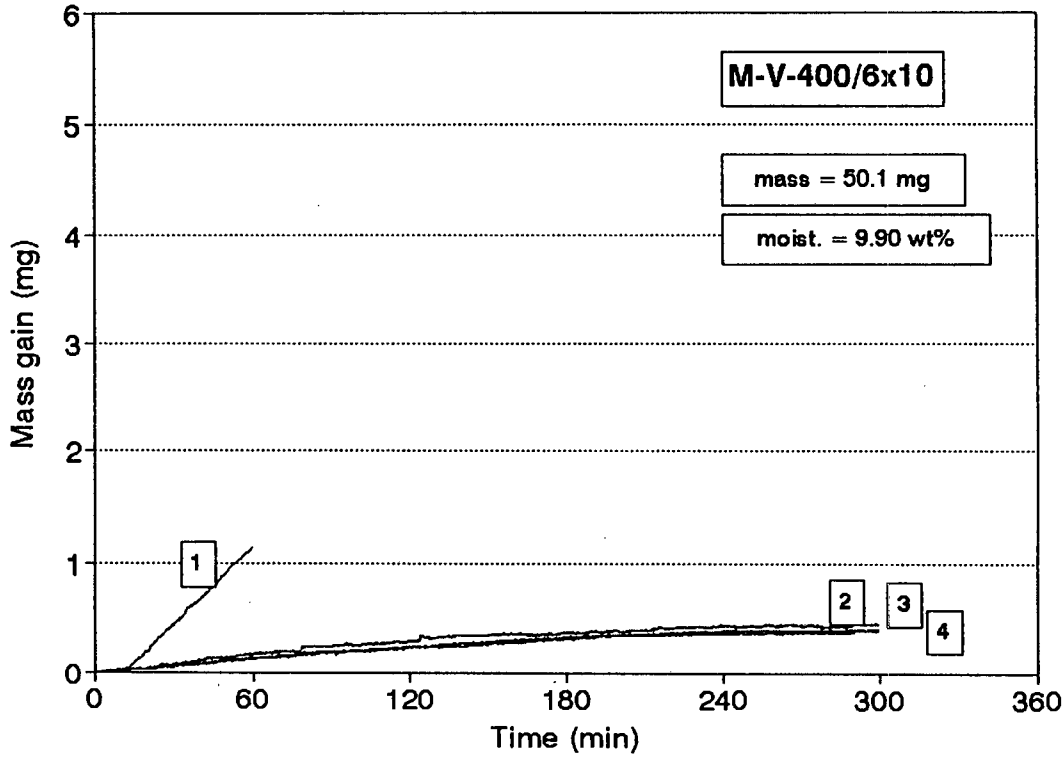

FIGURE A-IX.20: Adsorption profiles of sample M-V-400/6x10

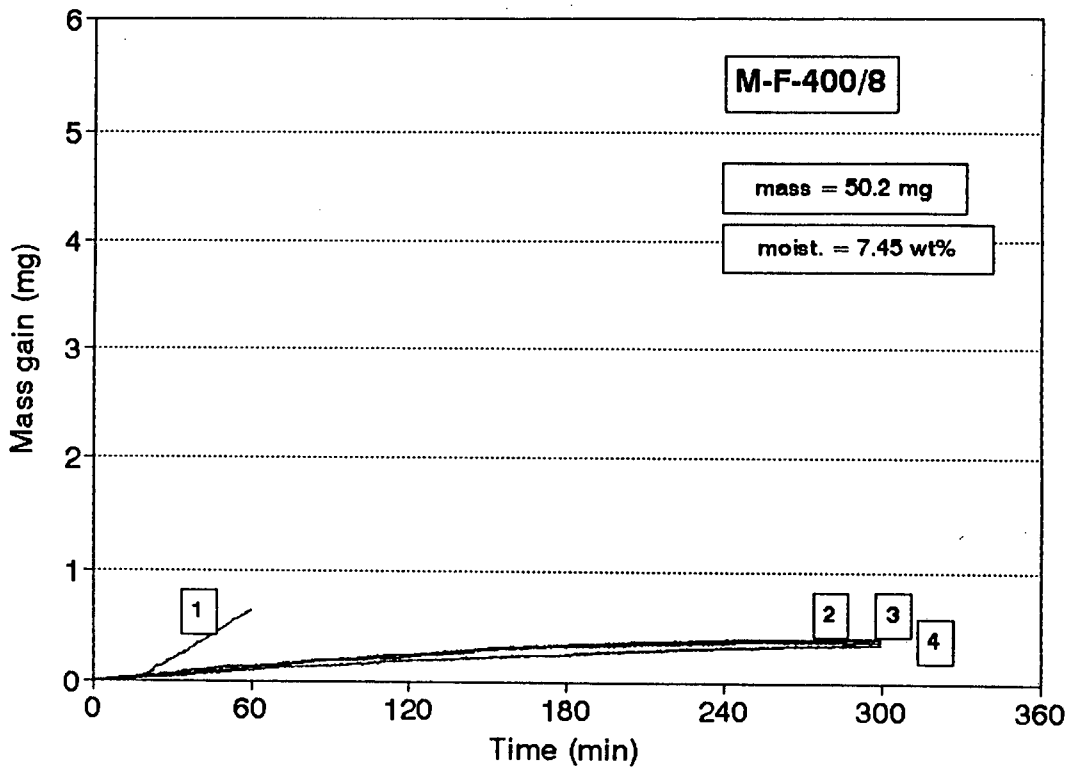

FIGURE A-IX.21: Adsorption profiles of sample M-F-400/8

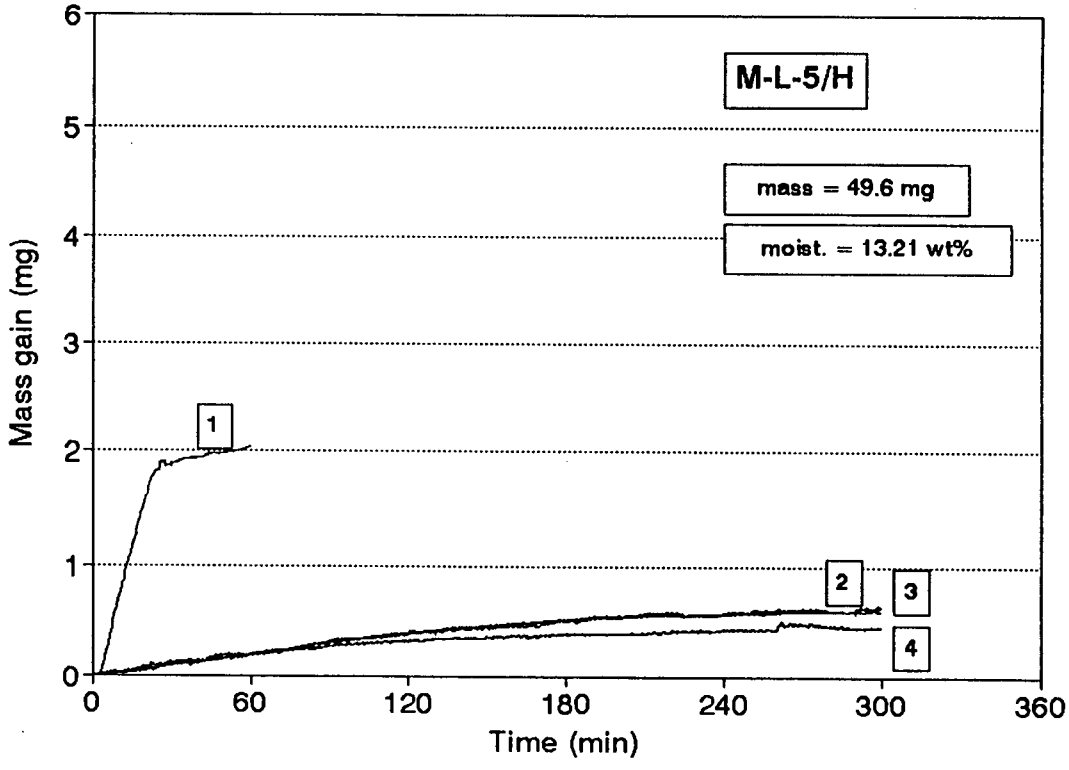

FIGURE A-IX.22: Adsorption profiles of sample M-L-5/H

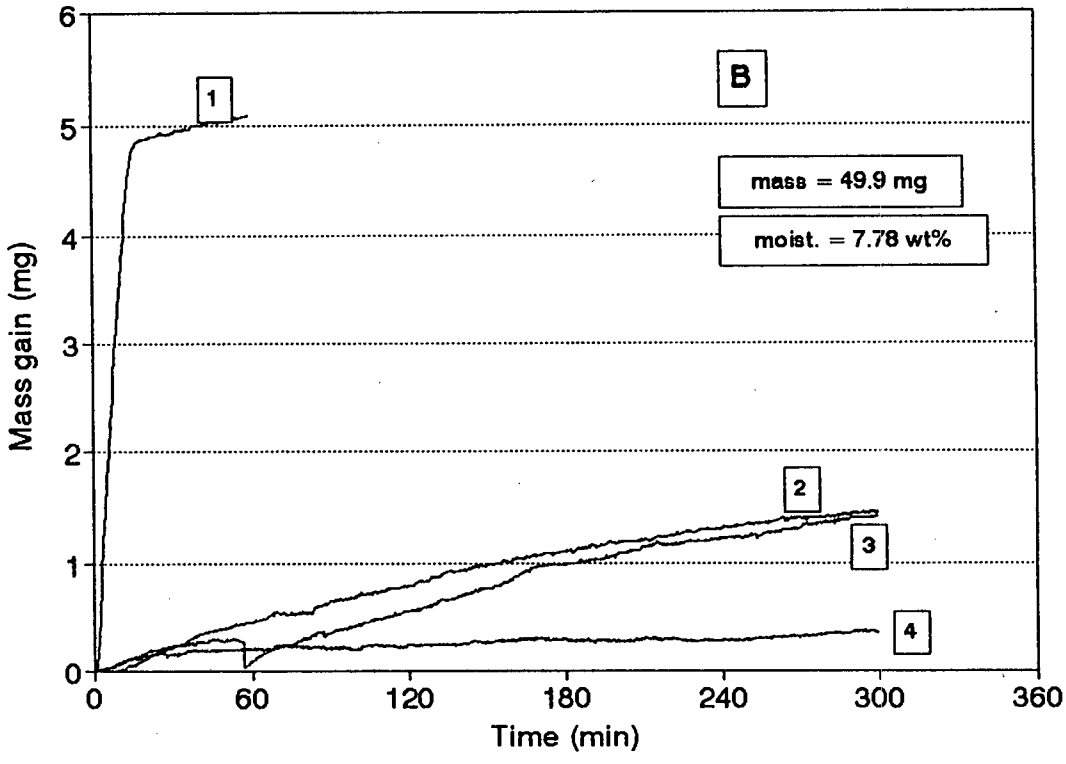

FIGURE A-IX.23: Adsorption profiles of sample B

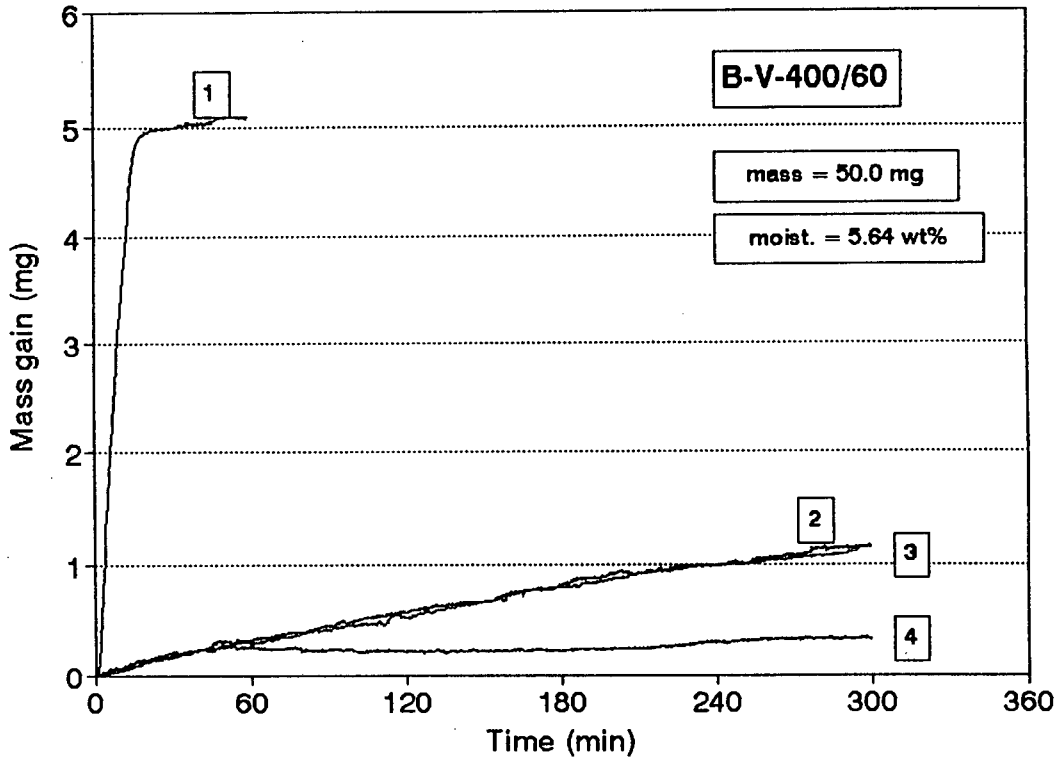

FIGURE A-IX.24: Adsorption profiles of sample B-V-400/60

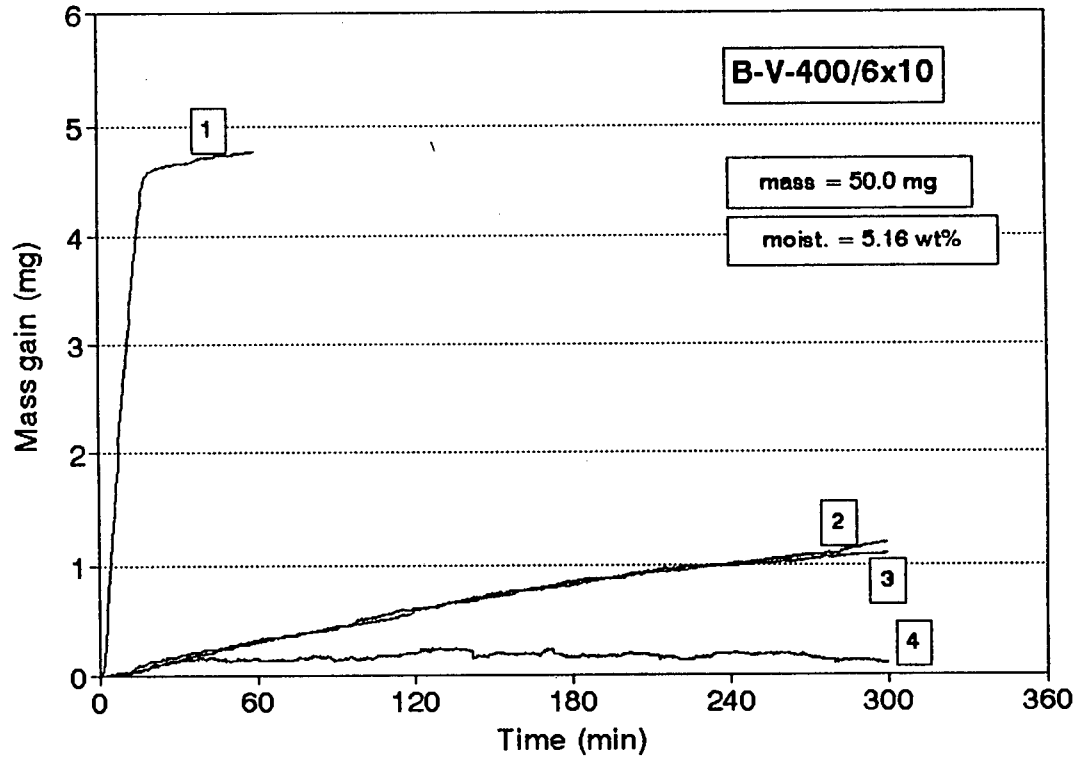

FIGURE A-IX.25: Adsorption profiles of sample B-V-400/6x10

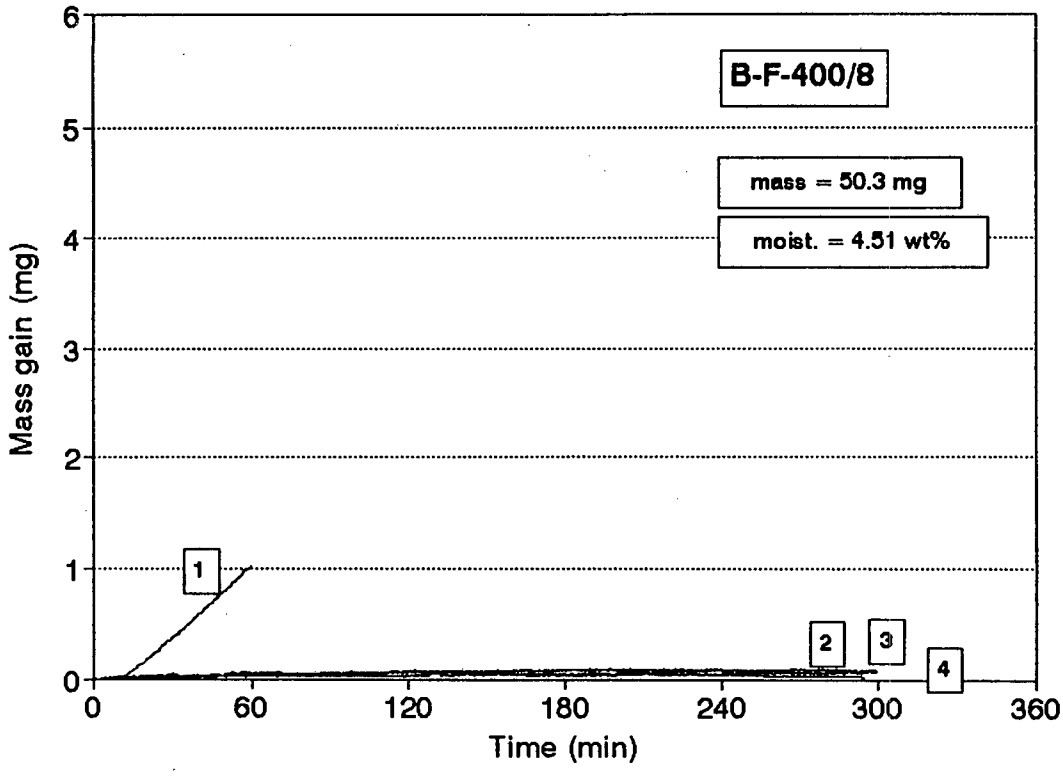

FIGURE A-IX.26: Adsorption profiles of sample B-F-400/8

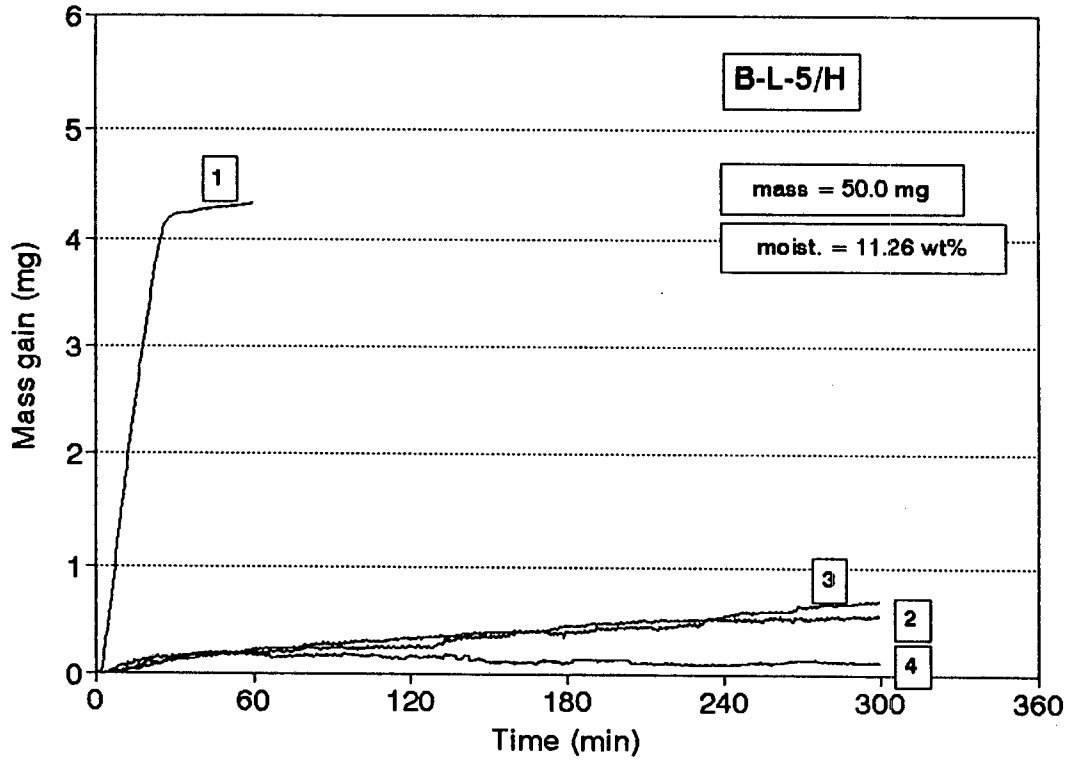

FIGURE A-IX.27: Adsorption profiles of sample B-L-5/H

APPENDIX X: 1,3,5-TRIISOPROPYL BENZENE RUN DATA

The conversions and mass balances were calculated using the following relationships (see Section 3.4.2.2):

where

$Rc_t = [A_{tipb} / A_{is}]_t$ (t = time)
$Rc_{bp} = [A_{tipb} / A_{is}]_{bp}$ (bp = by-pass)

$Rm_t = [(A_{tot} - A_{is}) / A_{tot}]_t$ (t = time)
$Rm_{bp} = [(A_{tot} - A_{is}) / A_{tot}]_{bp}$ (bp = by-pass)

and

$$\text{Conversion (\%)} = 100 \times [1 - (Rc_t / Rc_{bp})]$$
$$\text{Mass Balance (\%)} = 100 \times [Rm_t / Rm_{bp}]$$

TABLE A-X.1: TiPB reaction data for sample Z (crushed)

	Z (crushed)							
Temp.	Reactor	270		Pressure	(mbar)	505		
(degC)	c-Hexane	14		Flows	c-Hexane	8		
	TiPB	58.6		(ml/min)	TiPB	91		
By-Pass	c-Hexane	1,3,5-TiPB	Total - cH	Total Area		c-Hexane (%)	1,3,5-TiPB (%)	TiPB/c-H
1	1060045	173197	324226	1384271		85.96	14.04	0.1634
2	346857	49896	85881	432738		87.42	12.58	0.1439
3	561870	88347	133802	695672		86.41	13.59	0.1572
4	799084	130881	147989	947073		85.93	14.07	0.1638
5	869020	128032	145099	1014119		87.16	12.84	0.1473
Total	1668104	258913	293088	1961192		173.09	26.91	0.3111
Average	834052	129457	146544	980596		86.54	13.46	0.1556
	10 min.	20 min.	30 min.	40 min.	50 min.	60 min.		
c-Hexane	761062	885849	297506	498328	917836	356339		
1,3,5-TiPB	33175	42288	13710	25496	45198	18562		
5.7	27198	32861	11211	10862	14870	11789		
12.6	9120	11230	3599	3118	196	2032		
20.5	6682	2226	120	15576	30256	11291		
25.2	44192	55417	17511	107	312	71		
other	10178	20888	6457	37173	75880	19478		
Total Area	891607	1050759	350114	590660	1084548	419562		
Area - cH	130545	164910	52608	92332	166712	63223		
TiPB/c-H	0.0436	0.0477	0.0461	0.0512	0.0492	0.0521		
% Conv.	72.0	69.3	70.4	67.1	68.3	66.5		
Mass Bal.	98.0	105.0	100.5	104.6	102.9	100.8	Ri / Rbp	R=Ahc/At

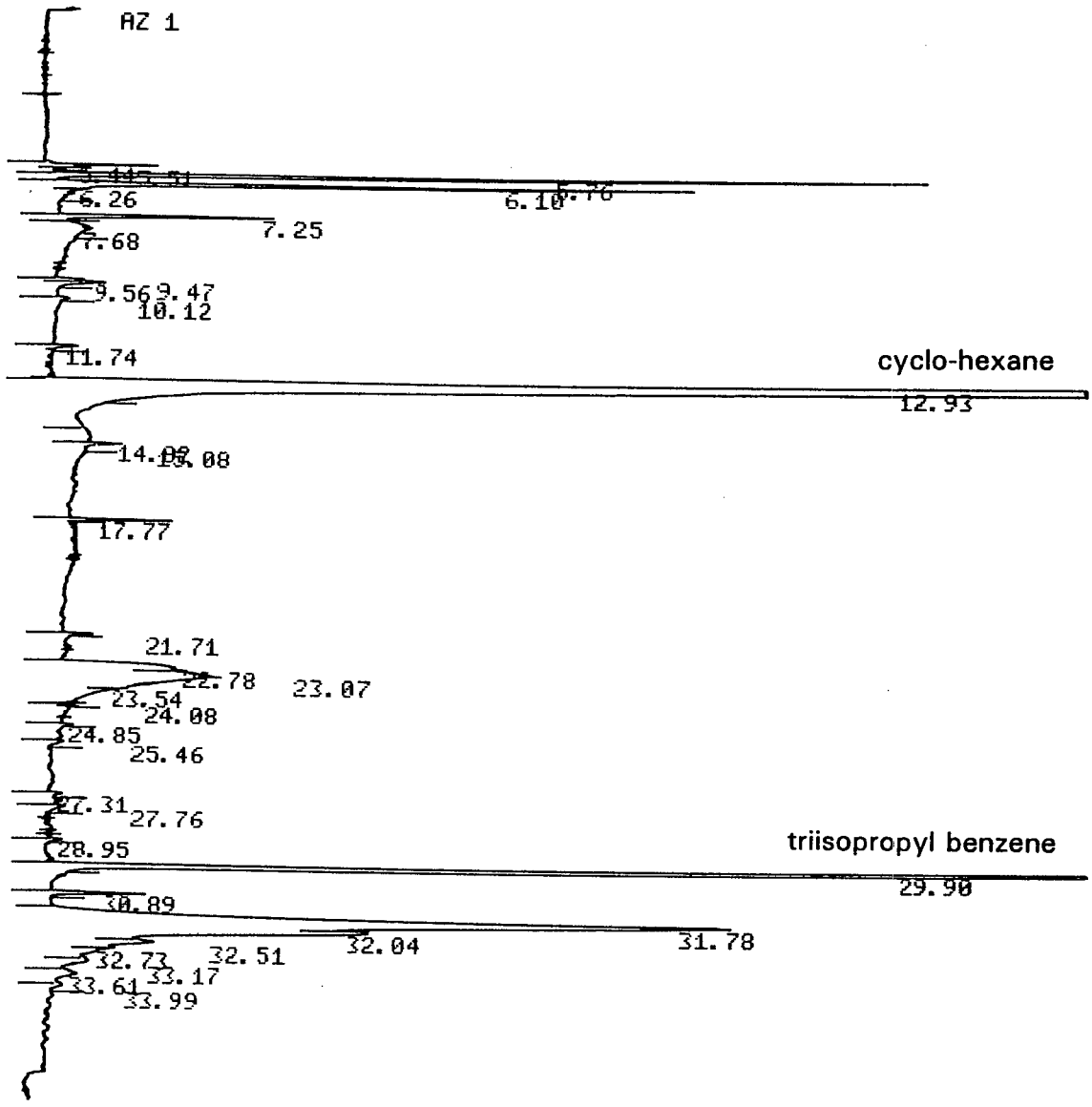

FIGURE A-X.1: Typical spectrum of the conversion of 1,3,5-triisopropyl benzene

TABLE A-X.2: TiPB reaction data for sample Z-V-400/6x10

	Z-V-400/6x10							
Temp.	Reactor	271		Pressure	(mbar)	501		
(degC)	c-Hexane	13		Flows	c-Hexane	8		
	TiPB	59.3		(ml/min)	TiPB	92		
By-Pass	c-Hexane	1,3,5-TiPB	Total - cH	Total Area		c-Hexane (%)	1,3,5-TiPB (%)	TiPB/c-H
1	0	0	0	0		0.00	0.00	0.0000
2	217008	81346	98986	315994		72.74	27.26	0.3749
3	375040	108140	116663	491703		77.62	22.38	0.2883
4	386685	109707	117157	503842		77.90	22.10	0.2837
5	338726	93659	100469	439195		78.34	21.66	0.2765
Total	1317459	392852	433275	1750734		306.59	93.41	1.2234
Average	**329364.8**	**98213**	**108318.8**	**437683.5**		**76.65**	**23.35**	**0.3059**
	10 min.	20 min.	30 min.	40 min.	50 min.	60 min.		
c-Hexane	359775	331964	373892	334987	321552	366281		
1,3,5-TiPB	92711	87818	104822	93833	90710	101161		
5.7	3693	3788	3377	3548	5133	4500		
12.6	6357	5723	6527	5885	5773	6041		
20.5	2695	2479	3123	2780	2769	2838		
25.2	2133	1501	1680	1975	1417	1379		
other	6409	7288	9336	7844	1403	6786		
Total Area	473773	440561	502757	450852	428757	488986		
Area - cH	113998	108597	128865	115865	107205	122705		
TiPB/c-H	0.2577	0.2645	0.2804	0.2801	0.2821	0.2762		
% Conv.	**15.7**	**13.5**	**8.3**	**8.4**	**7.8**	**9.7**		
Mass Bal.	**97.2**	**99.6**	**103.6**	**103.8**	**101.0**	**101.4**	Ri / Rbp	R=Ahc/At

TABLE A-X.3: TiPB reaction data for sample Z-V-400/6x10 (crushed)

	Z-V-400/6x10 (crushed)							
Temp.	Reactor	270		Pressure	(mbar)	497		
(degC)	c-Hexane	14		Flows	c-Hexane	8		
	TiPB	59.1		(ml/min)	TiPB	92		
By-Pass	c-Hexane	1,3,5-TiPB	Total -cH	Total Area		c-Hexane (%)	1,3,5-TiPB (%)	TiPB/c-H
1	0	0	0	0		0.00	0.00	0.0000
2	256193	81237	92149	348342		75.92	24.08	0.3171
3	323107	99974	105537	428644		76.37	23.63	0.3094
4	495318	151489	162804	658122		76.58	23.42	0.3058
5	76125	22067	30907	107032		77.53	22.47	0.2899
Total	1150743	354767	391397	1542140		306.40	93.60	1.2222
Average	**287685.8**	**88692**	**97849.25**	**385535**		**76.60**	**23.40**	**0.3056**
	10 min.	20 min.	30 min.	40 min.	50 min.	60 min.		
c-Hexane	485915	445884	472104	516319	546615	517791		
1,3,5-TiPB	93801	89327	92778	103923	106200	100714		
5.7	16875	16602	16532	16245	17755	18335		
12.6	6467	5103	6222	5427	5751	5305		
20.5	27142	26732	27734	31067	32223	30005		
25.2	3075	2946	3048	3464	3210	3523		
other	9685	7273	5386	10468	21979	16282		
Total Area	642960	593867	623804	686913	733733	691955		
Area - cH	157045	147983	151700	170594	187118	174164		
TiPB/c-H	0.1930	0.2003	0.1965	0.2013	0.1943	0.1945		
% Conv.	**36.8**	**34.4**	**35.7**	**34.1**	**36.4**	**36.3**		
Mass Bal.	**96.2**	**98.2**	**95.8**	**97.9**	**100.5**	**99.2**	Ri / Rbp	R=Ahc/At

TABLE A-X.4: TiPB reaction data for sample M

	M							
Temp.	Reactor	200		Pressure	(mbar)	493		
(degC)	c-Hexane	15		Flows	c-Hexane	8		
	TiPB	58.6		(ml/min)	TiPB	92		
By-Pass	c-Hexane	1,3,5-TiPB	Total - cH	Total Area		c-Hexane (%)	1,3,5-TiPB (%)	TiPB/c-H
1	0	0	0	0		0.00	0.00	0.0000
2	0	0	0	0		0.00	0.00	0.0000
3	1687438	206441	226130	1913568		89.10	10.90	0.1223
4	1717512	208212	242745	1960257		89.19	10.81	0.1212
5	1205060	147671	158761	1363821		89.08	10.92	0.1225
Total	4610010	562324	627636	5237646		267.37	32.63	0.3661
Average	**1536670**	**187441**	**209212**	**1745882**		**89.12**	**10.88**	**0.1220**
	20min.	10 min.	10 min. R	20 min. R	30 min. R	30 min.		
c-Hexane	1484811	1614154	1507756	1257608	1090078	1375913		
1,3,5-TiPB	28888	40062	56296	53475	50428	65982		
5.7	27751	31065	25739	21597	18587	24249		
12.6	9492	10233	1638	804	130	913		
20.5	11505	15211	21566	21977	12913	22685		
25.2	589	1899	3979	5580	5601	7802		
other	21955	46262	49699	35411	36030	38138		
Total Area	1584991	1758886	1666673	1396452	1213767	1535682		
Area - cH	100180	144732	158917	138844	123689	159769		
TiPB/c-H	0.0195	0.0248	0.0373	0.0425	0.0463	0.0480		
% Conv.	**84.1**	**79.7**	**69.4**	**65.2**	**62.1**	**60.7**		
Mass Bal.	**52.7**	**68.7**	**79.6**	**83.0**	**85.0**	**86.8**	Ri / Rbp	R=Ahc/At

TABLE A-X.5: TiPB reaction data for sample M (crushed)

	M (crushed)							
Temp.	Reactor	200		Pressure	(mbar)	500		
(degC)	c-Hexane	14		Flows	c-Hexane	8		
	TiPB	57.9		(ml/min)	TiPB	91		
By-Pass	c-Hexane	1,3,5-TiPB	Total - cH	Total Area		c-Hexane (%)	1,3,5-TiPB (%)	TiPB/c-H
1	0	0	0	0		0.00	0.00	0.0000
2	0	0	0	0		0.00	0.00	0.0000
3	1906270	209404	224939	2131209		90.10	9.90	0.1099
4	1708753	187254	204922	1913675		90.12	9.88	0.1096
5	1670362	183701	194751	1865113		90.09	9.91	0.1100
Total	5285385	580359	624612	5909997		270.32	29.68	0.3294
Average	**1761795**	**193453**	**208204**	**1969999**		**90.11**	**9.89**	**0.1098**
	10 min	20 min	30 min.	40 min. R	50 min. R	60 min. R		
c-Hexane	895402	1547682	1507213	1339046	1538797	1606726		
1,3,5-TiPB	314	13087	21355	25033	32716	35397		
5.7	4789	39630	41335	38318	43899	44101		
12.6	476	7104	5119	4567	4712	4174		
20.5	0	28024	29767	30654	37391	36528		
25.2	173	6190	7066	7554	10217	9019		
other	15716	22110	21531	26472	24260	26337		
Total Area	916870	1663827	1633386	1471644	1691992	1762282		
Area - cH	21468	116145	126173	132598	153195	155556		
TiPB/c-H	0.0004	0.0085	0.0142	0.0187	0.0213	0.0220		
% Conv.	**99.7**	**92.3**	**87.1**	**83.0**	**80.6**	**79.9**		
Mass Bal.	**22.2**	**66.0**	**73.1**	**85.3**	**85.7**	**83.5**	Ri / Rbp	R=Ahc/At

TABLE A-X.6: TiPB reaction data for sample M-V-400/6x10

	M-V-400/6x10							
Temp.	Reactor	199		Pressure	(mbar)	504		
(degC)	c-Hexane	13		Flows	c-Hexane	8		
	TiPB	58.9		(ml/min)	TiPB	92		
By-Pass	c-Hexane	1,3,5-TiPB	Total - cH	Total Area		c-Hexane (%)	1,3,5-TiPB (%)	TiPB/c-H
1	1894208	206616	228288	2122496		90.17	9.83	0.1091
2	2009081	219428	239789	2248870		90.15	9.85	0.1092
3	1983874	223509	243620	2227494		89.87	10.13	0.1127
4	1947645	219415	246223	2193868		89.87	10.13	0.1127
5	2118301	228807	250220	2368521		90.25	9.75	0.1080
Total	9953109	1097775	1208140	11161249		450.32	49.68	0.5516
Average	**1990622**	**219555**	**241628**	**2232250**		**90.06**	**9.94**	**0.1103**
	10 min.R	20 min.	30 min.	40 min.	50 min.	60 min.R		
c-Hexane	2404411	1878482	1947638	1773107	1818761	2303501		
1,3,5-TiPB	219656	173052	184465	169455	173192	220681		
5.7	16076	12171	11888	11140	10395	13331		
12.6	2148	1138	896	746	904	1191		
20.5	6278	5304	5591	4304	4099	5851		
25.2	603	517	642	209	385	568		
other	22981	39621	29287	30087	32091	25434		
Total Area	2672153	2110285	2180407	1989048	2039827	2570557		
Area - cH	267742	231803	232769	215941	221066	267056		
TiPB/c-H	0.0914	0.0921	0.0947	0.0956	0.0952	0.0958		
% Conv.	**17.2**	**16.5**	**14.2**	**13.4**	**13.7**	**13.2**		
Mass Bal.	**92.6**	**101.5**	**98.6**	**100.3**	**100.1**	**96.0**	Ri / Rbp	R=Ahc/At

TABLE A-X.7: TiPB reaction data for sample M-V-400/6x10 (crushed)

	M-V-400/6x10 (crushed)							
Temp.	Reactor	200		Pressure	(mbar)	509		
(degC)	c-Hexane	14		Flows	c-Hexane	8		
	TiPB	59.2		(ml/min)	TiPB	92		
By-Pass	c-Hexane	1,3,5-TiPB	Total - cH	Total Area		c-Hexane (%)	1,3,5-TiPB (%)	TiPB/c-H
1	1931698	197118	213460	2145158		90.74	9.26	0.1020
2	1904449	196775	209628	2114077		90.64	9.36	0.1033
3	1873767	192409	207217	2080984		90.69	9.31	0.1027
4	1867709	182887	202943	2070652		91.08	8.92	0.0979
5	838445	82922	99975	938420		91.00	9.00	0.0989
Total	8416068	852111	933223	9349291		454.14	45.86	0.5049
Average	**1683214**	**170422**	**186644.6**	**1869858**		**90.83**	**9.17**	**0.1010**
	10 min.	20 min.	30 min.	40 min.	50 min.	60 min.		
c-Hexane	2229131	2054445	1250923	2009710	1092026	2400546		
1,3,5-TiPB	21644	39204	32748	58876	36181	82367		
5.7	29928	37445	18057	41083	15800	50545		
12.6	7317	7629	1892	4293	1054	4899		
20.5	10812	21760	11983	27256	13276	34384		
25.2	1695	4932	3596	7534	3908	10808		
other	31360	30248	24966	24025	27948	49124		
Total Area	2331887	2195663	1344165	2172777	1190193	2632673		
Area - cH	102756	141218	93242	163067	98167	232127		
TiPB/c-H	0.0097	0.0191	0.0262	0.0293	0.0331	0.0343		
% Conv.	**90.4**	**81.1**	**74.1**	**71.0**	**67.2**	**66.0**		
Mass Bal.	**44.1**	**64.4**	**69.5**	**75.2**	**82.6**	**88.3**	Ri / Rbp	R=Ahc/At

TABLE A-X.8: TiPB reaction data for sample B (crushed)

	B (crushed)							
Temp.	Reactor	161		Pressure	(mbar)	506		
(degC)	c-Hexane	15		Flows	c-Hexane	8		
	TiPB	59.3		(ml/min)	TiPB	91		
By-Pass	c-Hexane	1,3,5-TiPB	Total - cH	Total Area		c-Hexane (%)	1,3,5-TiPB (%)	TiPB/c-H
1	0	0	0	0		0.00	0.00	0.0000
2	1673687	197392	223082	1896769		89.45	10.55	0.1179
3	1540104	178630	197256	1737360		89.61	10.39	0.1160
4	1888825	217729	238755	2127580		89.66	10.34	0.1153
5	1609997	186027	213589	1823586		89.64	10.36	0.1155
Total	5038926	582386	649600	5688526		268.91	31.09	0.3468
Average	**1679642**	**194129**	**216533.3**	**1896175**		**89.64**	**10.36**	**0.1156**
	14 min.	20 min.	30 min.	40 min.	50 min.	60 min.		
c-Hexane	1666705	1613454	1501845	1560775	1146233	1240368		
1,3,5-TiPB	16062	33153	52451	80392	68927	77569		
5.7	4121	6512	9128	11555	9095	10533		
12.6	0	0	0	81	0	0		
20.5	0	273	1523	2758	3376	6933		
25.2	0	0	1896	3033	5936	9940		
other	31084	28544	28940	26418	26733	24771		
Total Area	1717972	1681936	1595783	1685012	1260300	1370114		
Area - cH	51267	68482	93938	124237	114067	129746		
TiPB/c-H	0.0096	0.0205	0.0349	0.0515	0.0601	0.0625		
% Conv.	**91.7**	**82.2**	**69.8**	**55.4**	**48.0**	**45.9**		
Mass Bal.	**26.1**	**35.7**	**51.5**	**64.6**	**79.3**	**82.9**	Ri / Rbp	R=Ahc/At

TABLE A-X.9: TiPB reaction data for sample B-V-400/6x10

	B-V-400/6x10							
Temp.	Reactor	160		Pressure	(mbar)	501		
(degC)	c-Hexane	14		Flows	c-Hexane	8		
	TiPB	57.9		(ml/min)	TiPB	92		
By-Pass	c-Hexane	1,3,5-TiPB	Total - cH	Total Area		c-Hexane (%)	1,3,5-TiPB (%)	TiPB/c-H
1	1633478	175844	205599	1839077		90.28	9.72	0.1077
2	1860138	200971	217544	2077682		90.25	9.75	0.1080
3	1661266	190718	204210	1865476		89.70	10.30	0.1148
4	1462359	164988	179942	1642301		89.86	10.14	0.1128
5	1736033	197378	215347	1951380		89.79	10.21	0.1137
Total	4859658	553084	599499	5459157		269.35	30.65	0.3413
Average	**1619886**	**184361**	**199833**	**1819719**		**89.78**	**10.22**	**0.1138**
	10 min.	20 min.	30 min.	40 min.	50 min.	60 min.		
c-Hexane	1979765	1702628	1366047	1630603	1521669	1257361		
1,3,5-TiPB	66172	82321	82130	108213	109062	99675		
5.7	7119	9390	8315	10065	9761	7805		
12.6	0	0	0	35	96	0		
20.5	0	0	0	2190	3337	2920		
25.2	0	342	749	2374	4423	5296		
other	26107	42423	17405	21688	24665	19443		
Total Area	2079163	1837104	1474646	1775168	1673013	1392500		
Area - cH	99398	134476	108599	144565	151344	135139		
TiPB/c-H	0.0334	0.0483	0.0601	0.0664	0.0717	0.0793		
% Conv.	**70.6**	**67.5**	**47.2**	**41.7**	**37.0**	**30.3**		
Mass Bal.	**43.6**	**66.7**	**67.1**	**74.2**	**82.4**	**88.4**	Ri / Rbp	R=Ahc/At

TABLE A-X.10: TiPB reaction data for sample B-V-400/6x10 (crushed)

	B-V-400/6x10 (crushed)							
Temp.	Reactor	160		Pressure	(mbar)	499		
(degC)	c-Hexane	15		Flows	c-Hexane	8		
	TiPB	58.7		(ml/min)	TiPB	92		
By-Pass	c-Hexane	1,3,5-TiPB	Total - cH	Total Area		c-Hexane (%)	1,3,5-TiPB (%)	TiPB/c-H
1	0	0	0	0		0.00	0.00	0.0000
2	1952150	175017	193997	2146147		91.77	8.23	0.0897
3	1858823	171417	195434	2054257		91.56	8.44	0.0922
4	1928275	178661	194110	2122385		91.52	8.48	0.0927
5	1568191	146528	159664	1727855		91.45	8.55	0.0934
Total	5355289	496606	549208	5904497		274.53	25.47	0.2783
Average	**1785096**	**165535**	**183069.3**	**1968166**		**91.51**	**8.49**	**0.0928**
	10 min.	20 min.	30 min.	40 min.	50 min.	60 min.		
c-Hexane	1418233	1728005	1545633	1722720	1464199	1700032		
1,3,5-TiPB	33146	53817	59621	75143	70912	84959		
5.7	5883	8901	9462	11203	9770	11252		
12.6	0	0	0	0	0	61		
20.5	0	0	2612	4748	4227	5364		
25.2	389	408	2347	6863	6325	8397		
other	27978	28417	28077	29040	26876	40631		
Total Area	1485629	1819548	1647752	1849717	1582309	1850696		
Area - cH	67396	91543	102119	126997	118110	150664		
TiPB/c-H	0.0234	0.0311	0.0386	0.0436	0.0484	0.0500		
% Conv.	**74.8**	**66.4**	**58.4**	**53.0**	**47.8**	**46.1**		
Mass Bal.	**48.8**	**54.1**	**66.6**	**73.8**	**80.2**	**87.5**	Ri / Rbp	R=Ahc/At

REFERENCES

"No man has a good enough memory to make a good liar"

REFERENCES

The references are listed in alphabetical order of the first author. Where more than one publication by the same first author has been listed, the references are listed in chronological order.

Akporiaye, D., Chapple, A.P., Clark, D.M., Dwyer, J., Elliott, I.S. and Rawlence, D.J., *Stud. Surf. Sci. Catal.*, **28**, 351-357 (1986)

Amenomiya, Y. and Cvetanovic, R.J., *J. Phys. Chem.*, **67**, 144-147 (1963a)

Amenomiya, Y. and Cvetanovic, R.J., *J. Phys. Chem.*, **67**, 2046-2049 (1963b)

Amenomiya, Y. and Cvetanovic, R.J., *J. Phys. Chem.*, **67**, 2705-2708 (1963c)

Amenomiya, Y., Chenier, J.H.B. and Cvetanovic, R.J., *J. Phys. Chem.*, **68**, 52-57 (1964)

Amenomiya, Y. and Cvetanovic, R.J., *J. Catal.*, **18**, 329-337 (1970)

Andersen, B., *in* "Propene Oligomerization over Steam Dealuminated and Boron and Phosphorus Modified ZSM-5", PhD Thesis, University of Cape Town (1991)

Anderson, J.R., Foger, K., Mole, T., Rajadhyaksha, R.A. and Sanders, J.V., *J. Catal.*, **58**, 114-130 (1979)

Anderson, J.R., Chang, Y.-F. and Hughes, A.E., *Catal. Lett.*, **2**, 279-286 (1989a)

Anderson, J.R., Chang, Y.-F. and Western, R.J., *J. Catal.*, **118**, 466-482 (1989b)

Apelian, M.R., Degnan, T.F. and Fung, A.S., U.S. Patent 5,234,872 (1993)

Apelian, M.R., Fung, A.S., Kennedy, G.J. and Degnan, T.F., *J. Phys. Chem.*, **100**, 16577-16583 (1996)

Argauer, R.J. and Landolt, G.R., U.S. Patent 3,702,886 (1972)

Aronson, M.T., Gorte, R.J. and Farneth, W.E., *J. Catal.*, **98**, 434-443 (1986)

Barrer, R.M., *J. Chem. Soc.*, 2158 (1948)

Barrer, R.M., *Zeolites*, **1**, 130-140 (1981)

Barrer, R.M., *in* "Hydrothermal Chemistry of Zeolites", Academic Press, London (1982)

Barrer, R.M., *in* "Zeolite Synthesis", ACS Symp. Ser. 398, ACS, Occelli, M.L. and Robson, H.E (Eds.), Washington DC, 11-27 (1989)

Behrsing, T., Jaeger, H. and Sanders, J.V., *Appl. Catal.*, **54**, 289-302 (1989)

Bergna, H.E., Keane, M., Ralston, D.H., Sonnichsen, G.C., Abrams, L. and Shannon, R.D., *J. Catal.*, **115**, 148-158 (1989)

Bessel, S. and Seddon, D., *J. Catal.*, **105**, 270-275 (1987)

Beyer, H. and Belenykaja, I., *Stud. Surf. Sci. Catal.*, **5**, 203-210 (1980)

Bhat, Y.S. and Halgeri, A.B., *Appl. Catal.*, **101**, 95-104 (1993)

Bhat, Y.S., Das, J. and Halgeri, A.B., *Appl. Catal.*, **115**, 257-267 (1994)

Bhat, Y.S., Das, J. and Halgeri, A.B., *J. Catal.*, **155**, 154-157 (1995)

Bhat, Y.S., Das, J., Rao, K.V. and Halgeri, A.B., *J. Catal.*, **159**, 368-374 (1996)

Bhatia, S., Beltramini, J. and Do, D.D., *Catal. Rev.-Sci. Eng.*, **31**(4), 431-480 (1989-90)

Bibby, D.M., Milestone, N.B., Patterson, J.E. and Aldridge, L.P., *J. Catal.*, **97**, 493-502 (1986)

Borade, R.B. and Clearfield, A., *Microporous Materials*, **5**, 289-297 (1996)

Breck, D.W., *in* "Zeolite Molecular Sieves", Robert E. Krieger Publishing Company, Inc., Malabar, Florida USA (1974)

Brinker, C.J. and Scherer, G.W., *in* "Sol-Gel Science: The Physics and Chemistry of Sol-Gel Processing", Academic Press, Inc., San Diego, (1990)

Bülow, M., Caro, J., Völter, J. and Kärger, J., *Stud. Surf. Sci. Catal.*, **34**, 343-354 (1987)

Camblor, M.A. and Pérez-Pariente, J., *Zeolites*, **11**, 202-210 (1991)

Cejka, J., Zilkova, N., Wichterlova, B., Eder-Mirth, G. and Lercher, J.A., *Zeolites*, **17**, 265-271 (1996)

Chamoumi, M., Brunel, D., Fajula, F., Geneste, P., Moreau, P. and Solofo, J., *Zeolites*, **14**, 282-289 (1994)

Chao, K. and Chern, J., *Zeolites*, **8**, 82-85 (1988)

Choudhary, V.R. and Akolekar, D.B., *J. Catal.*, **117**, 542-548 (1989)

Choudhary, V.R. and Akolekar, D.B., *J. Molec. Catal.*, **66**, 215-222 (1991)

Corma, A., Martinez, A., Arrayo, P.A., Monteiro, J.L.F. and Sousa-Aguiar, E.F., *Appl. Catal.*, **142**, 139-150 (1996)

CRC Handbook of Chemistry and Physics, 63rd Edition, Weast R.C. (Ed.), CRC Press, Boca Raton, Florida USA (1982-1983)

Csicsery, S.M., *in* "Zeolite Chemistry and Catalysis, ACS Monograph 171", Rabo, J.A. (Ed.), 680-713 (1979)

Cvetanovic, R.J. and Amenomiya, Y., *Advances in Catalysis*, **17**, 103-149 (1967)

Cvetanovic, R.J. and Amenomiya, Y., *Catalysis Reviews*, **6**(1), 21-48 (1972)

Das, J., Bhat, Y.S. and Halgeri, A.B., *Catal. Lett.*, **20**, 349-357 (1993)

Das, J., Bhat, Y.S. and Halgeri, A.B., *Indian Journal of Chemistry*, **35A**, 690-692 (1996)

Datka, J., Kolidziejski, W., Klinowski, J. and Sulikowski, B., *Catal. Lett.*, **19**, 159-165 (1993)

Demmin, R.A. and Gorte, R.J., *J. Catal.*, **90**, 32-39 (1984)

Derouane, E.G., Gilson, J.P., Gabelica, Z., Mousty-Desbuquoit, C. and Verbist, J., *J. Catal.*, **71**, 447-448 (1981)

Derouane, E.G., *J. Catal.*, **100**, 541-544 (1986)

Derouane, E.G. and Gabelica, Z., *Journal of Solid State Chemistry*, **64**, 296-304 (1986)

De Vos Burchart, E., Van Bekkum, H. and Van de Graaf, B., *Zeolites*, **13**, 212-215 (1993)

Dwyer, J., Fitch, F.R., Machado, F., Qin, G., Smyth, S.M. and Vickerman, J.C., *J. Chem. Soc., Chem. Commun.*, 422-424 (1981)

Eapen, M.J., Reddy, K.S.N and Shiralkar, V.P., *Zeolites*, **14**, 295-302 (1994)

Feijen, E.J.P., Martens, J.A. and Jacobs, P.A., *Stud. Surf. Sci. Catal.*, **84**, 3-21 (1994)

Fetting, F. and Dingerdissen, U., *Chem. Eng. Technol.*, **15**, 202-212 (1992)

Flanigen, E.M., Bennett, J.M., Grose, R.W., Cohen, J.P., Patton, R.L. and Kirchner, R.M., *Nature*, **271**, 512-516 (1978)

Fletcher, J.C.Q., *in* "The acidity of synthetic mica-montmorillonite and its activity for propene oligomerization", PhD Thesis, University of Cape Town (1984)

Forni, L. and Magni, E., *J. Catal.*, **112**, 437-443 (1988)

Forni, L., Vatti, F.P. and Ortoleva, E., *Zeolites*, **12**, 101-106 (1992)

Forni, L., Vatti, F.P. and Ortoleva, E., *Microporous Materials*, **3**, 367-375 (1995)

Fraenkel, D., Cherniavsky, M. and Levy, M., *in* "Proceedings, 8th International Congress on Catalysis, Berlin, 1984," Vol IV, 545-554, Dechema, Frankfurt-am-Main (1984)

Fraenkel, D., Cherniavsky, M., Ittah, B. and Levy, M., *J. Catal.*, **101**, 273-283 (1986)

Fraenkel, D. and Levy, M., *J. Catal.*, **118**, 10-21 (1989a)

Fraenkel, D. and Levy, M., *J. Catal.*, **118**, 487-493 (1989b)

Fyfe, C.A., Gobbi, G.C. and Kennedy, G.J., *Chem. Lett.*, 1551-1554 (1983)

Gabelica, Z., Blom, N. and Derouane, E.G., *Appl. Catal.*, **5**, 227-248 (1983)

Gallezot, P., Leclercq, C., Guisnet, M. and Magnoux, P., *J. Catal.*, **114**, 100-111 (1988)

* Gilson, J.-P., *in* "Zeolite Microporous Solids: Synthesis, Structure, and Reactivity", NATO ASI Ser. Vol. 352, Derouane, E.G., Lemos, F., Naccache, C. and Ribeiro, F.R. (Eds.), Kluwer Academic Publishers, Dordrecht, 19-48 (1992)

Gorte, R.J., *J. Catal.*, **75**, 164-174 (1982)

Gründling, C., Eder-Mirth, G. and Lercher, J.A., *J. Catal.*, **160**, 299-308 (1996)

Guisnet, M. and Magnoux, P., *Appl. Catal.*, **54**, 1-27 (1989)

Haag, W.O., Lago, R.M. and Weisz, P.B., *Disc. Faraday Soc.*, **72**, 317-330 (1982)

Haag, W.O. and Chen, N.Y., *in* "Catalyst Design Progress and Perspectives", Hegedus, L.L, John Wiley and Sons, 165-170 (1987)

Handreck, G.P. and Smith, T.D., *Zeolites*, **10**, 746-752 (1990)

Hardenberg, T.A.J., Mertens, L., Mesman, P., Muller, H.C. and Nicolaides, C.P., *Zeolites*, **12**, 685-689 (1992)

Hegde, S.G., Kumar, R., Bhat, R.N. and Ratnasamy, P., *Zeolites*, **9**, 231-237 (1989)

Herz, R.K., Kiela, J.B. and Marin, S.P., *J. Catal.*, **73**, 66-75 (1982)

Hibino, T., Niwa, M., Murakami, Y., Sano, M., Komai, S. and Hanaichi, T., *J. Phys. Chem.*, **93**, 7847-7850 (1989) *

Hibino, T., Niwa, M. and Murakami, Y., *J. Catal.*, **128**, 551-558 (1991)

Hibino, T., Niwa, M. and Murakami, Y., *Zeolites*, **13**, 518-523 (1993)

Hidalgo, C.V., Itoh, H., Hattori, T., Niwa, M. and Murakami, Y., *J. Catal.*, **85**, 362-369 (1984)

Higgins, J.B., LaPierre, R.B., Schlenker, J.L., Rohrman, A.C., Wood, J.D., Kerr, G.T. and Rohrbaugh, W.J., *Zeolites*, **8**, 446-452 (1988)

Hughes, A.E., Wilshier, K.G., Sexton, B.A. and Smart, P., *J. Catal.*, **80**, 221-227 (1983)

Hunger, B, Hoffmann, J., Heitsch, O. and Hunger, M., *Journal of Thermal Analysis*, **36**, 1379-1391 (1990)

Itabashi, K., Fukushima, T. and Igawa, K., *Zeolites*, **6**, 30-34 (1986)

Iwamoto, M., Tajima, M. and Kagawa, S., *J. Chem. Soc., Chem. Commun.*, 598-600 (1986)

Jacobs, P.A. and Martens, J.A., *Stud. Surf. Sci. Catal.*, **33**, 100-103 (1987)

Jacobs, P.A., *in* "Zeolite Microporous Solids: Synthesis, Structure, and Reactivity", NATO ASI Ser. Vol. 352, Derouane, E.G., Lemos, F., Naccache, C. and Ribeiro, F.R. (Eds.), Kluwer Academic Publishers, Dordrecht, 3-18 (1992)

Jansen, J.C., Engelen, C.W.R. and Van Bekkum, H., *in* "Zeolite Synthesis", ACS Symp. Ser. 398, ACS, Occelli, M.L. and Robson, H.E (Eds.), Washington DC, 257-273 (1989)

Jansen, J.C., *Stud. Surf. Sci. Catal.*, **58**, 77-136 (1991)

Jansen, J.C., private communication (1998)

Jones, D.M. and Griffin, G.L., *J. Catal.*, **80**, 40-46 (1983)

Kapustin, G.I., Brueva, T.R., Klyachko, A.L., Beran, S. and Wichterlova, B., *Appl. Catal.*, **42**, 239-246 (1988)

Karge, H.G. and Dondur, V., *J. Phys. Chem.*, **94**, 765-772 (1990)

Karge, H.G., *Stud. Surf. Sci. Catal.*, **58**, 531-570 (1991)

Karge, H.G., Dondur, V. and Weitkamp, J., *J. Phys. Chem.*, **95**, 283-288 (1991)

Katovic, A., Subotic, B., Smit, I., Despotovic, A. and Curic, M., *in* "Zeolite Synthesis", ACS Symp. Ser. 398, ACS, Occelli, M.L. and Robson, H.E (Eds.), Washington DC, 124-139 (1989)

Kazansky, V.B., *Acc. Chem. Res.*, **24**, 379 (1991)

Kazansky, V.B., *Stud. Surf. Sci. Catal.*, **85**, 251-272 (1994)

Kerr, G.T., *J. Phys. Chem.*, **72**, 2594-2596 (1968a)

Kerr, G.T., *J. Phys. Chem.*, **73**, 2780-2782 (1968b)

Kim, J.-H., Ishida, A., Okajima, M. and Niwa, M., *J. Catal.*, **161**, 387-392 (1996)

Kiskinova, M., Griffin, G.L. and Yates, J.T.,Jr., *J. Catal.*, **71**, 278-287 (1981)

Koegler, J.H., Van Bekkum, H. and Jansen, J.C., *Zeolites*, **19**, 262-269 (1997)

Kofke, G.T.J., Gorte, R.J. and Farneth, W.E., *J. Catal.*, **114**, 34-45 (1988)

Kofke, G.T.J. and Gorte, R.J., *J. Catal.*, **115**, 233-243 (1989)

Kofke, G.T.J., Gorte, R.J., Kokotailo, G.T. and Farneth, W.E., *J. Catal.*, **115**, 265-272 (1989)

Kokotailo, G.T., Lawton, S.L., Olson, D.H. and Meier, W.M., *Nature*, **272**, 437-438 (1978)

Kühl, G.H., *in* "Proc. 3rd Int. Conf. on Molecular Sieves, Recent Progress Reports", Uytterhoeven, J.B. (Ed), Paper 127, 227-229, Univ. Leuven Press (1973)

Kühl, G.H., *J. Phys. Chem. Solids*, **38**, 1259-1263 (1977)

Lago, R.M., Haag, W.O., Mikovsky, R.J., Olson, D.H., Hellring, S.D., Schmitt, K.D. and Kerr, G.T., *Stud. Surf. Sci. Catal.*, **28**, 677-684 (1986)

Lee, C.S., Park, T.J. and Lee, W.Y., *Appl. Catal.*, **96**, 151-161 (1993)

Leu, L-J., Hou, L-Y., Kang, B-C., Li, C., Wu, S-T. and Wu, J-C., *Appl. Catal.*, **69**, 49-63 (1991)

Li-feng, C., Wacker, T. and Rees, L.V.C., *J. Chem. Soc., Faraday Trans. I*, **85(1)**, 33-45 (1989)

Liu, X. and Xu, R., *J. Chem. Soc., Chem. Commun.*, 1837-1839 (1989)

Maache, M., Janin, A., Lavalley, J.C., Joly, J.F. and Benazzi, E., *Zeolites*, **13**, 419-426 (1993)

Magnoux, P., Cartraud, P., Mignard, S. and Guisnet, M., *J. Catal.*, **106**, 242-250 (1987)

Martens, J.A., Geerts, M., Grobet, P.J. and Jacobs, P.A., *J. Chem. Soc., Chem. Commun.*, 1418-1419 (1990)

Matsuda, T., Kimura, T., Herawati, E., Kobayashi, C. and Kikuchi, E., *Appl. Catal.*, **136**, 19-28 (1996)

Meier, W.M., *in* "Molecular Sieves", Society for Chemical Industry, London (1968)

Meier, W.M. and Olson, D.H., *in* "Atlas of Zeolite Structure Types", Structure Commission of IZA, Third Revised Edition, Butterworth-Heinemann (1992)

Meier, W.M., Olson, D.H. and Baerlocher, Ch., *in* "Atlas of Zeolite Structure Types", Structure Commission of IZA, Fourth Revised Edition, Butterworth-Heinemann (1996)

Middleditch, B.S., *in* "Practical Mass Spectrometry", Middleditch, B.S. (Ed), Plenum Press, New York (1979)

Mirth, G., Cejka, J., Krtil, J. and Lercher, J.A., *Stud. Surf. Sci. Catal.*, **88**, 241-248 (1994)

Moon, G.C., *in* "The Synthesis and Characterization of Zeolite Beta", MSc Thesis, University of Cape Town (1995)

Moscou, L., *Stud. Surf. Sci. Catal.*, **58**, 1-12 (1991)

Nagy, J.B., Gabelica, Z. and Derouane, E.G., *Zeolites*, **3**, 43-49 (1983)

Namba, S., Inaka, A. and Yashima, T., *Zeolites*, **6**, 107-110 (1986)

Nayak, V.S. and Choudhary, V.R., *J. Catal.*, **81**, 26-45 (1983)

Nayak, V.S. and Choudhary, V.R., *Appl. Catal.*, **10**, 137-145 (1984)

Neuber, M., Dondur, V., Karge, H.G., Pachedo, L., Ernst, S. and Weitkamp, J., *Stud. Surf. Sci. Catal.*, **37**, 461-469 (1988)

Neuber, M. and Weitkamp, J., *in* "Proceedings, 8th International Zeolite Conference", Amsterdam, July 1989, Jansen, J.C., Moscou, L. and Post, M.F.M. (Eds), 425-426 (1989)

Niewenhuys, B.E., Ponec, V., Van Koten, G., Van Leeuwen, P.W.N.M. and Van Santen, R.A., *Stud. Surf. Sci. Catal.*, **79**, 89-158 (1993)

Niwa, M., Kato, S., Hattori, T. and Murakami, Y., *J. Chem. Soc, Faraday Trans. I*, **80**, 3135-3145 (1984a)

Niwa, M., Morimoto, S., Kato, M., Hattori, T. and Murakami, Y., Preprint from the 8th Int. Congr. Catal., **IV**, 701-711 (1984b)

Niwa, M., Kato, M., Hattori, T. and Murakami, Y., *J. Phys. Chem.*, **90**, 6233-6237 (1986a)

Niwa, M., Hidalgo, C., Hattori, T. and Murakami, Y., *Stud. Surf. Sci. Catal.*, **28**, 297-304 (1986b)

Niwa, M., Iwamoto, M. and Segawa, K., *Bull. Chem. Soc. Jpn.*, **59**, 3735-3739 (1986c)

Niwa, M., Kawashima, Y., Hibino, T. and Murakami, Y., *J. Chem. Soc, Faraday Trans. I,* **84**, 4327-4336 (1988a)

Niwa, M., Sawa, M. and Murakami, Y., *in* "Proceedings of the 9th International Congress on Catalysis", Phillips, M.J. and Ternan, M. (Eds), Calgary, June 26 - July 1, 1988, Vol I, Chemical Institute of Canada, Ottawa (1988b)

Niwa, M. and Murakami, Y., *J. Phys. Chem. Solids*, **50**, 487-496 (1989)

Niwa, M., Yamazaki, K. and Murakami, Y., *Ind. Eng. Chem. Res.*, **30**, 38-42 (1991)

Niwa, M., Katada, N. and Murakami, Y., *J. Catal.*, **134**, 340-348 (1992)

Niwa, M., Yamazaki, K. and Murakami, Y., *Ind. Eng. Chem. Res.*, **33**, 371-374 (1994)

Niwa, M., Katada, N., Sawa, M. and Murakami, Y., *J. Phys. Chem.*, **99**, 8812-8816 (1995)

O'Donovan, A.W., O'Connor, C.T. and Koch, K.R., *Microporous Materials*, **5**, 185-202 (1995)

Parikh, P.A., Subrahmanyam, N., Bhat, Y.S. and Halgeri, A.B., *Appl. Catal.*, **90**, 1-10 (1992)

Parikh, P.A., Subrahmanyam, N., Bhat, Y.S. and Halgeri, A.B., *J. Molec. Catal.*, **88**, 85-92 (1994)

Parrillo, D.J., Adamo, A.T., Kokotailo, G.T. and Gorte, R.J., *Appl. Catal.*, **67**, 107-118 (1990)

Parrillo, D.J. and Gorte, R.J., *J. Phys. Chem.*, **97**, 8786-8792 (1993)

Pereira, C. and Gorte, R.J., *Appl. Catal.*, **90**, 145-157 (1992)

Pérez-Pariente, J., Martens, J.A. and Jacobs, P.A., *Appl. Catal.*, **31**, 35-64 (1987)

Pope, C.G., *Zeolites*, **10**, 28-31 (1990)

Post, J.G. and Van Hooff, J.H.C., *Zeolites*, **4**, 9-14 (1984)

Ratnasamy, P., Bhat, R.N., Pokhriyal, S.K., Hedge, S.G. and Kumar, R., *J. Catal.*, **119**, 65-70 (1989)

Richter, M., Janchen, J., Jerschkewitz, H.-G., Parlitz, B. and Schreier, E., *J. Chem. Soc, Faraday Trans. I,* **87**, 1461-1466 (1991)

Rieck, J.S. and Bell, A.T., *J. Catal.*, **85**, 143-153 (1984)

Röger, H.P., Möller, K.P. and O'Connor, C.T., *Microporous Materials*, **8**, 151-157 (1997)

Röger, H.P., Möller, K.P. and O'Connor, C.T., accepted by *Microporous and Mesoporous Materials* (1998)

Rollmann, L.D., *J. Catal.*, **47**, 113-121 (1977)

Rollmann, L.D. and Walsh, D.E., *J. Catal.*, **56**, 139-140 (1979)

Rollmann, L.D., U.S. Patent 4,203,869 (1980)

Rollmann, L.D., *Stud. Surf. Sci. Catal.*, **68**, 791-797 (1991)

Sand, L.B., *Pure and Applied Chemistry*, **52**, 2105-2113 (1980)

Santilli, D.S. and Zones, S.I., *Catal. Lett.*, **7**, 383-388 (1990)

Santilli, D.S., Harris, T.V. and Zones, S.I., *Microporous Materials*, **1**, 329-341 (1993)

Sato, S., Tokumitsu, M., Sodesawa, T. and Nozaki, F., *Bull. Chem. Soc. Jpn.*, **64**, 1005-1007 (1991)

Sauer, J., *J. Molec. Catal.*, **54**, 312-323 (1989)

Sawa, M., Niwa, M. and Murakami, Y., *Appl. Catal.*, **53**, 169-181 (1989)

Sawa, M., Kato, K., Hirota, K., Niwa, M. and Murakami, Y., *Appl. Catal.*, **64**, 297-308 (1990a)

Sawa, M., Niwa, M. and Murakami, Y., *Zeolites*, **10**, 307-309 (1990b)

Sawa, M., Niwa, M. and Murakami, Y., *Zeolites*, **12**, 175-179 (1992)

Scherzer, J., ACS Symp. Series 248, 157-200 (1984)

Schulz, H. and Nehren, S., *Erdöl und Kohle*, **39**, 93 (1986)

Schulz, H., Zhao Siwei and Baumgartner, W., *Stud. Surf. Sci. Catal.*, **34**, 479-492 (1987)

Schwarz, J.A., Russell, B.G. and Harnsberger, H.F., *J. Catal.*, **54**, 303-317 (1978)

Sharma, S.B., Meyers, B.L., Chen, D.T., Miller, J. and Dumesic, J.A., *Appl. Catal.*, **102**, 253-265 (1993)

Sheng, T.-C. and Gay, I.D., *J. Catal.*, **145**, 10-15 (1994)

Silva, J.M., Ribeiro, M.F., Ramôa Ribeiro, F., Benazzi, E., Gnep, N.S. and Guisnet, M., *Zeolites*, **16**, 275-280 (1996)

Skeels, G.W. and Breck, D.W., *in* "Proc. 6th Intern. Zeolite Conf.", Reno, July 1983, Olson, D.H. and Bisio, A. (Eds), Butterworth, Guildford, 87-96 (1984)

Smith, J.V., *in* "Zeolite Chemistry and Catalysis, ACS Monograph 171", Rabo, J.A. (Ed) 1-79 (1979)

Stach, H., Jänchen, J., Jerschkewitz, H.-G., Lohse, U., Parlitz., B. and Hunger, M., *J. Phys. Chem.*, **96**, 8473-8479 (1992)

Suib, S.L., Stucky, G.D. and Blattner, R.J., *J. Catal.*, **65**, 174-178 (1980)

Szostak, R., *in* "Molecular Sieves - Principles of Synthesis and Identification", Davis, B.H. (Ed.), Van Nostrand Reinhold, New York (1989)

Szostak, R., *Stud. Surf. Sci. Catal.*, **58**, 153-199 (1991)

Szostak, R. *in* "Handbook of Molecular Sieves", Van Nostrand Reinhold, New York (1992)

Thiart, J.J. and Hlavacek, V., *AIChE Journal*, **41(8)**, 1926-1943 (1995)

Topsoe, N.-Y., Pedersen, K. and Derouane, E.G., *J. Catal.*, **70**, 41-52 (1981)

Tronconi, E. and Forzatti, P., *J. Catal.*, **93**, 197-200 (1985)

Tsai, T.-C. and Wang, I., *Appl. Catal.*, **77**, 209-222 (1991)

Uytterhoeven, J.B., Christner, L.G. and Hall, W.K., *J. Phys. Chem.*, **69**, 2117-2126 (1965)

Van den Brekel, C.H.J., *Philips Res. Rep.*, **32**, 118 (1977)

Van der Gaag, F.J., Jansen, J.C. and Van Bekkum, H., *Appl. Catal.*, **17**, 201-211 (1985)

Van Santen, R.A., *Stud. Surf. Sci. Catal.*, **85**, 273-294 (1994)

Von Ballmoos, R. and Meier, W.M., *Nature*, **289**, 782-783 (1981)

Wadlinger, R.L., Kerr, G.T. and Rosinski, E.J., U.S. Patent 3,308,069 (1967)

Wang, I., Ay, C.-L., Lee, B.-J. and Chen, M.-H, Proc. 9th Int. Congr. Catalysis, Calgary, 324-331 (1988)

Wang, I., Ay, C.-L., Lee, B.-J. and Chen, M.-H, *Appl. Catal.*, **54**, 257-266 (1989)

Ward, J.W., *J. Catal.*, **9**, 225-236 (1967)

Warzywoda, J., Edelman, R.D. and Thompson, R.W., *Zeolites*, **11**, 318-324 (1991)

Weitkamp, J., Schwark, M. and Ernst, S., *Chem.-Ing.-Tech.*, **61**, 887-888 (1989)

Whittemore, O.J., *Am. Mineral.*, **57**, 1146-1151 (1972)

Yue, Y.-H., Tang, Y., Liu, Y. and Gao, Z., *Ind. Eng. Chem. Res.*, **35**, 430-433 (1996)

Yue, Y.-H., Tang, Y., and Gao, Z., *Stud. Surf. Sci. Catal.*, **105**, 2059-2064 (1997)

Zholobenko, V.L., Kustov, L.M., Kazansky, V.B., Loeffler, E., Lohser, U., Peuker, Ch. and Oehlmann, G., *Zeolites*, **10**, 304-306 (1990)

Zones, S.I., *Zeolites*, **9**, 458-467 (1989)